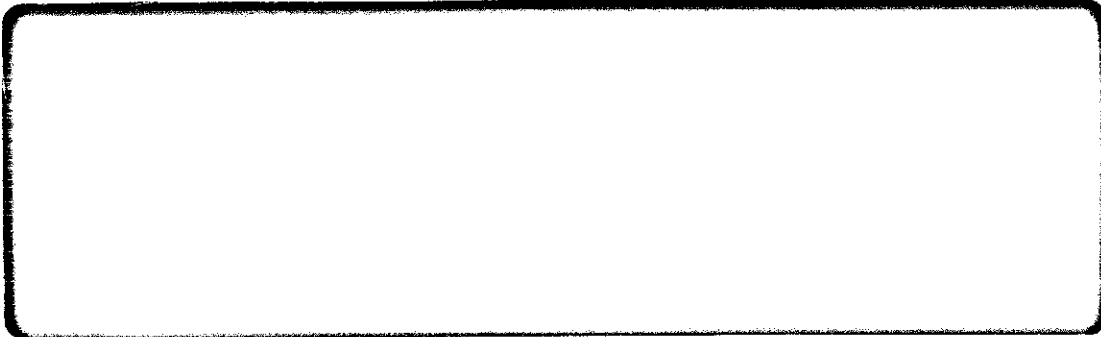


FLOW RESEARCH, INC.



NASA-CR-114696) THE CONSTRUCTION AND
OPERATION OF A WATER TUNNEL IN
APPLICATION TO FLOW VISUALIZATION STUDIES
OF AN OSCILLATING (Flow Research, Inc.,
Kent, Wash.) 76 p HC \$6.00 CSDL 14B

N74-15946

Unclas

G3/11 29375



FLOW RESEARCH REPORT NO. 13

THE CONSTRUCTION AND OPERATION OF A WATER TUNNEL
IN APPLICATION TO FLOW VISUALIZATION STUDIES
OF AN OSCILLATING AIRFOIL*

by

John H. Olsen
and
Hsien Ta Liu

May, 1973

Flow Research, Inc.
1819 South Central Avenue
Kent, Washington 98031

*This work is supported by AMES Directorate, USAAMRDL under NASA Ames
Research Center Contract NAS2-6927.

I

Table of Contents

	<u>Page</u>
List of Symbols	1
List of Figures	ii & iii
I. Introduction	1
II. Description of Apparatus	1
2.1 The Water Tunnel	1
2.2 The Oscillating Mechanism	3
2.3 High Power Flash Lamp	4
2.4 The Hydrogen Bubble Generator	5
2.5 The Light Detector Circuit	6
III. Procedures of Operation	7
IV. Results of Operation	10
V. Additional Tasks	12
5.1 Feedback Control System	12
5.2 Elimination of Reflection from the Rear Window	14
5.3 Other Flow Visualization Techniques	15
5.3.1 Description of the Thymol Blue Experiments	15
5.3.1.1 Principle of the Thymol Blue Technique	15
5.3.1.2 Experimental Setup	16
5.3.2 Results of Thymol Blue Experiments	17
VI. Concluding Remarks	20
References	
Appendix A - Figures	

The Construction and Operation of a Water Tunnel
in Application to Flow Visualization Studies
of an Oscillating Airfoil*

by

John H. Olsen and Hsien Ta Liu
Flow Research, Inc., Kent, Washington 98031

Abstract

Flow Research, under contract (NAS2-6927) with the NASA Ames Research Center has constructed a water tunnel and investigated the flow field adjacent to an oscillating airfoil. The design and operational procedures of the tunnel are described in detail. Hydrogen bubble and thymol blue techniques are used to visualize the flow field.

Results of the flow visualizations are presented in a series of still pictures and a high speed movie. These results show that the stall is more complicated than simple shedding from the leading edge or the trailing edge, particularly at relatively low frequency oscillations comparable to those of a helicopter blade. Therefore, any successful theory for predicting the stall loads on the helicopter blades must treat an irregular separated region rather than a discrete vortex passing over each blade surface.

*This work is supported by NASA Ames Research Center under Contract No. NAS2-6927.

List of Symbols

a	Major axis of an ellipse
b	Minor axis of an ellipse
C	Chord length of an airfoil
f	Oscillating frequency of an airfoil
K_t	Nondimensional oscillating frequency of an airfoil
n	Power index
p	Pressure
R_e	Reynolds number
t	time
x	Horizontal coordinate axis
y	Vertical coordinate axis
ϵ	Oscillating amplitude of an airfoil
ν	Kinematic viscosity
θ_o	Mean angle of attack of an airfoil
θ	Angle of attack of an airfoil
θ_{max}	Maximum angle of attack of an airfoil

List of Figures

- Fig. 1. View of Entire Tunnel
- Fig. 2. Tunnel Test Section
- Fig. 3. Test Section Window Installation
- Fig. 4. D.C. Motor and Driveshaft
- Fig. 5. Contraction Contours
- Fig. 6. Oscillating Mechanism
- Fig. 7. Wedge & Slot for Model Drive
- Fig. 8. Differential Mechanism
- Fig. 9. Flashlamp Power Circuit
- Fig. 10. Water Tunnel Flash Tube Trigger
- Fig. 11. Flashlamp Power Supply and Trigger
- Fig. 12. Hydrogen Bubble Generator
- Fig. 13. Light Detector Circuit
- Fig. 14. Hydrogen Bubble Generator and Trigger
- Fig. 15. Moment Diagrams of an Oscillating Airfoil (NACA 0012).
Pitch Axis = 1/4 Chord.
- Fig. 16. Hydrogen Bubble Traces of Boundary Layer Flow Patterns on an
Oscillating Airfoil. Run No. 1: $\theta_o = 10.9^\circ$, $\epsilon = +20.0^\circ$, $K_t = .111$,
 $R_e = .577 \times 10^6$.
- Fig. 17. Hydrogen Bubble Traces of Boundary Layer Flow Patterns on an
Oscillating Airfoil. Run No. 2: $\theta_o = 10.9^\circ$, $\epsilon = +20.0^\circ$, $K_t = .282$,
 $R_e = .577 \times 10^6$.
- Fig. 18. Hydrogen Bubble Traces of Boundary Layer Flow Patterns on an
Oscillating Airfoil. Run No. 3: $\theta_o = 10.9^\circ$, $\epsilon = +20.0^\circ$, $K_t = .532$,
 $R_e = .577 \times 10^6$.
- Fig. 19. Hydrogen Bubble Traces of Boundary Layer Flow Patterns on an
Oscillating Airfoil. Run No. 4: $\theta_o = 15.8^\circ$, $\epsilon = +20.0^\circ$, $K_t = .111$,
 $R_e = .577 \times 10^6$.
- Fig. 20. Hydrogen Bubble Traces of Boundary Layer Flow Patterns on an
Oscillating Airfoil. Run No. 5: $\theta_o = 15.8^\circ$, $\epsilon = +20.0^\circ$, $K_t = .282$,
 $R_e = .577 \times 10^6$.
- Fig. 21. Hydrogen Bubble Traces of Boundary Layer Flow Patterns on an
Oscillating Airfoil. Run No. 6: $\theta_o = 15.8^\circ$, $\epsilon = +20.0^\circ$, $K_t = .532$,
 $R_e = .577 \times 10^6$.

List of Figures (Cont'd)

- Fig. 22. Hydrogen Bubble Traces of Boundary Layer Flow Patterns on an Oscillating Airfoil. Run No. 7: $\theta_o = 18.6^\circ$, $\epsilon = +20.0^\circ$, $K_t = .111$, $R_e = .577 \times 10^6$.
- Fig. 23. Hydrogen Bubble Traces of Boundary Layer Flow Patterns on an Oscillating Airfoil. Run No. 8: $\theta_o = 18.6^\circ$, $\epsilon = +20.0^\circ$, $K_t = .282$, $R_e = .577 \times 10^6$.
- Fig. 24. Hydrogen Bubble Traces of Boundary Layer Flow Patterns on an Oscillating Airfoil. Run No. 9: $\theta_o = 18.6^\circ$, $\epsilon = +20.0^\circ$, $K_t = .595$, $R_e = .516 \times 10^6$.
- Fig. 25. Hydrogen Bubble Traces of Boundary Layer Flow Patterns on an Oscillating Airfoil. Run No. 10: $\theta_o = 20.0^\circ$, $\epsilon = +20.0^\circ$, $K_t = .111$, $R_e = .577 \times 10^6$.
- Fig. 26. Hydrogen Bubble Traces of Boundary Layer Flow Patterns on an Oscillating Airfoil. Run No. 11: $\theta_o = 20.0^\circ$, $\epsilon = +20.0^\circ$, $K_t = .282$, $R_e = .577 \times 10^6$.
- Fig. 27. Hydrogen Bubble Traces of Boundary Layer Flow Patterns on an Oscillating Airfoil. Run No. 12: $\theta_o = 20.0^\circ$, $\epsilon = +20.0^\circ$, $K_t = .595$, $R_e = .516 \times 10^6$.
- Fig. 28. Moment diagrams correspond to the high Reynolds number movie conditions - Run Series II.
- Fig. 29. Feedback Control Circuit Diagram.
- Fig. 30. Relative Deviations of Tunnel Speed with and without the Feedback Control System in Circuit.
- Fig. 31. Improved photographs of Hydrogen Bubble Traces with the Installation of a Black Background.
- Fig. 32. Visualization of Boundary Layer Flow Patterns on an Oscillating Airfoil with the Thymol Blue Technique. $\theta_o = 12.5^\circ$, $\epsilon = \pm 14^\circ$, $V = 1$ fps, $K_t = .05$.
- Fig. 33. Visualization of Boundary Layer Flow Patterns on an Oscillating Airfoil with the Thymol Blue Technique. $\theta_o = 12.5^\circ$, $\epsilon = \pm 14^\circ$, $V = 1$ fps, $K_t = .10$.
- Fig. 34. Visualization of Boundary Layer Flow Patterns on an Oscillating Airfoil with the Thymol Blue Technique. $\theta_o = 12.5^\circ$, $\epsilon = \pm 14^\circ$, $V = 1$ fps, $K_t = .24$.

I. Introduction

Contract NAS2-6927 involves the design, construction, operation, and delivery to Ames of a water tunnel. The first three phases of this work have been completed and are described in this final report. The material presented here covers a description of apparatus, procedures and results of operation, and concluding remarks. A high speed movie is also included as a portion of results of operation. Additional work supplementing the main contract is also described.

II. Description of Apparatus

The material presented in this section covers the following items:

- a) a description of the basic tunnel which may be used for a wide variety of experiments;
- b) the oscillating mechanism used to produce pitching motions on a two dimensional airfoil;
- c) a high power flash lamp that can be synchronized with the shutter of a high speed camera or with the airfoil oscillation;
- d) a hydrogen bubble generator for marking the fluid for flow visualization;
- e) a light detector circuit used to synchronize the flash or other electronic device with the phase of the airfoil oscillation as detected by photocells.

2.1 The Water Tunnel

A view showing the entire tunnel is given in figure 1. With the exception of the fiberglass contraction and plexiglas test section windows, all parts are of 304 stainless steel. The first and second elbows downstream of the test section are commercial long turn elbows. The third and fourth elbows are sharp 90° bends with turning vanes.

The tunnel is supported by a steel framework with adjustable pad feet. A platform is fastened to the frame to serve the dual purposes of a cat-walk for working on the tunnel and a table for holding instruments and other experimental apparatus.

The tunnel can be pressurized to 15 PSIG ($1.05 \times 10^4 \text{ Kg/m}^2$) in the test section to avoid cavitation on the models. At this pressure a Reynolds number of 200,000 per inch (7.87×10^6 per meter) can be obtained on a model with a pressure coefficient as low as -10 . The test section cross section is 8.4" x 12" (.213m x .305m) to keep the same proportions as the 7' x 10' (2.3m x 3.05m) Ames wind tunnels.

The water in the tunnel is kept clean by a continuous 10μ filtration system. Water is withdrawn from the third elbow, pumped through a 10μ filter and returned to the first elbow. The same pumping system is used to withdraw water from the tunnel for changing models or experiments. Two large storage tanks are provided to hold the water during work on the tunnel as well as to provide mixing tanks for adding various flow visualization chemicals.

The test section consists of 4 plexiglas windows mounted on a stainless steel frame (figure 2). The windows are simply rectangular plates with a step cut out around the edges. They can be easily manufactured and changed so that complete experiments can be bolted to a window and easily inserted in the tunnel. The windows are sealed by "o" rings in the steel frame and held in place by clamps. See figure 3 for details.

The pump is a three bladed impeller from an axial flow irrigation pump. The impeller is carried in a Lignum Vitae (a hard self lubricating wood) bearing. The driveshaft passes out through the second elbow where it is turned by an SCR (Silicon Controlled Rectifier) DC motor. (Figure 4). The impeller thrust is carried by bearings in the elbow.

The SCR speed control is controlled by a box on a flexible cable so that the operator can vary the speed from any convenient position. The SCR control is fed by a 230V three phase line which splits within the

control to supply power to the SCR, the filter pump, and the high power flash lamp. A feedback control system, which reduces the tunnel speed variation to approximately a factor of ten, has been installed and is described in a later section.

The screen section is immediately in front of the contraction. It contains two sections of honeycomb and four screens to provide a uniform flow into the contraction. A plexiglas air dome is mounted on top of the screen section to provide an air bleed and to control the pressure within the tunnel. (See figure 1) The air dome is connected by hose to the downstream end of the test section to provide a steady pressure in the test section. During operation, the air bleed valve between the dome and the screen section is closed.

The contraction also serves as a round to rectangular transition between the circular screen section and the rectangular test section. It is formed by a series of contracting super-ellipses whose x-y coordinates are given by the formula

$$\left(\frac{x}{a}\right)^n + \left(\frac{y}{b}\right)^n = 1$$

As n varies from 2 to infinity the curves change from ellipses to rectangles. The major and minor axes are given by a and b . A set of contours for the contraction is given in figure 3.

2.2 The Oscillating Mechanism

The particular experiments to be performed for this contract involve a study of the flow about pitching two dimensional airfoils. The mechanism described here provides a pitching amplitude of up to $\pm 20^\circ$ about any mean angle from 0° to 20° .

Figure 6 shows the basic mechanism. A reciprocating motion is provided by a crank with a long connecting rod. This motion is very nearly a pure sinusoid ($\pm 0.5\%$). The reciprocating motion is converted to rotary motion by a rack and gear. The torque applied to the model is measured by a

torque tube with a strain gauge bridge. The angular position of the model is recorded from a position transducer on the rack. Thus, moment and angle of attack can be recorded both as functions of time and as functions of each other.

The model is driven by a 1" x 3/16" (.025m x .0048m) rectangular tang held to the driving shaft by a tapered wedge (see figure 7). Wires for the hydrogen bubble generation pass through the tang and the driveshaft and through a seal at the rear end of the driveshaft.

The crankshaft and flywheel are driven by an SCR controlled DC motor through a pair of cone pulleys. A 67 to 1 frequency adjustment is possible. A disc with 10 evenly spaced holes on its perimeter is fastened to the crankshaft to provide interruption of a photocell circuit used to measure the crankshaft speed. A second disc is attached to the crankshaft through a differential gear unit so that it can be rotated with respect to the crankshaft while the mechanism is running (see figure 8). The position of a hole in this disc can then be changed relative to the crank position and used to trigger the flash lamp at any desired phase of the oscillation. In fact, the flow can be observed in slow motion by continuously rotating the differential spider.

2.3 High Power Flash Lamp

A Xenon water cooled flash lamp capable of 500 flashes per second at 6 joules per flash is provided for lighting the flow field for photographic purposes. It is mounted in a housing with baffles and lenses to provide an approximately 2 dimensional sheet 1/2" (.013m) wide and about 18 inches (.457m) long. In operation a commercially available strobe lamp is flashed in synchronism with the high power lamp. This light is used to illuminate a sign-board containing experimental information. Thus, each photograph contains a picture of the flow field as well as a record of the experimental conditions.

The lamp is powered by a commercial 8 kilowatt 2,000 volt supply. A pulse forming network for flashing the lamp is added to the supply. The network has two modes of operation. The first, an RC charging circuit is

used for low frequency operation up to about 15 flashes per second. This mode is used primarily for still photographs and visual examination of the flow field. Additional capacitance can be placed in the circuit external to the supply to increase the flash energy to 3000 joules for single flash operation. A second resonant charging mode is available for high speed operation up to 500 flashes per second. In this mode the lamp is operating at a frequency very close to the maximum frequency determined by the extinction of the lamp. Consequently the lamp occasionally may remain on, tripping the breakers and power supply. This mode is used only for short bursts of high speed movies lasting up to 30 seconds. A change from the RC mode to the resonant charging mode is accomplished by opening the rear door of the power supply and simply moving a banana jack from one place to another. Figure 9 is a schematic of the circuit.

The lamp is fired by providing a high voltage pulse to a trigger wire wrapped around the flash tube. This high voltage pulse is generated by the circuit given in figure 10. The pulse can be initiated either by a switch closure or by a small pulse. The pulse generator and power supply share a common cabinet shown in figure 11.

2.4 The Hydrogen Bubble Generator

The function of the hydrogen bubble generator is to provide DC power on demand for the purpose of electrolyzing water to form bubbles for flow visualization markers. The generator can be operated in two modes: in the continuous mode it serves as a steady DC power supply forming a continuous sheet of bubbles. In the pulse mode, the DC power turns on only during the time a photocell is exposed to light. The pulse mode can be used for forming time lines for synchronizing bubble formation with phases of the motion. An output pulse is provided at the instant the DC power is on for the purpose of synchronizing other instrumentation with the bubble formation. A circuit diagram for the hydrogen bubble generator is given in figure 12.

2.5 The Light Detector Circuit

The function of this circuit is to provide output pulses keyed to a photocell input. Two output functions are available. The first gives output pulses at the instant the photocell turns on. This output can be used for running a tachometer, or for continuous flashing of the light in conjunction with the differential gearing arrangement mentioned earlier. Two other outputs give a single pulse at the first photocell input after a switch has been depressed. They are used primarily for obtaining a single flash at a fixed phase of the motion for still photographs. The circuit diagram for the trigger circuit is given as figure 13. The trigger circuit and hydrogen bubble generator are mounted in a common chassis shown in figure 14.

III. Procedures of Operation

This section provides step by step instructions for the operation of the water tunnel and accessory equipment. These instructions should be observed carefully to avoid possible damage to the equipment. Before operating any of this equipment, make sure that it is assembled correctly according to the descriptions in Section II and other supplemental documents.

1. To fill the water tunnel
 - a. Check all joints and test section windows to see that they are tightened appropriately.
 - b. Open the upper and lower valves of the air dome (important)
 - c. Fill the two storage tanks with water. Chemical additives may be mixed in the tank by circulating the solution along the path between the filter and the tank.
 - d. Pump water from tanks (one at a time) to the tunnel. Refill the large tank after emptied.
 - e. Be ready to stop the filling when water starts entering the air dome. Stop the filling pump and close the valves connecting the tanks and the tunnel when the air dome is about 3/4 filled.
 - f. Switch on the main drive pump. Vary the tunnel speed on the remote control box #1 to free captured air bubbles in the tunnel.
 - g. Water level in the air dome will drop when captured air bubbles are released. Refill it up to 3/4 level.
 - h. Close both air dome valves.
2. To set tunnel speed.
 - a. Release any trapped air bubbles in the lines of the manometer.
 - b. Adjust zero level of the mercury column in the manometer.
 - c. When high tunnel speed ($\Delta p > 2$ in Hg or 6.91×10^2 kg/m²) is desired, pressurize the tunnel to 15 PSIG (1.05×10^4 kg/m²) with air through the pressure regulator valve to prevent cavitation on the model.

- d. Turn potentiometer clockwise slowly to obtain the desirable speed or pressure difference (with the airfoil oriented at zero degrees angle of attack).
 - e. Always operate the tunnel at a speed lower than the critical speed at which cavitation on the model starts.
3. To set oscillating amplitude and frequency of the airfoil:
- a. Check to be sure all elements are correctly assembled.
 - b. Disconnect the connecting rod from the flywheel. Adjust the length of the threaded rod and connect the connecting rod to one of the 8 holes on the flywheel such that the desired values θ_0 and ϵ are obtained.
 - c. Connect the V-belt to the selected pair of pulleys. For best regulation choose the pulleys giving the highest motor speed possible.
 - d. Tighten the nut on the threaded rod to eliminate any undesirable hesitating motion of the oscillation. It may be necessary to adjust the play in the gear teeth by tightening the tapered gib behind the rack.
 - e. Switch on the driving motor (remote control box #2) and power supply #1 (for the bubble generator and the optical signal detector).
 - f. Increase airfoil oscillating frequency by turning in clockwise direction the potentiometer on the remote control box #2. The oscillating frequency may be measured accurately by displaying the pulse signal of the photocell on an oscilloscope.
4. To generate hydrogen bubbles:
- a. Connect the electrodes on the airfoil to the power supply #1 output terminals.
 - b. Switch on power supply #1 and turn (clockwise) the variable transformer to its maximum position.
 - c. Switch on the bubble generator with the variable transformer in the zero position. Then, turn to the required setting.

5. To operate the flashlamp
 - a. Set circuit connection (RC or LC mode) and connect the output leads from power supply #2 (high voltage) to the end terminals on the flashlamp chassis according to one of the two operational modes:
 - (1) single shot mode = RC connection;
 - (2) continuous shot mode = LC connection plus a one ohm resistor between positive lead and the terminal.Connect the single pulse output wire to the center terminal.
 - b. Close cabinet door of power supply #2 and switch power on (primary and main switches).
 - c. Wait for about 2 minutes then press the red button on the front panel.
 - d. Turn variable transformer clockwise to reach the operational DC voltage (minimum 1100V)
 - (1) single shot mode: up to 2000V;
 - (2) continuous shot mode: \approx 1300 V.
 - e. Turn on water circulation through the flashlamp for cooling.
 - f. Test flashlamp by pressing the remote control switch (connected directly to the front panel of power supply #2).
 - g. To activate the synchronized mode, connect the output from the detector marked "AUX SYNC" to the front panel of power supply #2. Switch on power supply #1. Adjust the phase angle on the dial of the differential gear on the detector panel. The flashtube will be triggered the first time the airfoil passes the adjusted phase angle after the "RESET" remote switch is pressed.

IV. Results of Operation

Results of operation are presented in the forms of several series of photographs and a high speed movie. Figure 15 shows the x-y plots of instantaneous moments (y) versus phase angles or angles of attack (x). For a particular run, the output signals of the pitching moment strain gauge and of the phase angle strain gauge were stored on the screen of an oscilloscope and recorded photographically. The moment strain gauge was calibrated against known moments applied to it. The moment diagram due to bearing friction only (lower diagram of each photograph) was first recorded with the airfoil oscillating at very low frequency (about 75 rpm) and with no tunnel speed. The moment diagram due to the sum of bearing friction and aerodynamic forces (upper diagram) was then recorded with the airfoil oscillating at a frequency f and with a tunnel speed V specified for the particular run. The zero point for the angle signal is not needed because the extremes are known from the crank geometry. These moment diagrams provide a useful reference for correlating with the flow visualization photographs.

Figures 16 through 27 show twelve series of dynamic boundary layer flow patterns traced by the hydrogen bubbles. In each figure, there are thirty six individual photographs (Figures 16a through 27a) with 10° increments in phase angle unless otherwise specified. These photographs were taken with the use of the differential gear unit described in Section II-2. For a particular run, the mean angle θ_0 and the oscillating amplitude ϵ were first adjusted. The zero phase angle was then adjusted by aligning the centers of the hole on the disc and of the photocell. The alignment was made with the airfoil held at zero angle of attack on the increasing phase of motion and with the phase adjustment lever held at zero phase angle on the indicator. When the lever was held fixed the disc rotated at the same speed as the flywheel that drove the model and the photocell was activated at a constant phase of the motion. When the lever was moved it rotated the spider in the differential and changed the phase at which the photocell was activated. The photocell signal triggered the flash tube at the adjusted phase angle on the indicator and the image was recorded by the still picture camera. The phase angle and photographic film were then advanced and a new angle photographed. In this case, the flashlamp was operated under the RC mode (see sections II-3 and III-5). Ten most important photographs near stall and reattachment were

selected from each of the thirty-six photo sets. They are shown in Figures 16b through 27b to give greater detail.

It is of great interest to investigate the separation and reattachment of the boundary layer during each cycle of oscillation of the model. Visualization of the cyclic motion may be greatly enhanced by watching the slow motion of the oscillation. A high speed movie taken at 400 frames/second was therefore especially prepared for this purpose. In the movie, there were two run series denoted by low and high Reynolds numbers, respectively. Each series is composed of twelve runs which were arranged as follows:

RUN SERIES I or II		
Change of θ_0 and ϵ		
↓ Increase of k_t	1	4
	2	5
	3	6
	7	8
	9	10
	11	12

It should be noted that Run II-12 has a slightly lower Reynolds number than the others in the same series to reduce cavitation on the model. The films used are Kodak 4-X negative film 7224. In this case, the flashlamp was operated under the LC mode (see sections II-3 and III-5). Figure 28 shows the moment diagrams for the conditions of Run Series II.

It can be observed that the shape of the moment diagram traces (Figure 15) depends more heavily on the dimensionless frequency K_t rather than on the mean angle of attack. On each moment diagram, there is a region in which the traces are highly non-repeatable. This occurs when the airfoil is near and beyond stall. The regions of nonrepeatability correspond with the fluctuating separation regions as can be seen from Figures 16 through 27. No distinct vortices shedding from either the leading edge or the trailing edge are observed in the still picture (except for $K_t = .595$) and in the movie. Similar observations have been also reported elsewhere (Olsen 1971a). Since the helicopter blade operates at relatively low frequency having approximately the same range ($K_t = .05$ to $.595$) considered here, any successful theory for predicting the stall loads must treat an irregular separated region rather than a discrete vortex passing over the surface.

V. Additional Tasks

Three additional tasks supplementing the main contract were completed to improve the overall performance of the water tunnel.

1. Installation of a feedback control system to reduce variations of the tunnel speed.
2. Elimination of reflection from the rear test section window to improve optical quality for flow visualization.
3. Further research work on the development of other flow visualization techniques, especially of the thymol blue experiments.

These three tasks and their results are described in detail in this section.

5.1 Feedback Control System

It was observed that the tunnel speed varies by about 5% when the model moved in and out of stall due to the change of drag on the model. A feedback control system (FCS) to reduce the above variation by approximately a factor of ten was designed and installed as one of the additional tasks for the contract. This section gives a detailed description of the FCS.

Basically, the FCS consisted of a differential pressure transducer together with an interfacing circuit between the transducer and the control circuit of the main-drive pump. The pressure transducer chosen for this purpose was a variable reluctance, unidirectional, differential model (CJVR-10PSID) made by C. J. Enterprises at Panorama City, California. Its basic element is a flat pressure sensing diaphragm which is field replaceable for other pressure ranges. Corrosive liquids or gases may be applied to both sides of the diaphragm. An optional carrier demodulator Model CJCD 3049 is furnished to deliver an output 0 - 5 VDC. The transducer was connected between pressure taps at the screen section and the test section for velocity sensing. These pressure taps are separate from those used for the manometer to avoid coupling between manometer oscillations and the FCS. The interfacing circuit diagram is shown in Figure 29. It delivers a signal through the main control circuit, which compensates any deviation from the set tunnel speed sensed by the transducer, to speed up or slow down the main drive pump accordingly.

Two control switches were added on the remote control box of the main drive pump. One of them is an on-off switch of the transducer circuit and the other is a ten turn pot for controlling the tunnel speed. When the switch is in the off position, the FCS is not operational.

The operational procedures for the feedback control system are as follows:

1. Turn the two control knobs counter-clockwise all the way.
2. Press the "on" switch of the main drive pump.
3. Switch on the feedback control system.
4. Adjust the feedback control potentiometer (10 turns) to the desired tunnel speed (with the airfoil oriented to zero degree of angle of attack).
5. When the FCS switch is in "off" position, the FCS is not operational. The tunnel speed may be set as described in Section III.

Figure 30 shows the variation of tunnel speed versus the pitching frequency of the airfoil both with and without the FCS in circuit. As can be seen from the figure, significant improvements with the FCS in circuit are achieved at very low pitching frequency. Unfortunately, the frequency response of the FCS is limited by the large inertia of the huge volume of water in the tunnel and of the main-drive flywheel. A simple test indicates that there is a delay of about 5 seconds for the tunnel to reach a set speed in response to a step change of current applied to the motor. Further improvements, however, may be achieved by installing a fast response drag compensated device such as a butterfly valve to counter-balance the drag variations induced by the model. Such a device, which will be driven by the present FCS, may be installed easily at one of the joints downstream of the model.

5.2 Elimination of Reflection from the Rear Window

It was also observed that the reflection from the rear test section window, especially from the stainless steel disc, washed out some details on the photographs showing the hydrogen bubble traces. One of the additional tasks was to design and to install a device to eliminate the reflection from the rear window. Black plastic engraving pieces with

Satin finish were therefore installed to cover the stainless steel disc and other area along the trailing zone of the airfoil. The plastic pieces were flush with the surface of the window. They were attached to the rear window with nylon screws so that they could be replaced with different colored pieces suitable for other visualization techniques. On one of the plastic pieces, reference marks of angle of attack spaced in increments of one degree (from -20° to $+40^{\circ}$) with maximum deviation of $\pm 1/10$ degree were scribed. These marks would be used to aid in the interpretation of motion pictures. Figure 31 shows a few hydrogen bubble traces with the black plastic pieces installed.

5.3 Other Flow Visualization Techniques

In addition to the hydrogen bubble technique, the pearl essence and the thymol blue techniques were also explored. The pearl essence technique required simply mixing of .02% by weight of pearl essence (made by the Mearl Corporation, New York) with water. The lighting arrangement was the same as that for the hydrogen bubble technique (slot light). The fine suspended pearl essence particles which were silvery in color traced the flow pattern as a whole quite clearly. The traces marked the disturbed (turbulent) and the undisturbed (streamlined) regions distinctly. It did not trace, however, the boundary layer flow pattern alone as distinctly as the hydrogen bubbles or the thymol blue solution did. One of the reasons was that the diffusion of light from the fine particles between the directly illuminated region and the camera decreased the sharpness of the photographs.

Prior to the investigation of the pearl essence technique, a few preliminary experiments with the thymol blue technique had been launched. The results showed great potential of the latter in observing motions of laminar separation region and the onset of turbulent separation (stall). Because these are the most interesting phenomena to be studied, major effort was spent to improve the thymol blue technique. Therefore, the rest of this section is devoted to describing the thymol blue technique in detail and the improvements made to better the photographic quality.

5.3.1 Description of the Thymol Blue Experiment

5.3.1.1 Principle of the Thymol Blue Technique

The thymol blue technique which introduces dye in a liquid is due to Baker (1966). It uses a pH indicator, and is applicable in aqueous solutions. Two electrodes are placed in a solution of thymol blue (thymol sulphonephthalein) titrated near to the end point of the acidic side ($\text{pH} \approx 8.0$). A d.c. voltage is impressed between the electrodes which triggers the change of color on the surface of the negative (-) electrode because the color of the basic form of thymol blue (blue) is different from the acidic form (yellow). One of the main advantages of this technique over others is that it introduces a thin layer of truly neutrally buoyant colored fluid with no disturbance to the flow field. Baker (1966) used originally both a single wire ($5.08 \times 10^{-5} \text{ m}$) and networks of wires to measure fluid velocities in the range 0 - .05 m/sec.

In the investigations, the whole airfoil was used as the negative electrode and the tunnel wall as the positive one. With such an arrangement, a thin layer of colored fluid (deep blue) which traced truly the boundary layer region around the airfoil would be generated around the surface of the airfoil. Therefore, the flow characteristics in the vicinity of the airfoil could then be studied by photographic means.

5.3.1.2 Experimental Setup

The working fluid was prepared by adding .150 kilograms of thymol blue to the water tunnel with a capacity of 1000 gal. (3782 Kg) to produce approximately a .004% by weight solution. The solution was titrated near to the end point ($\text{pH} \approx 8.0$) by adding 1N-NaOH until it turned deep blue, then adding 1N- H_2SO_4 to cause the solution to be on the acid (yellow) side of the end point.

5.3.1.2 (continued)

Na_2SO_4 was added to the solution (2.5% by weight) to increase its conductivity. The resistance of the airfoil to tunnel current path was measured to be about 5 ohms. A d.c. power supply with a maximum voltage output of 20 VDC controlled by connecting with a variable transformer was used as the voltage source for the electrodes. The maximum allowable voltage and current were approximately 10 VDC and 2 amp respectively before bubbles, generated on the surface of the airfoil, disturbed the flow field. No detectable corrosion, however, was observed on the surface of the airfoil even at a higher supplying voltage than 10 VDC (at about 5 amp). At such high voltage and current, the brass airfoil tended to be darkened after a short period of use. A sodium light was originally used for illumination to improve optical quality of the system. With the setup described above, the separation region could barely be observed from photographic prints. Improvements on the technique were definitely desirable in order to obtain quantitative measurements, especially at high tunnel speeds. A few revisions, which improved to a great extent the optical quality, were made:

1. A 165 μF capacitor was connected in parallel with the present 8 μF capacitor of the original circuit design. As a result, the energy per flash (RC mode) increased from a maximum of 16 joules to 356 joules, a factor of about 20. It should be noted that with the 165 F capacitor in circuit, the high voltage power supply must be operating only under the RC mode. It was found that the lamp operating at 1500V with ASA 400 film gave sufficient light for photographs to be taken at f 16 with a corresponding large depth of field.
2. Additional white plastic engraving pieces (satin finish) which are interchangeable with the black pieces described in section 5.2, were made to improve the background optical quality.

3. A new airfoil with the same dimension as the original one was made. The new one was plated with .001 in hard chrome (satin finish); this special treatment of the airfoil was designed to enhance the contrast between the blue fluid and the airfoil surface by avoiding the darkening mentioned above.
4. Several alternatives to suppress the generation of hydrogen bubbles on the negative (-) electrode were investigated. At the present stage, pressurization of the test section up to 16 PSI was the only effective way which allowed the supplying current to be raised by a factor of 1.2. Several chemical additives such as hydrogen peroxide were tested, but no apparent suppression was observed. In fact, the hydrogen peroxide bleached out the blue color of the fluid to some extent.

5.3.2 Results of the Thymold Blue Experiment

The improvements just described considerably improved the thymol blue technique. With the present facility, the optical quality of the system has been optimized such that motions within the boundary layer can be identified clearly on photographic prints. Figures 32 through 34 are therefore specially arranged to bring out several salient features of the boundary layer flow characteristics of an oscillating airfoil. These features, a few of which are believed never to have been observed in the literature, are described in the following.

In general, a sequence of events can be observed from the figures during the cyclic change of the angle of attack θ . The occurrence of these events shows a definite delay, which leads to the delay of stall, with increasing nondimensional frequency K_t . At $\theta = 0$, the boundary layer is essentially laminar and attached to the airfoil surface. A

small portion at the trailing edge shows signs of laminar separation especially for cases with low K_t . As θ increases, a laminar separation region starts forming at the trailing edge and travels toward the leading edge. The separation region which shows a formation of cellular structure along the lateral direction on the airfoil surface is three dimensional in shape. A wavy formation then develops and travels upstream trailing the leading edge of the separation region. It is trailed by a turbulent tail beyond which the regular wavy formation is disturbed. The higher the non-dimensional frequency K_t , the more well defined the wavy formation is. The maximum number of waves observed on the airfoil surface is about four to five. The wavy formation persists for about one tenth of a complete cycle and then turns into irregular patches. The irregular patches finally become turbulent accompanied by a sudden thickening of the boundary layer directly above these patches. The sudden thickening of the turbulent boundary layer is also observable from the hydrogen bubble traces shown in the high speed movie and still photographs (Figures 16 through 27). With further increase of θ , the turbulent boundary layer just developed is being washed downstream. Until this moment, the boundary layer at the leading edge always attaches to the surface as can be seen from the figures. The boundary layer at the leading edge separates before long with still further increases of θ and turbulent separation of the entire layer follows almost instantly. The thickness of the separated layer grows and reaches a maximum at $\theta = \theta_{max}$. During the following half cycle, the events described above reverse their order of occurrence except that there is no wavy formation observed. The separation region re-attaches at the leading edge and then is transported smoothly toward the trailing edge. A complete cycle thus finishes. It should be noticed that the wavy formation is observed only when the airfoil is oscillating. Under a semi-static condition, the separation region simply moves back and forth on the airfoil surface during a cycle of oscillation which is very much different from the phenomena under a dynamic condition. Again, no distinct vortices shedding from either the leading edge or the trailing edge are observed in the thymol blue experiments ($K_t = .05 \sim .24$). This supports the remarks made at the end of Section IV.

At the present stage, the photographs in Figure 32 through 34 show only qualitative features as described above. Quantitative measurements which are necessary for a complete understanding of separation and the stall mechanism of an oscillating airfoil, are however obtainable with further development of the present technique.

VI. Concluding Remarks

The water tunnel built for the present contract is a revised version of the original design established at Boeing Scientific Research Laboratory (Olsen 1971b). Improvements were included to upgrade the general performance of the tunnel. Major revisions and improvements of the original design are summarized as follows:

1. Suppression of cavitation on the model was achieved by building a pressurization unit with pressure up to 15 PSIG ($1.05 \times 10^4 \text{ kg/m}^2$) applied to the test section.
2. An improved design of the bearing and seals for the propeller was installed to provide smooth and long life operation.
3. The oscillating amplitude was increased from $\pm 10^\circ$ to $\pm 20^\circ$. The present mechanism provides accurately sinusoidal oscillations with deviation of .5% (3% for the original design).
4. Black plastic pieces (satin finish) engraved with reference marks of angle of attack were installed on the rear test section window to eliminate reflection which washed out details of hydrogen bubble traces.
5. A feedback control system was added to the main drive circuit to reduce variations of tunnel speed especially at relatively low frequency of oscillation.

In addition to the hydrogen bubble technique, the pearl essence and the thymol blue techniques were also investigated. It was found that the former was superior to the latter so far as visualization of boundary layer flow characteristics was concerned. Improvements to the thymol blue technique resulted from the following changes:

1. A new airfoil plated with 0.001 in. ($2.5 \times 10^{-5} \text{ m}$) hard chrome with satin finish was built to enhance optical contrast between the boundary layer fluids (blue) and the airfoil surface.

2. White plastic pieces (satin finish) inter-changeable with the black pieces were made to enhance background contrast.
3. Pressurization of the test section up to 15 PSIG (1.05 kg/m^2) $\times 10^4$ suppressed generation of excess of hydrogen bubbles which allowed increased current density and hence concentration of dye on the airfoil surface.
4. A 165 μF capacitor was added in parallel with the existing 8 μF capacitor to increase the energy per flash by a factor of 20, which provided more than sufficient lighting for still photographs at an f stop of 16.

One of the most important findings with the thymol blue technique is that it traces clearly and truly the boundary layer flow patterns in great detail. Of all the observations, the development of the wavy formations on the airfoil surface attracts most of our attention. This phenomenon indicates that it is certainly worthwhile to conduct further investigations.

References:

- Baker, D. J. (1966). A technique for the precise measurement of small fluid velocities, J. Fluid Mech., Vol. 26, Part 3, pp. 573-575.
- Olsen, J. H. (1971a). Flow Visualization Experiments on Pitching Airfoils, Boeing Document D210-10450-1, Boeing Scientific Research Laboratories, Seattle, Washington.
- Olsen, J. H. (1971b). Design and Operation of the BSRL Water Tunnel, Boeing Document D180-14130-1, Boeing Scientific Research Laboratories, Seattle, Washington.

APPENDIX A

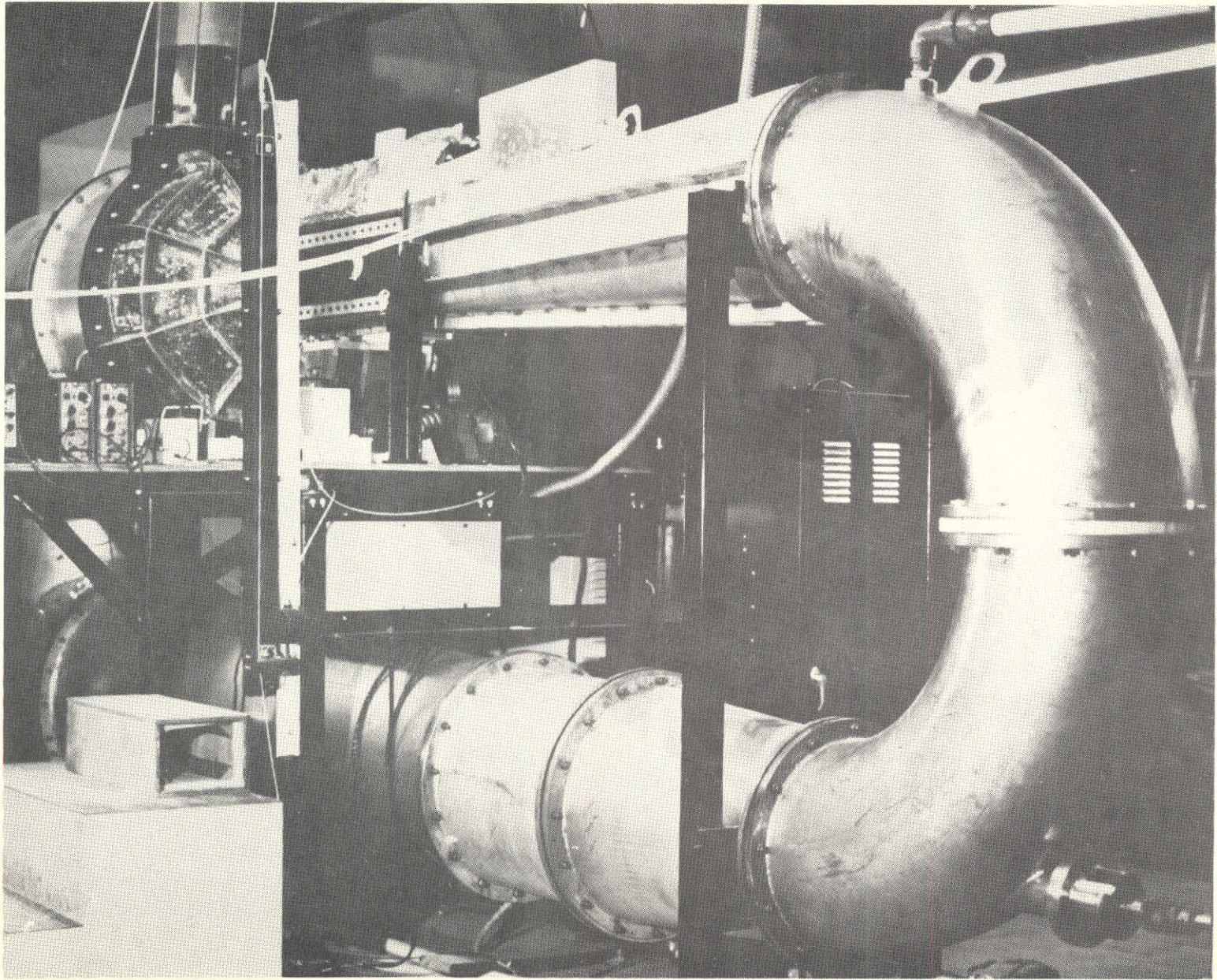


Figure 1. View of Entire Tunnel

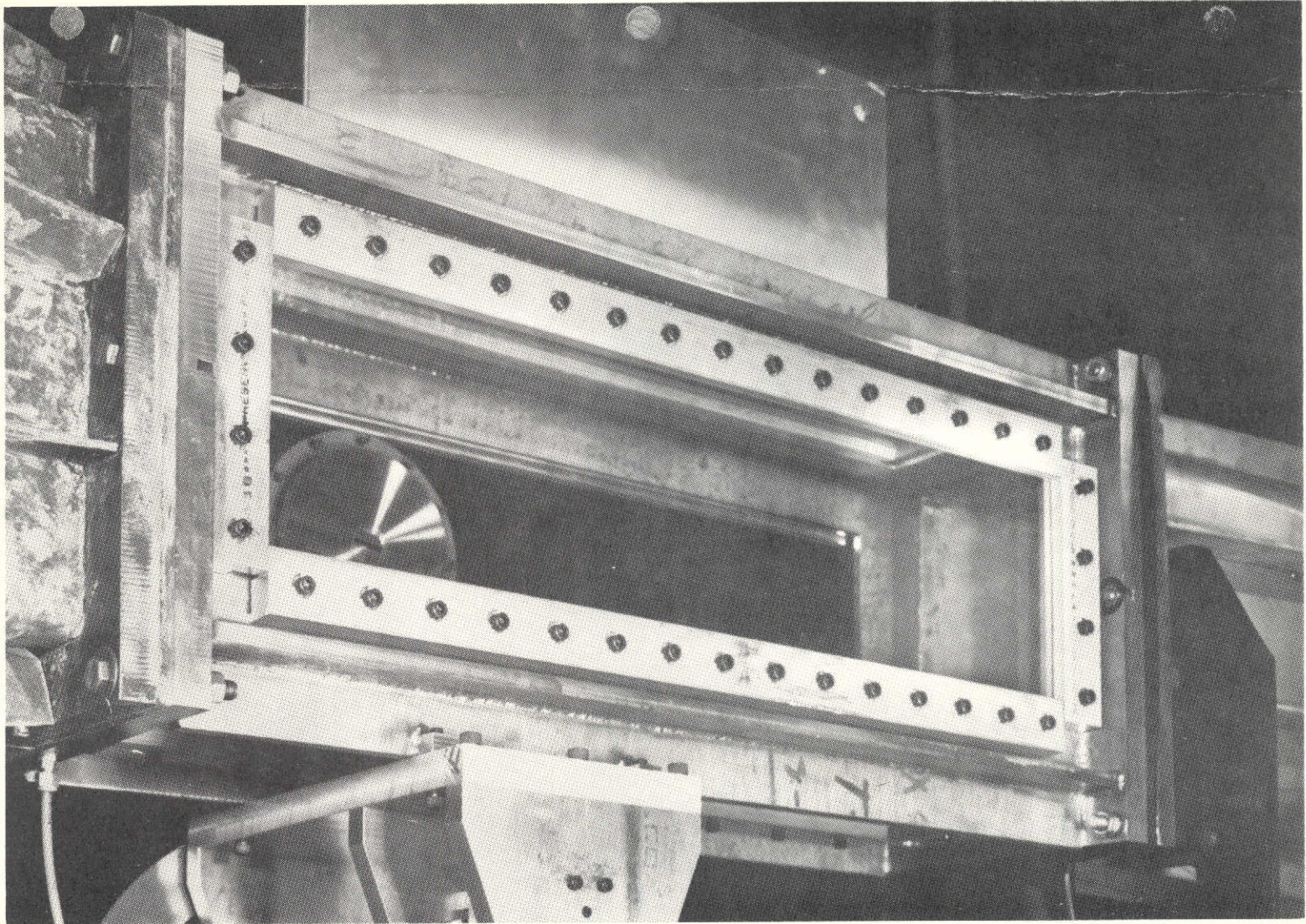


Figure 2. Tunnel Test Section

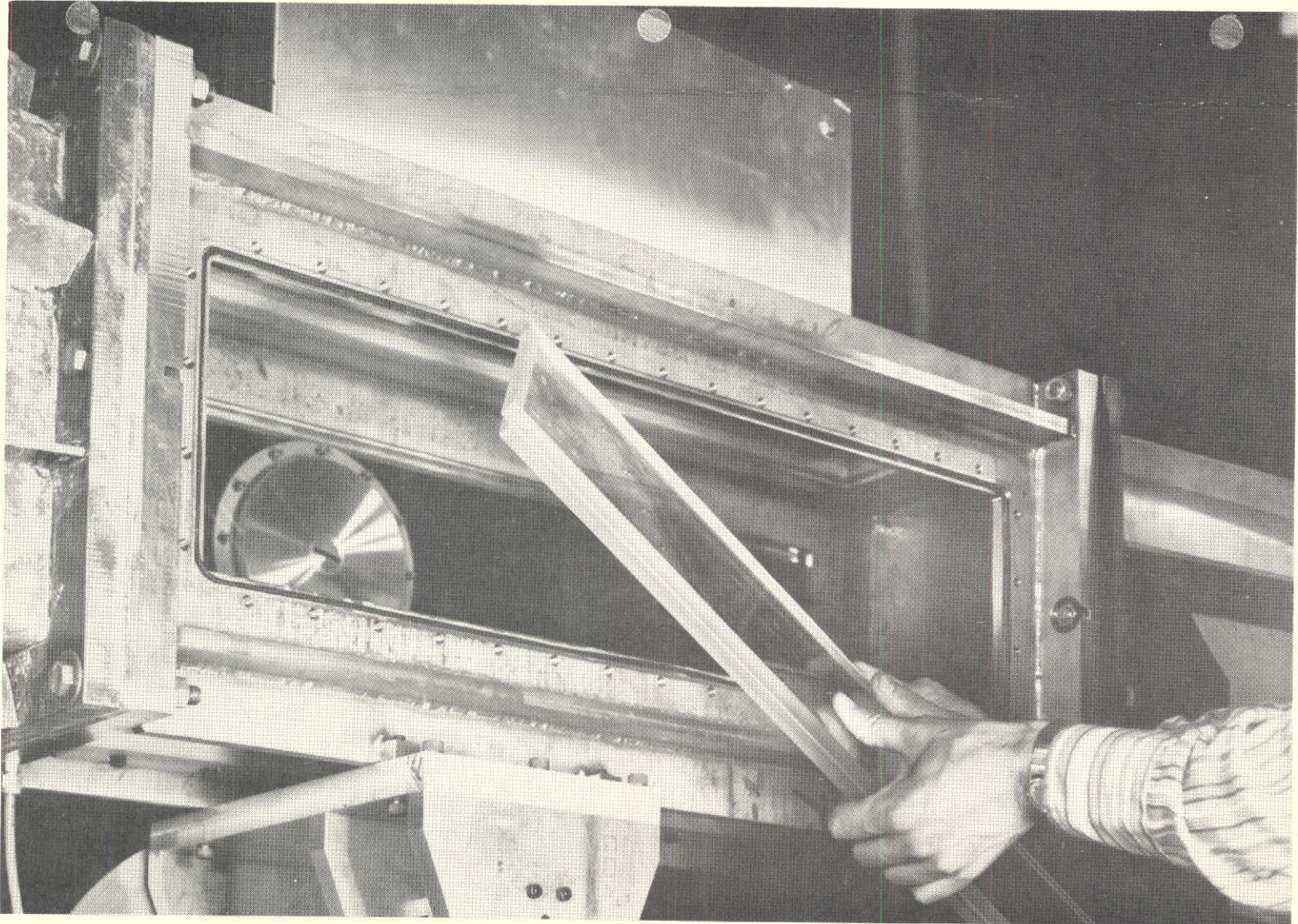


Figure 3. Test Section Window Installation

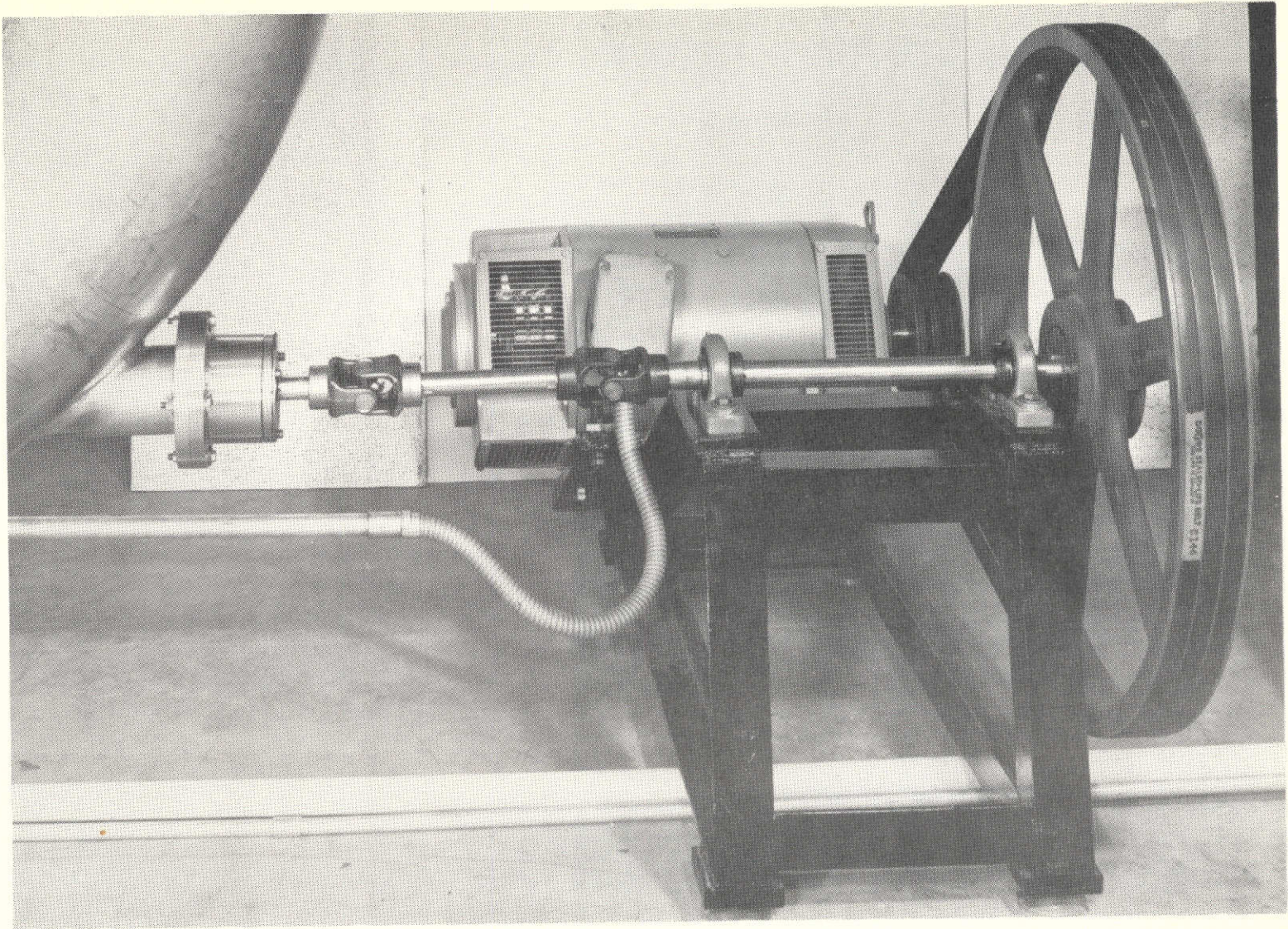


Figure 4. D.C. Motor and Driveshaft

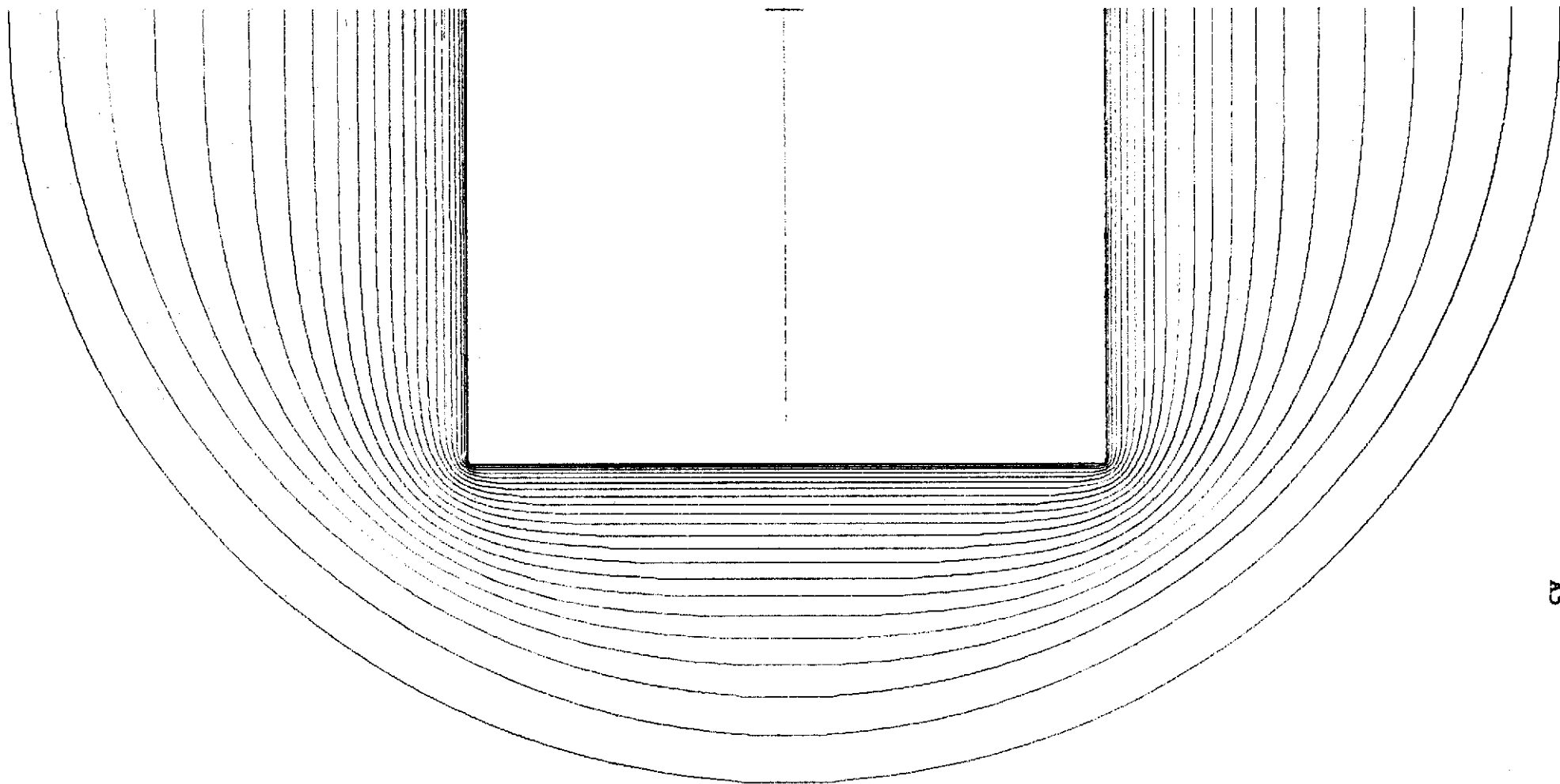


Figure 5. Contraction Contours

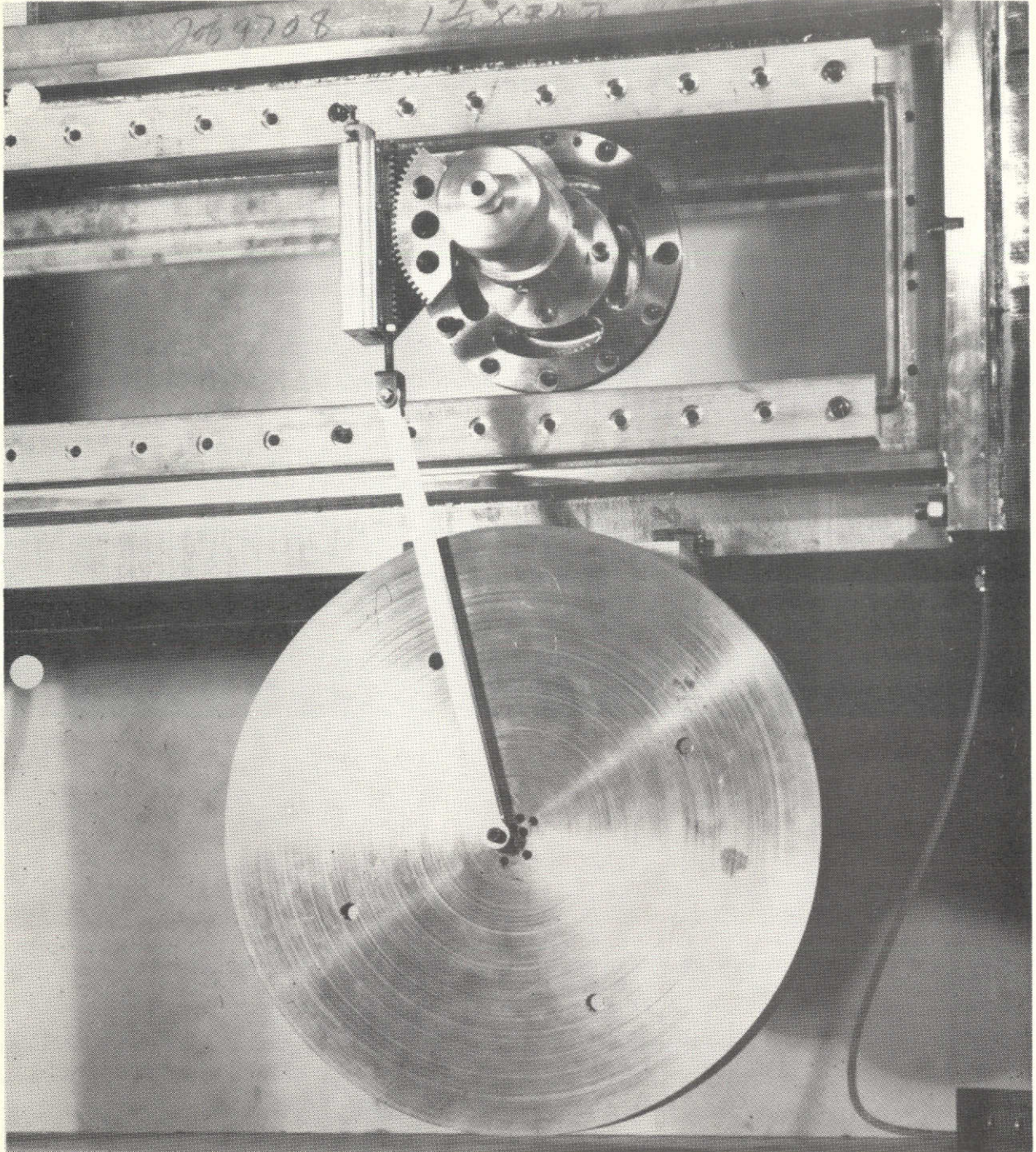


Figure 6. Oscillating Mechanism

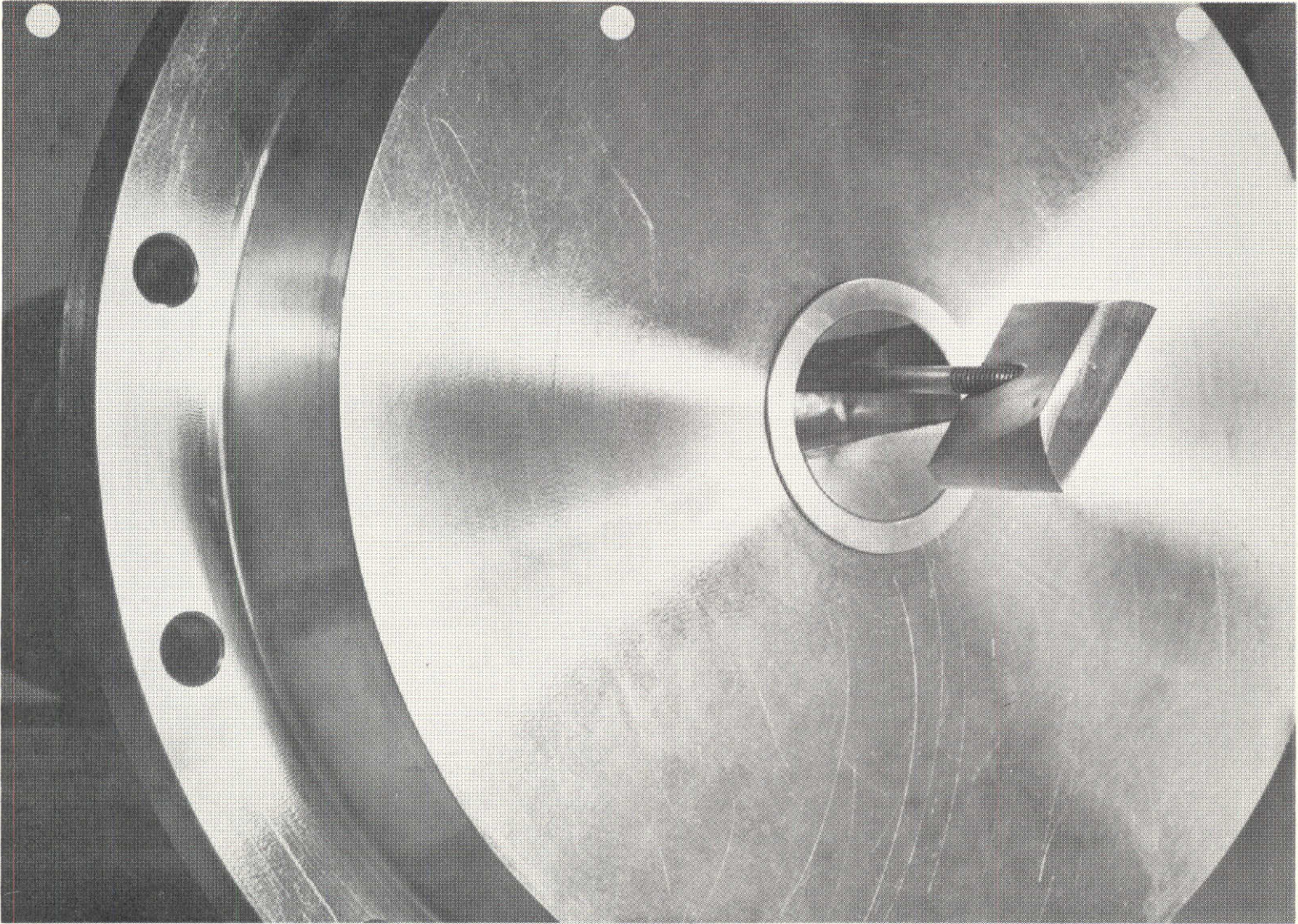


Figure 7. Wedge & Slot for Model Drive

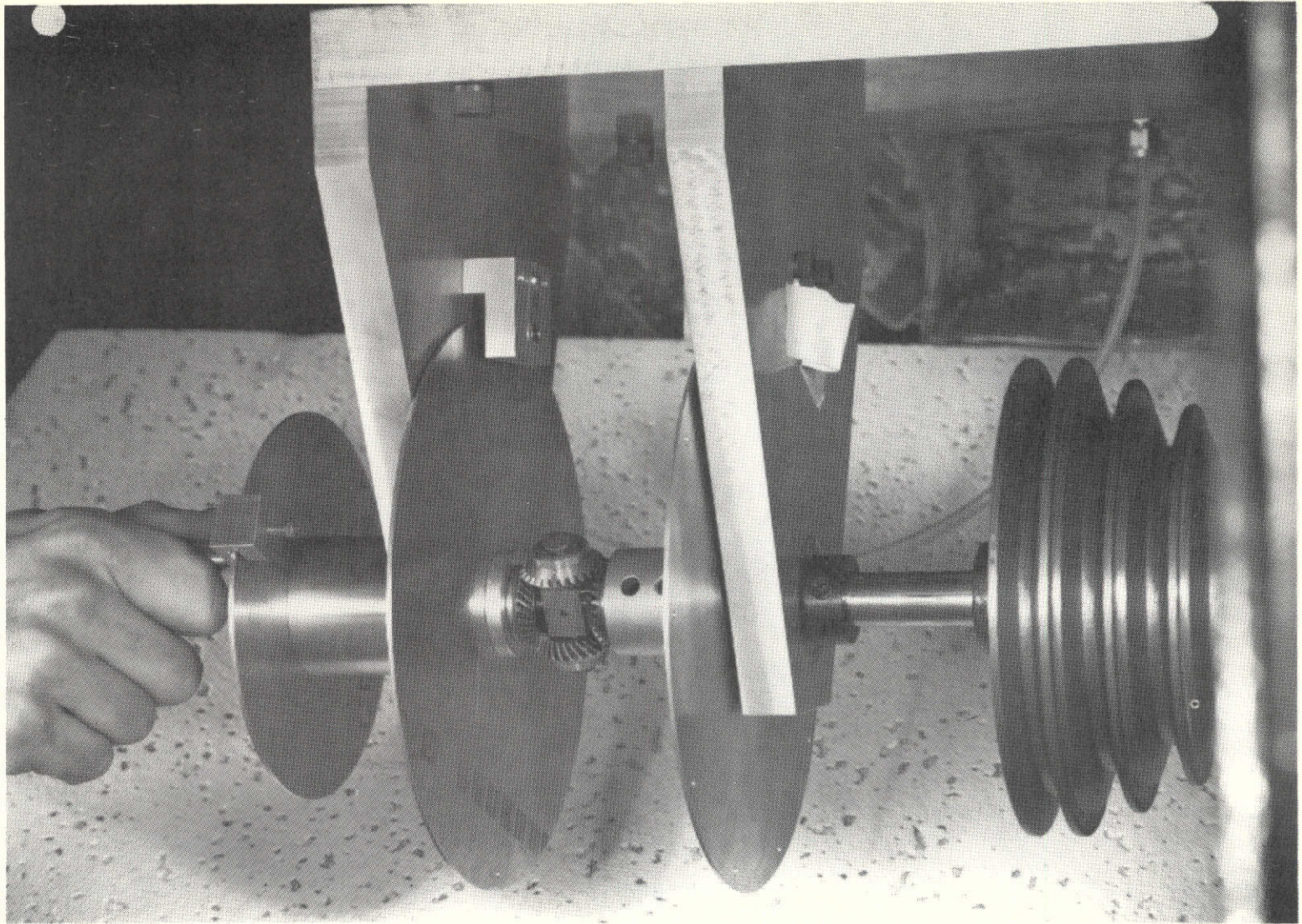


Figure 8. Differential Mechanism

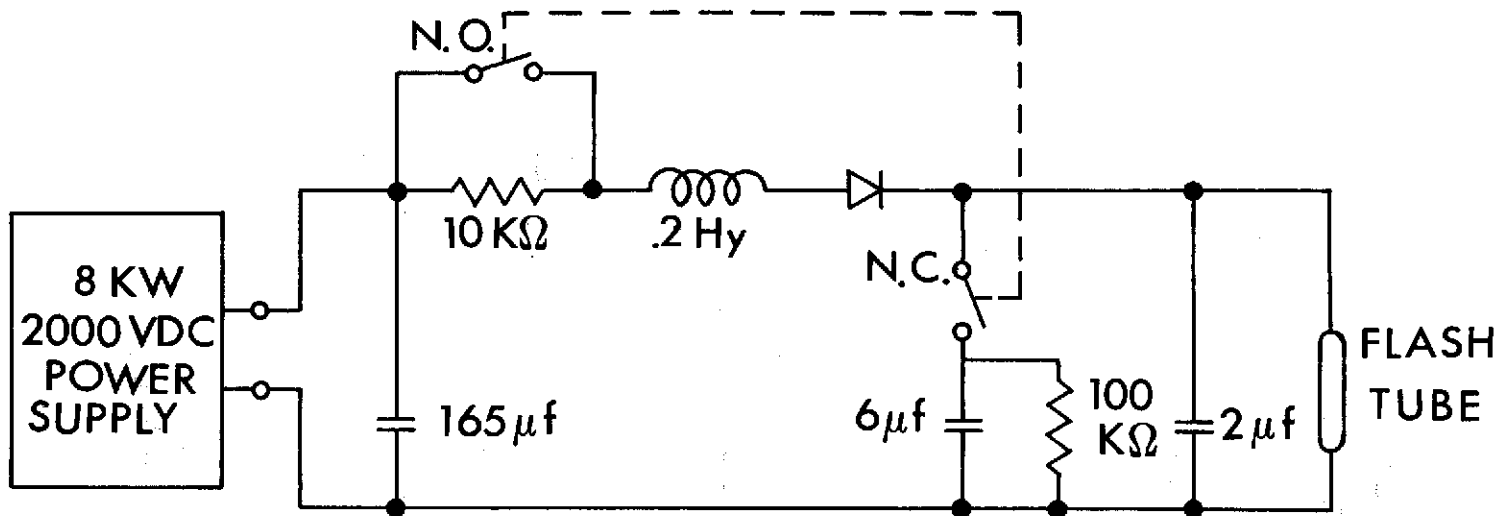


Figure 9. Flashlamp Power Circuit

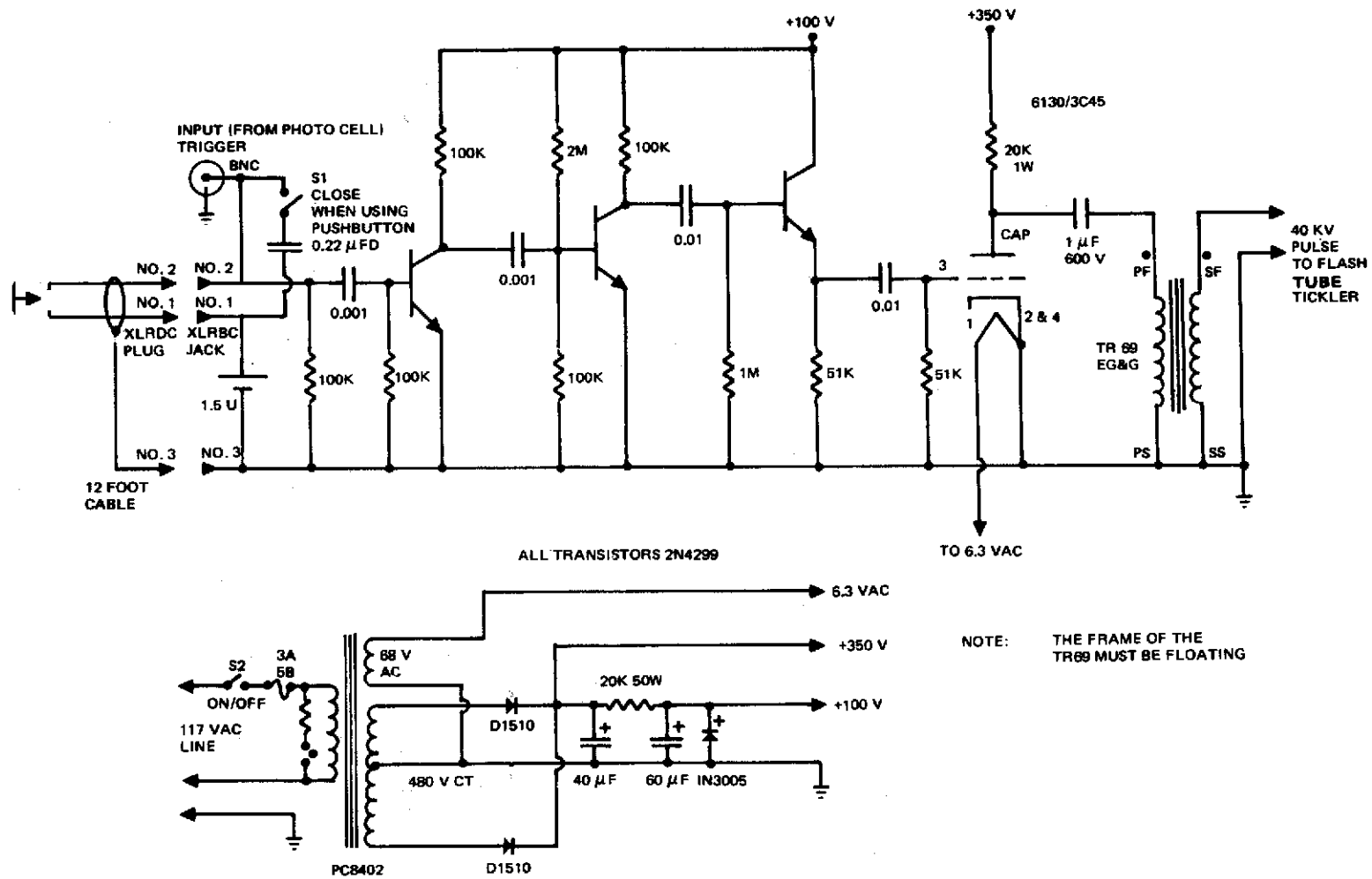


Figure 10. Water Tunnel Flash Tube Trigger

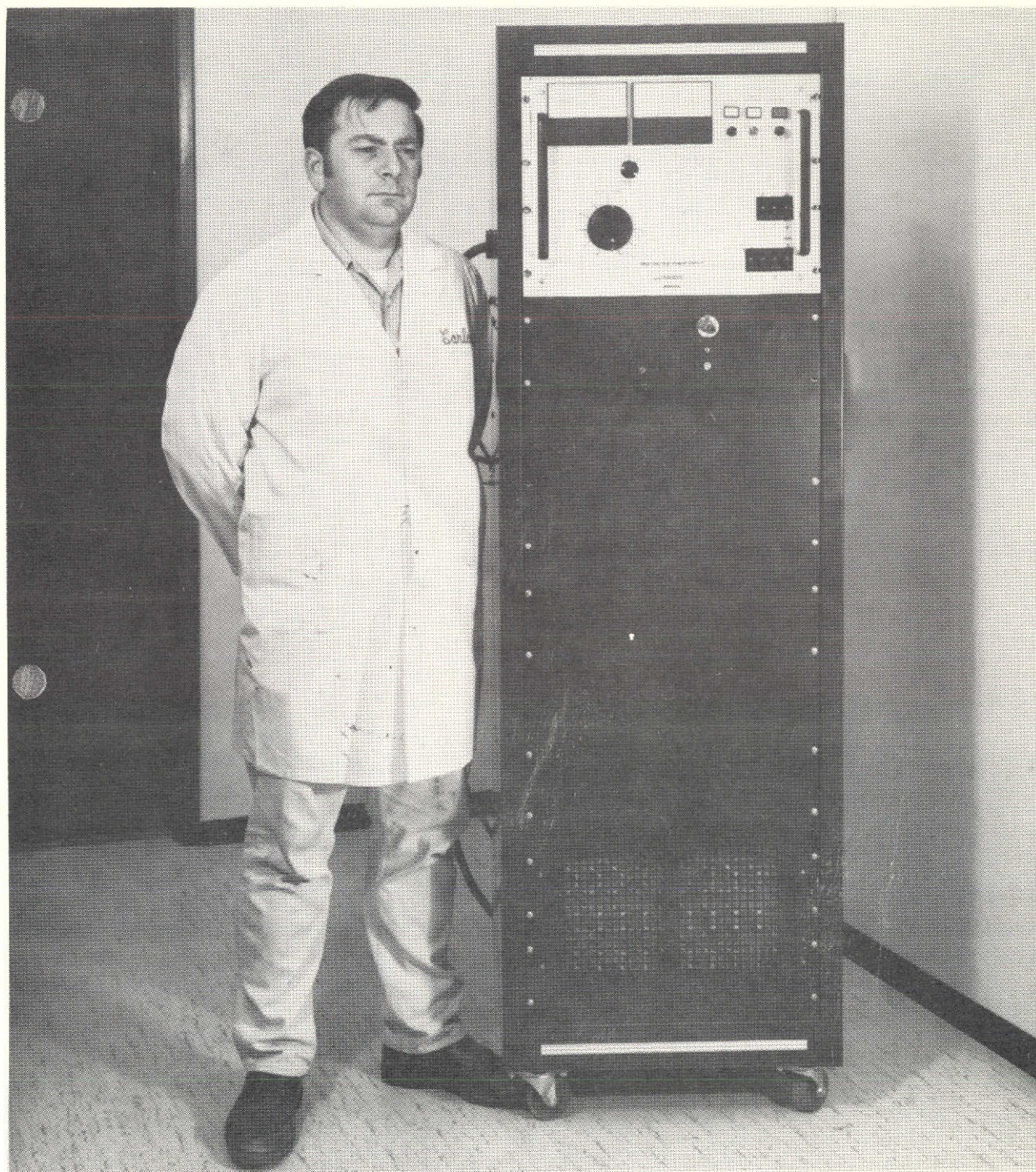


Figure 11. Flashlamp Power Supply and Trigger

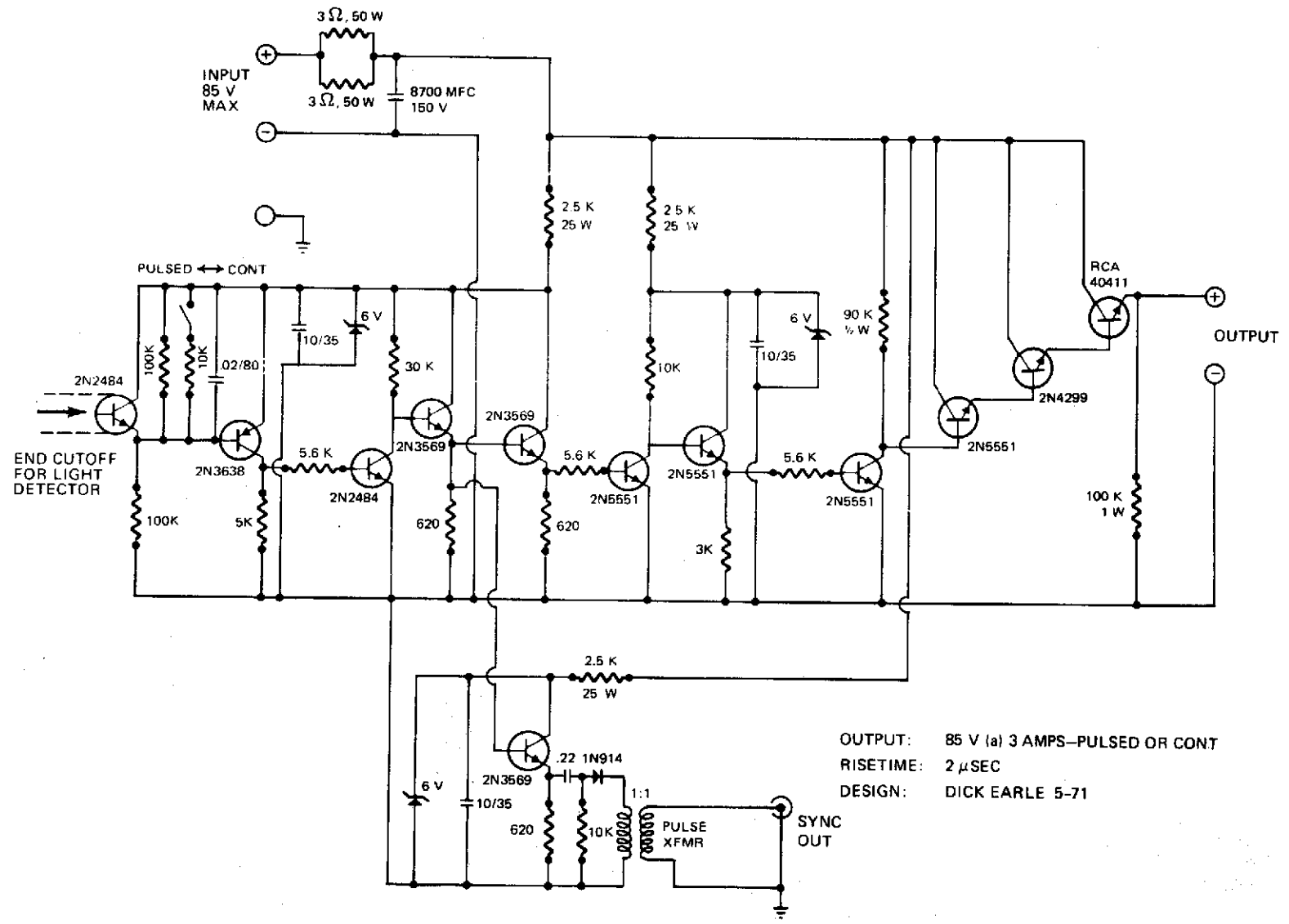
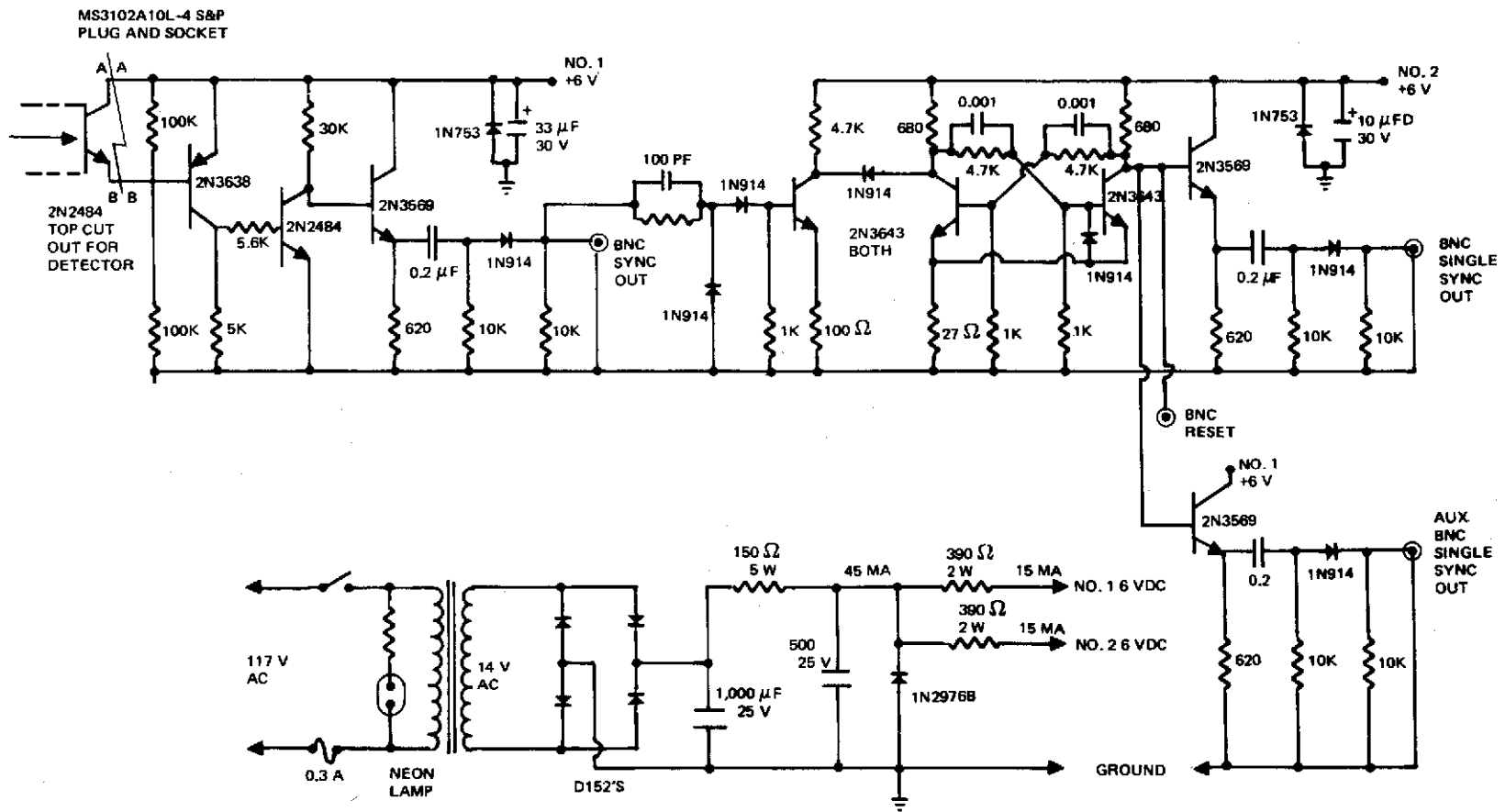


Figure 12. Hydrogen Bubble Generator



AL3

Figure 13. Light Detector Circuit

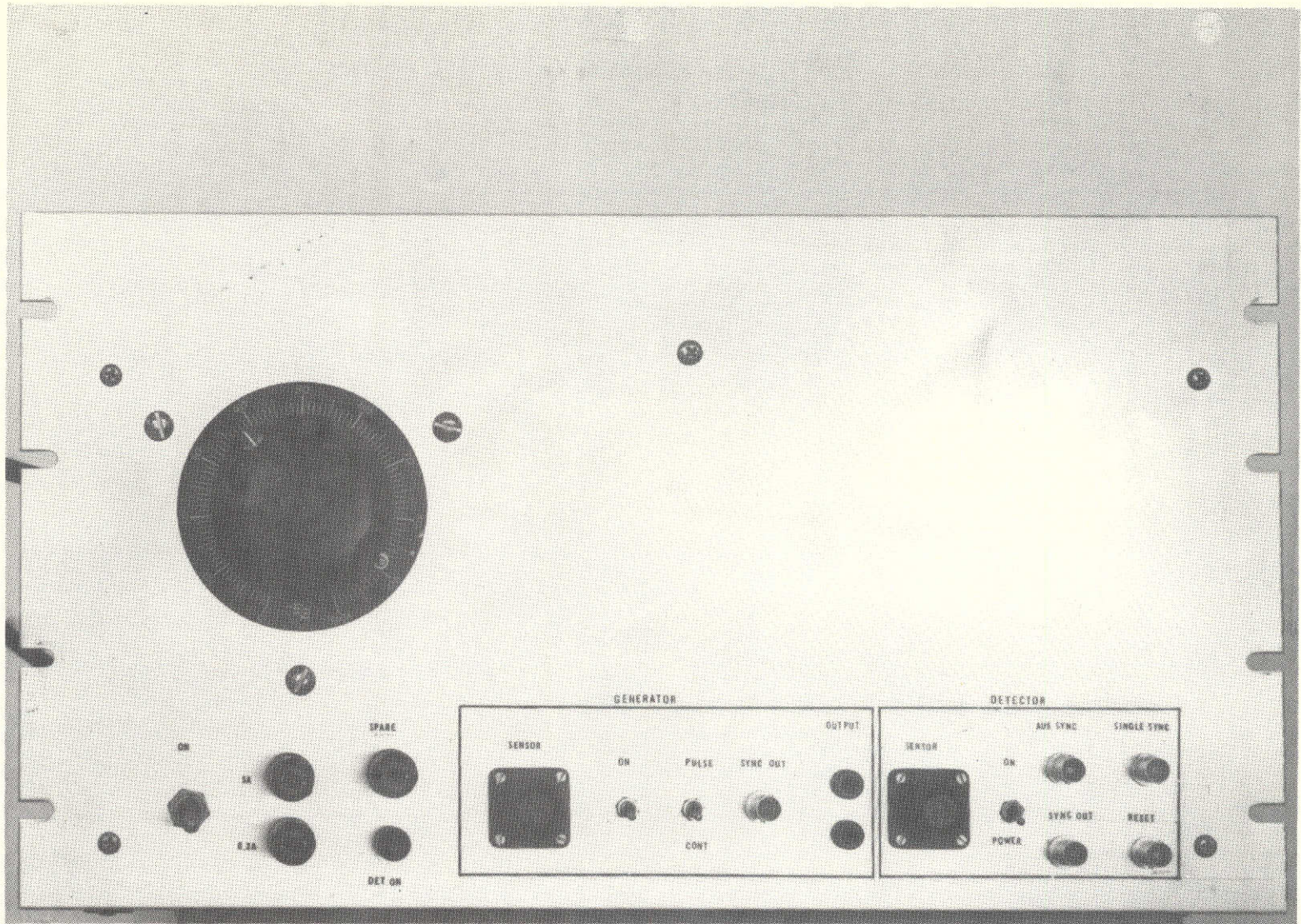


Figure 14. Hydrogen Bubble Generator and Trigger

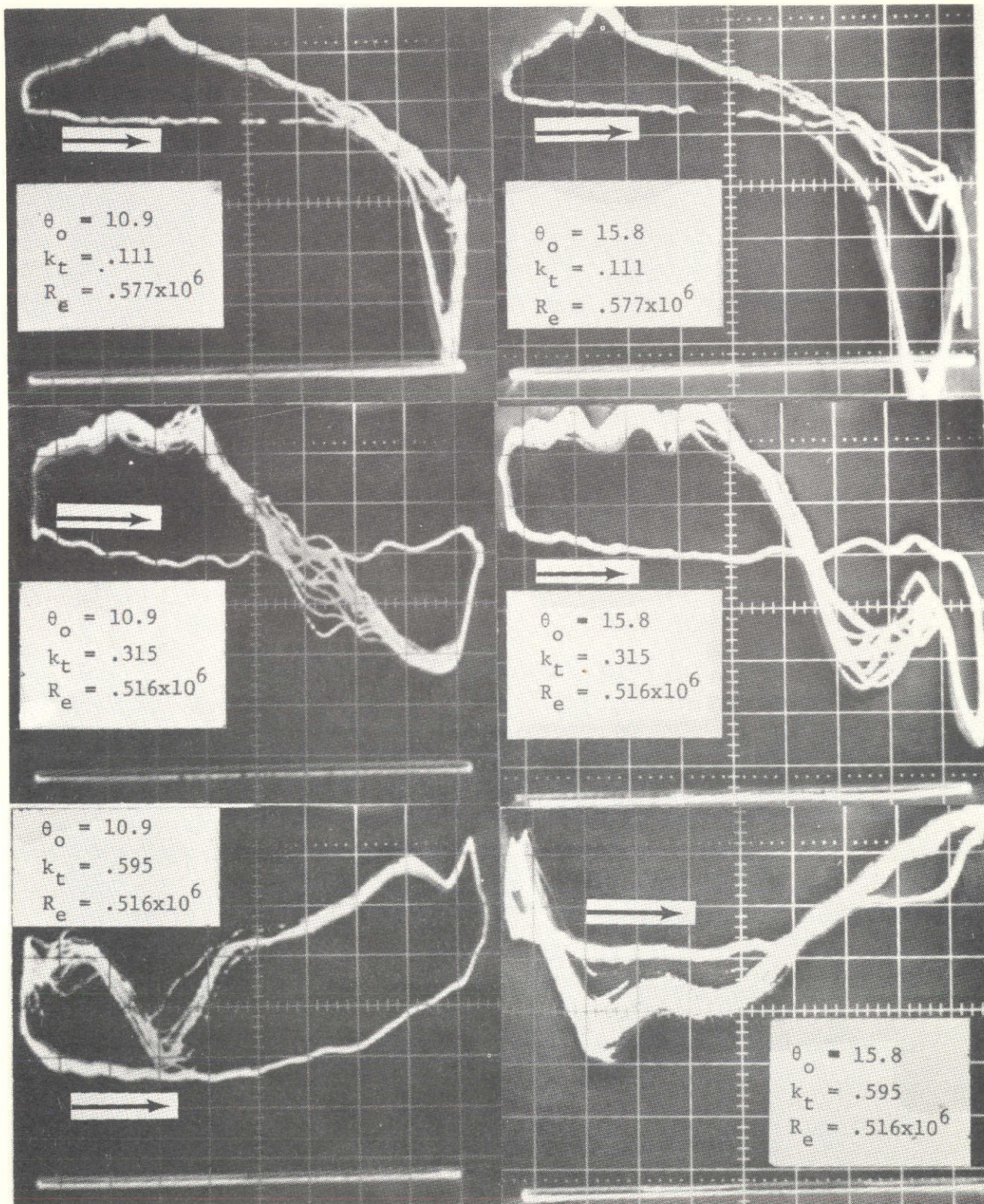


Figure 15. Moment Diagrams of an Oscillating Airfoil (NACA 0012). Pitch Axis = $\frac{1}{4}$ Chord. $\epsilon = \pm 20$. Scale = .58 Kg-m/major division.

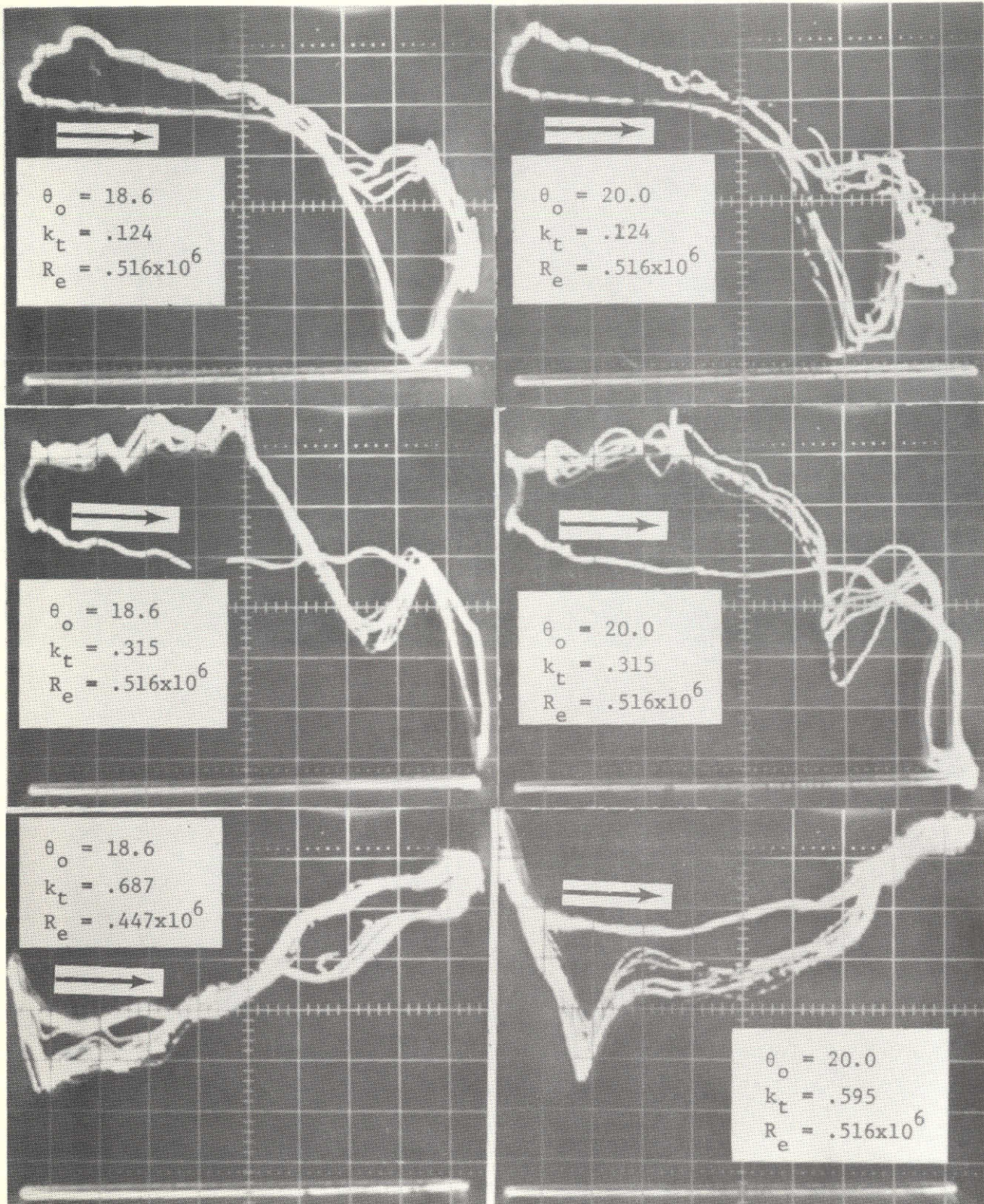


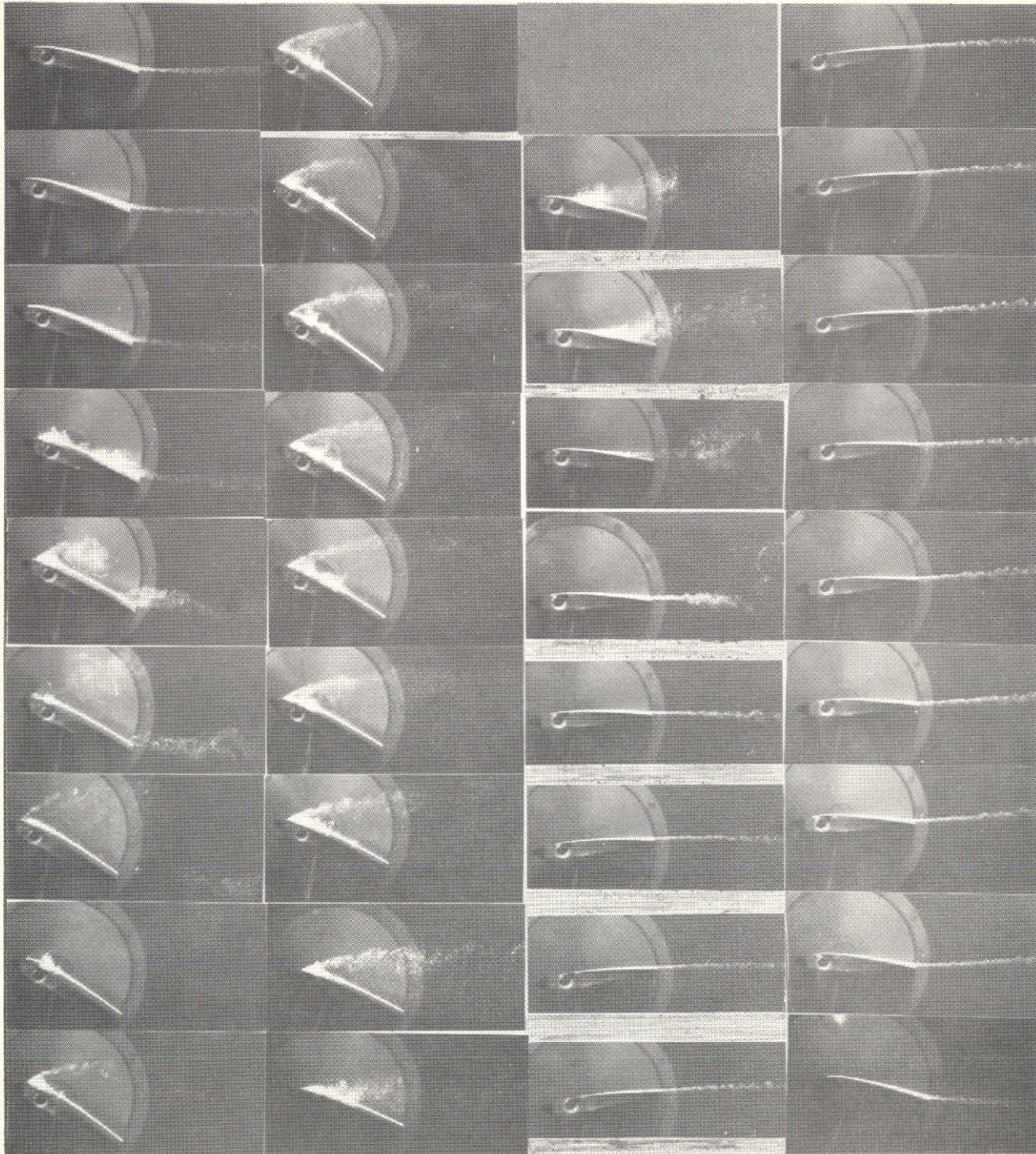
Figure 15. Moment Diagrams of an Oscillating Airfoil (NACA 0012). Pitch Axis = $\frac{1}{4}$ Chord. $\epsilon = \pm 20$. Scale = .58 Kg-m/major division.

00

90

180

270



80

170

260

350

RUN NO.1

AIRFOIL NACA 0012 $C = 4''$

$\theta_0 = 10.9$ $\epsilon = 20.0$

$k_T = .111$ $Re = .577 \times 10^6$

PITCH AXIS = $\frac{1}{4}$ CORD

FIGURE 16A.

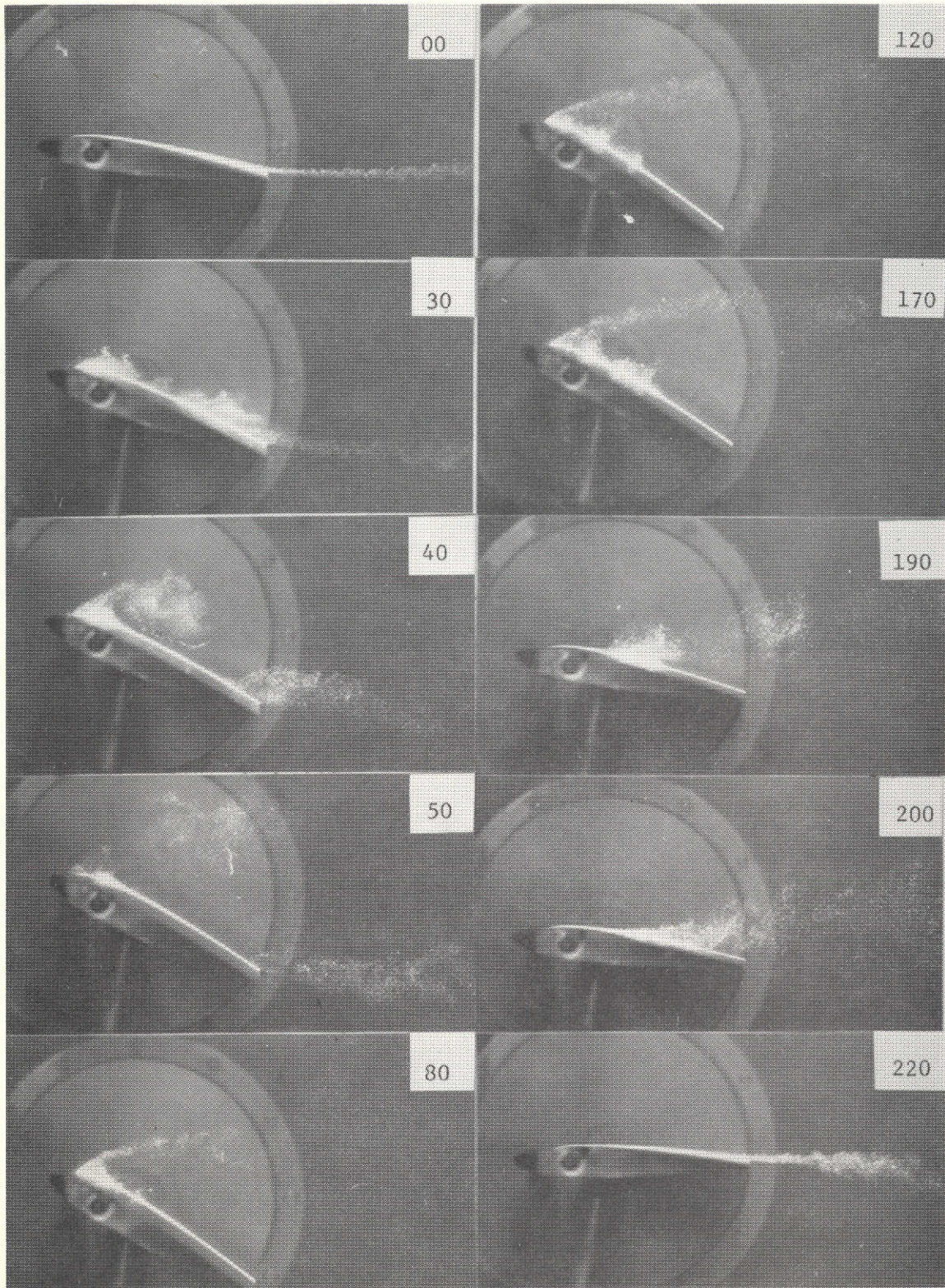


Figure 16b

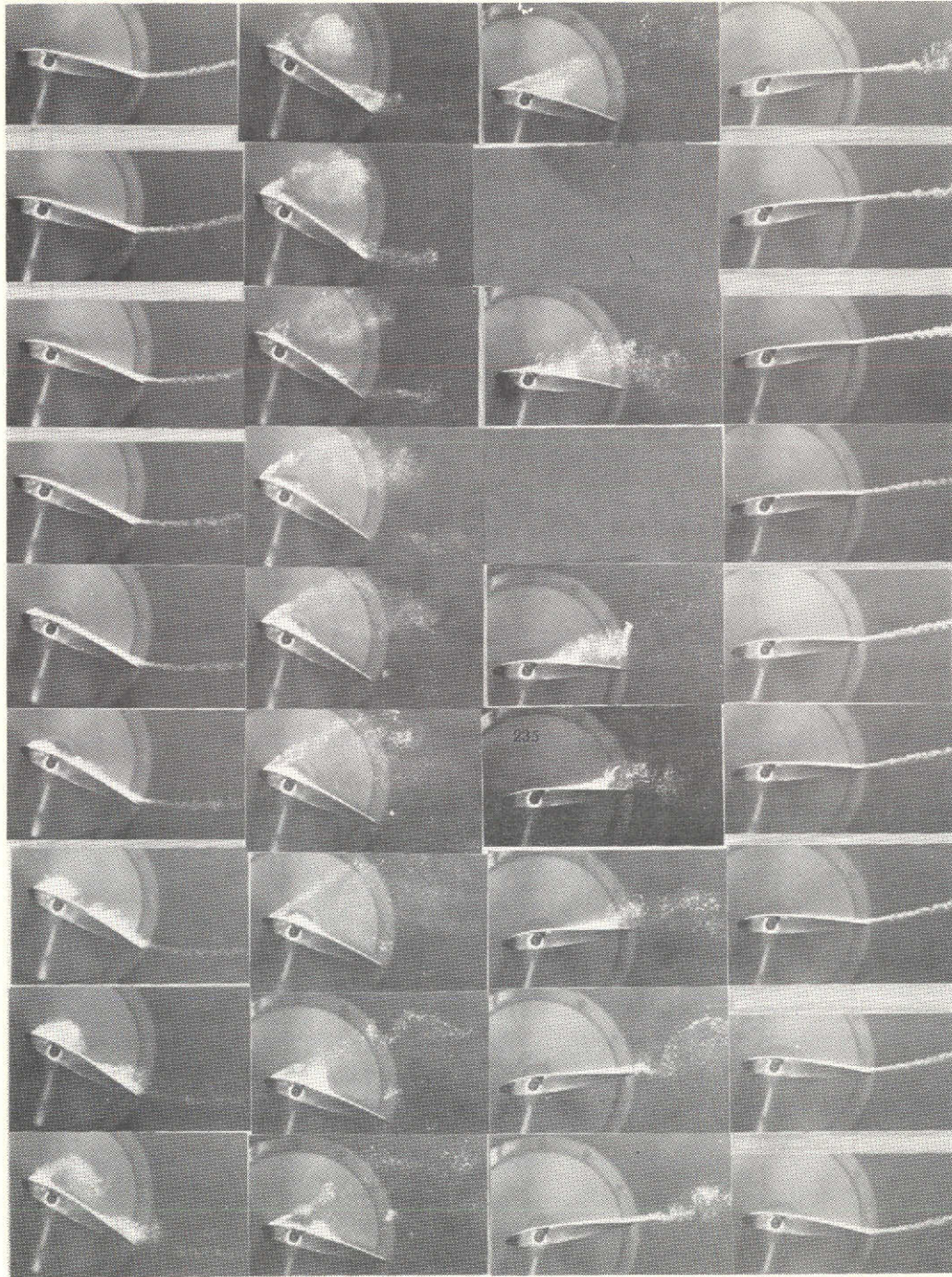
00

90

A19

180

270



80

170

260

350

RUN NO. 2

AIRFOIL NACA 0012 $C = 4^\circ$

$\theta_0 = 10.9$ $\epsilon = 20.0$

$k_T = .282$ $Re = .577 \times 10^6$

PITCH AXIS = $\frac{1}{4}$ CORD

FIGURE 17A.

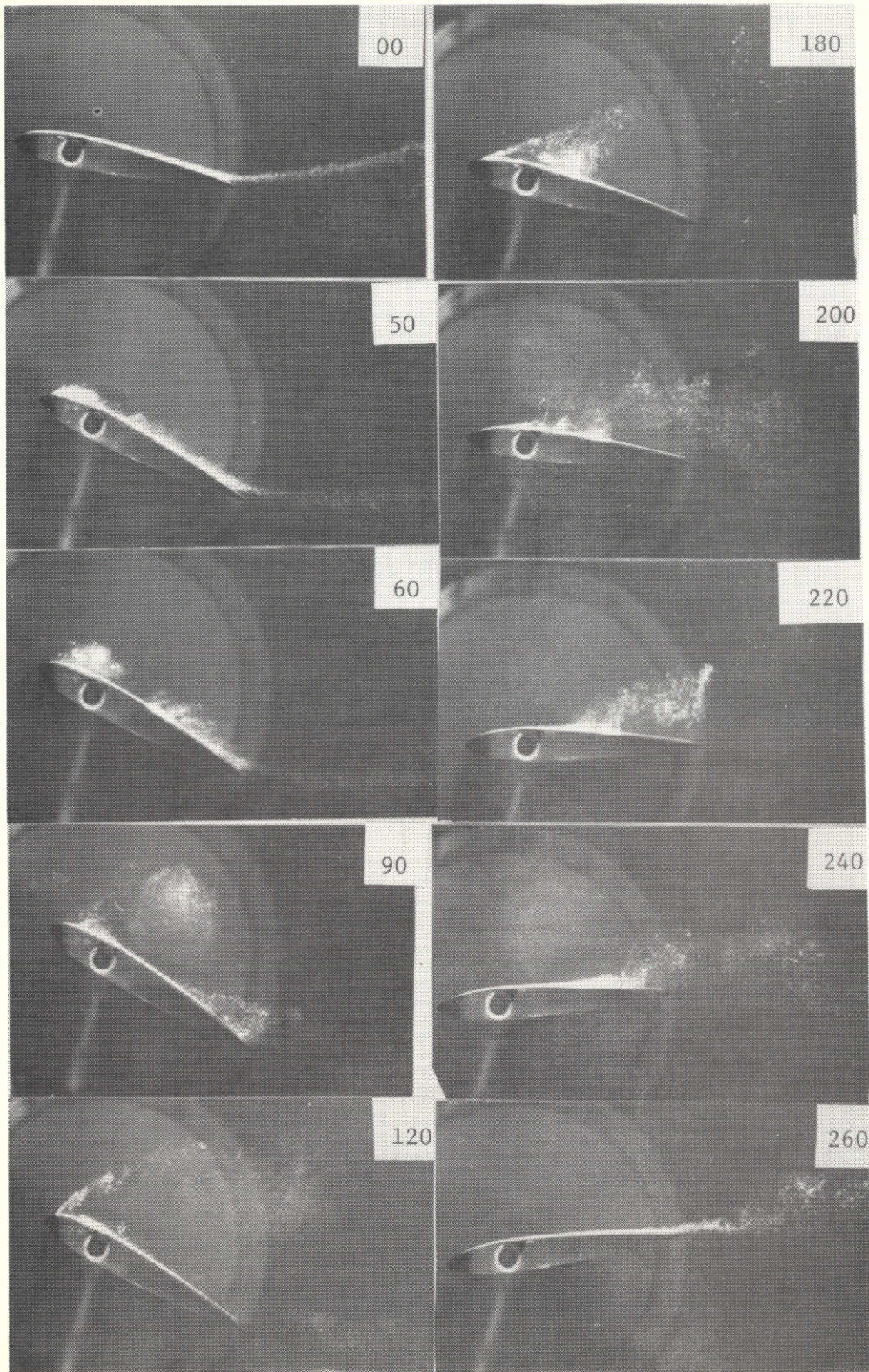


Figure 17b

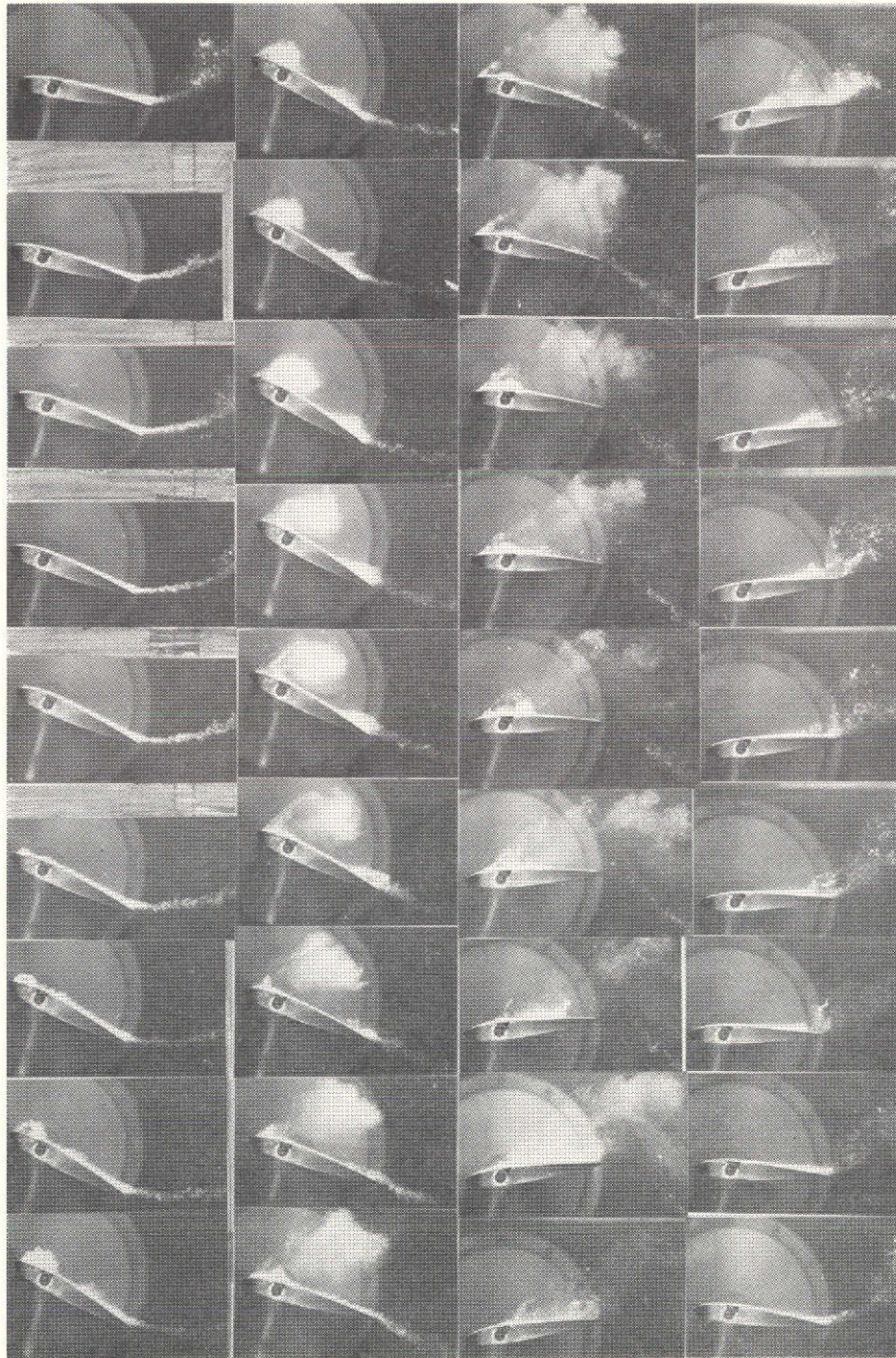
00

90

A21

180

270



80

170

260

350

RUN NO. 3

AIRFOIL NACA 0012 C = 4"

$\theta_0 = 10.9$ $\epsilon = 20.0$

$k_T = .532$ $Re = .577 \times 10^6$

PITCH AXIS = $\frac{1}{4}$ CORD

FIGURE 18A.

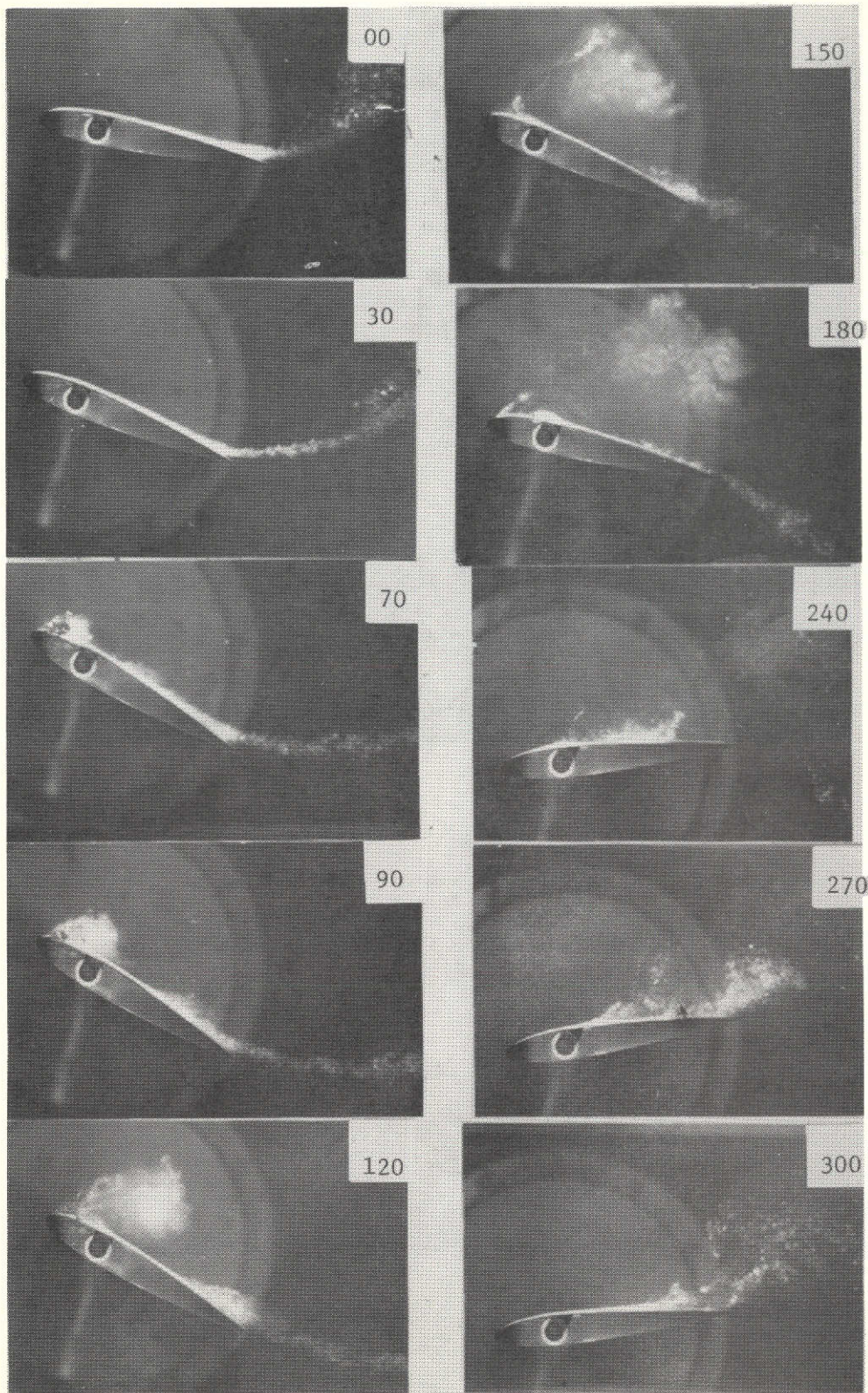
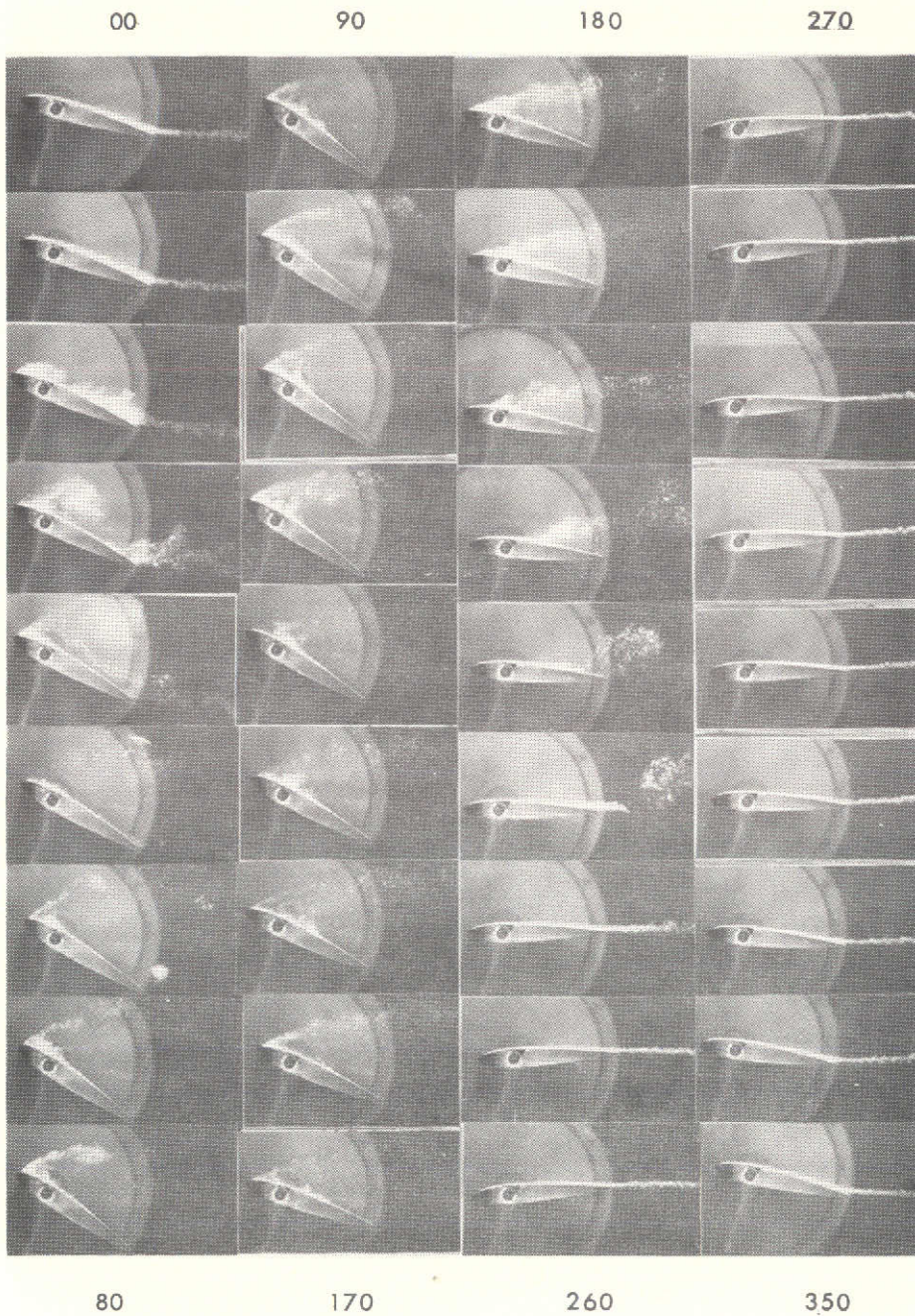


Figure 18b



RUN NO. 4

AIRFOIL NACA 0012 $C = 4''$

$\theta_0 = 15.8$ $\epsilon = 20.0$

$k_T = .111$ $Re = .577 \times 10^6$

PITCH AXIS = $\frac{1}{4}$ CORD

FIGURE 19A.

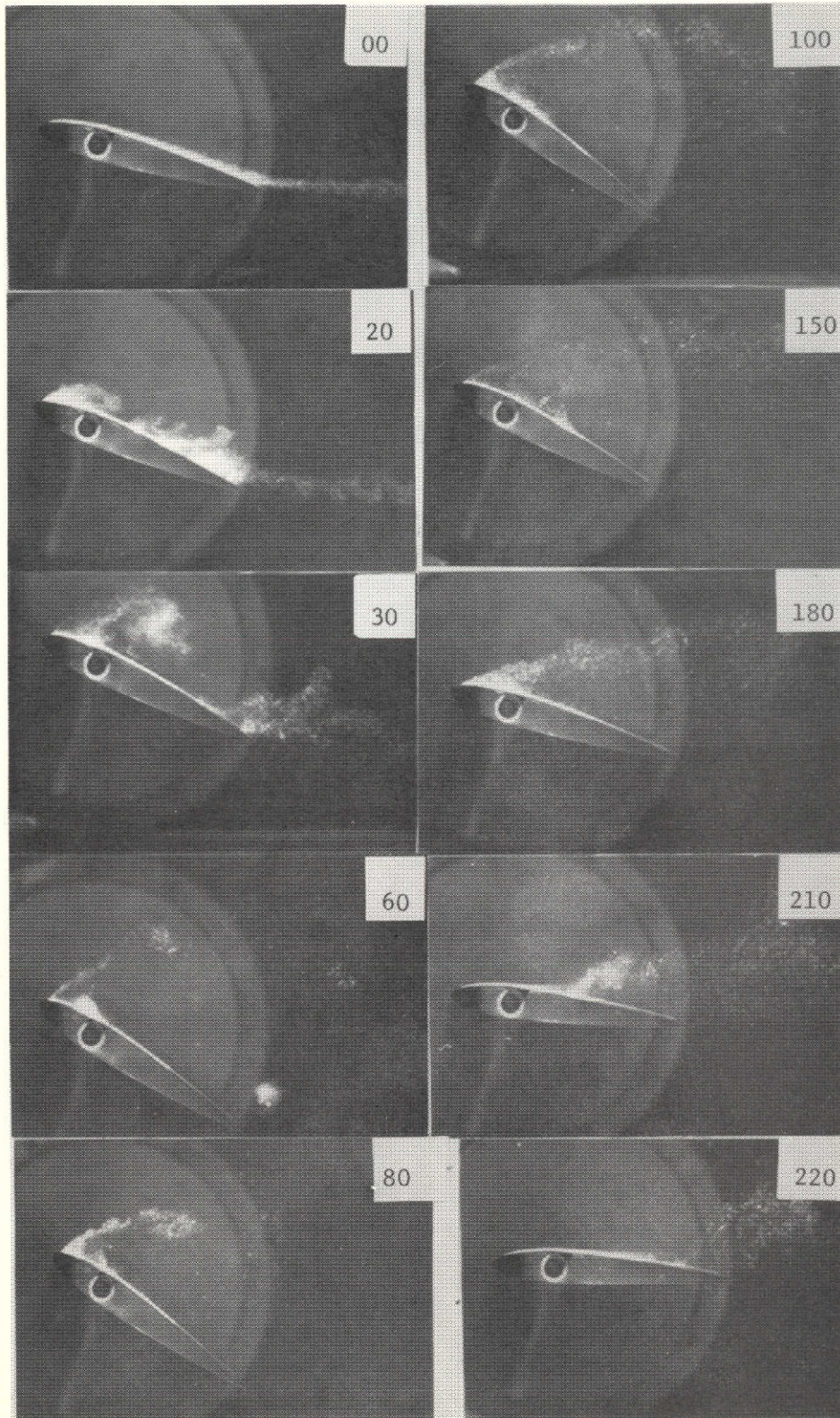
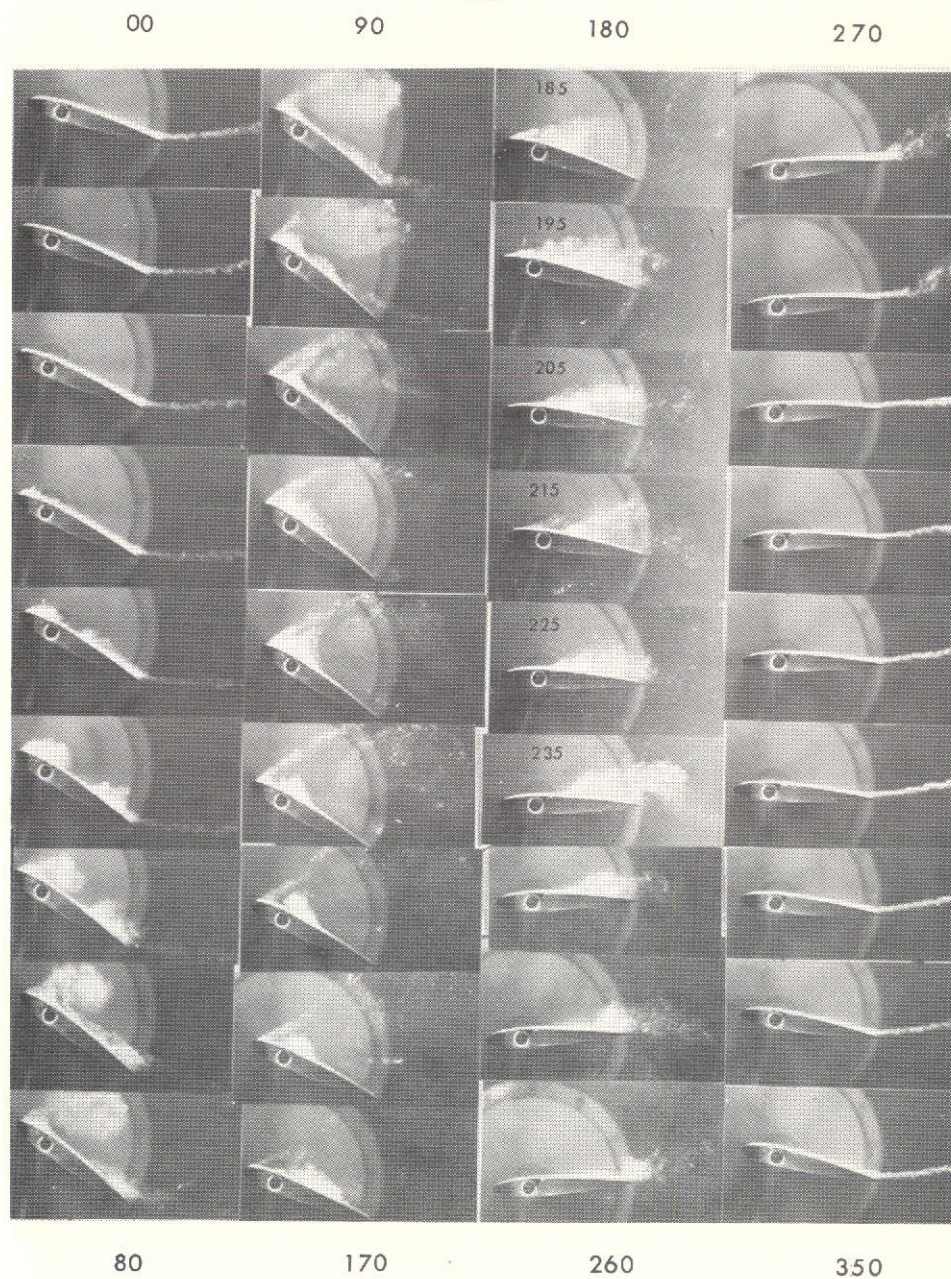


Figure 19b



RUN NO. 5

AIRFOIL NACA 0012 $C = 4''$

$\theta_0 = 15.8$ $\epsilon = 20.0$

$k_T = .282$ $Re = .577 \times 10^6$

PITCH AXIS = $\frac{1}{4}$ CORD

FIGURE 20A.

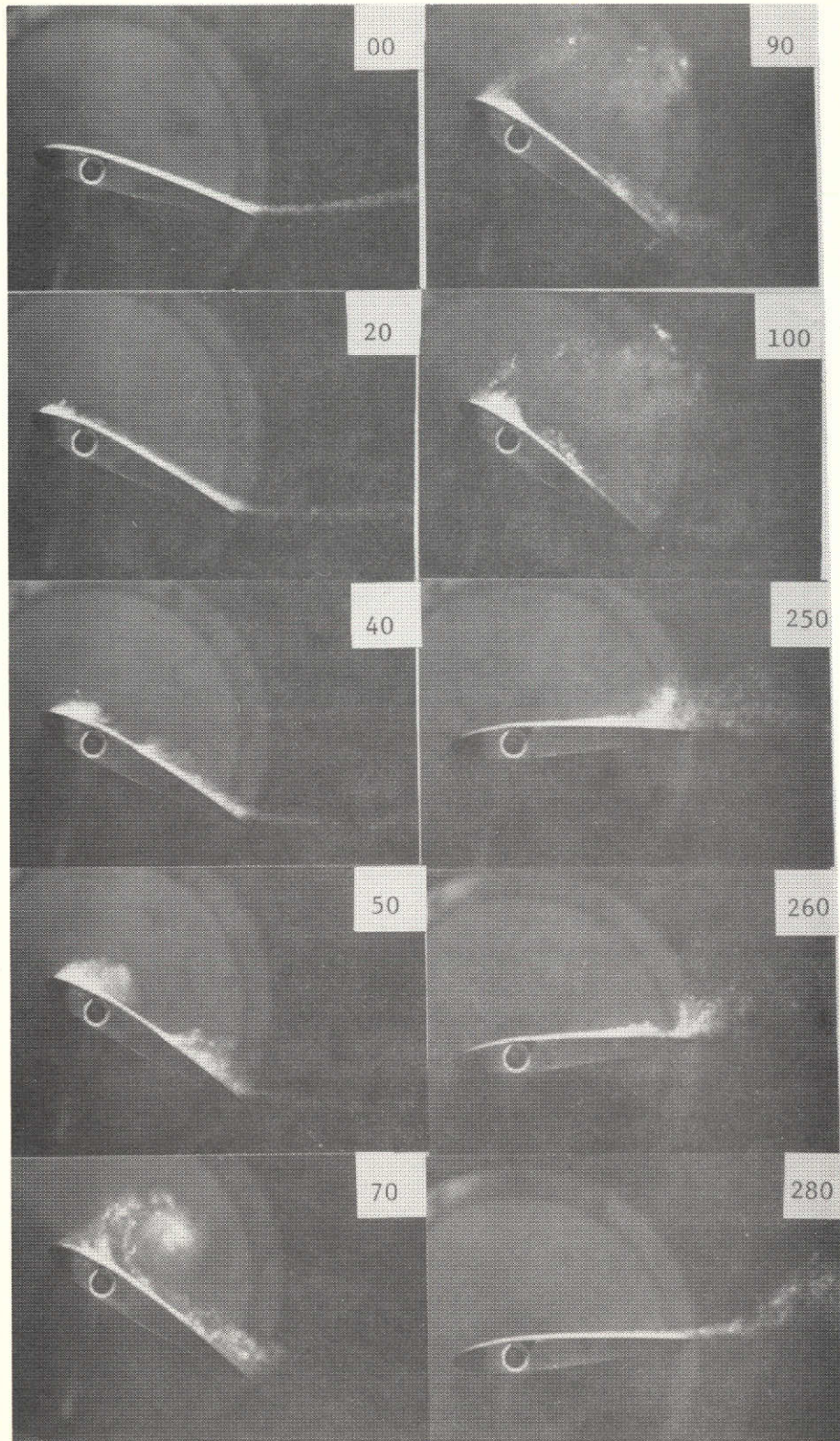


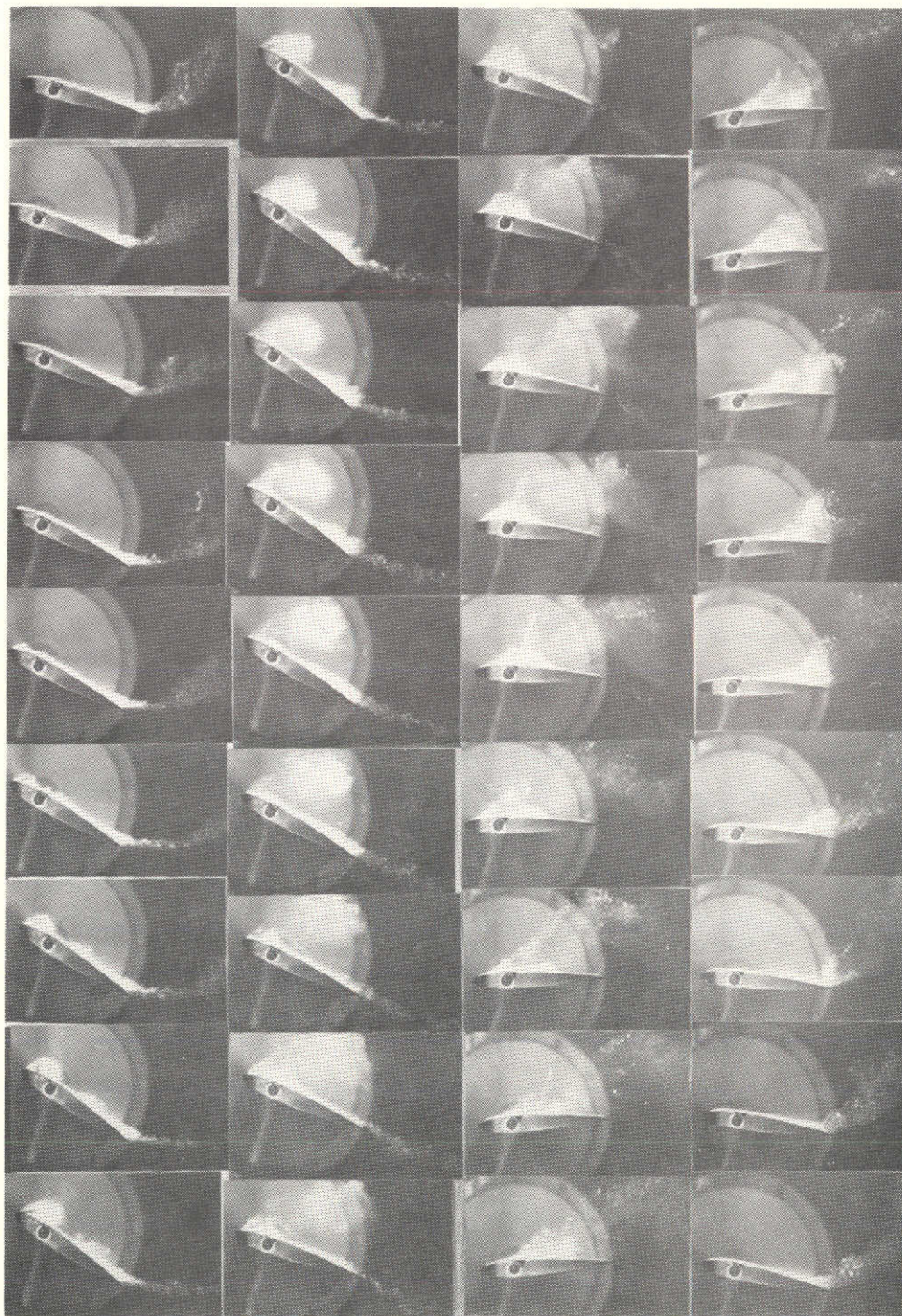
Figure 20b

00

90

180

270



80

170

260

350

RUN NO. 6

AIRFOIL NACA 0012 $C = 4'$ $\theta_0 = 15.8$ $\epsilon = 20.0$ $k_T = .532$ $Re = .577 \times 10^6$ PITCH AXIS = $\frac{1}{4}$ CORD

FIGURE 21A.

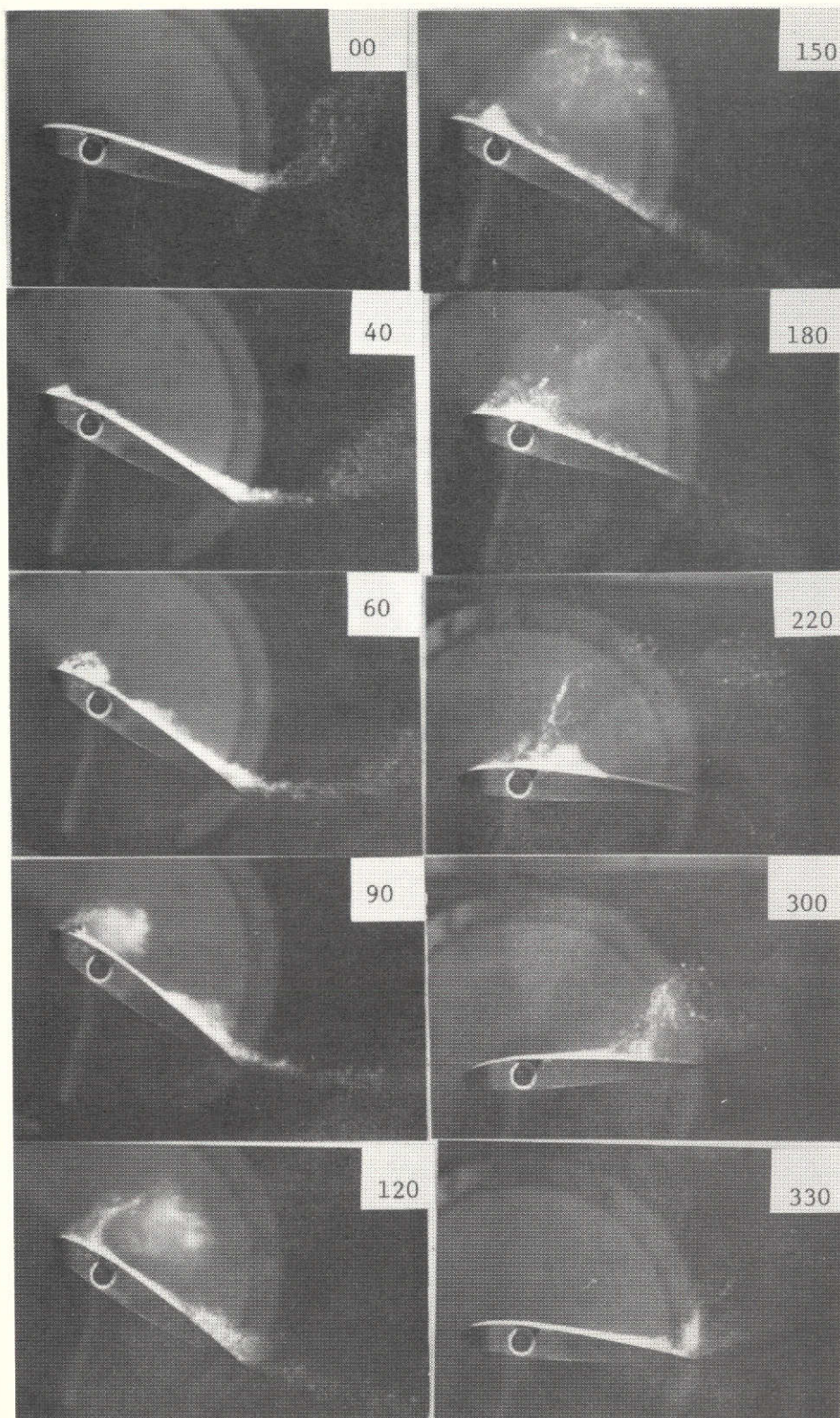


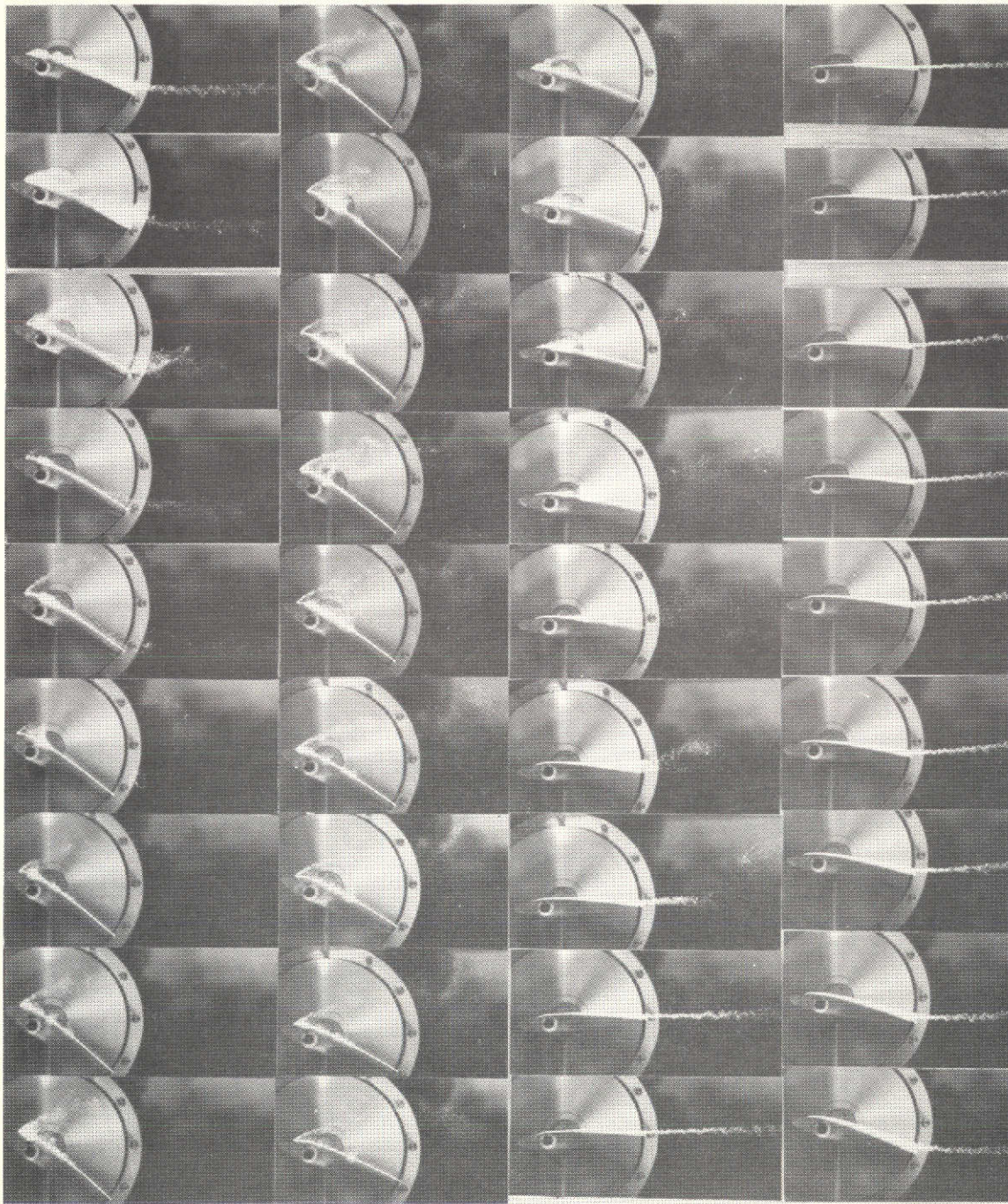
Figure 21b

00

90

180

270



80

170

260

350

RUN NO. 7

AIRFOIL NACA 0012 $C = 4''$ $\theta_o = 18.6$ $\epsilon = 20.0$ $k_T = .111$ $R_e = .577 \times 10^6$ PITCH AXIS = $\frac{1}{4}$ CORD

FIGURE 22A.

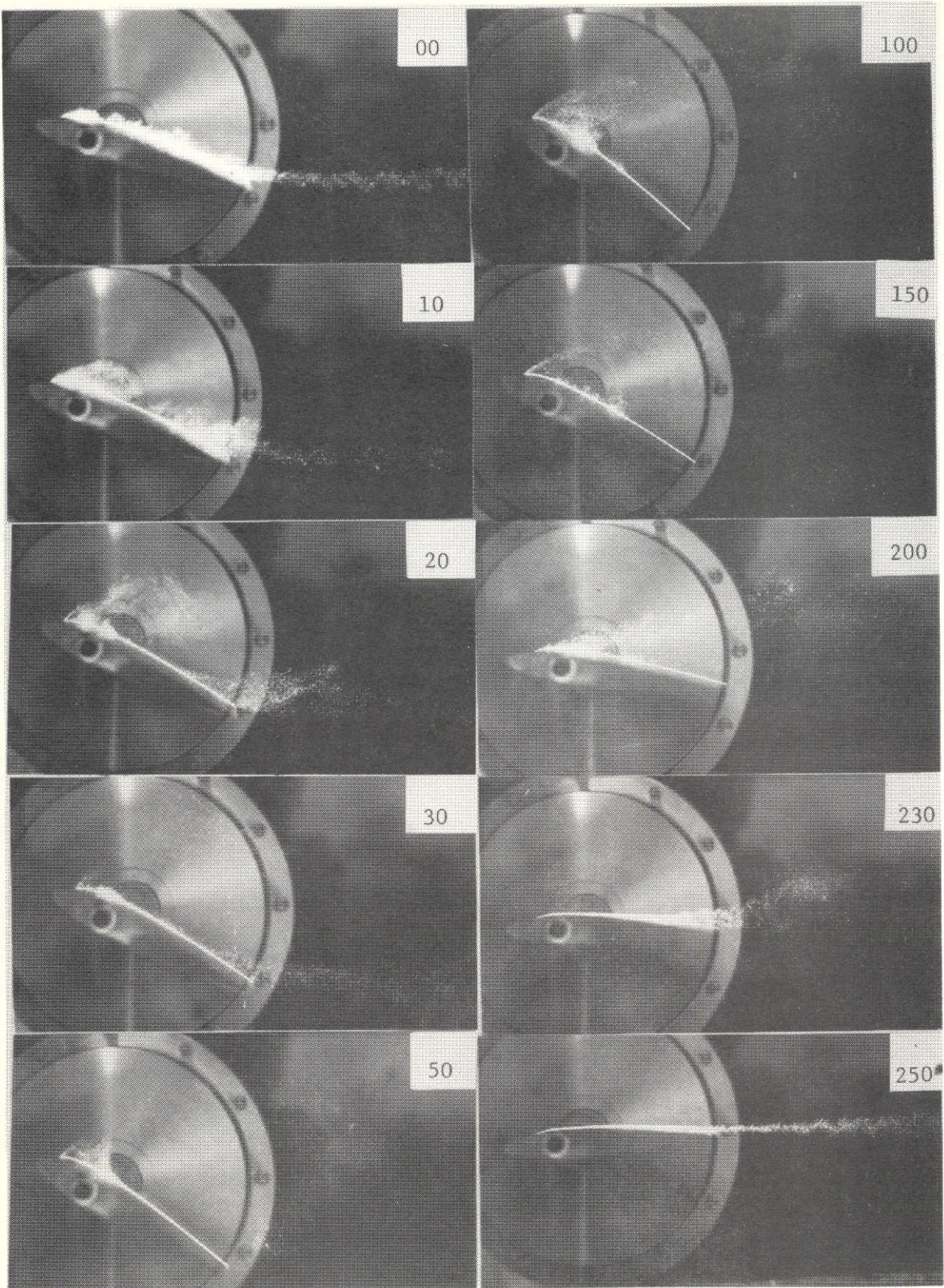


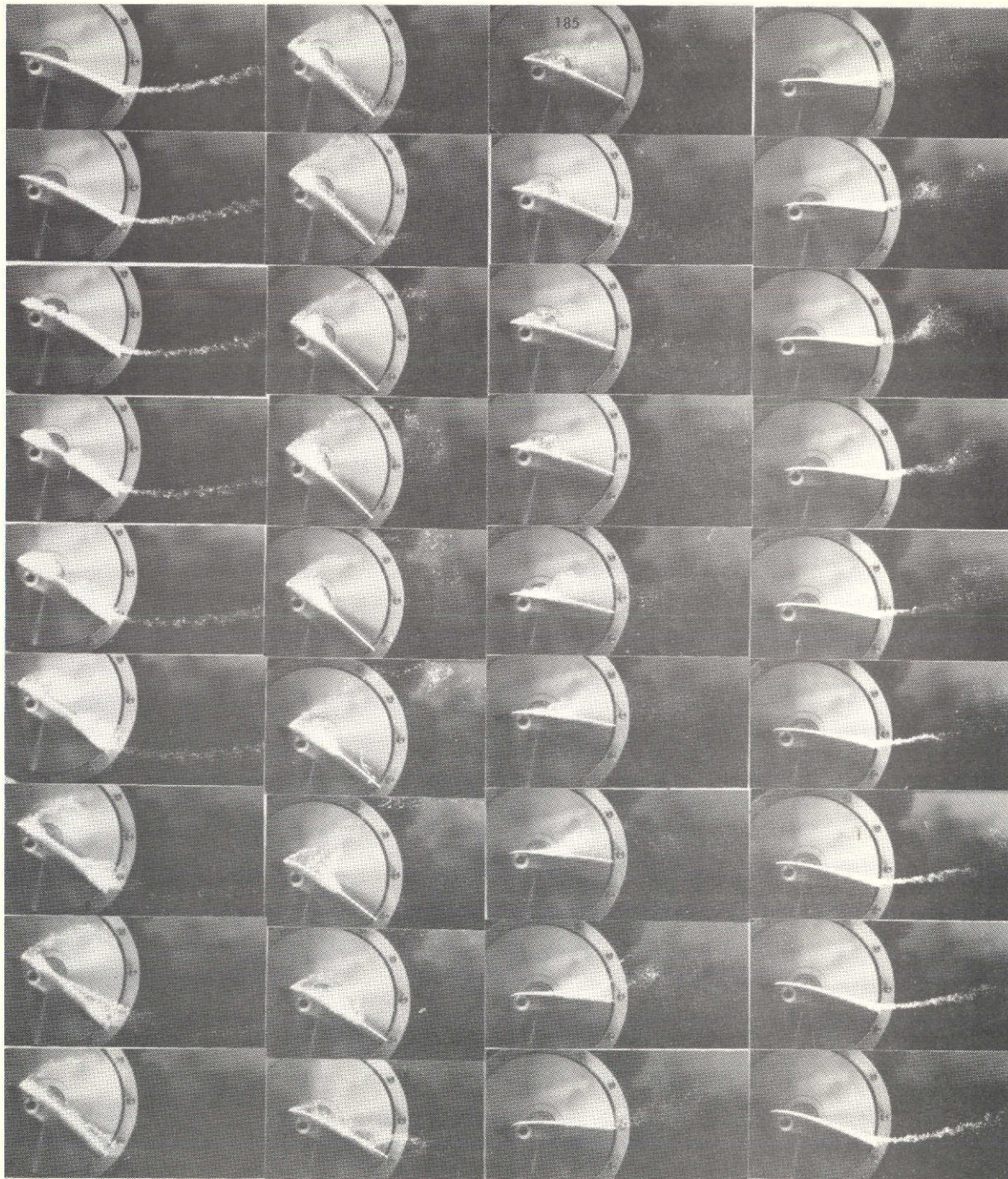
Figure 22b

00

90

180

270



80

170

260

350

RUN NO. 8

AIRFOIL NACA 0012 $C = 4''$ $\theta_0 = 18.6$ $\epsilon = 20.0$ $k_T = .282$ $Re = .577 \times 10^6$ PITCH AXIS = $\frac{1}{4}$ CORD

FIGURE 23A.

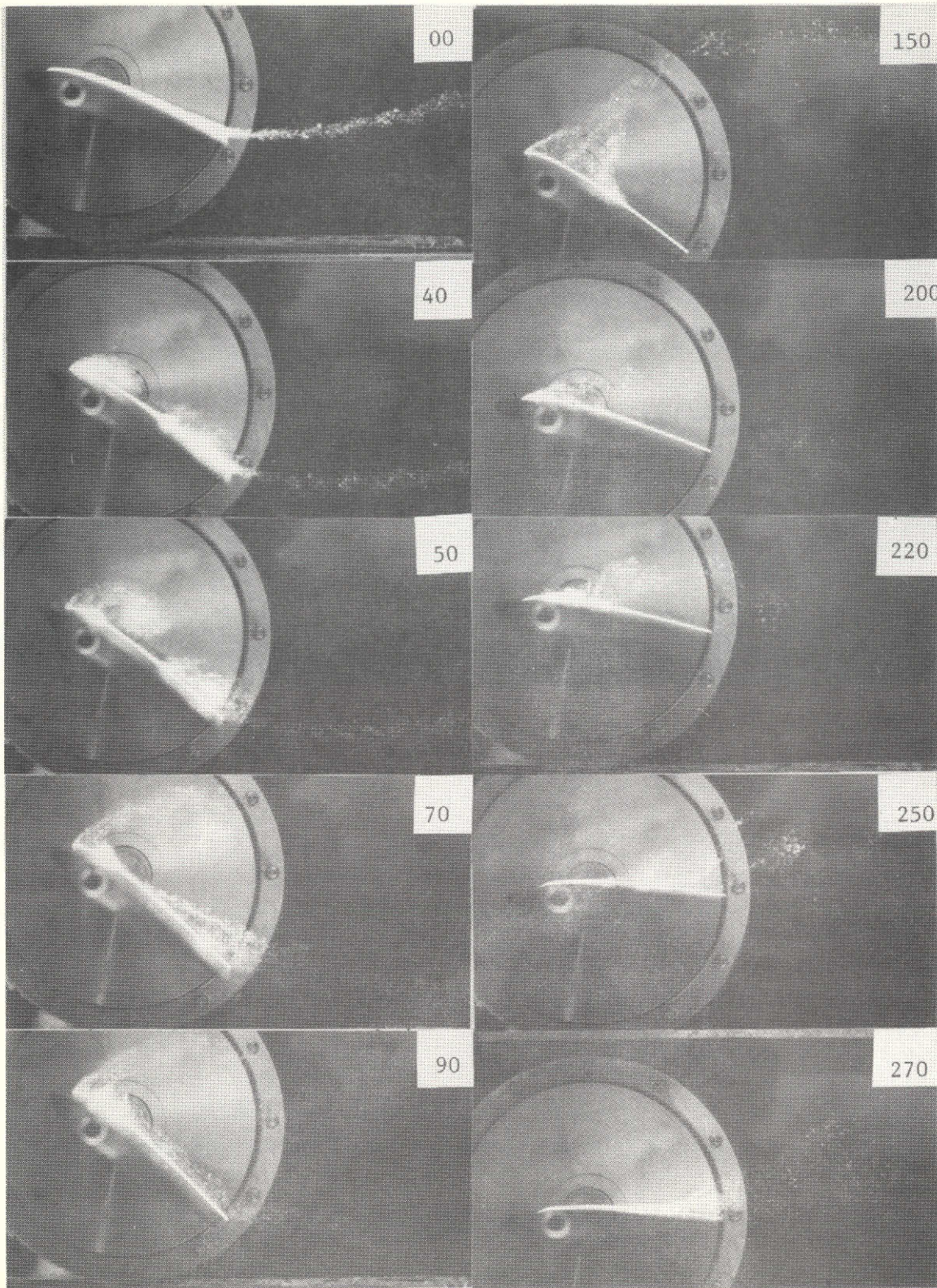


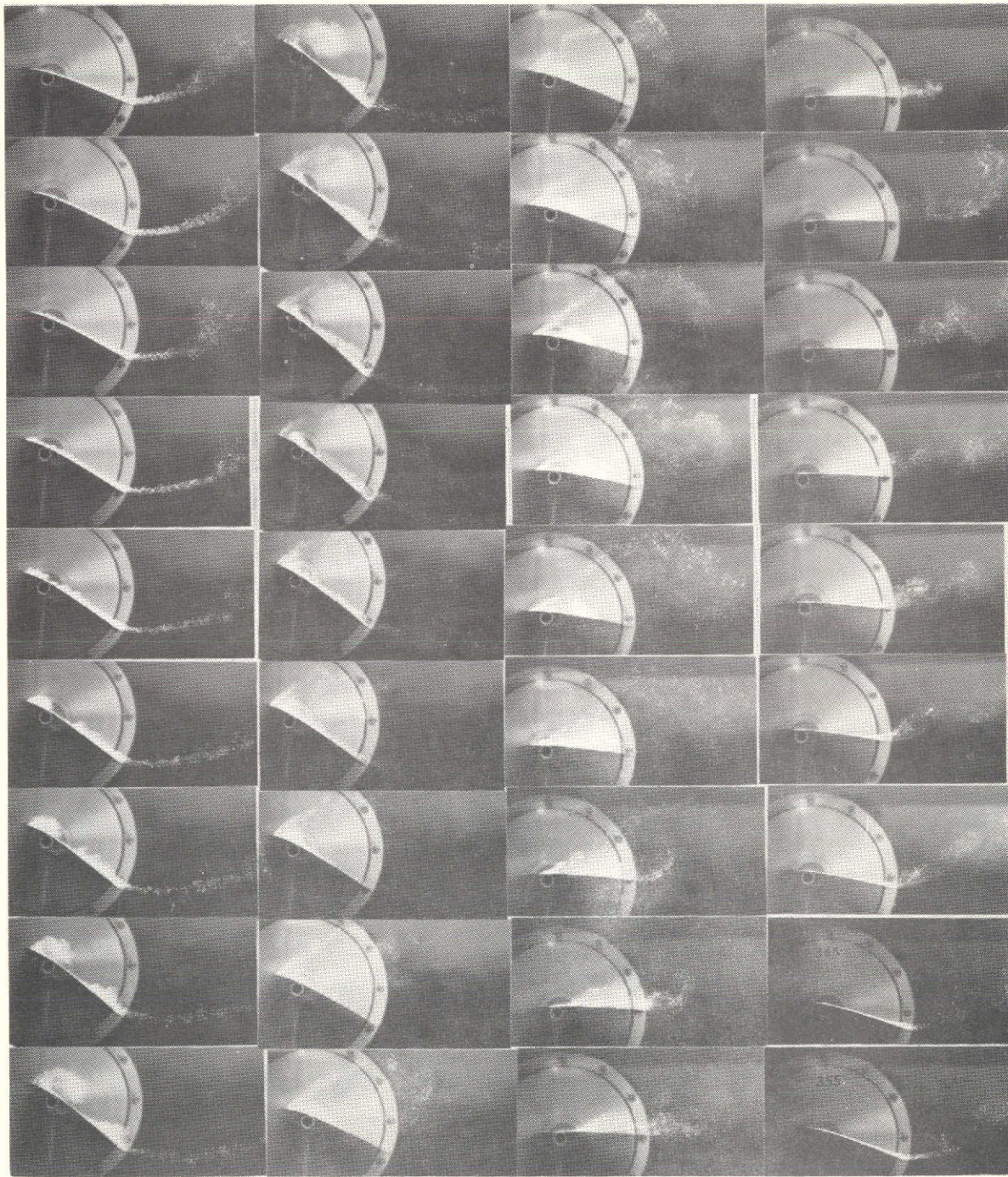
Figure 23b

00

90

180

270



80

170

260

350

RUN NO. 9

AIRFOIL NACA 0012 $C = 4^\circ$ $\theta_0 = 18.6$ $\epsilon = 20.0$ $k_T = .595$ $Re = .516 \times 10^6$ PITCH AXIS = $\frac{1}{4}$ CORD

FIGURE 24A.

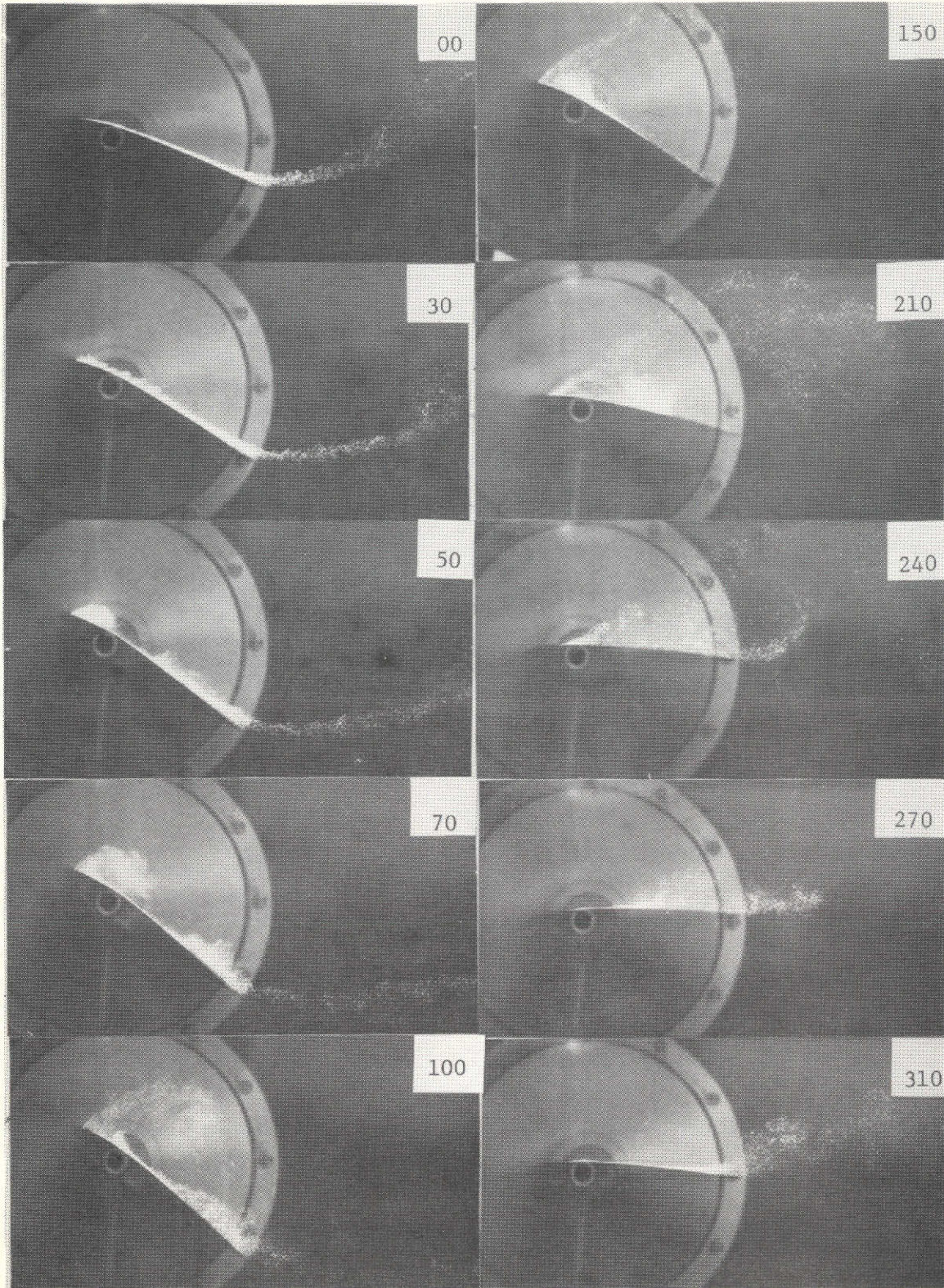


Figure 24b

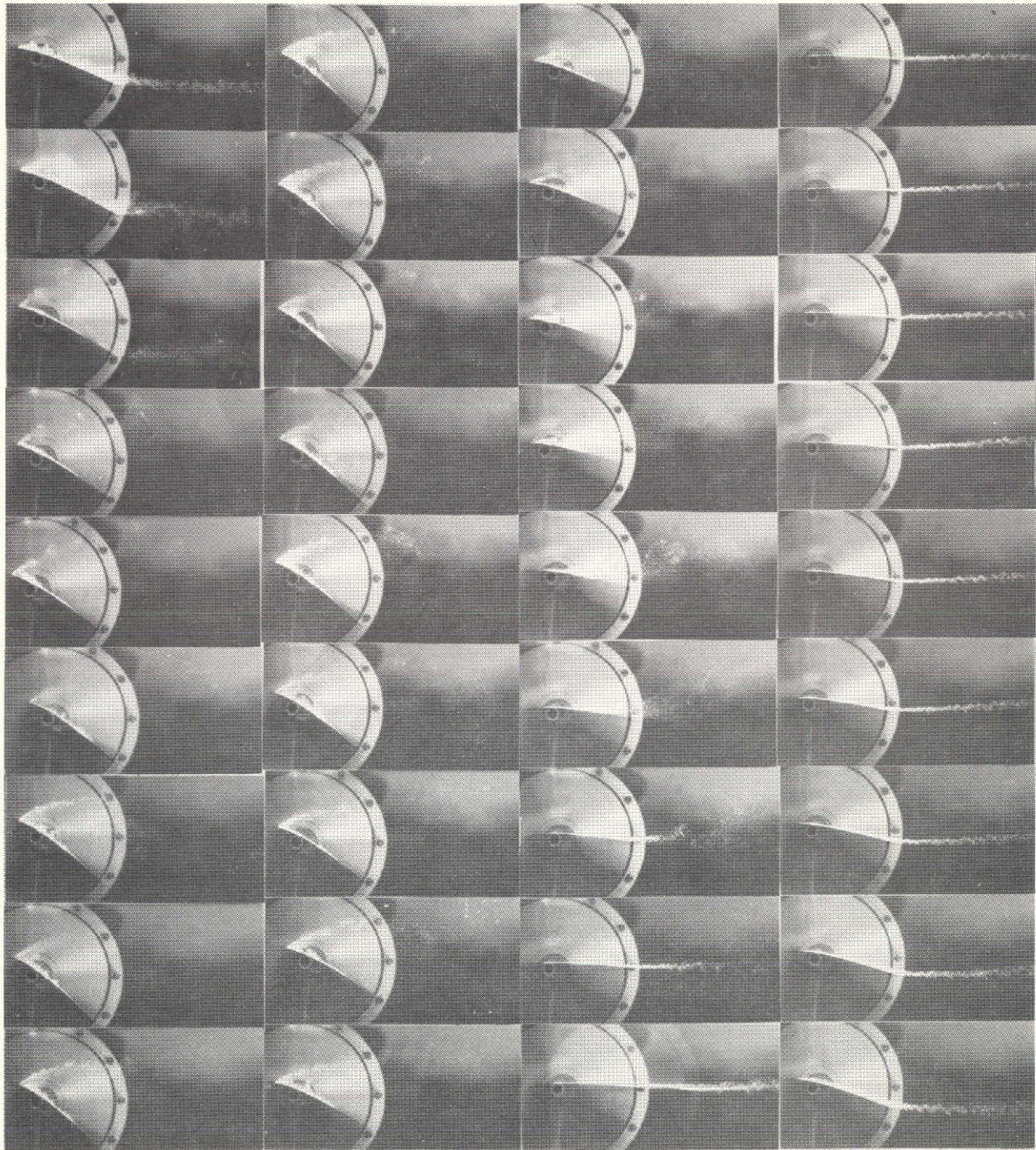
00

90

A35

180

270



80

170

260

350

RUN NO. 10

AIRFOIL NACA 0012 $C = 4''$

$\theta_0 = 20.0$ $\epsilon = 20.0$

$k_T = .111$ $Re = .577 \times 10^6$

PITCH AXIS = $\frac{1}{4}$ CORD

FIGURE 25A.

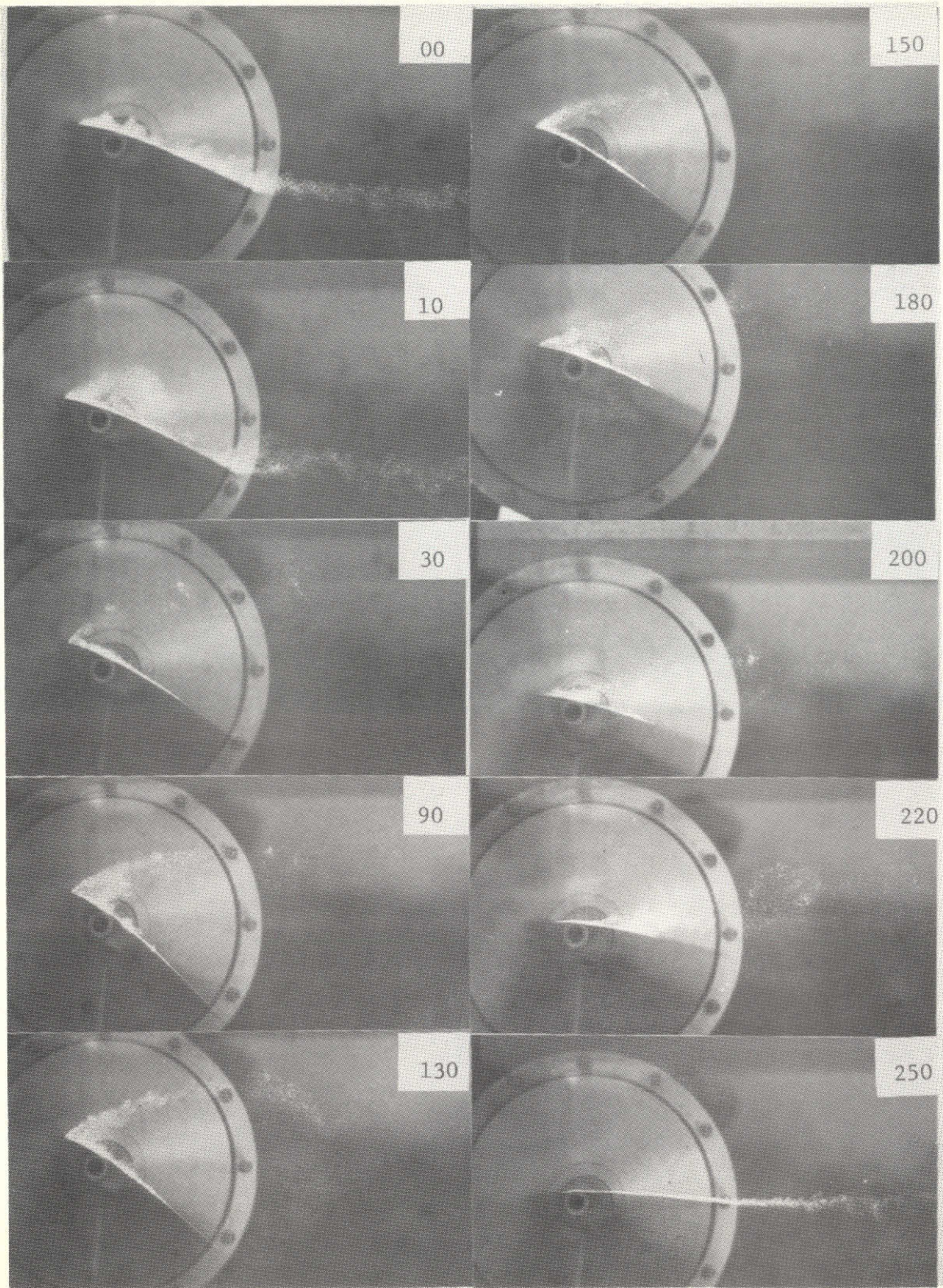


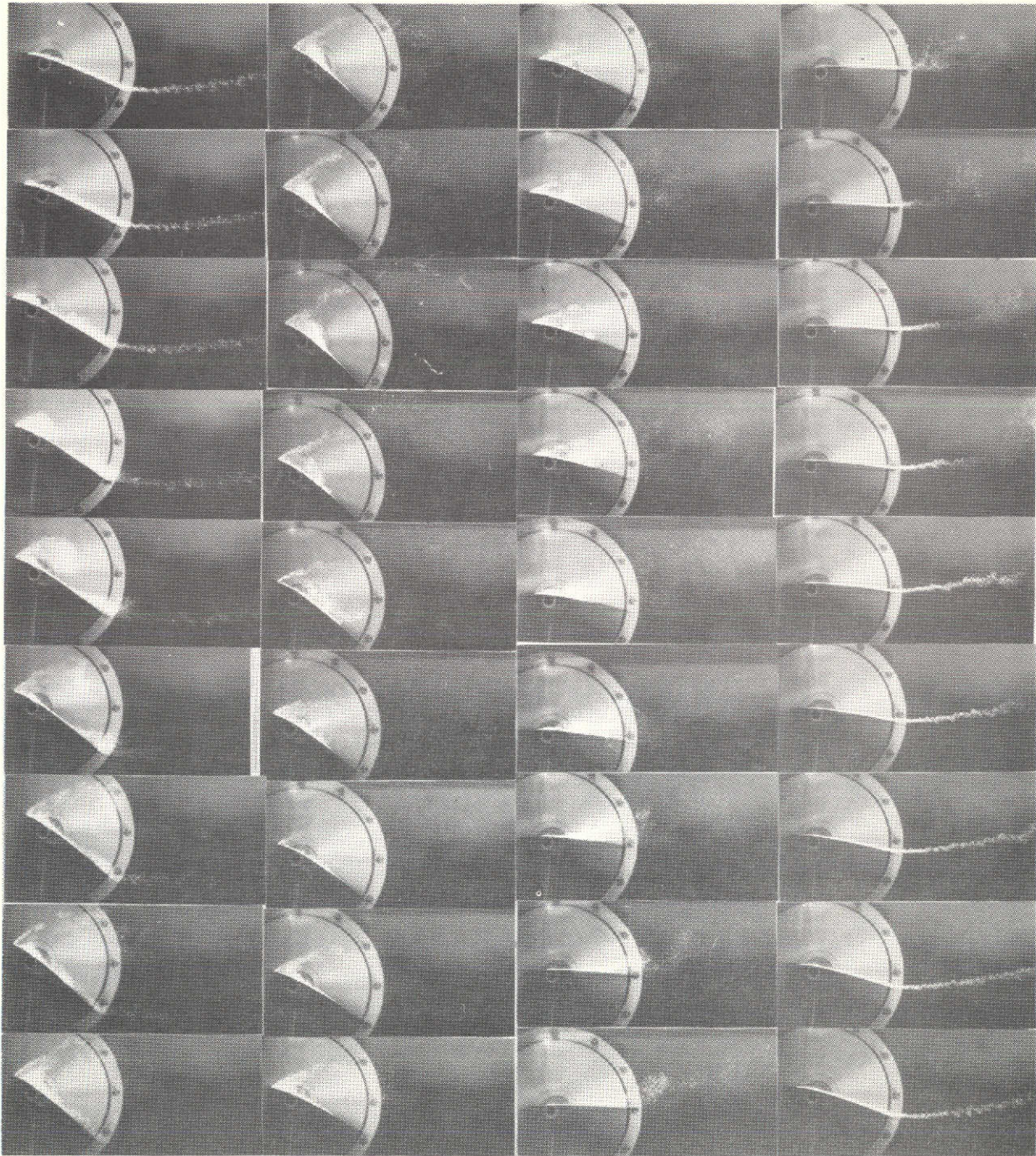
Figure 25b

00

90

180

270



80

170

260

350

RUN NO. 11

AIRFOIL NACA 0012 $C = 4^\circ$ $\theta_0 = 20.0$ $\xi = 20.0$ $k_T = .282$ $R_e = .577 \times 10^6$ PITCH AXIS = $\frac{1}{4}$ CORD

FIGURE 26A.

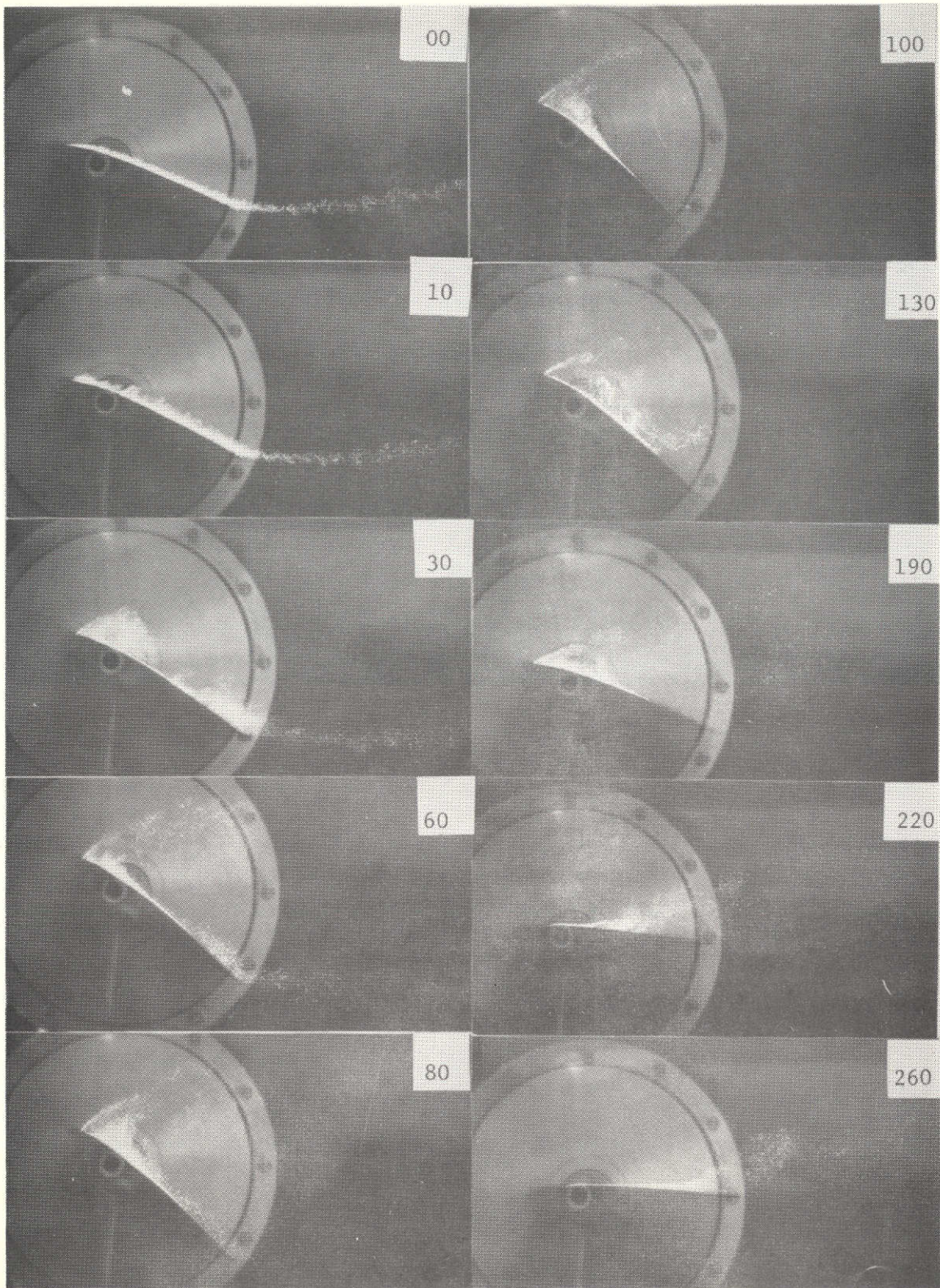


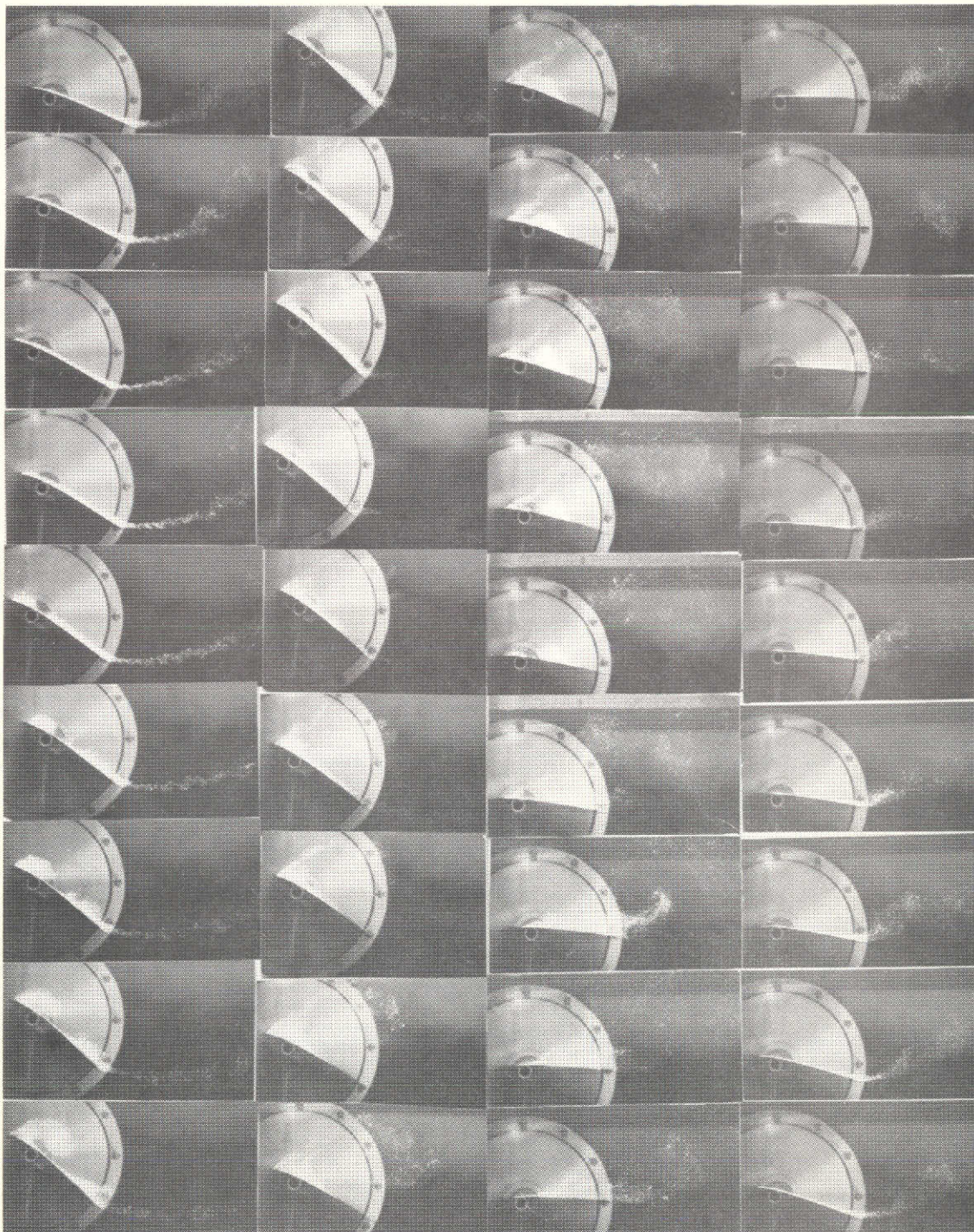
Figure 26b

00

90

180

270



80

170

260

350

RUN NO. 12

AIRFOIL NACA 0012 $C = 4^\circ$ $\theta_0 = 20.0$ $\epsilon = 20.0$ $k_T = .595$ $Re = 516 \times 10^6$ PITCH AXIS = $\frac{1}{4}$ CORD

FIGURE 27A.

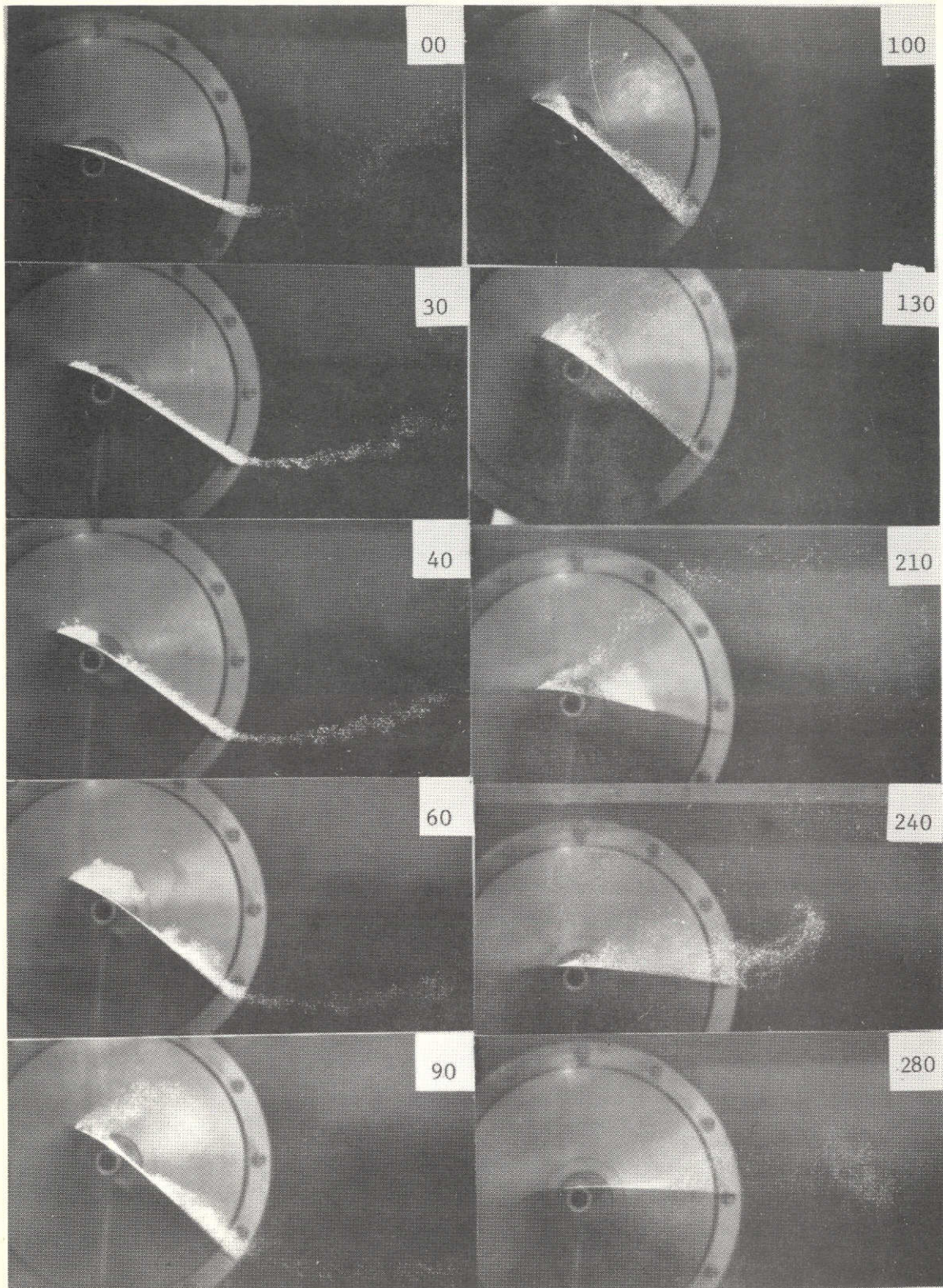


Figure 27b

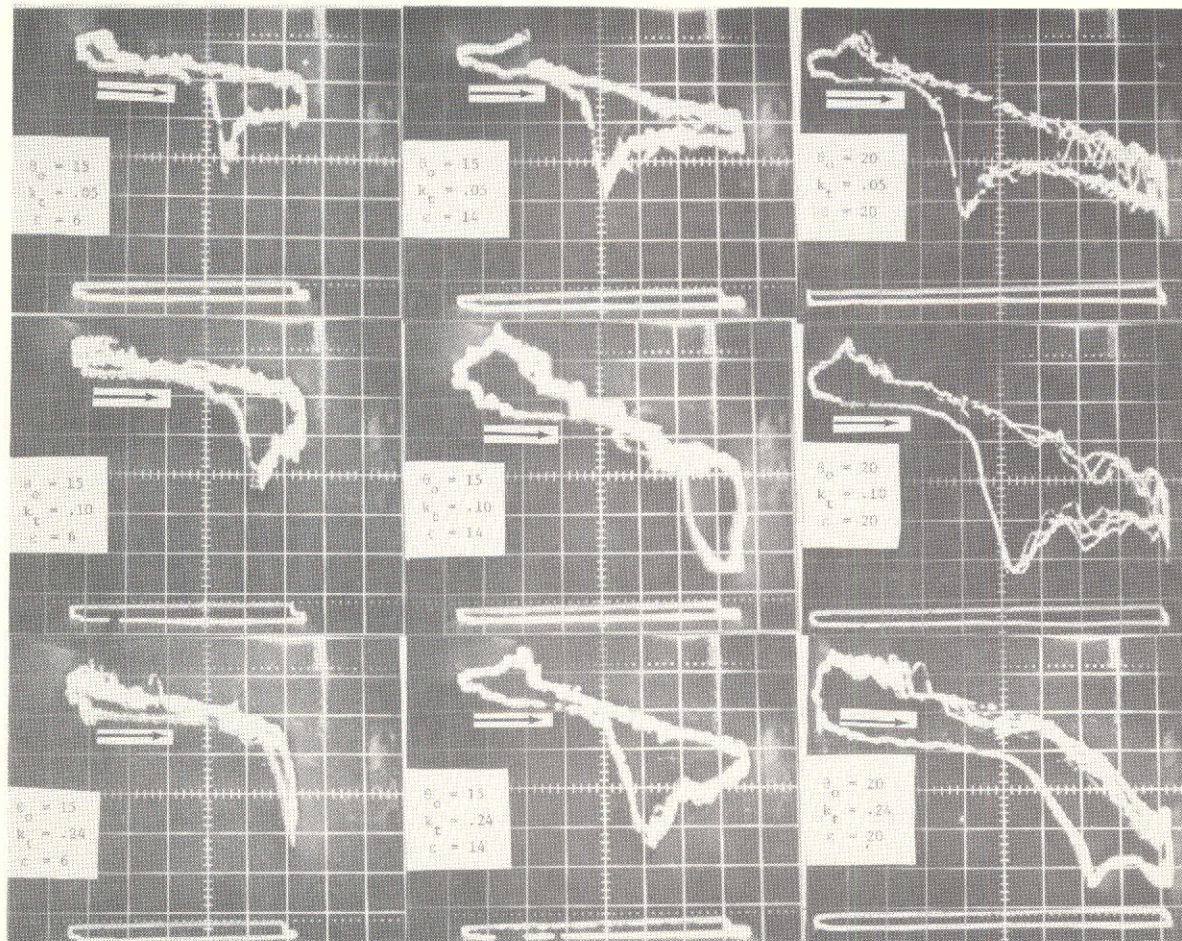
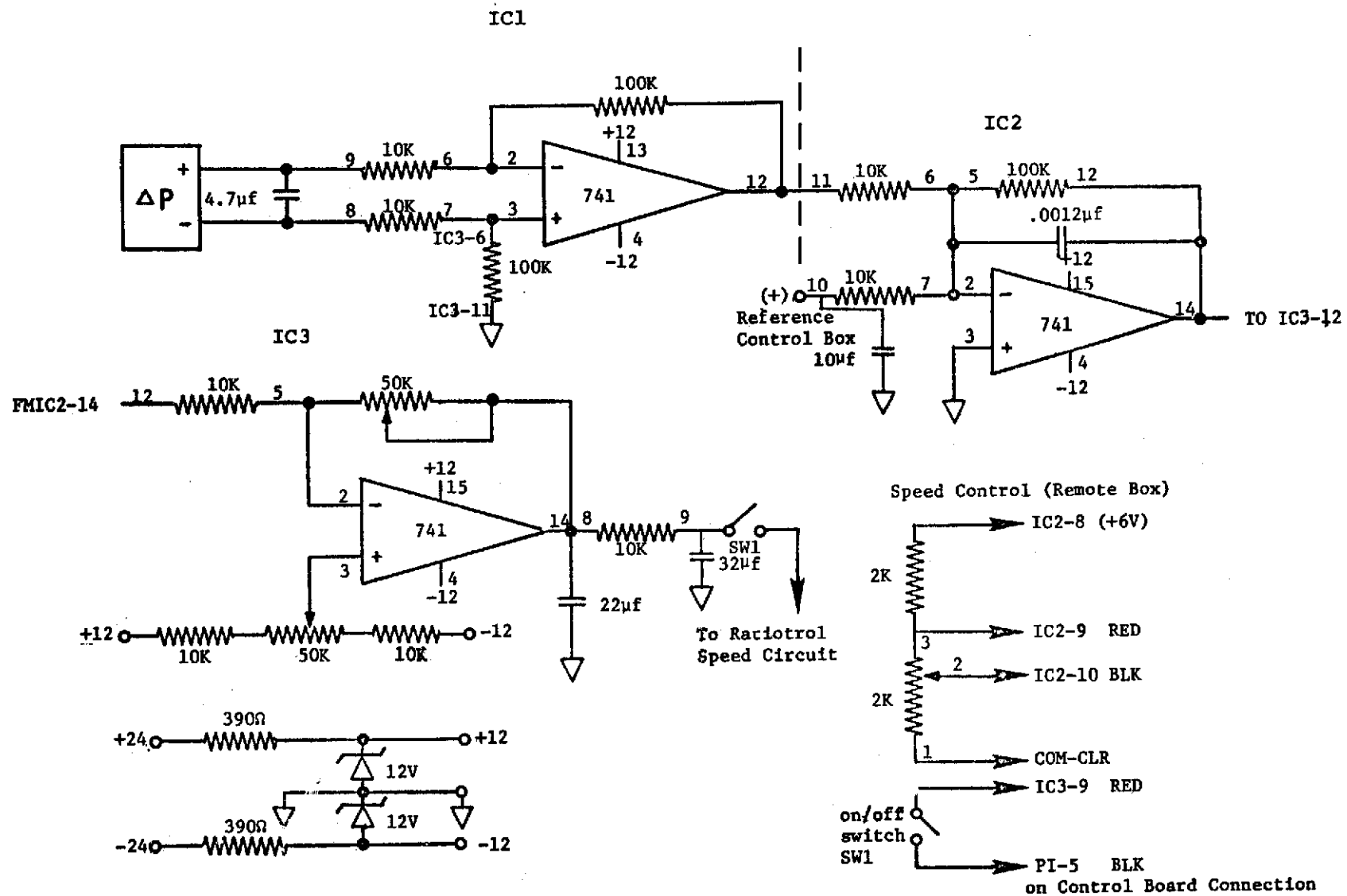


FIGURE 28. MOMENT DIAGRAMS CORRESPONDING TO THE HIGH REYNOLDS NUMBER MOVIE CONDITIONS - RUN SERIES II. SCALE = .58 KG-M / MAJOR DIVISION, $Re = .7 \times 10^6$.



A42

Figure 29. Feedback Control Circuit Diagram

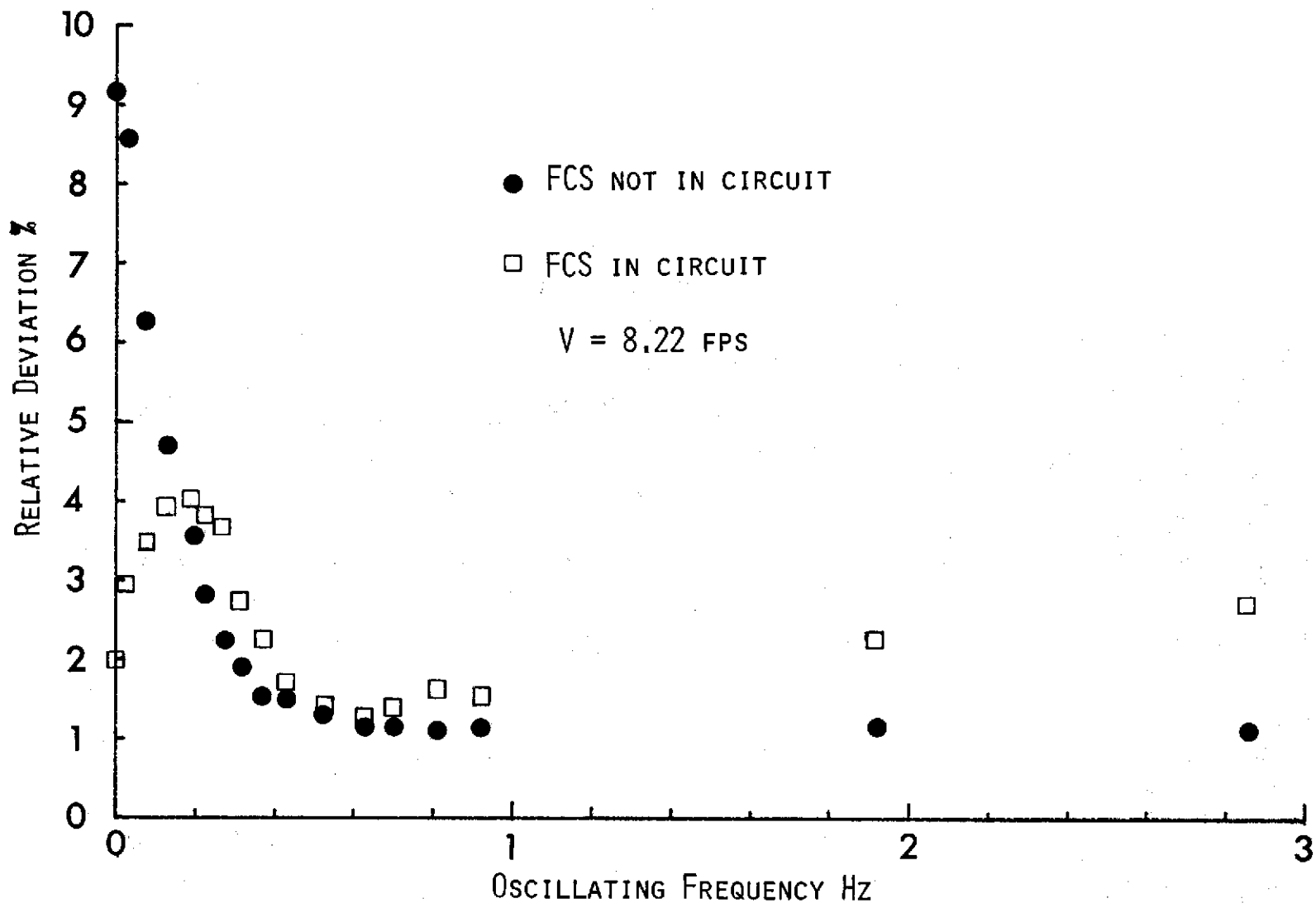


Figure 30. Relative Deviations of Tunnel Speed with and without the Feedback Control System in Circuit.

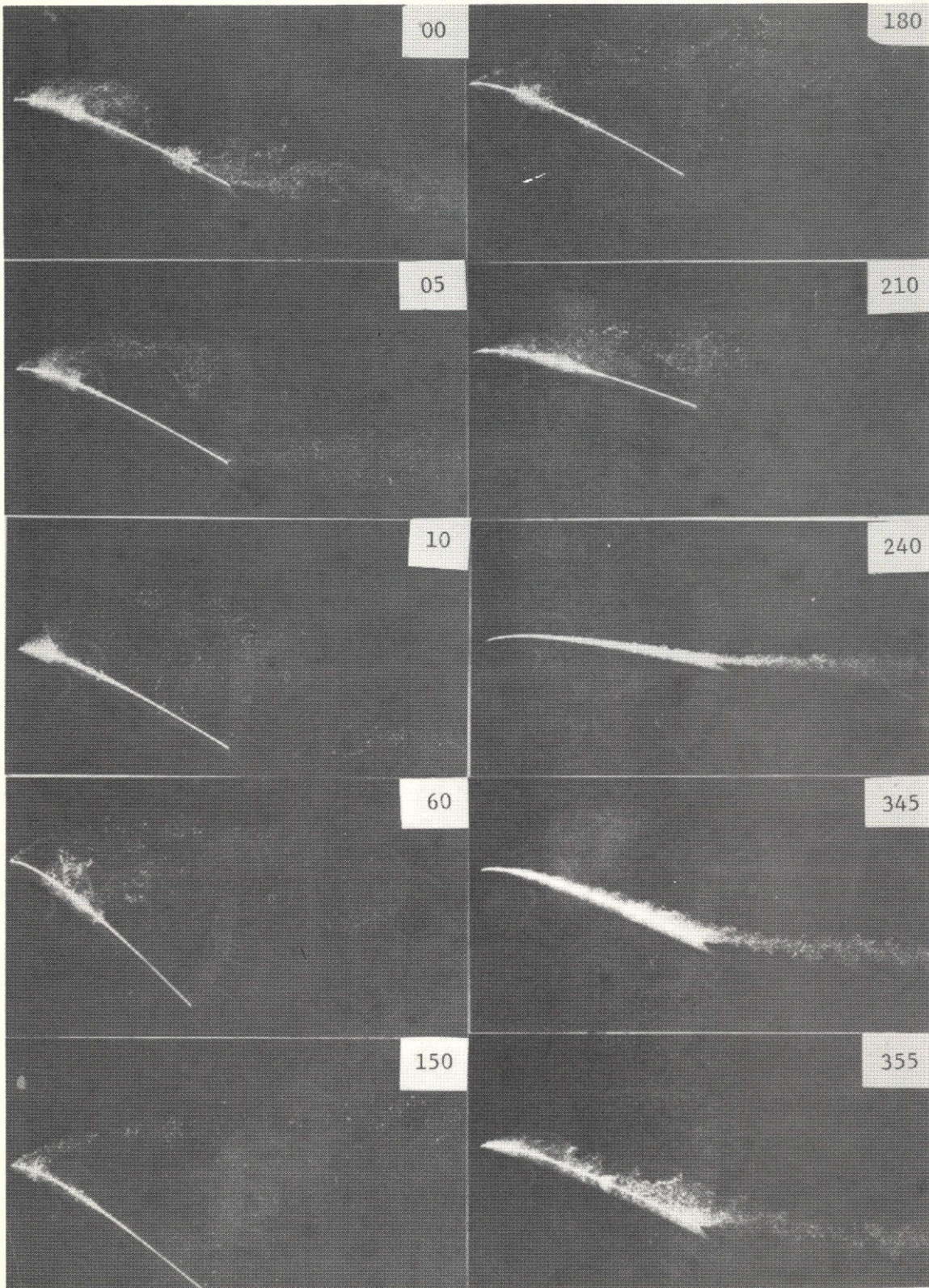
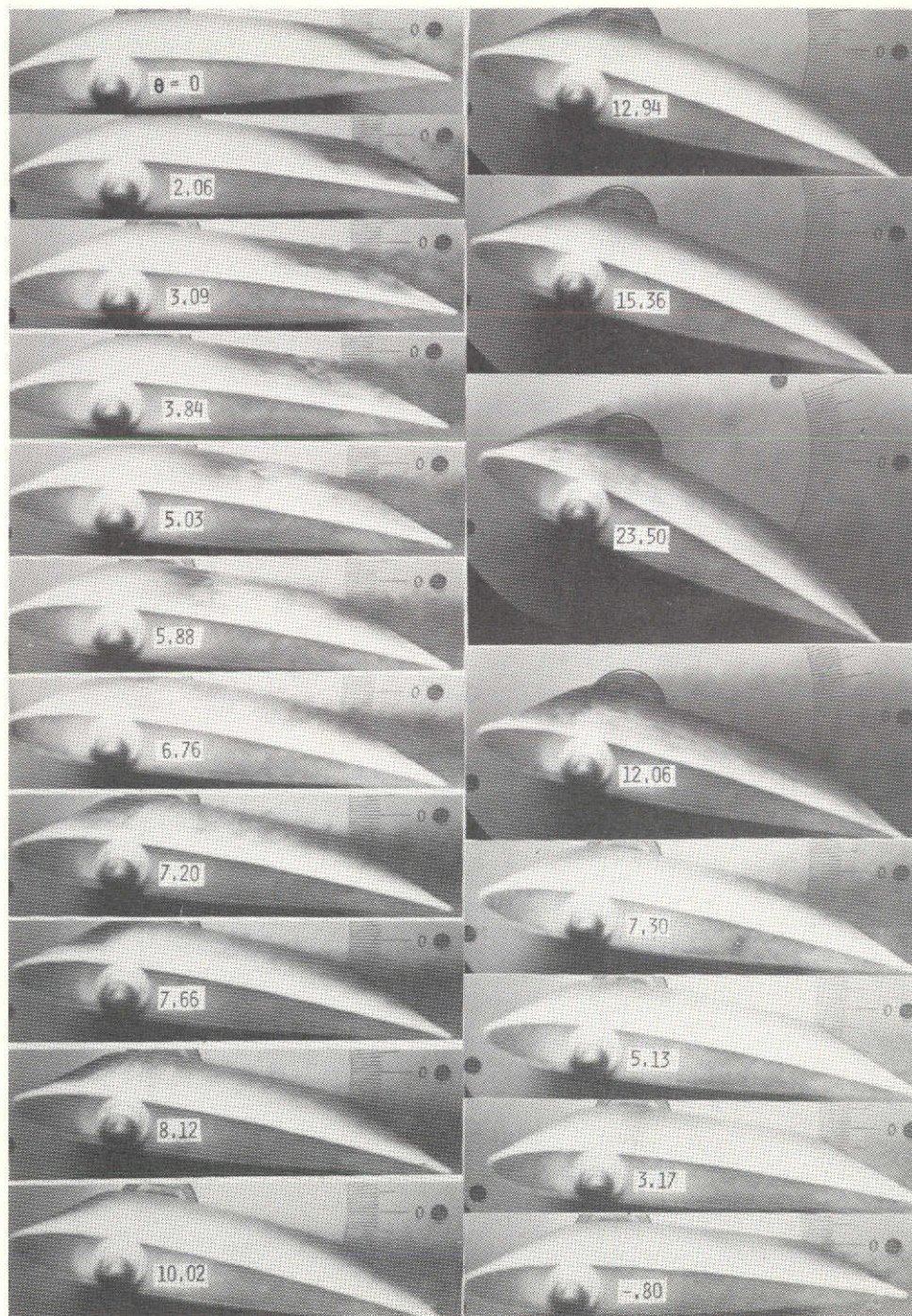


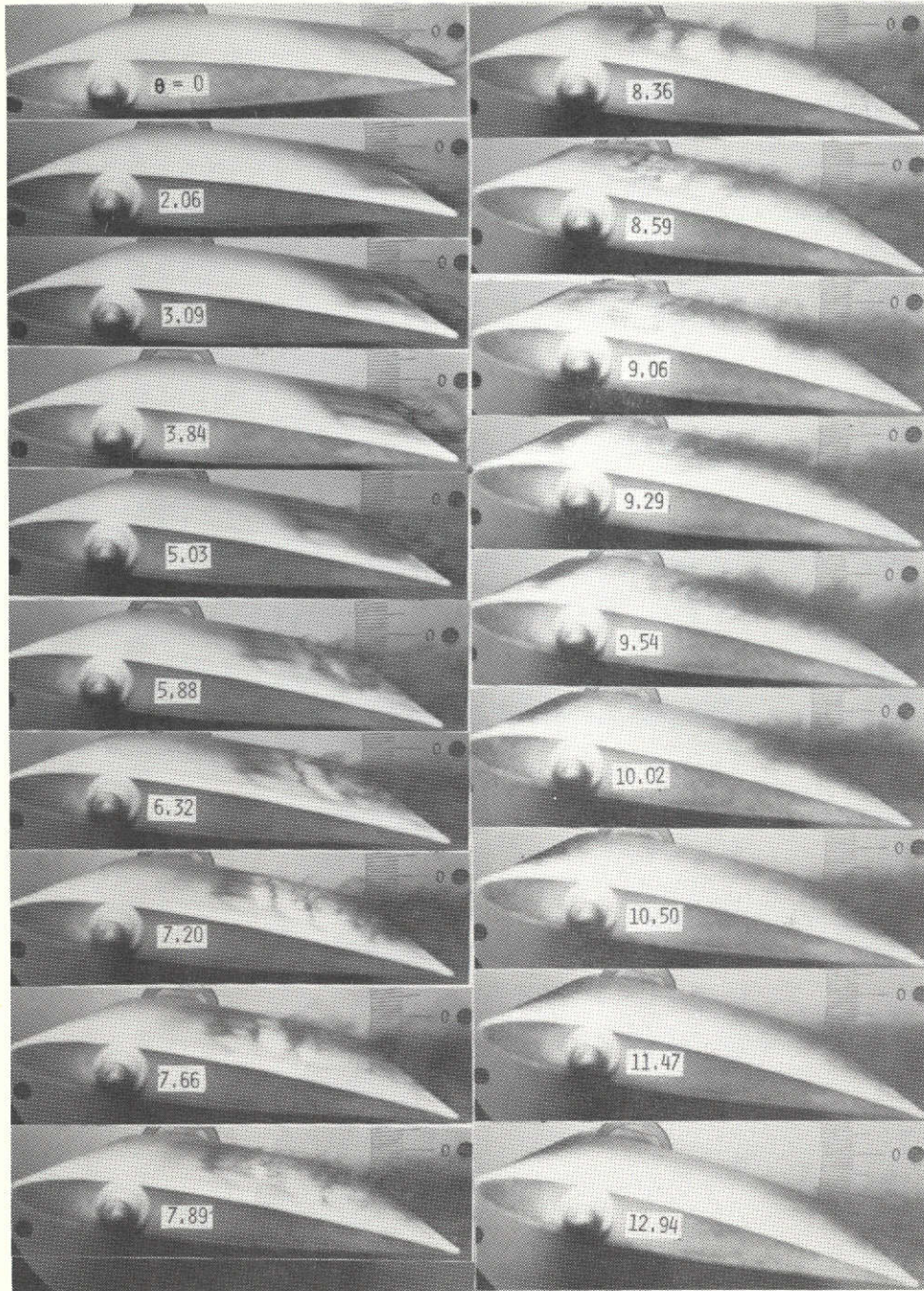
Figure 31. Improved Photographs of Hydrogen Bubble Traces with the Installation of a Black Background. $K_t = .1$, $Re = .35 \times 10^6$, $\theta_0 = 20$, $\epsilon = \pm 20$.



$V = 1 \text{ FPS}$ $K_T = .05$ $Re = .3 \times 10^5$

$\theta_0 = 22.25$ $\epsilon = \pm 13.75$

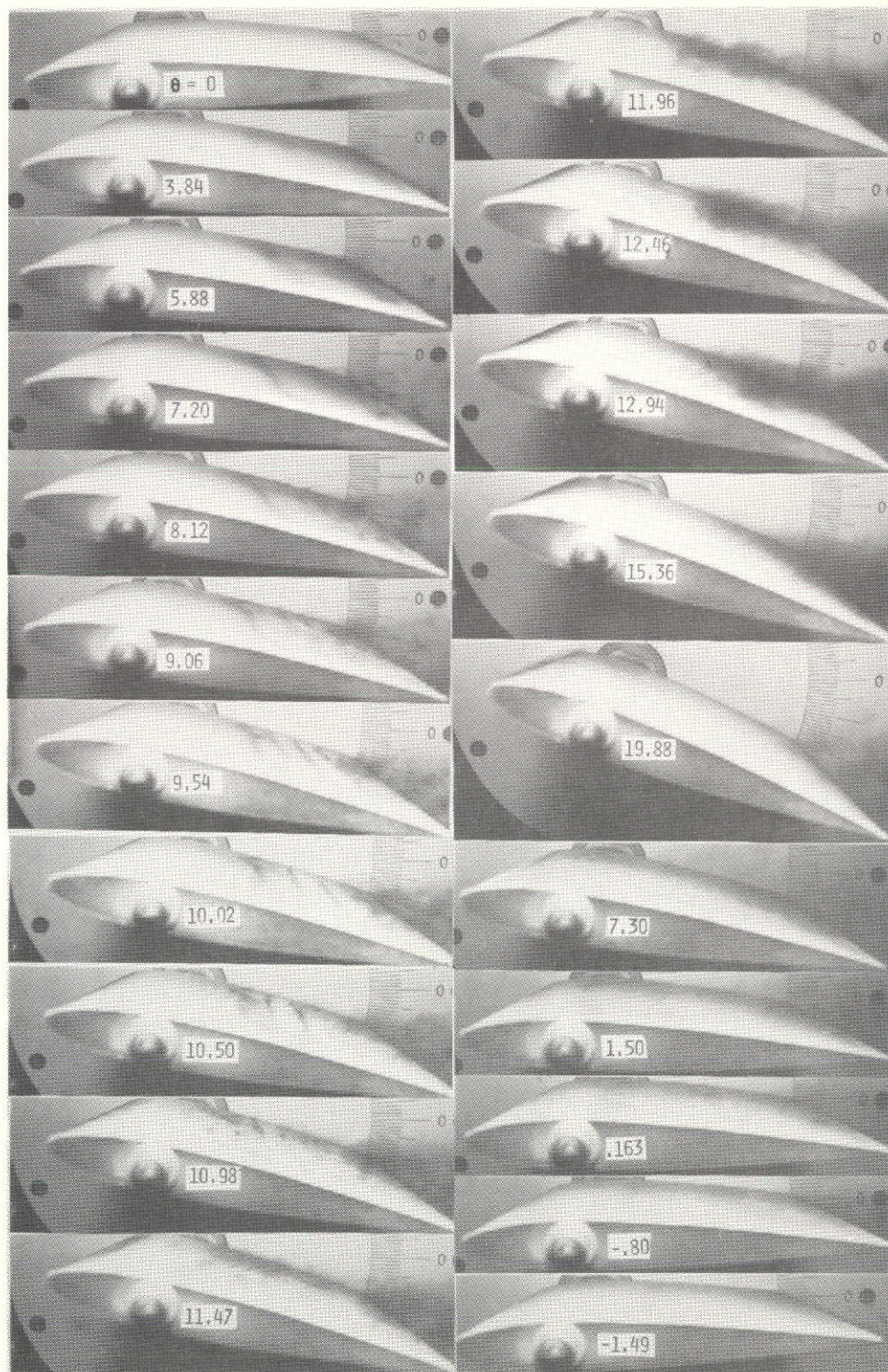
FIGURE 32



$$V = 1 \text{ FPS} \quad K_T = .10 \quad R_E = .3 \times 10^5$$

$$\theta_0 = 12.25 \quad \epsilon = \pm 13.75$$

FIGURE 33



$$V = 1 \text{ FPS} \quad K_T = .24 \quad R_E = .3 \times 10^5$$

$$\theta_0 = 12.25 \quad e = \pm 13.75$$

FIGURE 34

In the first case, the particles suspended in the fluid flow /83 approach by their properties and shape solid undeformed rods or plates with dimensions on the order of 10^3 - 10^5 Å. These particles themselves are birefringent; however, in a fluid which is not subjected to the effect of the appropriate field of force, the solution will appear to be optically isotropic as a result of the disordering caused by the rotational brownian motion of these particles. A certain region of the fluid becomes birefringent only when the particles are statistically ordered in the fluid as a result of the effect of the tangential stresses. The effect of the tangential stresses on the ordering of the particles is of course disturbed by the brownian motion of these particles, so that the resulting statistical ordering is the result of the effect of the tangential stresses in the fluid and the brownian motion of the particles. Hence, the ordering is not static, but we have the case when the direction in which the particles are oriented on the average, and hence also the direction of the optical axis of the fluid layer formed by these particles are given by the direction of the longer axes of the particles at the instant when the angular velocity of the particles is a minimum. The degree of orientation can be characterized by the parameter $\alpha = G/\Phi$, where G is the velocity gradient and Φ is the rotational diffusion constant. Φ is a measure of the intensity of the Brownian motion and it depends on the dimensions and shape of the particles in the fluid. To each velocity gradient G corresponds a certain distribution of the orientation directions of the rod-shaped particles. As the gradient G (or the parameter α) increases, this distribution narrows, and the birefringence value increases. The first group includes, for example, the tobacco mosaic virus, clays such as halloysite, bentonite, and also various proteins.

The second group includes polymers. Their particles can be replaced for theoretical considerations by a spherical or a dumbbell model. However, these particles are deformed in the fluid flow as a result of the effect of the tangential stresses (similarly as in the photoelastic phenomenon), for example, spheres are deformed into ellipsoids, resulting in their optical anisotropy. In the entire fluid region subjected to the effect of forces, the birefringence value is also affected by the orientation of the deformed particles. We can also include in this group pure fluids in which the direction of the statistical orientation of the molecules almost does not vary with the magnitude of the velocity gradient G , so that for them the birefringence formed depends mainly on the deformation of the molecules.

In addition to the birefringence value, another datum must be known for practical application, i.e. the so-called orientation angle (extinction angle) χ , which is defined as the angle

subtended by the principal optical axis of the fluid layer at a certain point and the direction of the flow at this point. By measuring Δn and χ at the selected point of the two-dimensional fluid flow layer, we can determine from these data under certain assumptions (see p. 81) the magnitudes of the velocity gradient G and the local direction of the flow, since for all groups of fluids it was determined that Δn and χ are functions of the velocity gradient G (see Fig. 54):

$$\Delta n = f(G), \quad (33)$$

$$\chi = g(G). \quad (34)$$

To determine the experimental values of the quantities Δn and χ for the relations (33) and (34), equipment called, according to Cvetkov [139], a dynamooptimeter is used. This equipment is based on the principle of a rotary viscosity meter. It consists of two coaxial cylinders, one of which can be rotated. The measured fluid in the space between the two cylinders is observed with the aid of a polariscope.

The use of temporary birefringence to obtain characteristics of the flow is based on the fundamental relations (33) and (34). This means that by measuring the birefringence value at various points of the fluid flow region it is possible to determine, on the basis of relation (33), at these points the magnitude of the velocity gradient G , and from it, with the aid of the orientation angle χ additional data without disturbing the flow by any measuring sensor. Also it is necessary to determine for the fluid used the behavior of the functions $f(G)$ and $g(G)$ which can be done, for example, with the aid of the dynamooptimeter that was mentioned. Of course, those fluids for which $f(G)$ is linear in the required range of velocity gradients and χ is nearly constant in the same range are most suitable. (The proper fluids and their use for hydrodynamic purposes were studied by Weller [140]).

Since the flow when the behavior of the functions $f(G)$ and $g(G)$ is determined with the aid of the dynamooptimeter is a flow where the direction of the velocity gradient is perpendicular to the direction of the flow, when the method is applied to other cases the question arises whether this condition must be preserved. A reliable use of the temporary birefringence to obtain characteristics of the flow in more complex cases would require that the question be answered and that the assumption that the direction of the velocity gradient in colloidal solutions can be determined on the basis of the value of the orientation angle χ be confirmed. However, so far, the necessary experimental and theoretical prerequisites are not yet available.

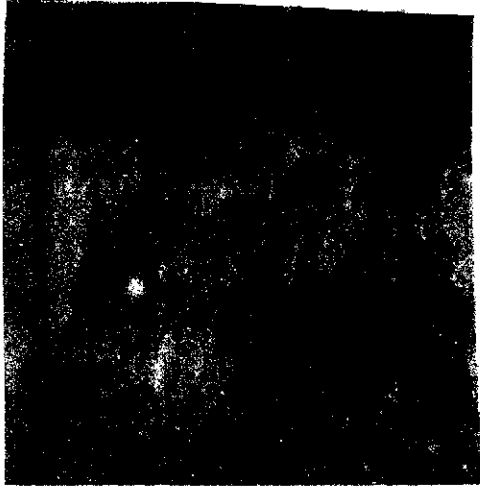


Fig. 54. Birefringence and extinction angle versus velocity gradient.

The experimental equipment which takes advantage of temporary birefringence to study the flow consists of a channel in which the flow must be studied or into which objects are inserted, the flow around which interests us. The bounding surfaces of the channel which are parallel to the plane of two-dimensional flow which is studied in the channel consists of plane-parallel glass plates. The channel is attached to a unit which ensures the passage of the fluid and the entire set forms the hydraulic tunnel. Basically, two layouts are possible. One is a gravitational

tunnel, a combination in which the fluid flows out from the reservoir of the channel under the effect of its own weight. This tunnel can also be equipped so that the fluid that flows out is brought back to the reservoir in which a constant level is maintained. The second combination is a circulation tunnel, a closed hydraulic circuit in which a pump ensures the circulation of the fluid. The disadvantage of this layout is that the character of the flow can be affected by the vibrations caused in the fluid by the pump, which is a disadvantage, especially when transient phenomena are observed. This basic hydraulic unit has a companion optical equipment unit, a polariscope, which is entirely analogous to the polariscopes used in photoelasticity. It consists of two polarization filters (or nicols), a light source, and possibly also of a quarter-wave plate and compensator.

Two methods can be used during the measurements. We can either measure individual points in the channel or observe the entire measurement space simultaneously. The first method is time consuming, but it is useful in cases when it is necessary to determine the birefringence values in a small part of the channel (for example, in the boundary layer), especially when a low-sensitivity fluid is used or when the flow has a small velocity gradient. The cover glass of the channel has a mesh, and with the aid of the polarization equipment, the birefringence values are measured by the compensator at the points which correspond to the intersections of the mesh, or the entire polariscope is mounted on a slide bed with the aid of which the axis of the polariscope can be set in the desired position. When small parts of the channel are measured using single-ray equipment, very small changes in the position of the ray can be obtained with the aid of a rotary glass plane-parallel plate inserted in the path of the ray before the inlet to the channel. During such exact measurements, of course, it is

necessary to take into account the effect of the birefringence of the cover glasses on the values that are obtained. The basic schematic diagram of the equipment for the case when nicols and the Babinet-Soleil compensator are used, is given in Fig. 55. However, a polariscope with polarization filters can also be used and the birefringence value can be measured using a goniometric compensator, which is common practice in photoelasticimetry.

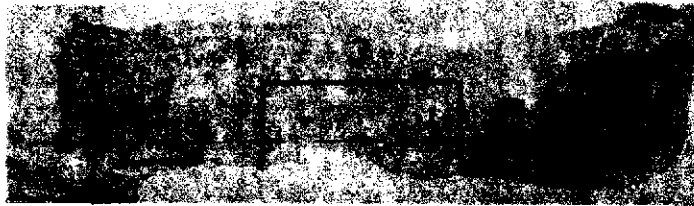


Fig. 55. Single-ray polariscope (1. light source; 2. nicol polarizer; 3. analyzed fluid; 4. compensator; 5. nicol analyzer).



Fig. 56. Polariscope for the analysis of a flow field of relatively large dimensions (1. light source; 2. condenser; 3. polarizing filter polarizer; 4 and 6. quarter-wave plate; 5. analyzed fluid layer; 7. polarizing filter analyzer; 8. objective; 9. camera).

Another method can also be used in cases when the velocity gradient and the sensitivity of the fluid are such that in the flow region analyzed birefringence occurs whose value causes a phase shift of the split rays which corresponds to several times the wavelength of the light used. Interference fringes are then formed behind the analyzer which can be photographed or plotted, and the required characteristics of the flow can then be determined from them. The schematic diagram of the optical part of the equipment used for this method is given in Fig. 56. These methods are suitable in both versions for the study of cases of plane flow. Therefore, the rays of light that are used must be perpendicular to the plane of flow during their passage through the channel.

The origin of interference fringes, for example, in fluids with undeformable particles (these fluids which have a high sensitivity are most suitable for visualization of flow using the method under consideration) can be explained as follows. The particles which have birefringent properties are arranged in the two-dimensional fluid flow by the tangential forces into rows (in the sense of their orientation distribution). A row

of such oriented particles behaves like a crystal from the standpoint of optical properties and splits the incident ray of linearly polarized light into two linearly polarized rays whose vibration directions are mutually perpendicular and lie in the orientation plane (i.e. in the plane given by the statistical orientation direction of the longer axes of the oriented particles) and in the plane perpendicular to it. The refractive index for the two vibration directions is not the same. Therefore, the split rays propagate through the fluid at different velocities c_1 and c_2 and leave it with a shift in phase. Both rays require different times for passage through a fluid layer of thickness t :

$$\tau_1 = \frac{t}{c_1} = \frac{t}{c} n_1, \quad \tau_2 = \frac{t}{c_2} = \frac{t}{c} n_2;$$

where c is the velocity of light in vacuum, and n_1 and n_2 are the absolute refractive indices of the two rays under consideration in the fluid forming the layer. Hence, the time difference is

$$\Delta\tau = \frac{t}{c} \Delta n,$$

which corresponds to a phase shift

$$\varepsilon = 2\pi \frac{\Delta\tau}{\frac{\lambda}{c}} = 2\pi \frac{t}{\lambda} \Delta n. \quad (35)$$

The analyzer, whose polarizing plane is perpendicular to the polarizing plane of the polarizer, are the two rays which have the same frequency and amplitude and are oriented in the same vibration direction so that they can interfere. The conditions which determine when the dark interference fringes will be formed follow from the following expression (36). From the graphical representation (see Fig. 57) it follows for the amplitude A_r of the emanating light that

$$A_r^2 = A_0^2 \cdot \sin^2 2\gamma \cdot \sin^2 \frac{\varepsilon}{2},$$

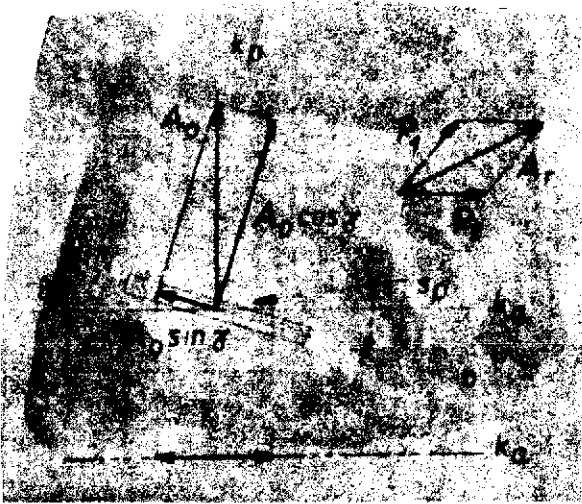
where A_0 is the original amplitude of each of the two rays, and the meaning of the angle γ is obvious from Fig. 57 (s_p denotes the direction of the flow). Since the intensity of the light is proportional to the square of the amplitude, we obtain

for the ratio of the intensity J_0 of the ray entering the fluid under consideration to the intensity J_r of the ray leaving the analyzer the relation

$$\frac{J_r}{J_0} = \frac{A_r^2}{A_0^2} = \sin^2 2\gamma \cdot \sin^2 \frac{\epsilon}{2} = \sin^2 2\gamma \cdot \sin^2 \left(\pi \frac{t}{\lambda} \Delta n \right), \quad (36)$$

where we did not take into account light absorption.

Hence, the light will vanish (dark fringes) in the following cases (we assume of course that $J_0 \neq 0$):



a) for $\gamma = 0^\circ$ or $\gamma = 90^\circ$, i.e. when the optical axis of the fluid layer has the same direction as the vibration direction of the analyzer or polarizer. The dark lines in the field of view corresponding to these conditions are called isocline lines, with the aid of which the statistical orientation direction of the particles can be determined. The isocline lines vanish when circular polarized light is used, which is obtained from linearly polarized light with the aid of quarter-wavelength plates.

187

b) the next case when the intensity of the emanating light drops to zero is given by the condition $\sin \epsilon/2 = 0$. This condition is only

satisfied when $\Delta n = 0$, i.e. when the velocity gradient $G = 0$. Thus those points in the field of view will be dark where the velocity gradient is zero. By analogy with the terminology used in photoelasticimetry, these points can be called singular points or possibly lines.

The condition $\sin \epsilon/2 = 0$ can also be satisfied according to (35) when

$$\pi \frac{t}{\lambda} \Delta n = i\pi, \quad \text{where } i = 1, 2, 3, \dots$$

87a

The points in the fluid flow where such condition is satisfied appear as dark only when observed in monochromatic light. In white light, these fringes resulting from interference at a particular wavelength become a bundle of colored interference fringes corresponding to the wavelenths of the white light components. These fringes are called isochromatic lines. Since they satisfy $\Delta n = i(\lambda/t) = \text{const}$, they are actually the locus of the points in the plane of flow at which Δn has the same value.

Assuming that relations (33) and (34), which are found experimentally in the case when the velocity gradient is perpendicular to the direction of the flow (see p. 76) can be used for the general case of flow, it is possible to determine from the isoclinic lines with the aid of the orientation angle χ the direction of the flow.

If we select a fluid for which $\Delta n = kG$, where k is a constant, the isochromatic lines connect the points with a constant velocity gradient G , since in this case $G = i(\lambda/kt) = \text{const}$ along the isochromatic line. $i = 1$ is associated with the isochromatic line which is closest to the singular line; therefore, it is called a first-order isochromatic line and the velocity gradient has the same magnitude $G = 1(\lambda/kt) = \lambda/kt$ at all points on the line; $i = 2$ is associated with the next isochromatic line (second-order isochromatic line), and the magnitude of the velocity gradient at its points is $G = 2(\lambda/kt)$.

Thus, for example, for a completely developed laminar flow between parallel plane plates, we obtain the image of the isochromatic lines in the form of a system of parallel dark fringes at equal distances from one another (see Fig. 58 a) which corresponds to a parabolic velocity profile. In the subsequent photographs (Fig. 58 b, c) are interference images obtained during the flow around a cylinder between parallel walls at a very low Reynolds number [144].

788

Since the magnitudes of the gradient can be determined on the perimeter of the streamlined bodies, the magnitudes of the frictional resistance can also be determined. During turbulent flow, the sharpness and connectedness of the fringes disappears, so that although they cannot be used to determine quantitatively the characteristics of the flow in the sense that was mentioned, they can be used to analyze transition phenomena [142].

The photographs of the interference images that are presented were made with the aid of equipment whose basic hydraulic unit consists of a simple gravitational tunnel. The channel is bounded by parallel walls. The passage from the reservoir to the channel is designed continuously by bending these walls. The sides of the transverse rectangular cross section of the channel

789



Fig. 58. Interference images obtained using the birefringence method during the flow [144]: a) flow between parallel plane plates; b), c) flow around a cylinder at a very low Reynolds number.

are: width 2 cm, depth $t = 15$ cm. Hence, the ratio of the depth to the width is 7.5. The selected ratio must be sufficiently high to suppress the effect of the forces exerted by the transparent walls of the channel on the fluid. These walls are perpendicular to the direction of the rays of the light used and parallel to the plane of the model of the two-dimensional flow which must be obtained. However, a high value of this ratio leads to difficulties during photography. The fluid that was

used was a gelatin solution in the initial gelatinized state. Hence, the motion of the gel in the channel was very slow [144].

3.2. Methods in Group 3 Which Are Suitable to Visualize the Flow of Gases

Some methods from group 3 are very often used to visualize the flow of gases, since they provide quantitative data in certain cases and are also suitable for studying flows with high (supersonic) velocities. The compressibility of gases is the property without which these methods could not be used. When these methods are used, advantage is taken of the changes in the refractive index of the gas flow caused by pressure changes and thus also changes in the density or possibly temperature. Since these changes in the refractive index cannot be seen by the naked eye, in most cases various optical apparatus is used for their visualization, and the associated methods can be classified into several main groups. In the first three groups, light refraction is the basic phenomenon which makes visualization possible. Therefore, we will call all these methods refraction methods. They are also called schlieren methods (from the German word "die Schliere"). The next two groups take advantage of light interference. Finally, the last groups include methods based on taking advantage of the dependence of the attenuation of various types of electromagnetic and corpuscular radiation on the density of the gas through which this radiation passes.

Hence, in Section 3.2 we will discuss the following methods or groups of methods:

1. the shadow method
2. diaphragm schlieren methods
3. diaphragm schlieren method with a colored image
4. interferometric methods
5. phase contrast method
6. methods based on taking advantage of the attenuation of electromagnetic or corpuscular radiation during passage through the gas flow.

These methods will be discussed in detail in Sections 3.2.1 through 3.2.6, and whenever necessary, these numbers will also be used to describe them, i.e. for example, diaphragm schlieren methods with a colored image will be called methods in group 3.2.3, etc.

In all methods from group 3.2 the information about the flow is basically obtained from the local changes in the illumination of the field of view of the observation equipment, for example, from the changes in the state when the medium is at rest. When we observe a ray of light passing through the gas layer that is analyzed (see Fig. 59) we find that if the layer is homogeneous /90

the particle is incident to the screen S at the point P at the instant t in the direction θ (characterized, for example, by the three corresponding direction cosines), whereas if there are inhomogeneities in the layer, the ray is incident at a point P* at the instant t* in the direction θ^* , which results in a local change in the illumination of the screen. Using optical apparatus, it is possible to obtain on the screen either a record of the phase shift corresponding to the time difference $\tau = t^* - t$ (methods in group 3.2.4) or a record of the deviation $\varepsilon = \theta^* - \theta$ (methods in group 3.2.2) or a record of the displacement of the track $\Delta P = \overline{P^*P}$ (methods in group 3.2.1) or possibly a combination of these records. The corresponding τ , ε and ΔP must then be found from the records, and from these the local values of the absolute refractive index $n = n(x,y,z)$ of the object through which the rays pass. From the values n that were found, the local density values of the object can be calculated, and from these, subsequently, other data.

To obtain results which will aid in evaluating quantitatively the images of the flow obtained by the methods in group 3.2, we will use the following arguments.

Suppose that a bundle of parallel rays passes through a medium which is bounded by the two parallel planes 1 and 2 at a distance $x_2 - x_1$ from one another. The incident rays are perpendicular to plane 1, which is closer to the light source, and they are parallel to the direction of the X axis of a rectangular Cartesian coordinate system. The optical properties of the medium are characterized by the absolute refractive index n of the light used. Suppose that the medium has such inhomogeneities that n changes continuously in the planes which are perpendicular to the X axis and does not change in the directions which are parallel to the X axis, hence, we have a plane field, i.e. $n = f(y,z)$. The shape of the ray of light in such a medium is described by the Fermat principle, according to which the optical path of the ray is extremal. The optical path covered by the rays between two points which will be denoted by 1 and 2 since concretely we assumed that the first point lies in the plane 1 and the second in the plane 2, is given by the expression

/91

$$\int_1^2 n ds, \quad (37)$$

where ds is an elementary arc of the trajectory of the ray. This expression is a functional, i.e. generally it takes on different values on each curve connecting the points 1 and 2. According to Fermat's principle, the actual trajectory is the

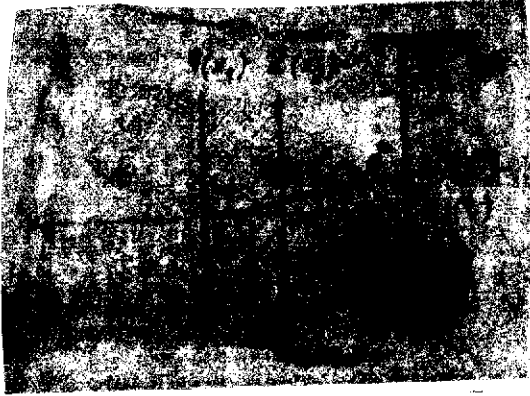


Fig. 59.

curve on which the functional (37) has an extremum. Since the necessary condition for the extremum of the functional is that its first variation vanish [20], the relation

$$\delta \int_1^2 n ds = 0. \quad (38)$$

must hold on the actual trajectory.

Expressing the trajectory of the the ray as the intersection of cylindrical surfaces

$$(39)$$

we have

$$y = f_1(x), \quad z = f_2(x),$$

$$ds = \sqrt{dx^2 + dy^2 + dz^2} = dx \sqrt{1 + \left(\frac{dy}{dx}\right)^2 + \left(\frac{dz}{dx}\right)^2} = \sqrt{1 + y'^2 + z'^2} dx$$

Hence relation (38) can be written in the form

$$\delta \int_1^2 n \sqrt{1 + y'^2 + z'^2} dx = 0. \quad (40)$$

It has been proved in the calculus of variations [20] that the function (39) for which the functional (37) has an extremum, i.e. the function satisfying condition (40), must be the solution of a system of so-called Euler differential equations. In our case, the Euler equations have the form:

$$\begin{aligned} \frac{\partial n}{\partial y} \sqrt{1 + y'^2 + z'^2} - \frac{d}{dx} \left(n \frac{y'}{\sqrt{1 + y'^2 + z'^2}} \right) &= 0, \\ \frac{\partial n}{\partial z} \sqrt{1 + y'^2 + z'^2} - \frac{d}{dx} \left(n \frac{z'}{\sqrt{1 + y'^2 + z'^2}} \right) &= 0. \end{aligned} \quad (41)$$

The expressions $y' = dy/dx$, $z' = dz/dx$ are the angular deflections of the passing light from the original direction, which was parallel to the direction of the X axis. These deflections are very small in the usual cases that will be discussed, so that their squares can be ignored in comparison with unity. (This and additional simplifications lead to errors in the quantitative evaluation, since they do not take into account the already existing deflection of the ray from the original direction in the layer that is studied. This is further compounded by the effect of the glass covers of the measurement space on the flow. The boundary layer on these walls is responsible for the fact that in concrete cases the flow in the tunnel is not exactly planar. If very accurate results must be obtained in the evaluation, these errors must be limited by means of various corrections which complicates the calculation [146, 146a]).

Ignoring y'^2 and z'^2 compared to one, equations (41) take on the form

$$\begin{aligned}\frac{\partial n}{\partial y} &= \frac{d}{dx} (ny'), \\ \frac{\partial n}{\partial z} &= \frac{d}{dx} (nz').\end{aligned}\tag{42}$$

In these equations n is independent of x , since we assumed a plane field $n = n(y, z)$, and consequently the partial derivatives $\partial n / \partial y$ and $\partial n / \partial z$ are also independent of x . However, the quantities y' and z' depend on x . Integrating each equation in (42) with respect to the variable x from $x = x_1$ to $x = x_2$, we obtain:

$$\begin{aligned}\frac{\partial n}{\partial y} (x_2 - x_1) &= n[y'(x_2, y, z) - y'(x_1, y, z)], \\ \frac{\partial n}{\partial z} (x_2 - x_1) &= n[z'(x_2, y, z) - z'(x_1, y, z)].\end{aligned}\tag{43}$$

The relations that were obtained can be further simplified formally. As a consequence of the assumption that the incident rays are perpendicular to plane 1 (the plane $x = x_1$), $y'(x_1, y, z) = 0$, $z'(x_1, y, z) = 0$. Therefore, without making an error we will write henceforth, for brevity, y' instead of $y'(x_2, y, z)$ and similarly z' instead of $z'(x_2, y, z)$. Of course,

we must remember that y' , z' now mean the angular deflections of the ray passing through plane 2 (the plane $x = x_2$) at the point with the coordinates x_2 , y , z , from the direction of the X axis.

Using the notation that was just introduced, from equations (43) we obtain the relations

$$\begin{aligned}\frac{\partial n}{\partial y} &= \frac{ny'}{x_2 - x_1}, \\ \frac{\partial n}{\partial z} &= \frac{nz'}{x_2 - x_1},\end{aligned}\tag{44}$$

from which the $\partial n/\partial y$, $\partial n/\partial z$ can be determined, i.e. the y-th and z-th component of the gradients of the refractive index (the x-th component is zero, since by assumption n is independent of x) at any point of the field, provided we know from the experiment the angular deflections of the rays when they leave the layer whose thickness is $x_2 - x_1$. Although theoretically we must always substitute the local value $n = n(y, z)$ of the refractive index (which is unknown and for which we try to prove that it can be determined at least approximately), we can substitute the refractive index n_0 instead of n (in cases that will be discussed below) of the substance forming the medium flow in the case when the flow does not cause inhomogeneities in it. Hence, for example, the refractive index of the medium flow outside the inhomogeneous region that is examined can be substituted. This procedure can be justified by the fact that the value of the refractive index varies insignificantly from point to point in comparison with the change in the gradient of the refractive index. /93

If n_0 is the refractive index of the medium flow at the point with coordinates x , y_0 , z_0 , i.e. $n_0 = n(y_0, z_0)$, the relations

$$\begin{aligned}n(y, z_0) &= n_0 + \int_{y_0}^y \frac{\partial n}{\partial y} dy, \\ n(y_0, z) &= n_0 + \int_{z_0}^z \frac{\partial n}{\partial z} dz,\end{aligned}\tag{45}$$

hold, since by assumption the refractive index is independent of x . These relations are derived without any physical considerations, only on the basis of a simple mathematical argument. The relations show that if the components of the gradient of the

refractive index have already been determined (on the basis of experimental data) according to (44), by integrating them the values of the refractive index can be determined at any point of the field. In practice, of course, the corresponding integration must be a numerical or graphical integration, since the components $\partial n/\partial y$, $\partial n/\partial z$ of the gradient of the refractive index determined from the experimental data are obviously only known numerically, not analytically.

It was already mentioned that the corresponding local changes in the density of the medium flow can be inferred from the local changes in its refractive index. The relation

$$\frac{n^2 - 1}{n^2 + 2} \frac{1}{\rho} = \text{const} \quad (46)$$

is valid, where n is the absolute refractive index and ρ is the density of the transparent medium under consideration. This relation expresses the fact that, during a change in the density of the transparent medium caused, for example, by the effect of pressure, the specific refraction does not change (the Lorenz-Lorentz law). Further if the absolute index of the medium under consideration differs very little from one, for example, as in air, the left member in equation (46) can be modified approximately as follows:

$$\frac{n^2 - 1}{n^2 + 2} = \frac{(n + 1)(n - 1)}{n^2 + 2} \approx \frac{2(n - 1)}{3},$$

so that (46) takes on, in this case, the form:

$$\frac{n - 1}{\rho} = K, \quad (47)$$

where K is a constant, giving the Gladstone-Dale relation.

The value of the constant K can be determined by substituting the corresponding values for ρ and n . Thus, for example, under normal conditions (0°C, 760 torr) for sodium light at wavelength $\lambda = 0.589 \mu\text{m}$, air has a refractive index $n_0 = 1.000292$, and the density of the air is $\rho_0 = 1.293 \text{ kg}\cdot\text{m}^{-3}$, hence for air the value of the constant K is $K_0 = 2.26 \cdot 10^{-4} \text{ kg}^{-1}\cdot\text{m}^3$.

Equation (47) implies:

$$\begin{aligned}\frac{\partial n}{\partial y} &= K \frac{\partial \rho}{\partial y}, \\ \frac{\partial n}{\partial z} &= K \frac{\partial \rho}{\partial z},\end{aligned}\tag{48}$$

hence it is obvious that using equations (48) and (44) the density gradient or the density at an arbitrary point of the field can be determined directly from the values of y' , z' that were determined experimentally[4, 5, 5a, 147, 156, 162].

Let n_0 be the refractive index of air (or another gas) in the layer whose thickness is $x_2 - x_1$, and let ρ_0 be the density. If the density of the air in the layer changes to the value ρ , the refractive index of air changes to the value n . If n is greater than n_0 , the time needed for the passage of the ray through the layer in the second case (for the refractive index n) is greater than in the first case (for the refractive index n_0) by the time

$$\tau = \frac{x_2 - x_1}{c} (n - n_0),\tag{49}$$

where c is the velocity of light in a vacuum. After it leaves the layer, the ray enters in both cases the same surrounding medium in which the velocity of the light is c' , its density is ρ , and the absolute refractive index is $n' = c/c'$. In this surrounding medium, the displacement

$$\Delta s = c' \tau = \frac{n - n_0}{n'} (x_2 - x_1).\tag{50}$$

along the trajectory corresponds to the time shift τ . If we determine τ or Δs from the results of the experiment, we can determine the difference between the change in the refractive index n of air, for example, during flow, and the original refractive index n_0 of air, for example, when it was quiescent in the layer studied.

195

The necessary experimental data are obtained with the aid of various optical devices which will now be described together with a more detailed analysis of the individual methods.

3.2.1. Shadow Method

The simple refractive method uses the simplest equipment. This method is based on a phenomenon which was observed during the passage of light through transparent objects (glass objects, gas layers) with local inhomogeneities [161]. The pencil of rays entering the object at all points of its cross section with the same intensity impinges after the passage through the object on the screen with local changes in the intensity, and subsequently points with greater and smaller illumination corresponding to the inhomogeneities on the object appear on the screen (turbidities, schlieren, from the German "die Schlieren"). Certain characteristics of the flow can be determined on the basis of similar changes in the screen illuminated by the pencil of rays that passed through an airflow layer (or another gas). For example, the region occupied by the wake, the shape and type of shock wave, the local Mach number, the region of turbulent flow, etc. can be determined from their image on the screen.

The local relative change $\Delta A/A$ in the illumination A of the screen corresponding to the inhomogeneities in the air layer depends on the changes in the gradient of the refractive index at the corresponding points of the layer. This relation can be expressed approximately by expression (57) below which is derived using the following argument:

We introduce in the plane of the screen whose distance from the layer is L rectangular Cartesian coordinates y, z (we are still using the same coordinate systems and the same notation as on pages 84-89). The illumination A of the screen by the light rays passing through a layer without inhomogeneities will be described by the function $A = A(y, z)$. Now let us study the ray (Fig. 59) which is incident to the screen the point $P(y, z)$ (when there are no inhomogeneities in the layer). If there are inhomogeneities in the layer, the same ray will be incident at some point P^* with the coordinates

$$y^* = \varphi_1(y, z), \quad z^* = \varphi_2(y, z). \quad (51)$$

Assuming that the functions φ_1, φ_2 are continuous, all rays which after passage through the layer without inhomogeneities were incident at an element of area dS of the screen which includes the point P , will be incident after passage through an inhomogeneous layer at a certain element of area dS^* of the screen, which includes the point P^* . Hence, by the definition of illumination we will have, for the ratio of the illumination, $A^*(y^*, z^*)$ by the rays passing through the

inhomogeneous layer at the point P* (on the area dS*) of the screen to the original illumination A(x,y) at the point P (on the area dS)

$$\frac{A^*(y^*, z^*)}{A(y, z)} = \frac{dS}{dS^*} \quad (52)$$

The ratio dS/dS* can be expressed, as is well known, with the aid of the Jacobian of the image (51). During its calculation we will apply similar simplifying assumptions as on p. 85, i.e. we will assume that the differences $\Delta y \equiv y^* - y$, $\Delta z \equiv z^* - z$ are small, and that their first derivatives are small compared to 1, so that the products of these derivatives can be ignored. In this case we obtain, for the Jacobian J, using the identities $y^* = y + \Delta y$, $z^* = z + \Delta z$

$$J = \begin{vmatrix} \frac{\partial y^*}{\partial y} & \frac{\partial z^*}{\partial y} \\ \frac{\partial y^*}{\partial z} & \frac{\partial z^*}{\partial z} \end{vmatrix} = \begin{vmatrix} 1 + \frac{\partial(\Delta y)}{\partial y} & \frac{\partial(\Delta z)}{\partial y} \\ \frac{\partial(\Delta y)}{\partial z} & 1 + \frac{\partial(\Delta z)}{\partial z} \end{vmatrix} \approx 1 + \frac{\partial(\Delta y)}{\partial y} + \frac{\partial(\Delta z)}{\partial z}; \quad (53)$$

The expression that we obtained is obviously positive, since we assumed that the partial derivatives in it are small compared to 1, so that $|J| = J$ holds. Since $dS/dS^* = 1/|J|$ holds for the ratio dS/dS* in relation (52), we can write (52) in the form

$$\frac{A}{A^*} = |J| = 1 + \frac{\partial(\Delta y)}{\partial y} + \frac{\partial(\Delta z)}{\partial z}. \quad (54)$$

Finally, we also note that

$$\Delta y = Ly', \quad \Delta z = Lz', \quad (55)$$

holds, where L is the distance of the screen from the layer, and y', z' are interpreted as on p. 85, so that their expressions given by equations (44) can be substituted for them. We will use such an expression for y', z' but we will write it formally differently. If, in the step from equations (42) to equations (43), the integrals in the left members are only

expressed symbolically, i.e. not evaluated, equations (44) can be written 97 formally somewhat differently, namely so that we obtain from them the expressions

$$y' = \frac{1}{n} \int_{x_1}^{x_2} \frac{\partial n}{\partial y} dx, \quad z' = \frac{1}{n} \int_{x_1}^{x_2} \frac{\partial n}{\partial z} dx. \quad (56)$$

for y' and z' . If we also set in these relations $n = n_0$, a possibility we discussed on p. 88 and substitute these in relations (55) which in turn are substituted again in (54), we obtain finally the sought expression for the relative change in the illumination (the so-called contrast)

$$\begin{aligned} \frac{\Delta A}{A} &= \frac{A - A^*}{A^*} = \frac{A}{A^*} - 1 = |J| - 1 = \frac{\partial(\Delta y)}{\partial y} + \frac{\partial(\Delta z)}{\partial z} = \\ &= \frac{L}{n_0} \int_{x_1}^{x_2} \left(\frac{\partial^2 n}{\partial y^2} + \frac{\partial^2 n}{\partial z^2} \right) dx, \end{aligned} \quad (57)$$

where the first equality is valid by the definition of the contrast.

However, the use of expression (57) for a quantitative evaluation of the density field is laborious and it is not used in practice except in a few exceptional cases. See also the remarks about the results obtained using the simple refraction method on p. 96.

It follows from equation (57) that the change in the illumination on the screen occurs at those points which correspond to the points of the layer at which $[(\partial^2 n / \partial y^2) + (\partial^2 n / \partial z^2)]$ is different from zero. To simplify the discussion, let us assume for a moment that n is only a function of y , i.e.

$n = f(y)$. Then $\frac{\Delta A}{A} = \frac{L}{n_0} \int_{x_1}^{x_2} \frac{\partial^2 n}{\partial y^2} dx$, so that a change in the

illumination will not occur when $\partial^2 n / \partial y^2 = 0$, i.e. when the gradient of the refractive index is either 0 (homogeneous field) or constant $[(\partial n / \partial y) = \text{const}]$. In the first case the rays will

not change their direction, and in the second case all rays of the pencil will be deflected from the original direction which they had before the layer when they leave the layer, but always by the same angle, so that the illumination on the screen will again be uniform. If, at some point of the layer, the relative change in the gradient of the refractive index is positive [$(\partial^2 n / \partial y^2) > 0$], the rays passing through the layer at the point corresponding to the larger y are more deflected when they leave the layer than the rays passing through the point corresponding to the smaller y , and the illumination in the corresponding region of the screen will be smaller than in the case when the layer has no inhomogeneities. Conversely, if the relative change in the gradient of the refractive index is negative [$(\partial^2 n / \partial y^2) < 0$], the illumination at the corresponding point on the screen will be increased (see Fig. 60) [5, 5a]. When we take into



Fig. 60.



Fig. 61.

account equations (48) it is obvious that dark points correspond to a positive relative change in the density gradient (an increasing density gradient) and lighter points to a negative relative change in the gradient. Thus, for example, the image of a shock wave (for a comparison with the previous argument we assume that the wave propagates in the direction of the positive y axis, see also Fig. 61) obtained by this method, is formed by two fringes, a dark fringe in the front part of the wave and a light fringe in the rear part of the wave.

The changes in the illumination are naturally greater during greater relative changes in the density gradient. Therefore, this method can be used advantageously for high subsonic and supersonic velocities when relatively great changes in the density gradient induced by observable changes in the illumination can occur.

The optical equipment needed to apply the method is usually arranged in two ways: a) with a divergent pencil of rays in the measurement space, b) with a parallel pencil of rays.

The first method does not require any lenses or mirrors. In the simplest case it consists of a high intensity point light source, a screen or possibly a camera (Fig. 62). The light sources used most often are high-pressure, high-performance discharge tubes. Optically, a spark discharge was used as the source, which was obtained by discharging the condenser through the spark gap, which is still used successfully (therefore this method is also called the spark method and the photographs that are obtained, spark photographs). This method was used to obtain images of the flow around projectiles in flight [162]. Spark illumination is still the most convenient means for the study of projectiles in flight, and it can also be used to study the motion of unstable pressure waves. Other light sources can also be used, such as arc lamps, bulbs and discharge tubes [146, 146a, 154, 155].

When a divergent beam of light is used, a magnified image is obtained. The best results were achieved with enlargements not exceeding 1.5 [153]. For small objects, for example, bullets from a rifle, a satisfactory distance of the screen or the film from the object is 15 cm, and of the spark, the light source, from the object, it is 1.2 m. However, the last distance can be up to 5 m when relatively large measurement spaces in tunnels are lit through.

/99

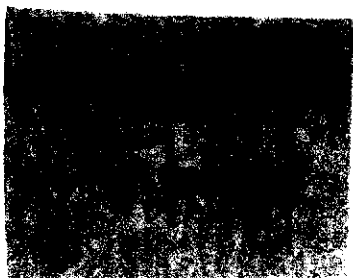


Fig. 62. Schematic diagram of simplest equipment for shadow method with divergent beam of light (1. light source; 2. analyzed gas layer; 3. screen).

Besides the advantages that can be obtained with the aid of enlargement, it is limited in all respects by the divergent rays, only to the use on objects and a field with a small span in the direction of the rays (projectiles, airplane bodies, propeller tips, etc. whose longer side is perpendicular to the direction of the rays).

To obtain images of the two-dimensional flow, the observed layer of air must be lit through by a parallel pencil of rays. To the

previous version, one lens or concave mirror is added (Fig. 63) and the light source is placed at their focus. The selected focal length should be as short as possible, to obtain with the given light source a high illumination on the screen. However, this must be done without detriment to the uniformity of the initial illumination on the screen and the sharpness of the images of the inhomogeneities. A reduction in the sharpness depends indirectly on the focal length f_1 , directly on the distance L of the inhomogeneity from the screen or film, and also directly on the

diameter d of the light source [174]. The sensitivity depends directly on the distance L . Since d cannot be reduced without limit, f_1 must be selected taking into consideration these factors. In some cases, it is advantageous to focus on the screen or the photographic plate (film) some plane inside the measurement space with the aid of another lens.

The lenses or mirrors used must be of first-class quality and defects in them must be corrected to prevent nonuniform illumination of the screen. Nevertheless, an instrument with cheap Fresnel lenses pressed from organic glass has been constructed. In some special cases, satisfactory results were obtained with the aid of this instrument [150].

Figs. 64 through 67 show photographs that were obtained by the shadow method.



Fig. 63. Schematic diagram of equipment for shadow method with parallel light beam (1. light source; 2. lens; 3. analyzed gas layer; 4. screen).

region of turbulent flow than in the laminar flow region, and the vaporized oil changes the refractive index more substantially in the turbulent boundary layer whose image is therefore clearer.

The oscillations of shock waves can be studied with the aid of an interrupted light source (stroboscope) [154, 158]. Although obtaining quantitative data about the distribution of the density in the observed field on the basis of photographic measurements or photographs is not sufficiently reliable and requires a great deal of care and caution during the technical photographic work, data about the distribution of the density near the front of a shock wave can be obtained [146, 162, 156].

This method was used subsequently to study the shape of three-dimensional shock waves and to obtain data about the processes that occur in them [165]. It is also used together with the so-called method of hot wires and other similar methods (see pp. 46 and 59). It was also used to obtain images of the flow around parts of an airplane during flight [168] and also to determine the state of the boundary layer and of the transition regions [159, 164]. Sometimes a very thin layer of volatile oil is applied to the surface of the streamlined body for this purpose [146a]. The oil vaporizes faster in the

/100

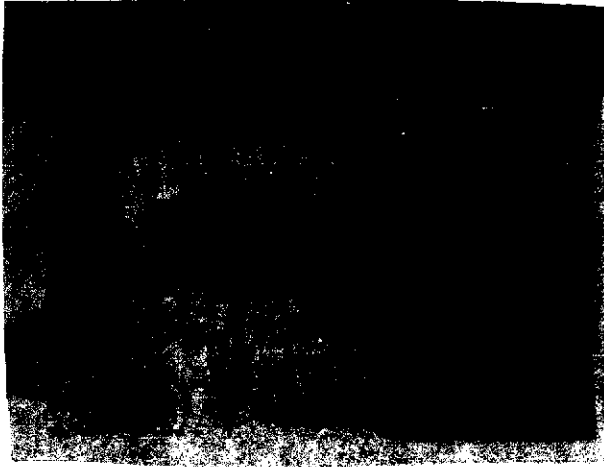


Fig. 64. Photograph obtained using shadow method during flow around a wing [5].



Fig. 65. Shadow image obtained during the study of the flow field around a projectile [146].

In other experiments that were carried out to obtain quantitative data about the density distribution in the entire observed layer a two-dimensional mesh (with square openings) is placed in front of the observed object in the direction of the light rays and the distortion in its image on the screen behind the observed object is used as the basis to determine the inhomogeneities in the object [162].

/102

The shadow method can also yield certain quantitative data about turbulence. When the turbulent layer is lit through, the local changes in the density have a similar effect on the passing, originally parallel rays as small converging and diverging lenses. The field with the local differences in the illumination is obtained on the screen placed immediately behind the layer in this manner (Fig. 68). The continuity of this illumination field and the density field have been described by mathematical relations, whose analysis makes it possible to determine certain statistical properties of the fluctuations in the density in the layer that is examined [146, 166].

A method for the study of three-dimensional flow has also been developed [170, 165].

3.2.2. Diaphragm Schlieren Methods

In addition to the qualitative data similar to those obtained by the previous method, it is possible to obtain more easily and better quantitative data about the distribution of the density in the entire region under consideration, i.e. for



Fig. 66. Shadow image of flow field in cascade. The photographs were included with the kind permission of the author [164].

example, to determine the density field in a two-dimensional gas flow layer, by using various versions of diaphragm schlieren methods. The method used most frequently to set up the optical apparatus is evident from Figs. 69 and 70. It is the so-called Toepler principle [173]. From the photographs obtained with the aid of diaphragm schlieren methods, it is possible to determine y' and z' by measuring the blackening (see p. 85) and subsequently from this the density gradient and the density field. However, diaphragm methods are used more frequently only to obtain basic data about the flow, mainly about shock waves, expansion and wake regions, and about the boundary layer. /103

A high-intensity light source, whose dimensions are small, is used. The source is placed in the focal plane of the first lens or mirror (Fig. 69), (or the source is lit through by the condenser at the slit at the focus of the first lens, in which case the light area of the slit is considered as the source).

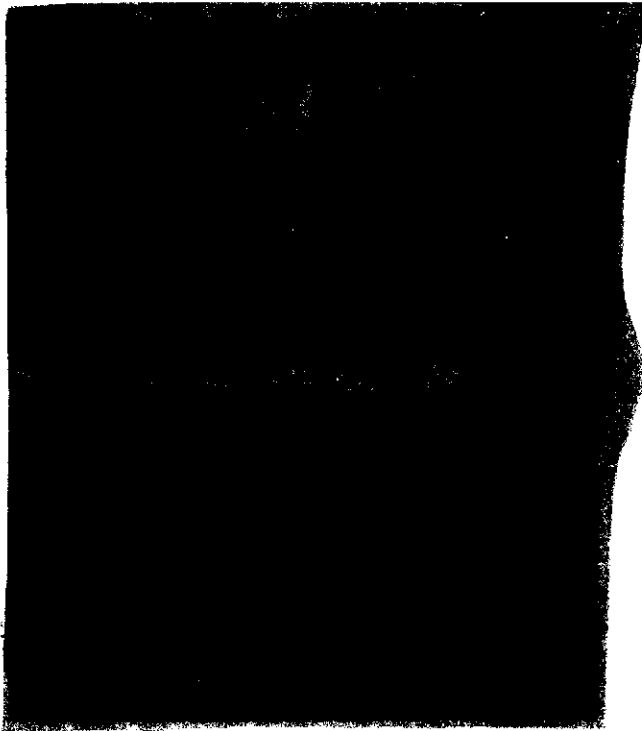


Fig. 67. Effect of exposure time during the shadow method [1]:

- a) exposure time $1/300$ sec;
- b) exposure time 10^{-5} sec.

The unstable oscillating character of the shock waves can be inferred from the sharper images of the shock waves in b) (during a very low exposure time).

screen. The reduction in the illumination depends on how large the part of the image of the light source is shaded by the diaphragm, i.e. (see Fig. 69) on the distance a of the edge of the diaphragm from the vertical axis of the equipment.

If the examined layer has inhomogeneities, the rays passing through these points are bent, and the corresponding part of the image of the source is displaced from the original point through a distance Δs . This of course changes the illumination at the corresponding point on the screen. We will now analyze, with the aid of Fig. 69, this case in greater detail [171, 174].

We will consider a light source with a slit whose width is b , whose height is h with luminance E , placed in the focal plane of the lens C_1 with focal length f_1 . If the area of the lens C_1 illuminated by the source is S , we derive easily, on the basis

If the layer is homogeneous a pencil of straight parallel rays passes through the layer that is examined (the measurement space in the tunnel). Then the second lens placed behind the measurement space forms the image of the light source in its own focal plane and the image of the measurement space which contains, for example, the studied model is obtained on the screen or the camera film. Lens C_3 is used to form the image. If the source has the same luminance at any point, the illumination on the screen where the rays impinge will be the same at all points. Now if, for example, a knife diaphragm (a diaphragm with a straight edge) is placed in the focal plane of the second lens in such a way that it intercepts a part of the rays incident to the screen or film, their illumination is reduced, but is again the same at all points on the illuminated area of the

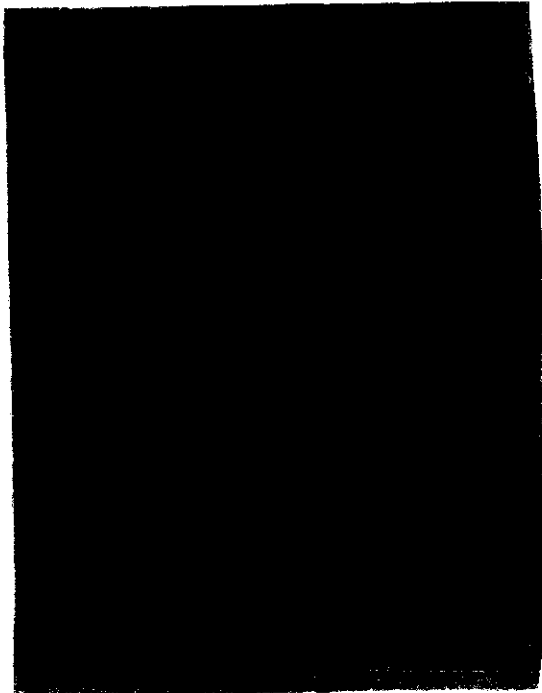


Fig. 68. Shadow image of wake [146].



Fig. 69. Schematic diagram of equipment for diaphragm schlieren method.

the dimensions $h' = h(f_2/f_1)$, $b' = b(f_2/f_1)$, where f_2 is the focal length of lens C_2 .

Suppose that the center of one of the longer sides of the (rectangular) source with the slit lies at the focus F_1 of the

of the definition of the luminance of the source for the approximate value Φ of the luminous flux incident at the lens C_1 the expression

$$\Phi = \frac{EbhS}{f_1^2} \quad (58)$$

If we ignore the effect of the losses and take into consideration that the rays arrive from the source to the screen only with small angular deflections from the direction of the optical axis of the entire equipment, then in the case when the diaphragm is outside the pencil of rays the same luminous flux Φ also impinges on the screen. The initial illumination of the screen, whose illuminated area is S' is therefore

$$A_0 = \frac{\Phi}{S'} \quad (59)$$

Denoting the linear enlargement obtained using the optical system that was described by m , we have $S'/S = m^2$, so that using (58) and (59), we obtain

$$A_0 = \frac{Ebh}{m^2 f_1^2} \quad (60)$$

The image of the source with the slit in the focal plane of the lens C_2 has



Fig. 70. Simplified schematic diagram of apparatus for diaphragm schlieren method: a) with mirrors; b) with one principal lens (1. light source; 2 and 2'. mirrors or possibly lens; 3. analyzed layer; 4. knife diaphragm; 5. screen).

At the bottom of the diagram is the schematic diagram of the light source in the case when a spark discharge is not used (as for example in Fig. 72 a, b), but an arc lamp or discharge tube is used (6. arc lamp or discharge tube; 7. condenser projecting the luminous discharge into the slit 1', 1' slit at the first focal point of the first mirror or lens; the light area of the slit is considered as the light source for the equipment). The objective is inserted between diaphragm 4 and screen 5, with the aid of which the image of the selected plane in the analyzed layer is formed on the screen or photographic plate.

lens C_1 . Then the center of the longer side of the image of the source lies at the focus F_2 of lens C_2 , and the image is on the side of the optical axis opposite to the source with the slit. Both sides that were mentioned are parallel.

Now if we shade a part of the image of the source by the knife diaphragm in such a way that the height of the image is equal along the entire length to the distance a of the edge of the diaphragm from the optical axis of the entire equipment (the edge of the diaphragm is parallel to the width b of the source with the slit!) the illumination on the screen is reduced from the value A_0 to the value A for which the relation

$$\frac{A}{A_0} = \frac{a}{h'} = \frac{af_1}{hf_2},$$

holds, so that in view of (60), we have

$$A = \frac{Eba}{m^2 f_1 f_2} \quad (61)$$

If the layer examined has such inhomogeneities that at certain points of the layer the component of the gradient of the refractive index which is perpendicular to the

edge of the diaphragm exists and is different from zero (if the edge of the diaphragm is parallel to the Z axis it is the component $\partial n/\partial y \neq 0$), the rays passing through these points will be curved. The rays which leave the layer then are deflected from the original direction by the angle ε whose tangent is equal to the quantity y' , which can be expressed either using the first equation in (44) or with the aid of the first equation in (56), obtaining:

$$\tan \varepsilon = y' = \frac{1}{n_0} \int_{x_1}^{x_2} \frac{\partial n}{\partial y} dx,$$

where $n = n(y, z)$ is the local refractive index in the layer and n_0 is interpreted as on p. 88, i.e. n_0 is the refractive index of the substance forming the flow medium in the case when the flow does not cause inhomogeneities in it. With regard to the direction of the Y axis it is considered to be the same, so that it is perpendicular to the edge of the diaphragm, i.e. perpendicular to the width d of the light source with the slit to which the edge of the diaphragm is parallel by hypothesis.

The displacement of the ray that has just been considered, which corresponds to a deflection of the ray by the angle ε from the original direction takes place in the plane perpendicular to the edge of the diaphragm, so that the corresponding parts of the image of the source in the focal plane of lens C_2 are shifted in the direction of the Y axis through the distance $\Delta s = f_2 y'$. This, of course, changes the illumination at the corresponding points on the image of the layer of the screen by the amount

$$\Delta A = \frac{f_2 y'}{f_1} A_0 = \frac{E b y'}{m^2 f_1}, \quad (62)$$

where the last equality is valid because of (60). The changes in the illumination will again, as before (see p. 93) be evaluated by the relative change in the illumination, the contrast, which we now denote by the symbol B . Using relations (62) and (61) we obtain for the contrast the expression

$$B = \frac{\Delta A}{A} = \frac{f_2 y'}{a} = \frac{\Delta s}{a}. \quad (63)$$

The change in the contrast caused by a unit deflection of the ray is the so-called sensitivity of the equipment C. Hence, according to (63), it is

$$C = \frac{dB}{dy'} = \frac{f_2}{a}, \quad (64)$$

where the first equality holds on the basis of the definition of the sensitivity C that was given. The possibility of increasing the sensitivity by changing the distance of the edge of the diaphragm from the optical axis of the entire equipment which follows from the above is limited due to diffraction phenomena causing changes in the illumination of the screen which do not correspond to the inhomogeneities in the examined layer and also do not correspond to the arguments that have been presented and which are based on ray optics. The effect of the diffraction phenomena does not matter during observations of a qualitative nature, so that for these purposes highly sensitive devices can be used; however, the fidelity (accuracy) of the quantitative measurements is reduced (especially those based on the measurement of changes in the illumination) which limits their use to cases in which a lower sensitivity is sufficient [162, 175, 180]. /107

Equation (62) is no longer valid when the image of the source (formed by the lenses C_1 and C_2 in the focal plane of the second lens) or a part of it is shifted entirely outside the diaphragm, or if the entire image is on the diaphragm. If this occurs, the image of the observed field (or a part of it) on the screen will have the illumination A_0 given by equation (60) or the illumination will be zero. This will also occur during larger deflections about which additional information cannot be obtained from the image on the screen. The largest possible shift of the image of the light source (or a part of it) which does not lead to a loss in sensitivity is, for $a = h'$, equal to the height of the image $h' = (f_2/f_1)h$ (Fig. 69). This corresponds to the deflection of the ray

(65)

$$y_{\max} = \frac{h}{f_1},$$

since

$$f_2 y_{\max} = \frac{f_2}{f_1} h = h'.$$

Similarly, for $a < h'$, the largest shift of the image of the source (or a part of it) in the direction away from the optical axis toward the edge of the knife diaphragm is a , which corresponds to the ray deflection

$$(y'_{\max})_{\text{toward the edge}} = \frac{a}{f_2},$$

since

$$f_2(y'_{\max})_{\text{toward the edge}} = a,$$

and the largest possible shift in the direction away from the edge toward the optical axis is $h' - a$, which corresponds to a ray deflection

$$(y'_{\max})_{\text{from edge}} = \frac{h}{f_1} - \frac{a}{f_2},$$

since

$$f_2(y'_{\max})_{\text{from edge}} = \frac{f_2}{f_1} h - a = h' - a.$$

If the same maximum range must be achieved for both these deflection directions, the diaphragm must be set so that it intercepts exactly one-half of the image of the light source, i.e. we must have $a = h'/2$, or, taking into consideration (65),

/108

$$a = \frac{hf_2}{2f_1} = \frac{1}{2} f_2 y'_{\max}. \quad (66)$$

We then have, for the sensitivity (64),

$$C = \frac{2}{y'_{\max}}. \quad (67)$$

From the above it follows that the maximum sensitivity that can be achieved for the given deflection range is inversely proportional to this deflection range and that it does not depend, for example, on the intensity of the source, etc. The feasible deflection range can be increased by increasing the height h of the light source with the slit or by reducing the

focal length f_1 of the first lens C_1 (or mirror), which follows from equation (65).

Now, substituting z from equation (66) in equation (61) we obtain for the illumination on the screen the relation

$$A = \frac{Eby'_{\max}}{2m^2f_1} = \frac{1}{2} A_0. \quad (68)$$

The guidelines for the design of the necessary optical equipment follow from the considerations of an approximate character that were given above. The most important parts are the two lenses C_1 and C_2 or the corresponding mirrors. From an optical standpoint, their quality must be high so that the inaccuracies arising during the refraction of light (or reflection in the case when mirrors are used) should not cause deflections of a smaller order of magnitude than the deflections caused by the inhomogeneities that are examined. The spherical and chromatic aberrations in the lens must be corrected as much as possible. The glass must be free of inhomogeneities, since all its local imperfections are observed on the screen. The objective of an astronomical telescope is most suitable for this purpose.

Compared to lenses the advantages of mirrors are that they do not have a chromatic aberration, that the inhomogeneities inside the glass do not matter and that mirrors with relatively large diameters are cheaper than lenses with the same diameter, since only one surface is treated in a mirror. An aluminum metal plating on the surface of the mirror is better than a silver plating, since it is more durable and the oxidized aluminum layers are transparent.

The focal length of the lens C_1 must be as small as possible, since this increases not only the feasible range, which is evident from equation (65), but also for the given enlargement the initial illumination on the screen, as shown by equations (60) and (68). This will also make it possible to use a large enlargement for the given illumination, which improves observation by the naked eye and facilitates a more precise adjustment of the apparatus. However, the selection of the smallest f_1 is limited by the requirement that a homogeneous pencil of parallel rays be obtained behind the lens C_1 . To obtain uniform illumination of the image of the source within 1% limits, the rays must enter the lens C_1 at a vertex angle which is smaller than 8° [171]. A similar limitation also applies to the use of mirrors. This requirement must also be satisfied by the second lens or mirror. A large focal length of the lens C_2 will increase the sensitivity of the equipment as shown by equation (64); however, when the equipment is adjusted

/109

for the maximum possible range it has no effect, according to (68), on the illumination, according to (65) on the range, and according to (67) on the sensitivity. The above gives the conditions for the selection of the lenses (mirrors).

Next, the properties of the light source must be selected so that the necessary enlargement is obtained without exceeding the feasible range. For this purpose, the maximum values of the deflections y' , z' which occur in various inhomogeneities in the gas flow must be known. It was established [174-176] that deflections greater than 0.005 rad occur very seldom. This means that if we take the value that was given as a bound, the height h of the source can be calculated from equation (65), since y'_{\max} and f_1 have already been selected. The initial illumination on this screen can then be increased by widening the source and also by choosing the smallest enlargement m at which details can still be distinguished.

The requirement of a high value of the initial illumination on the screen is justified by the fact that the observer's eye works in the maximum sensitivity range where it observes the relative changes in the illumination, the contrast. The eye actually reacts to changes in the brightness on the screen and when the basic value of the brightness on the screen is on an order of magnitude less than 3 nt [sic], the sensitivity of the eye to discriminating the contrast drops [174]. Hence, the minimum value of the initial (basic) illumination of this screen will be about 32 lux [174]. From these data and from the previously selected values, the necessary luminous power of the source can be determined, see equations (58) and (61).

When mirrors are used instead of lenses, the fact must be taken into account that both the source and the diaphragm are located outside the optical axis, so that the surface of the mirror should be taken, strictly speaking, as the surface obtained by rotating a parabola about an axis which is not identical with the axis of the parabola. However, normal parabolic and spherical mirrors are also used (with a focal length to aperture ratio greater than 10), since they can be obtained more easily and cheaper. To reduce the defects in the optical equipment when these mirrors are used, the angles α and β are selected as small as possible and equal or nearly equal (see Fig. 70a).

The source and the diaphragm are on opposite sides of the optical axis (of course, very close to it or in its immediate vicinity). This reduces both the astigmatism and the coma. It is advantageous if the equipment is adjusted so that the image of the source is deformed, as a result of the effect of the astigmatism, only in the direction parallel to the edge of the diaphragm.

The distance between the mirrors (or lenses) should be as small as possible to limit as much as possible the effect of the inhomogeneities of the surrounding medium between the mirrors. When mirrors are used, it is of course difficult from a design standpoint to reduce this distance, as in the case of lenses, so that the value of the distance between the mirrors fluctuates around twice the focal length of the mirror.

The light source must be placed exactly in the focal plane of the first mirror or lens. This can be achieved either by measuring the diameter of the pencil of rays between the lenses (mirrors) or the reflected image of the source on the screen placed for this purpose in the immediate vicinity of the source. A plane mirror is used for the reflection, which is inserted between the lenses (mirrors). The diaphragm must also be placed exactly in the focal plane of the second lens (mirror) and it must be positioned so that it can be adjusted exactly with the aid of micrometer screws and the distance a can be measured exactly. The edge of the diaphragm and the edges of the opening (source) must have the smallest possible unevennesses. Similarly, the lens or mirrors must be mounted on suspensions so that their position can be adjusted exactly, and the suspensions must be sufficiently rigid. This entire optical system as a whole must be as rigid as possible to prevent spontaneous changes in the position of its parts. In addition, the possible rotation of the entire optical system or the source together with the diaphragm about the optical axis must be kept in mind. This requirement occurs in certain methods used to obtain quantitative data.

/110

The activity of the tunnel can affect the adjustment of the equipment. Therefore, it is sometimes necessary to make the final adjustment under normal operating conditions in the tunnel [5, 5a].

It is important that the axes of the source with the slit and of the diaphragm be parallel. To achieve this, for example, a microscope can be used and the image of the source on the screen can be observed through it, or the image of the source and the diaphragm can be focused with the aid of the modified lens C_3 on the screen (by exchanging it). The normal task of the lens C_3 is to form the image of the inhomogeneity on the screen or the photographic plate or film. In the last two cases, the lens C_3 is the objective of the camera which is focused on the plane which is perpendicular to the light rays and cuts the measurement space in half.

Fig. 71 gives an outline of the equipment that was used successfully, which consists of two systems, a lens and mirror system [174], so that the practical adjustment of the optical

/111

equipment for the diaphragm refraction method can be well illustrated on it. The largest linear dimension of the observation field in the tunnel is 22.5 cm. The mirror system has two spherical mirrors with a 23.75 cm diameter and a focal length of 2.7 m, so that the apex angle of the conical pencil of rays is approximately 12° . The lens system which is used to observe details has two lenses with a 5 cm diameter and a focal length of 35 cm and it is mounted on a carriage so that its axis can be adjusted in any position along the measurement space, possibly so that the functioning of the mirror system is not disturbed. Both sets of equipment can also be used to obtain photographs with the aid of the shadow method on a photographic plate inserted behind the measurement space in the direction away from the source. The light source used for visual observation is the filament of the projector bulb, and for photography, the electric spark discharge with a duration on the order of 10^{-6} sec, obtained by discharging a condenser with a capacity of 0.01 μF charged to 20 kV. Using two different electrode arrangements, a slit and circular (approximately point) light source can be obtained. In the first case, two plane (metal sheet) 1 mm thick electrodes were clamped between two glass plates so that the ends of the electrodes were at a distance of 7 mm from one another, giving the 1×7 mm source with the slit drawn in Fig. 72. The arrangement of the electrodes for the point source used to obtain photographs with the aid of the simple refraction method is analogous. This arrangement provides a source with greater luminance than the source with a slit. It is also suitable, when greater sensitivity is required, but mainly for high quality observation, since the width of the image of the source changes during the displacement along the diaphragm, and hence also the sensitivity changes. The possibility of using as the light source a laser is discussed briefly on p. 147.

The equipment used widely in Czechoslovakia is a product of the Zeiss-Jena plant (Schlieren aufnahmegerat 80 [schlieren camera-80]) which can also be used to carry out the measurements using the grid and dye method (see pp. 114 and 119). Here the maximum diameter of the observed field is 80 mm [204] (Fig. 73 a). However, equipment for which the diameter of the observed field is 10 times as large is also being designed [194].

/112

In addition to such types of optical equipment of a basic character, systems which furnish stereoscopic records have also been designed [183, 184]. Such a system consists of two basic mirror systems by means of which the corresponding rays intersect inside the measurement space. The axes of the two systems deviate by a small angle from the perpendicular to the cover glass of the measurement space of the tunnel and lie in the same plane containing this perpendicular. The two corresponding cameras are focused on the plane where the rays from the two systems intersect. Another modification of the basic system

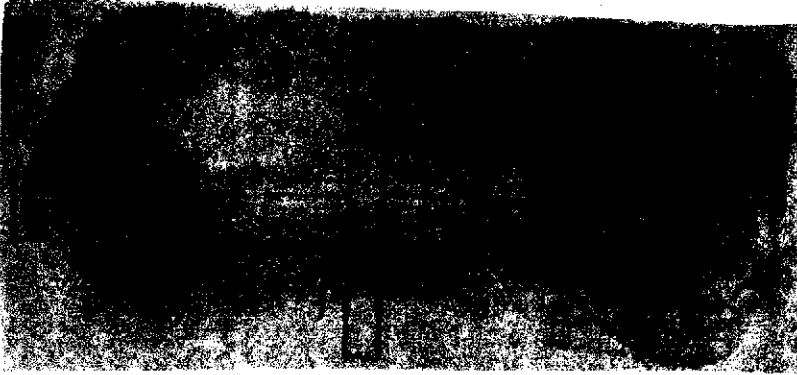


Fig. 71. Schematic diagram of equipment for the diaphragm method, consisting of two systems: a mirror system for the study of the entire cross section of the measurement space, and a smaller system attached to a displaceable optical bench, which is used for the study of details. When the independent mirror system is used, the equipment can also be used for the shadow method, by inserting the screen in the position marked in the diagram by the line 5 (1. light source of mirror system; 2. light source of small instrument; 3. screen, focusing screen or photographic instrument; 4. measurement space).

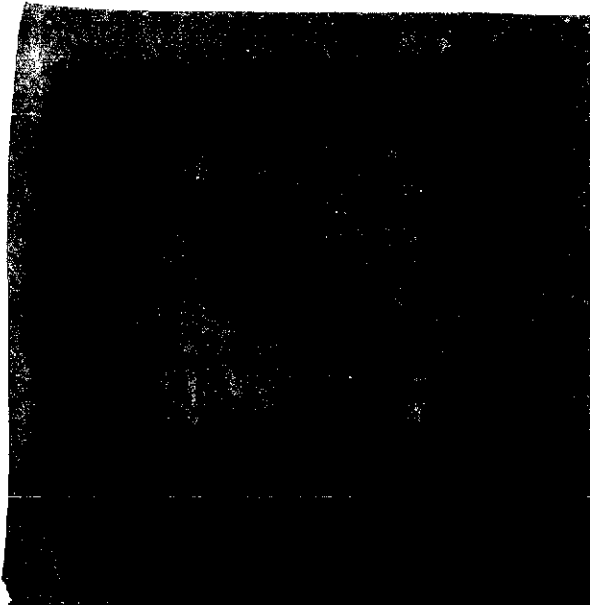


Fig. 72. Schematic diagram of the arrangement of electrodes for spark (discharge) sources of light (1, 2. electrodes).

makes it possible to determine the measurements in the selected planes of the measurement space through exact focusing [177].

To increase the sensitivity, the instruments were modified for two passages of the rays. It is particularly important to increase the sensitivity of the method during measurements at low pressures. However, it was observed in nitrogen at a density of $1.5 \cdot 10^{-3} \text{ kg} \cdot \text{m}^{-3}$ that even at such extremely low values, the shock wave can still be determined by the diaphragm method. At pressures equal to several percent of an atmosphere at which

/113

the equipment that was described can no longer be used, the sensitivity can be increased by adding sodium vapors to the air flow [197].

Often it is necessary to obtain simultaneously a record using two cameras or possibly a motion picture camera and also to study the image of the observed field on the screen. This can be achieved not only by splitting the rays immediately behind the light source, but also by having a mirrored surface



Fig. 73a. Schematic diagram of instrument manufactured by the firm Zeiss-Jena, GDR (Schlierenaufnahmegerat-80 [schlieren camera-80]) used in diaphragm methods [204]. 1. arc lamp or high-pressure mercury discharge tube; 2. condenser; 3. slit at focus of first principal lens; 4, 5. analyzed layer; 6. second principal lens; 7. image focal plane of second principal lens; 8. knife diaphragm; 9 and 10. objectives forming the image of the selected plane 5 in the analyzed layer on the focusing screen 11 of the camera built into the instrument; 12. folding mirror which can be used to reflect the rays through the objective 13 to the screen 14 for visual observation.

The U-shaped arrangement of the optical axis of the instrument with the aid of the plane mirror is of no basic significance. However, much smaller dimensions of the instrument and greater rigidity of the frame are obtained in this manner.

on the knife diaphragm. Additional images are obtained taking advantage of the reflection on the diaphragm [198, 199].

In addition to this more complex equipment, instruments are also used with one principal lens or mirror, in which the rays of the pencil passing through the medium that is examined are not parallel. The light source, its image and also the diaphragm are not in the focal planes (Fig. 73 b). An instrument

based on a similar principle with a single mirror has also been used in Czechoslovakia [209].

When we determined quantitatively the requirements on the design of the optical equipment and evaluated the properties of such equipment, we only considered a light source with a slit with a constant height h and a constant width b , which was parallel to the straight line edge of the knife diaphragm. This arrangement by means of which we want to obtain the quantitative data is most suitable for the measurements and therefore has been used most frequently. However, any other shape of the source can be used provided a diaphragm with a corresponding shape is used at the same time, for example, a circular source and a circular diaphragm having the shape of a small opaque disk.

One possible source is a source given by the shape of a filament in a bulb. The corresponding diaphragm for the source is obtained by inserting the photographic plate at the place where the image of the source is formed, i.e. in the focal plane of the second lens or mirror, where it is exposed and, after it is developed, inserted in the same plate where it serves as a diaphragm. Hence this is a procedure with an initial dark field (the dark field on the screen) since only those rays which were not curved in the observed medium pass through the diaphragm (if we ignore diffraction phenomena).

/114

Circular shaped sources and diaphragms with a circular aperture with the same diameter as that of the image of the source at the point of the diaphragm have also been used. Hence, during the initial adjustment, the illumination on the screen was at a maximum.

When irregularly shaped sources and the corresponding diaphragms are used, the records obtained on the screen do not correspond to the deflections of the rays only in one direction (as in the case when a light source with a slit and a knife diaphragm are used), but the rays are deflected in different directions when they are formed. Therefore, the evaluation of such records is laborious and difficult. In addition to this, the effect of the astigmatism of the system cannot be eliminated as in a source with a slit.

During the observation of objects with large gradients of the refractive index, a low sensitivity of the equipment must be selected which, however, may not be adequate to record the small gradients that can occur simultaneously in the observed object, or a greater sensitivity can be selected, but on the other hand, the feasible range can be exceeded so that information about points with large gradients is not obtained. The solution (with certain exceptions) can be obtained either on the basis of two photographs obtained with a low

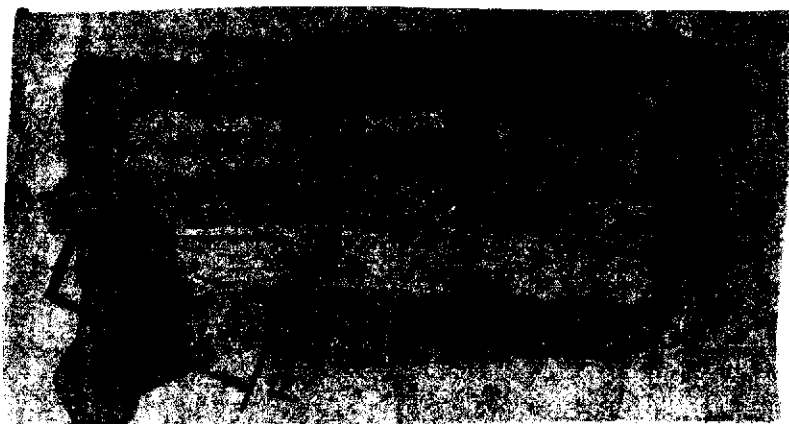


Fig. 73b. Schematic diagram of instrument manufactured by the firm Dätwyler, Switzerland used in the diaphragm method [147, 209]. (1. discharge tube; 2. condenser; 3. slit in first focal plane of mirror 10; 4. prism reflecting beam of rays through analyzed layer 13 to spherical mirror 10; the reflected rays again pass the measured layer and are shifted by prism 5 to the original direction of the optical axis; 6. knife diaphragm placed near image focal plane of the mirror 10; rotary prism reflecting rays either through objective 8 and plane mirror 11 to the screen 12, or through objective 9 to the projection screen).

and high sensitivity, where the observed object must have the same character in both cases, or with the aid of an exponentially expanding slit placed in such a way that the axis of symmetry of its image in the plane of the knife diaphragm is perpendicular to the edge of this diaphragm, or possibly a wedge filter can be used instead of the diaphragm (see p. 122) [178]. An L-shaped source with a slit is also used (two mutually perpendicular slits) and a corresponding L-shaped diaphragm [175]. However, in this case, it is necessary to take into account the fact that sharp images of each arm of the source (for example, the horizontal and vertical arm) are

obtained at different distances from the source as a result of the effect of the astigmatism, and therefore the diaphragm must be arranged accordingly. The mutual distance between the two images that were mentioned is on the order of several tenths to 1 mm in the commonly used systems. Sometimes, the diaphragm is replaced by a grid or only a single filament.

Two basic methods can be used to obtain the numerical values of the local refractive index and the local density in the layer that is analyzed with the aid of various types of diaphragm schlieren methods. In the first method, primarily equipment with a source with a slit and a knife diaphragm is used and the calculations are based on equations (44), (48), and (63). The following relations for the relative change in the illumination $(\Delta A/A)_y$ caused by the deflection of the ray in the direction of the Y axis and for the relative change in the illumination $(\Delta A/A)_z$ caused by the deflection of the ray in the

direction of the Z axis are obtained from these equations:

$$\begin{aligned} \left(\frac{\Delta A}{A}\right)_y &= \frac{f_2}{a} \frac{x_2 - x_1}{n_0} \frac{\partial n}{\partial y} = k_n \frac{\partial y}{\partial n} = k_n K \frac{\partial \rho}{\partial y} = k_c \frac{\partial \rho}{\partial y} \\ \left(\frac{\Delta A}{A}\right)_z &= \frac{f_2}{a} \frac{x_2 - x_1}{n_0} \frac{\partial n}{\partial z} = k_n \frac{\partial n}{\partial z} = k_n K \frac{\partial \rho}{\partial z} = k_c \frac{\partial \rho}{\partial z} \end{aligned} \quad (69)$$

where K is the constant from equation (47) and

$$k_n \equiv \frac{f_2}{a} \frac{x_2 - x_1}{n_0}, \quad k_c \equiv k_n K \quad \text{are also constants. Equations (69) imply that}$$

the contrast, i.e. the local relative change in the illumination on the screen or photographic plate is proportional to the component of the gradient of the refractive index or the density gradient at the corresponding point of the layer which is perpendicular to the edge of the diaphragm. Hence, if the edge of the diaphragm is parallel to the Z axis, the contrast $(\Delta A/A)_y$ appears on the screen or photographic plate, from which we can determine the y-th component of the gradient of the refractive index and the density gradient, i.e. $\partial n/\partial y$ and $\partial \rho/\partial y$. Now if we rotate the entire optical system about its optical axis through a 90° angle, we will record the contrast $(\Delta A/A)_z$ from which we determine the z-th component of the two gradients, and from the y-th and z-th components of the gradient we can determine the final value of the gradient of the refractive index and the density gradient, and from these, according to equation (45), the field of the refractive index and, from analogous equations for the density, the density field.

When the contrast $\Delta A/A$ is determined, the change in the illumination can be measured point by point with the aid of a modified luxmeter. The disadvantage of this method is that the same luminance of the source must be maintained throughout the entire photometric measurement time, and that the flow studied must be the same, which is almost impossible.

A better solution is to carry out photometric measurements on photographs. Of course, two photographs must be taken for two mutually perpendicular directions of the edge of the diaphragm (the source with the slit is always parallel to the edge of the diaphragm). When these are obtained, the flow need not be exactly the same. For this reason, equipment was built in which the beam from the slit of the source is optically split (through reflection) into two beams which behave like beams which emanated from two mutually perpendicular sources with slits. These two beams pass through the measured

layer (the tunnel), and after passage are separated over a greater distance by the mirrors and form in one camera on the same film at the same instant, two separated images. However, before that, each of the two beams passed through one of the two knife diaphragms whose edges are mutually perpendicular [179].

However, it is difficult to obtain photographs on which the blackened contrast is the same as the contrast when the film or photographic plate is illuminated during exposure. This is due to shortcomings in the quality of the photographic material and the imperfections of the photographic technological processes. Therefore, the procedure used introduces into the observed field a reference inhomogeneity (in German: "die Normalschliere") [162, 171]. For example, when the flow around a profile is photographed, a transparent object is inserted at the edge of the light beam at points through which the rays that were not affected by the inhomogeneities in the tunnel pass, whose effect is the same as that of an inhomogeneity with a known gradient of the refractive index (a change in the direction of the rays). Such an object may be, for example, a glass wedge with a very small refracting angle whose effect is the same as that of an inhomogeneity with a constant gradient of the refractive index, or a plane-concave lens with a small curvature of the concave side whose effect is the same as that of an inhomogeneity in which the gradient of the refractive index varies in a certain range. Then in the photograph at the point where the rays that pass through such reference inhomogeneity impinge in a small area whose blackening corresponds to the known gradient of the refractive index in the reference inhomogeneity that is used for the comparison. By comparing photometrically the blackening at individual points on the photograph with the blackening on this area, we can then determine the gradients of the refractive index around the streamlined body. It is more convenient to use a lens as the reference inhomogeneity, provided we select its curvature so that it behaves like an inhomogeneity in which the gradient of the refractive index varies in the range of values which apply to the problem under consideration.

/116

Another method of obtaining quantitative data may be called the filament or possibly the grid method. Also here the source has a slit, which is as narrow as possible, and instead of a knife diaphragm either a thin filament or several parallel filaments (grid) are inserted in the focal plane of the second lens, and in both cases the filaments are parallel to the axis of the slit. We will first consider only one filament which is placed at the distance a from the optical axis of the equipment in such a way that it is outside the image of the source with the slit, so that if the observed layer has no inhomogeneities, the screen is uniformly illuminated. However, if

inhomogeneities are formed in the layer, the rays are deflected from their original direction, and those rays whose angular deflection in the direction perpendicular to the filament is such that its tangent y_a' has the value $y_a' = a/f_2$ are intercepted by the filament (we used the subscript a since we assumed that the filament was at the distance a from the optical axis). Hence, shadows are formed on the screen at those points which correspond to the points in the layer at which, as a result of inhomogeneities, the rays were deflected by y_a' . From equations (44) and (48) it is obvious that the density gradient has at these points the value

$$\frac{\partial \rho}{\partial y} = \frac{1}{K} \frac{\partial n}{\partial y} = \frac{1}{K} \frac{n_0}{x_2 - x_1} y_a' = \frac{1}{K} \frac{n_0}{x_2 - x_1} \frac{a}{f_2} = k' a, \quad (70)$$

where $k' \equiv \frac{n_0}{K f_2 (x_2 - x_1)}$ is a constant. During the calculations

we took in equations (44) $n = n_0$, a possibility we discussed already on p. 90.

If we displace the filament through the distance a' from the optical axis, the dark shadows on the screen will now correspond to those points in the studied layer at which the component of the density gradient which is perpendicular to the direction of the filament has the value $(\partial \rho / \partial y) = k' a'$. Hence, when the filament method is used, the dark shadows on the screen denote those points in the layer that is examined at which the angular deflection of the rays deflected in the direction perpendicular to the filament is the same, and at which the density gradient and the gradient of the refractive index have a constant component in this direction. These dark shadows, or lines are called, according to Schardin, isophotes. A narrow slit can also be used instead of a filament. In this case, light shadows are obtained on a light field instead of dark shadows on a dark field. /117

By connecting several filaments into a grid or by using a special grid, isophotes of several orders are obtained in the same photograph. Since the image of the source has a width which is not zero and the shadows obtained are wide, this method does not yield sufficiently accurate results. In addition to this, to obtain a sufficient sensitivity, the grid must be very dense, i.e. the grid spacing must be small, which would lead to diffraction phenomena, which distort the image. Two photographs obtained by the filament or grid method are given in Fig. 74 [1, 174, 180, 181].

The work is more accurate when an arrangement is used where the grid is shifted in front of the image focal plane of

lens C_2 , see Fig. 75 [186, 147, 191, 175]. If there are no inhomogeneities in this region that is examined, the ray passing through the point P is parallel to the optical axis until the point Q, and then after refraction by lens C_2 , impinges at the point S of the image of the slit of the source (of course, before the grid G is inserted) and is then projected through the lens C_3 (projection lens, the objective of the camera) onto the screen T at the point P'. If an opaque strip of the grid G that was inserted intercepts this ray, the point P' and similarly other such points will be dark. Hence the screen will be covered by alternating dark and light lines.

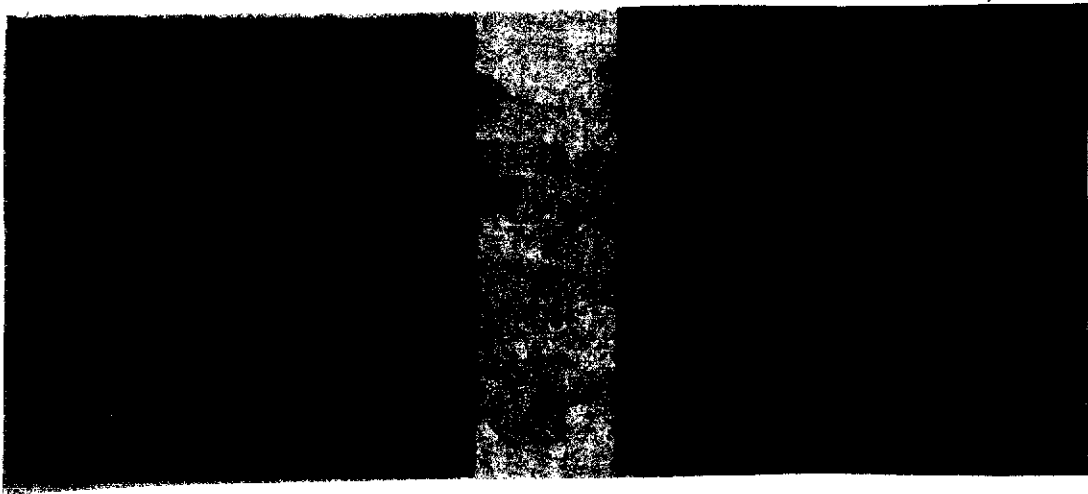


Fig. 74. Samples of images obtained using the filament method [1, 2, 181].

Let us assume now that the layer that is studied has inhomogeneities, so that the ray passing through the point P will now be deflected, say, upward by a small angle ϵ_p whose tangent has the value $\tan \epsilon_p = y'_p$ (the subscript P for the point P). This ray will arrive at the point Q' and then, after refraction by lens C_2 , at the point R, where $\overline{RS} = f_2 \cdot y'_p$, which can be determined with the aid of the lens equation. Hence, it is obvious that the ray will not pass through the same point of the grid as before, but will be incident on the screen again at the point P', since D and T are conjugate planes which change the illumination on the screen, i.e. in our case, the dark shadow will disappear at the point P' and will be shifted elsewhere. We can find out easily immediately where it is shifted to.

/118

Let M denote another point in the inhomogeneous layer that is examined, and let us assume that the ray passing through the

point M, which in the case of a homogeneous layer was parallel to the optical axis is deflected from the direction of the optical axis by the small angle ϵ_M and passes through the points N', A, and V, where $\overline{VS} = f_2 \cdot \epsilon_M$. When it is intercepted at the point A by an opaque strip of the grid which originally intercepted the ray passing through the point P which was not deflected, this means that the dark shadow which originally passed through the point P' was displaced so that it now passes through the point M' where the distance $\overline{P'M'}$ is equal to the product of the distance \overline{PM} and the enlargement m of the optical system formed by the lenses C₂ and C₃, i.e. $\overline{P'M'} = m \cdot \overline{PM}$.

The distance \overline{PM} which we do not know for the time being will be calculated as follows: from the similarity of the triangles QN'A and SVA, we obtain

$$\overline{QN'} = \frac{f_2 - l}{l} \overline{VS},$$

where $\overline{VS} = f_2 \cdot \epsilon_M$, as already stated, so that

$$\overline{QN'} = \frac{f_2 - l}{l} f_2 \epsilon_M$$

and we obtain for \overline{PM} (Fig. 75),

$$\overline{PM} = \overline{QN} = \overline{QN'} + \overline{N'N} = \frac{f_2 - l}{l} f_2 \epsilon_M + d \epsilon_M = \epsilon_M \left(\frac{f_2^2}{l} + d - f_2 \right).$$

With regard to the enlargement m of the system of lenses C₂, C₃, it is

$$m = \frac{f_2}{d - f_2} \frac{b(d - f_2)}{f_2^2} = \frac{b}{f_2},$$

where b is now the distance of the focal plane of the projection lens C₃ from its second principal plane. Hence, we finally obtain for the shift $\overline{P'M'} = m \cdot \overline{PM}$ of the dark shadow under

/119

consideration

$$\overline{P'M'} = m \overline{PM} = \frac{b}{f_2} \epsilon_M \left(\frac{f_2^2}{l} + d - f_2 \right) = k^* \epsilon_M, \quad (71)$$

where $k^* \equiv \frac{f_2 b}{f} + \frac{b(d - f_2)}{f_2}$ is a constant for a particular

optical system which does not depend on the characteristics of the grid. The displacement $\overline{P'M'}$ of the dark shadow (more precisely, the displacement of the shadow at a given point) is proportional to the error in the angle $\epsilon \sim y'$ at the point in the examined layer which corresponds to the displaced point of the shadow.

Although at first sight a dense grid should improve the accuracy (a grid with a small grid spacing), this is not the case, since diffraction phenomena interfere considerably. A sensible bound is four opaque strips per 1 mm [146]. The opaque and transparent strips between them usually have the same width; however, it is more advantageous if all opaque strips are narrower than the transparent strips. The same number of strips in the observation field of the screen can be achieved with a sparser grid by increasing the distance l (Fig. 75), which however reduces the sensitivity of the equipment. Hence, the selection of the properties of the equipment must be a compromise between these standpoints [175, 186, 147]. In addition to a source with a slit and a grid formed by parallel straight filaments, a circular source and a circular grid can be used, i.e. a grid in which the transparent and opaque strips have the form of concentric circles.

The use of diaphragm schlieren methods imposes an important requirement on the design of the tunnel, namely that the transparent glasses be plane parallel, without defects and internal strains.

Among all methods in group 3.2 diaphragm schlieren methods are used most frequently, since in comparison with the shadow method, they provide relatively reliable quantitative data about the density fields and, in comparison with interferometer methods, the required equipment is simpler, less sensitive and expensive and much easier to work with. /121

Figs. 77 through 80 give samples of photographs obtained using the diaphragm schlieren methods. Fig. 81 is a sample of the visualization of a boundary layer, in this case a turbulent boundary layer.

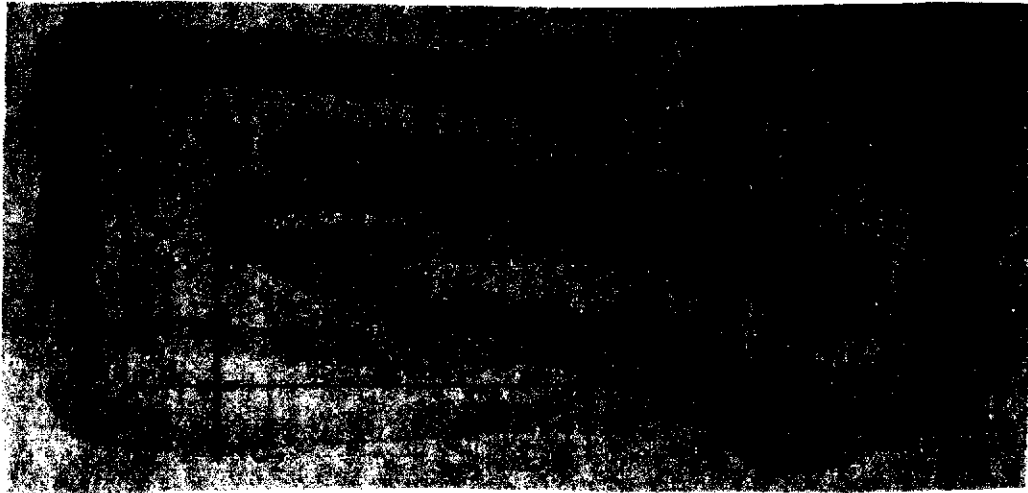


Fig. 75. Diagram illustrating grid schlieren method.

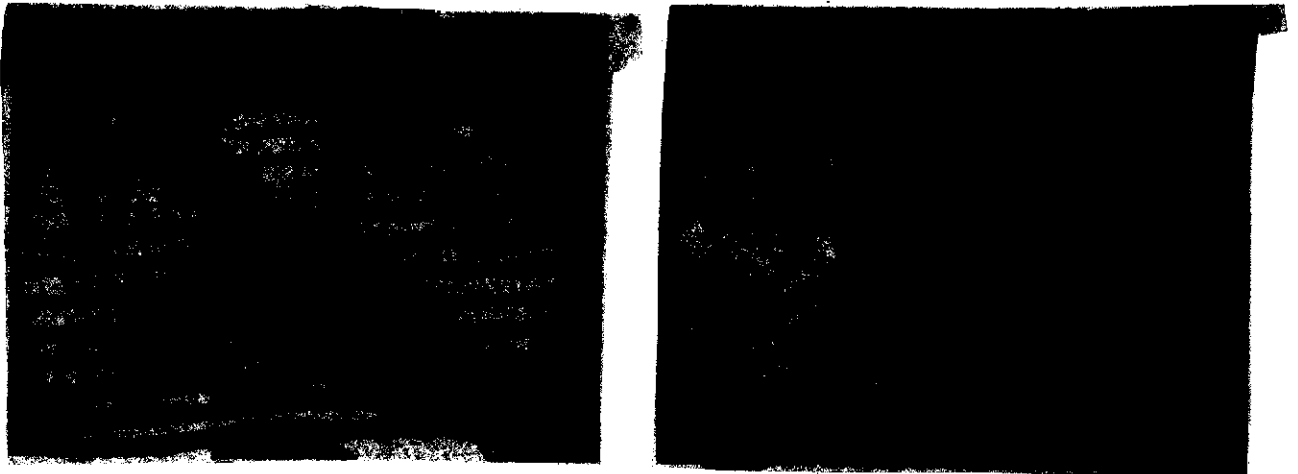


Fig. 76. Sample of images obtained by the grid method with the grid placed in front of the focus of the second lens C_2 (see Fig. 75), a) without flow, b) during flow. The photographs were included with the kind permission of the VZLÜ [expansion unknown] and the author [147].

3.2.3. Diaphragm Schlieren Methods with a Colored Image

/122

The methods that were described in the previous two sections, 3.2.1 and 3.2.2, provide information in the form of white and black photographs. Hence, in these cases, the eye must



Fig. 77. Photograph obtained using diaphragm method. Flow around a rhombic profile [5].

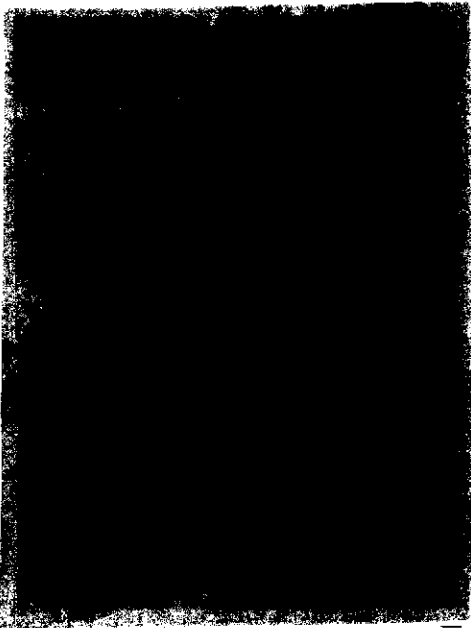


Fig. 78. Front pressure wave visualized by diaphragm method [146].

react to changes in the illumination (unless grid methods are used), an activity for which the eye is not particularly sensitive. A healthy eye records much more easily changes in color so that the observer can observe much more conveniently in the field of view of the appropriate equipment changes in the color of the basic field rather than changes in the illumination. The proposal for and application of the method which is used in this way are not new [162], even though this method has only been used recently in the study of flow [211, 210, 147, 191].

The principle of the method is such that the normal equipment for the diaphragm schlieren method is used, but a decomposing prism is inserted behind the slit of the white light source (for example, a direct vision prism), which decomposes the white light, and the optical system forms in the plane of the image of the source a spectrum whose image can be intercepted on the screen (Fig. 82). However, if a slit (a slit diaphragm) is inserted in the focal plane of the second lens C_2 (the plane of the image of the source) which is parallel to the spectral lines, the screen will be illuminated only by a part of the spectrum and by choosing appropriately the height of the slit diaphragm and the dimensions of the spectrum, the illumination on the screen will have the same

/123

color shade everywhere. This basic color of the illumination on the screen can be selected by choosing the position of this slit and it can also be changed by shifting the slit diaphragm across the spectrum in the direction perpendicular to the width of this slit. When the decomposed light passes through a



Fig. 79. Images of pressure waves obtained in stereoscopic equipment. The light beams of two independent systems for the diaphragm method intersect at a small angle in the measurement space [183].

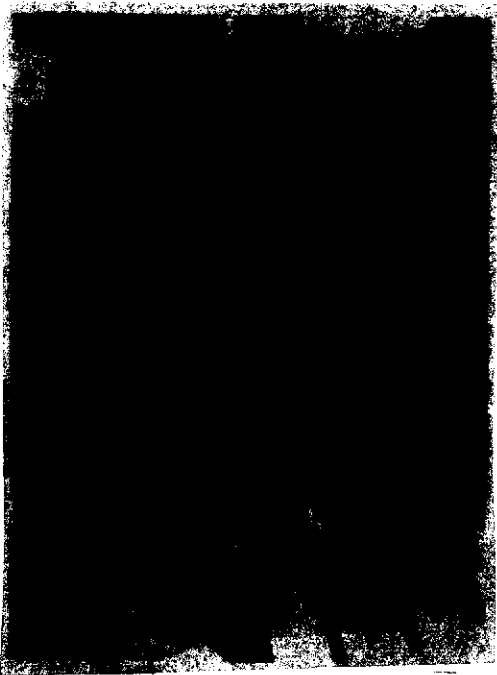


Fig. 80. Image obtained by diaphragm method during the study of flow through a cascade [10].

medium with a density gradient, the rays are deflected from the original direction, from the direction they would have if the density of the medium were constant. The deflected rays are intercepted by the slit diaphragm (i.e. they do not pass through its slit), so that the corresponding point on the screen will be illuminated by rays of a different color. To each color corresponds a certain value of the component of the density gradient which is perpendicular to the slit, which follows from equations (44) and (48).

The dimension (length) of the spectrum must be selected taking into consideration the magnitudes of the density gradient in the medium that is studied and the dimensions of the optical equipment. If the length of the spectrum is too large, the change

in the colors is not very noticeable and the sensitivity of the equipment is small. On the other hand, when the length of the spectrum is small, the measurement range of the equipment may be



Fig. 81. Visualization of boundary layer with the aid of the diaphragm method.

exceeded and those points on the screen which correspond to the points in the medium that is studied at which the magnitude of the gradient exceeds the measurement range are dark. When the length of the spectrum is properly selected for the study of a particular

case, all colors of the spectrum are represented in the image on the screen and no dark unilluminated points must appear on it. This means that the requirements on the design of the parts of the equipment and the manner in which it is constructed are basically the same as those used in the diaphragm schlieren method 3.2.2.

For example, if the basic illumination on the screen when this method is used has a green color, the deflections of the rays in one direction (these deflections lead to an increase in the illumination in the normal diaphragm schlieren method) cause a change in the green color to a color which lies closer to the red end of the spectrum, i.e. depending on the magnitude of the deflection that is considered, the green color changes through yellow to red, and starting with a certain magnitude of the deflection a dark spot appears at the corresponding points on the screen. Deflections in the opposite direction (deflections which in the diaphragm schlieren method lead to a drop in the illumination) result, depending on their magnitude, in a change from the green color through blue to violet.

In addition to a white light source, a source yielding a line spectrum (for example, an iron spectrum) can be used. In this case, both in the spectrum and in the image of the field, lines of various colors separated from one another by dark strips are formed instead of the continuous colored transitions. Images which are similar to those obtained when the diaphragm schlieren method with a grid is used are obtained; however, they are colored, which simplifies considerably their evaluation. /124

Light sources yielding a system of luminous colored strips obtained by decomposing the light can be replaced by a colored filter strips with selected color strips, which is inserted into the slit of any light source that passes through the filter. The filter can be obtained by photographing the chosen colored sample made from colored paper or by photographing the spectrum on a color print film or plate.

The method that was described only takes advantage of a single color change cycle, which limits either the range or the sensitivity of the method. Several color change cycles



Fig. 82. Schematic diagram of equipment for diaphragm method with colored image (1. light source; 2. decomposing straight vision prism; 3 and 5. principal lenses; 4. analyzed layer; 6. diaphragm; 7. objective; 8. focusing screen or camera.

strip an equal part of the width extends past the edge of the strip, i.e. the red and blue end of the spectrum. In this case, the screen is simultaneously illuminated by red and blue light and appears as a purple color. Now if the beam of light is deflected in the layer that is studied, the image of the source (the spectrum) on the grid is also displaced and more light, for example, from the blue end of the spectrum, will impinge on the screen than from the red end. As the rays are further deflected in the same direction, this relation will continue to change, so that as the deflections of the rays considered increase, the illumination on the screen will change the color from purple through blue, green, yellow, orange, and red, back to purple, which will appear again as soon as the displacement of the image of the source is equal to the grid spacing. Larger deflections will cause additional color change cycles in the illumination on the screen. Deflections of the rays in the direction opposite to that considered until now will cause an alternation of colors in the opposite sequence.

In some cases it is desirable to replace a grid with equally wide parallel strips by a grid in which the transmissive strips widen (Fig. 84), i.e. the width of the strips changes along their length). When such a grid is used the deflections of the rays (components of the density gradient) appear with the color changes on the screen which are perpendicular to the axes of the strips of the grid, whereas the deflections of the rays in the direction of the strips will manifest themselves in changes in the illumination as in the normal diaphragm schlieren method. A further improvement can be obtained with the aid of a grid which has several rows of grid systems with widening strips (Fig. 84). This increases the sensitivity of the equipment to deflections in the direction of the strips [178].

can be used when the slit diaphragm is replaced by a grid, i.e. by several slits, which increases the range while retaining sufficient sensitivity. The width of the transparent and opaque strips in the grid is the same and the grid spacing, in this case, twice the width of a strip in the grid, is approximately equal to the effective width of the image of the source, the spectrum.

Suppose that the image of the source falls onto an opaque strip of the grid so that on both sides of the

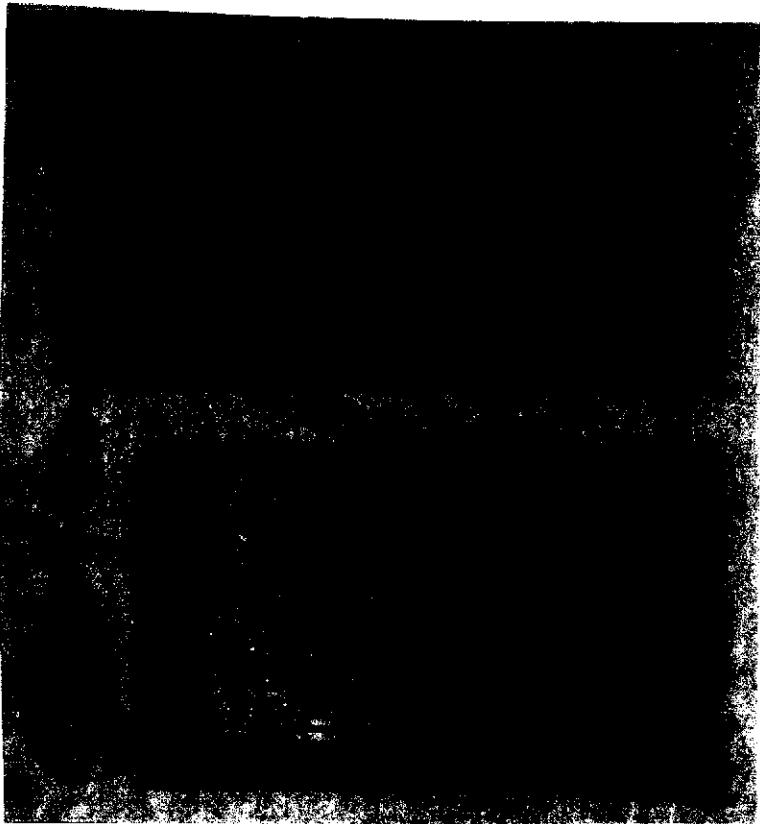


Fig. 84. Grid with widening strips.

A colored image of the inhomogeneities can also be obtained by other methods. The method in which the same equipment is used as in the grid diaphragm schlieren method (see p. 114) is suitable for large inhomogeneities, where the normal grid, located in the focal plane of the second lens, is replaced by a colored grid [162, 191] (see Fig. 85). The principle for other suitable equipment is given in Fig. 86. The middle strip of the plate D which is not cross-hatched radiates white light and the other strips glow in various colors. The size of the layer that is studied must be such that it does not extend past the

pencil of rays which radiates from the surface as luminous white light and enters the aperture of diaphragm C. If at some point in the layer there is an inhomogeneity deflecting the rays by the angle ϵ (its tangent was denoted in equation (44) and elsewhere by y'), in the observation field the point illuminated by the light of the same color at which the strip marked in Fig. 8 b by the letter b glows corresponds to this point. Hence, in this method, a certain deflection ϵ (a particular interval of values of the deflection ϵ) corresponds to each colored strip. The method is only suitable for large deflections ϵ and small dimensions of the layer that is studied, since otherwise the distance denoted by l in Fig. 86 is too large [162].

The methods that were described in this chapter are used very seldom even though they yield good results. The reasons are the difficulties which arise when colored photographs are taken and reproduced, since the inaccuracies in the reproduction of the colors in this method reduce considerably the accuracy of the results in the case when the density field is determined quantitatively.

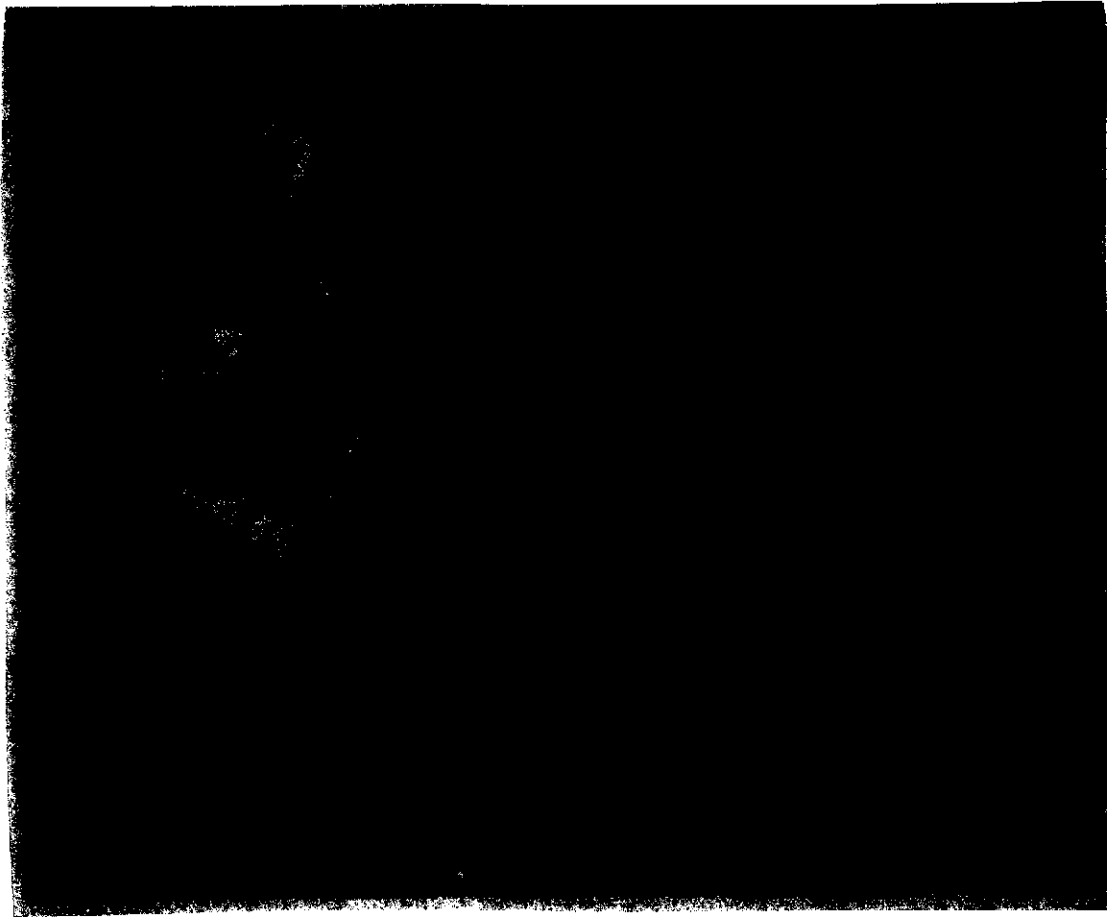


Fig. 85. Photograph obtained during flow through a cascade using colored grid placed in the image focal plane of second lens. The photograph was included with the kind permission of the VZLU [expansion unknown; probably Aviation Research Institute], and the author [191].

3.2.4. Interferometric Methods

The interferometric method requires in comparison with the methods in group 3.2 that were presented much more complex and expensive equipment, and the requirements on the service are also greater. Nevertheless, recently it has been used more and more frequently. The reason for this is that among all the methods in group 3.2 that were presented, it furnishes the most accurate data about the density field in the layer that is studied. These data can also be obtained from the interference images without particular difficulties, even though laboriously, without special instruments.

On p. 84 it was mentioned that if the refractive index of the layer that is studied whose thickness will henceforth be

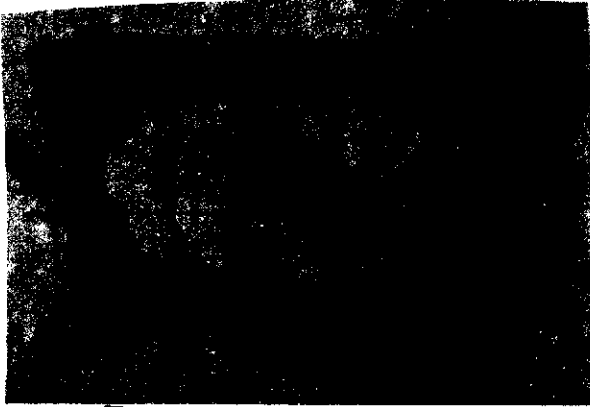


Fig. 86. Schematic diagram of equipment used to obtain colored images of pronounced inhomogeneities (M -- focusing screen; D -- colored grid filter; V -- analyzed layer; C -- diaphragm; O -- objective; T -- focusing screen).

denoted by l (until now in most cases this thickness was denoted by $x_2 - x_1$) changes from the original value n_0 to the value n , in each of these two cases the ray will leave the layer with a different phase. Hence the phase shift of the passing rays corresponds to a change of the refractive index in the layer, and to it, in the surrounding medium with the refractive index n' , corresponds the displacement Δs along the trajectory given by the relation

$$\Delta s = \frac{n - n_0}{n'} l, \quad (72)$$

which was given as (50) on p. 89.

When the change in the refractive index in the layer that is studied is not the same everywhere, i.e. if $n = n(y, z)$, the phase and trajectory shift will be a function of the coordinates y, z . This means that by determining the displacement Δs along the trajectories at various points of the inhomogeneous layer, it is possible to obtain data for determining the local values of the refractive index, from which in turn the local values of the density can be determined on the basis of the relation

/127

$$\frac{n - 1}{\rho} = \frac{n_0 - 1}{\rho_0} = K, \quad (73)$$

which we presented as (47) on p. 89.

The shift along the trajectory can be measured using interference, for example, in the following manner. Two rays are obtained from the same light source, one of which passes through the inhomogeneous layer in which we determine the field of the refractive index, and the other passes through the layer used for the comparison (for example, a layer with the same properties which the layer that is studied had when it had no inhomogeneities, and therefore had the same refractive index n_0 everywhere). If, after passage through the layers,

the rays are combined again, they interfere, provided they are coherent. If the trajectory difference at the point where the rays meet again is equal to an odd multiple of half the wavelength λ' of the light used (λ' is the wavelength of the light used in the medium in which interference occurs, which here is the medium which we called the surrounding medium with respect to the layer examined, and whose refractive index we denoted by n'), i.e. if at that point

$$\Delta s = (2k + 1) \frac{\lambda'}{2}, \quad \text{where } k = 0, 1, 2, 3, \dots \quad (74)$$

the light will be attenuated at this point, and if the intensities of the two rays are the same the light will vanish. Conversely, the light will be intensified at points where the trajectory difference of the interfering particles is equal to an even multiple of the wavelength, i.e. where

$$\Delta s = 2k \frac{\lambda'}{2} = k \cdot \lambda', \quad \text{where } k = 0, 1, 2, 3, \dots \quad (74')$$

The dark and light fringes that are formed are called interference fringes. The record, a photograph of these interference fringes, serves as the basis for determining the field of the local values of the refractive index in the layer that is examined. This means that the data about the layer that is examined are determined from the shape and grouping of the interference fringes or possibly from their changes.

The images of the phase shifts of the rays, the interference images, are obtained with the aid of interferometers. Hence, in principle, the Michelson (Fig. 87) or Jamin (Fig. 88) interferometers that are known from physics can be used [15, 16]. However, the Michelson interferometer has the disadvantage that the rays in it pass through the layer that is examined twice, which may cause inaccuracies when the records are evaluated. The difficulty in the Jamin interferometer is the small distance of the two separated beams which later interfere with one another, so that its use is limited to cases when one of the transverse dimensions, the dimensions in the directions perpendicular to the direction of the rays of the layer examined, is sufficiently small, as, for example, in the study of a boundary layer. The improper position of the plane in which the interference fringes are formed is another shortcoming in both instruments. The interferometer proposed by Mach, the Mach-Zehnder interferometer, is used exclusively for experimental aerodynamic purposes [223]. A sketch of this equipment

/128



Fig. 87. Schematic diagram of the Michelson interferometer [15, 16]. (1. light source; 2. lens forming parallel pencil of rays; 3. plane parallel glass plate with reflecting semipermeable layer; 4. plane parallel glass plate like 3 without reflecting layer; 5. fixed mirror; 6. displaceable mirror; 7. observation telescope into which luminous rays reflected by the mirrors 5 and 6 enter and interfere (8. image plane of reflecting surface of mirror 6).

(in physics, similar equipment is associated with the name Rozhdestvenskiy) is given in Fig. 89. Compared to the two types that were described, it has the advantage that the light passes through the examined layer only once, and that the separate beams can be separated from one another over a sufficiently large distance so that if necessary, only one beam passes through the measurement space and the other is completely outside this space.

The basic parts in a Mach-Zehnder interferometer are two plane mirrors S_1 and S_2 (Fig. 89) and two plane parallel semipermeable glass plates P_1 and P_2 (a semipermeable plate is a plate which reflects half the incident light and lets the other half through). These four basic parts are located in the instrument in such a way that when their centers are connected a rectangle or square or possibly another parallelogram is formed. The mirrors and glass plates during the measurements are either exactly parallel and subtend with the sides of the rectangle that was mentioned 45° angles, or at least one of these four elements is slightly deflected from the position that was mentioned as a result of a small rotation about the axis that passes through its center, for example, perpendicularly to the plane of the rectangle that was mentioned (for additional details, see p. 133) [226].

/129

Another part of the Mach-Zehnder interferometer is a point source of monochromatic light placed at the focus S of the collimator objective, or possibly the source is projected by the condenser onto the collimator slit which lies at the focus of its objective. Each light ray R emanating from the source S impinges on the plate P_1 which is semipermeable, i.e. it splits the ray R into two parts: the reflected and passing ray, whose intensities

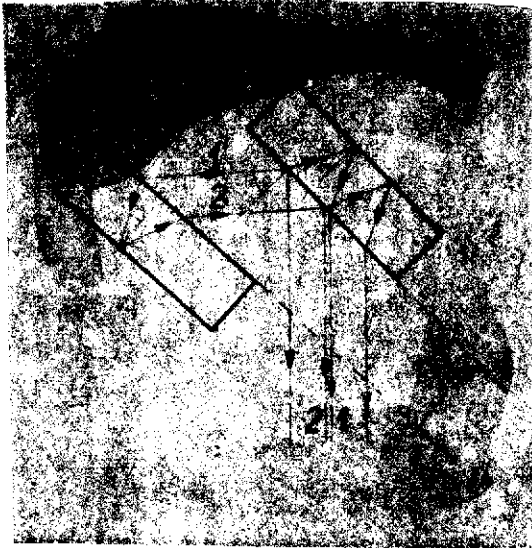


Fig. 88. Schematic diagram of Jamin interferometer [15, 16] (Z -- light source; A and B -- plane parallel glass plates; 1 and 2 -- rays which interfere with one another after reflection on plate B).



Fig. 89. Schematic diagram of Mach-Zehnder interferometer.

are approximately one-half of the intensity of the incident ray R. If the plate and mirrors are mounted so that they are parallel, the trajectory of the passing ray is determined by the points ABCD1 and the trajectory of the reflected ray by the points AEFD1.

A part of the luminous ray is also reflected at the point B, so that it follows the trajectory ABGMLK2, or, possibly, due to the subsequent reflection at point G, the trajectory ABGHK2. The reflection may also occur at the point D, so that a part of the original ray may also have the trajectory AEFDLK2. All rays which finally arrive at point 1 will have the same phase at this point, which also applies

to the rays arriving at point 2, both of which follow from the assumption that the mirrors and plates are parallel and exactly planar, that the two plates have the same properties and are exactly plane parallel, and that the medium between the plates and mirrors is completely homogeneous. The rays, incident at point 2 (and all similar rays) even though they have, in comparison with the rays arriving at point 1, a very small intensity, can nevertheless have a disturbing effect, since the common value of the phase of the rays at point 2 differs from the common value of the phase of the rays at point 1. Therefore, anti-reflexive layers on the plates are used to prevent them from impinging on the screen. Hence, we may consider only rays which are analogous to the rays passing through point 1 which will illuminate the screen uniformly. This satisfies to a certain extent all the assumptions and

requirements made on the properties of the parts of the interferometer which will be discussed later (see p. 140).

Now if in one branch (for example, in the branch AEF \bar{D} l, see Fig. 89) of the interferometer inhomogeneities are formed as a result of the flow in the air layer that is examined through which the rays from the branch pass, then, for example, the ray of the branch under consideration passing through point l will have at the point D a different phase than before. If this phase shift corresponds to a trajectory displacement which is equal to an odd multiple of half the wavelength, a dark spot is formed as a result of interference with the ray ABCDl at the point D (and also at the point l and all points on the segment \overline{Dl}); since the ray ABCDl is incident at D with the original phase. Similar pairs of rays will form additional dark spots. On the whole, dark fringes will be formed on the screen (or possibly dark regions which do not have exactly the form of fringes), and at each point of a particular fringe, the phase and hence also the trajectory difference of two rays which at that point are disturbed by interference will have the same value. For various k (k = 0, 1, 2, ...; see equation (74)) dark fringes of various orders will be formed.

We will now use (as before in most cases) the following notation:

a) n and ρ are the refractive index and the density at the point of the layer with the inhomogeneities that is examined through which the ray AEF \bar{D} l passes; c and λ are the velocity and wavelength of the monochromatic light used during the passage through the layer that is examined;

b) n_0 , ρ_0 , c_0 , and λ_0 are the symbols for the analogous magnitudes in the homogeneous layer used for the comparison which is located in the second branch of the interferometer, through which the ray ABCDl passed;

c) n', ρ' , c' and λ' will denote the analogous magnitudes in the surrounding medium.

The difference of the optical paths of the rays AEF \bar{D} l and ABCDl (and similar pairs of rays) is

$$\Delta s_{opt} = (n - n_0)l, \quad (75)$$

since the layer that is examined and the layer used for the comparison have the same thickness l. In the surrounding medium the path difference given by relation (72) corresponds to the above difference. From equations (72) and (74), we obtain for the changes in the refractive index at which the dark interference fringes are formed the relation

$$\frac{n - n_0}{n'} = \frac{1}{l} (2k + 1) \frac{\lambda'}{2}, \quad \text{where} \quad k = 0, 1, 2, 3, \dots \quad (76)$$

in which we can take, on the basis of (73),

$$n - n_0 = \frac{n_0 - 1}{\rho_0} (\rho - \rho_0), \quad (77)$$

so that we obtain for ρ

$$\begin{aligned} \rho &= \frac{\rho_0}{n_0 - 1} \frac{\lambda' n'}{l} \frac{2k + 1}{2} + \rho_0 \\ &= \frac{\rho_0}{n_0 - 1} \frac{\lambda_v}{l} \frac{2k + 1}{2} + \rho_0, \quad \text{where} \quad k = 0, 1, 2, 3, \dots \end{aligned} \quad (78)$$

in which the second equality holds because $n' = c_v/c' = \lambda_v/\lambda'$, where λ_v is the wavelength of the monochromatic light used in vacuum and c_v is the velocity of light in vacuum. Since λ_v and l are known and $\rho_0/(n_0 - 1) = 1/K$, according to (73), this fraction has a constant value which we can easily determine in advance (for example, for air we already calculated K on p. 89 and denoted the value by K_0 , so that for air the fraction under consideration will have the value $1/K_0$), and it suffices, obviously, if we determine the density ρ_0 of the layer used for the comparison and determine the order k of the interference fringe. After substitution in (78), we obtain the density along the line in the measurement space, which corresponds to the given interference fringe and hence indicates the points where the density ρ is the same. When the local density is known, additional data can be calculated, data about the local velocity, pressure, the Mach number and temperature [for example, 215, 217, 212, 239, 240, 242 and others].

A procedure which is often used is to determine the density at a point of the layer which corresponds to some point through which the interference fringe in the interference image passes on the basis of the measured static pressure at that point in the layer. This is usually done at several points in the layer. If the observed layer is bounded by glass walls, holes are drilled into them at selected points which are used for measurement of the static pressure. The images of these holes are in the field of view (Fig. 90), so that we can find the interference fringes passing through the centers of these images. If the interference fringe passes through the center

of a particular hole, the pressure at these points of the layer which correspond to the interference fringe under consideration may be considered to be equal to the static pressure measured at the point where the hole is located. However, since the pressure is measured at the point where the opening is the inlet into the measurement space, i.e. near the wall of the measurement space, and this pressure is not identical with the pressure at those points in the layer which lie on the line through the center of the opening across the layer, i.e. on the line perpendicular to the walls (cover glasses) of the measurement space, the accuracy of the data that were obtained is affected. However, any other method of measuring the pressure would disturb the flow.

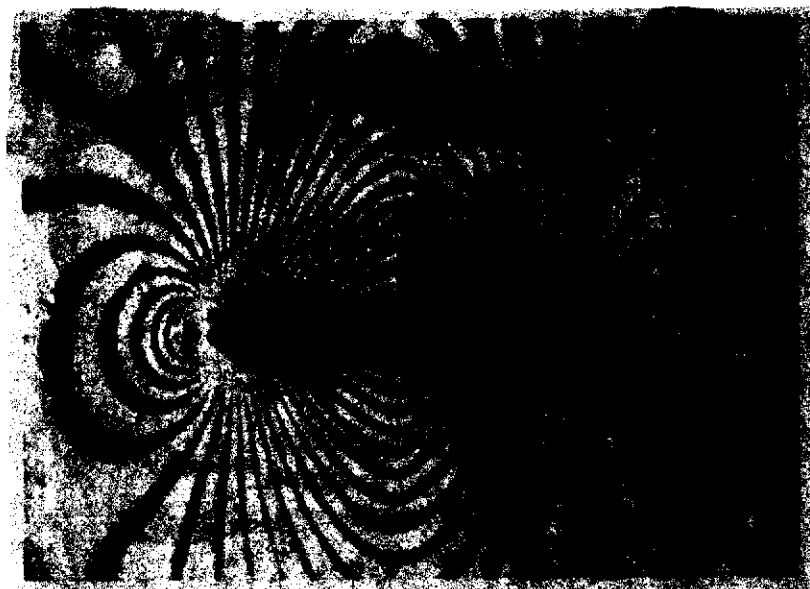


Fig. 90. Interferogram with images of openings used for measurement of static pressure [2]. (Interferometer adjusted for infinite width of fringe.)

The densities corresponding to two neighboring interference fringes differ according to (78) by /132

$$(\Delta \rho)_1 = \frac{\rho_0}{n_0 - 1} \cdot \frac{\lambda_w}{l}, \quad (79)$$

so that if we know the density corresponding to a particular interference fringe, we can easily determine the densities corresponding to other interference fringes. Of course, we must

know on which side of the interference fringe that was identified the density increases. When k is the order of the identified interference fringe, the fringes whose order is higher than k , and to which, according to (78), correspond higher values of the density are distributed from the fringe that was identified, in the direction toward the point where the velocity on the streamlined body is zero, since, at this point, the pressure is higher than at the points corresponding to the identified fringe. Fringes whose order is lower than k are distributed in the direction from the identified fringe toward the point where the velocity is a maximum (Figs. 91 and 92).

The plotting of interference images in the form of drawings which are later evaluated causes sometimes difficulties because of the great width of the interference fringes. This difficulty can be surmounted by subjecting the photographs to a special photographic process called equidensitometry [21], by means of which two very narrow lines are obtained from one wide fringe.

A Mach-Zehnder interferometer can also be used for the study of inhomogeneous layers in a different manner. By turning a mirror or plate, for example, by rotating the plate P_2 about the axis which passes through its center perpendicularly to the plane given by the centers of the plates and mirrors (the plane in Fig. 89), we obtain a case which is similar to the case in which the light passes through a wedge, in this case an air wedge. We will analyze what happens in such a case. The surrounding medium is considered to be entirely homogeneous and its refractive index is again denoted by n' .

The optical paths of the rays in both branches of the interferometer will now no longer be the same (even though, for the time being, we do not consider the insertion of the examined inhomogeneous layer in one branch of the interferometer and the layer used for the comparison in the other branch!). Their difference depends on the angle of rotation of the plate and on the distance of the ray from the axis about which the plate was rotated. Hence, we may assume that the pencil of rays passing through one branch of the interferometer (for example, the branch in which the measurement space will be inserted must, in comparison with the rays in the other branch, also pass perpendicularly through a wedge with a small refracting angle α , which has a refractive index that will be denoted by n_0). The rays in this branch, unlike the rays in the other branch, will have a trajectory displacement which, in the surrounding medium with refractive index n' , has the value

$$\Delta s = \frac{n_0}{n'} d = \frac{n_0}{n'} e \alpha, \quad (80)$$

where d is the thickness of the wedge at the point where the ray studied passes through the wedge and e is the distance of this point from the edge of the wedge.

It is obvious that for some e , conditions (74) will be satisfied after the light disappears. According to (74) and (80), the light will disappear when

$$e = (2k + 1) \frac{\lambda'}{2} \cdot \frac{n'}{\alpha n_0} = (2k + 1) \frac{\lambda_v}{2\alpha n_0}, \quad \text{where } k = 0, 1, 2, 3, \dots \quad (81)$$

and where $\lambda_v = \lambda'n'$ is the wavelength of the light that was used in vacuum. Hence, dark interference fringes will be formed in the field of view of the interferometer (Fig. 93) which are parallel to the edge of the wedge (i.e. to the axis about which the plate was turned). The distance b between two neighboring fringes will be the same everywhere and equal to

$$b = e_{k+1} - e_k = \frac{\lambda_v}{2\alpha n_0} (2k + 2 + 1 - 2k - 1) = \frac{\lambda_v}{\alpha n_0}. \quad (82)$$

(If the plate and mirrors are in mutually parallel positions, i.e. if $\alpha = 0$, according to (82), the distance b between the neighboring interference fringes (and their widths) will increase without limit. Therefore, in this case, which we already discussed on pp. 128-132, we talk about adjusting the interferometer to an infinite width of the fringe.)

Now if the inhomogeneous layer with refractive index n and thickness l is inserted in one branch (for example, the branch EF) of the interferometer, the trajectory difference (80) changes by a value which corresponds to the change in the refractive index from the value n_0 to the value n (we assume that in the place where the layer is inserted, the air was originally still, and therefore we use for the original refractive index the same notation as for the refractive index in the wedge considered above, which is also formed in still air). This change in the surrounding medium with refractive index n' is given by the expression $[(n - n_0)/n']l$, so that the total displacement along the trajectory of the ray passing through the branch containing the inhomogeneous layer that is examined, unlike the ray that passes through the second branch of the interferometer, in the surrounding medium with refractive index n' , will now be given by the expression

$$\Delta s = \frac{n_0}{n'} d + \frac{n - n_0}{n'} l. \quad (83)$$

/135

instead of expression (80). However, this means that the position of the original dark interference fringes will also change (i.e. those that were formed before the inhomogeneous layer that is examined was inserted in one branch of the interferometer, as a result of turning the plate P_2 ; see p. 133), since, due to the change in the trajectory difference of the rays, the condition for the vanishing of the light will now be satisfied for a different thickness d' of the wedge, i.e. at a different point e' . From equation (74) and equation (83), in which we will write d' instead of d on the basis of what has just been said, we find that the light will disappear as a result of interference when the condition

$$(2k + 1) \frac{\lambda'}{2} = \frac{n_0}{n'} d' + \frac{n - n_0}{n'} l = \frac{n_0}{n'} e' \alpha + \frac{n - n_0}{n'} l, \quad \text{where } k = 0, 1, 2, 3, \dots$$

is satisfied, where the second equality holds on the basis of the relation $d' = \alpha e'$, where α is the refracting angle of the wedge. From the above, we obtain for e' which gives the new position of the dark interference fringe, using the relation $\lambda' n' = \lambda_V$, the expression

$$e' = (2k + 1) \frac{\lambda_V}{2 \alpha n_0} - \frac{n - n_0}{\alpha n_0} l, \quad \text{where } k = 0, 1, 2, 3, \dots \quad (84)$$

When we compare the expression that was just obtained with expression (81) for e which gives the original position of the dark fringe, i.e. its position before the inhomogeneous layer that is examined was inserted in one branch of the interferometer, and also when we compare equations (80) and (83), we find that if $n - n_0$ is positive, the original displacement along the trajectory is increased and the change $\Delta e = e - e'$ in the position of the original interference fringe is in the direction of smaller d , i.e. in the direction toward the edge the wedge (to the axis about which the plate P_2 was turned; see p. 132) and the converse will hold when $n - n_0$ is negative. According to (81) and (84)

$$\Delta e = e - e' = \frac{n - n_0}{\alpha n_0} l, \quad (85)$$

so that we obtain, for the ratio of the change in the position of the fringe to the original distance b between the interference fringes with the aid of equation (82), first

$$\frac{\Delta e}{b} = (n - n_0) \frac{l}{\lambda_0} \quad (86)$$

and, taking into account (77),

$$\frac{\Delta e}{b} = \frac{l}{\lambda_0} \frac{n_0 - 1}{\rho_0} (\rho - \rho_0). \quad (87)$$

This equation determines the relation between the change in the position of the interference fringe and the change in the density. From the above we obtain, for the unknown density,

$$\rho = \frac{\Delta e}{b} \frac{\rho_0}{n_0 - 1} \frac{\lambda_0}{l} + \rho_0 = C_0 \Delta e + \rho_0, \quad (88)$$

where

$$C_0 \equiv \frac{\rho_0}{n_0 - 1} \frac{\lambda_0}{bl} \quad \text{is a constant; hence for } \Delta \rho = \rho - \rho_0$$

we obtain

$$\Delta \rho = C_0 \Delta e. \quad (89)$$

On the basis of expression (88), the density can be determined at any point of the layer that is examined provided we measure the change Δe in the position of the interference fringe as discussed in the next section. The unknown density ρ however is determined, according to (88), as a function of the density ρ_0 in the homogeneous reference layer, for which the surrounding medium can also be used. The original interference image formed by the parallel equidistant fringes with the spacing b given by relation (82) belongs to this reference layer. The reference medium for the density ρ_0 is the surrounding undisturbed atmosphere in the case when the flow around bodies in flight (projectiles, etc.) in the free atmosphere is studied, or during the study of axisymmetric outflow of air from a nozzle into the free atmosphere. During the observation of flow in tunnels, the reference medium is the air in the so-called compensation chamber which is inserted in the branch BC of the interferometer (the measurement space in the tunnel is inserted according to the previous prerequisite in the branch EF) or the undisturbed flow in the tunnel before the part of the measurement space that is examined [212]. In the last case, the

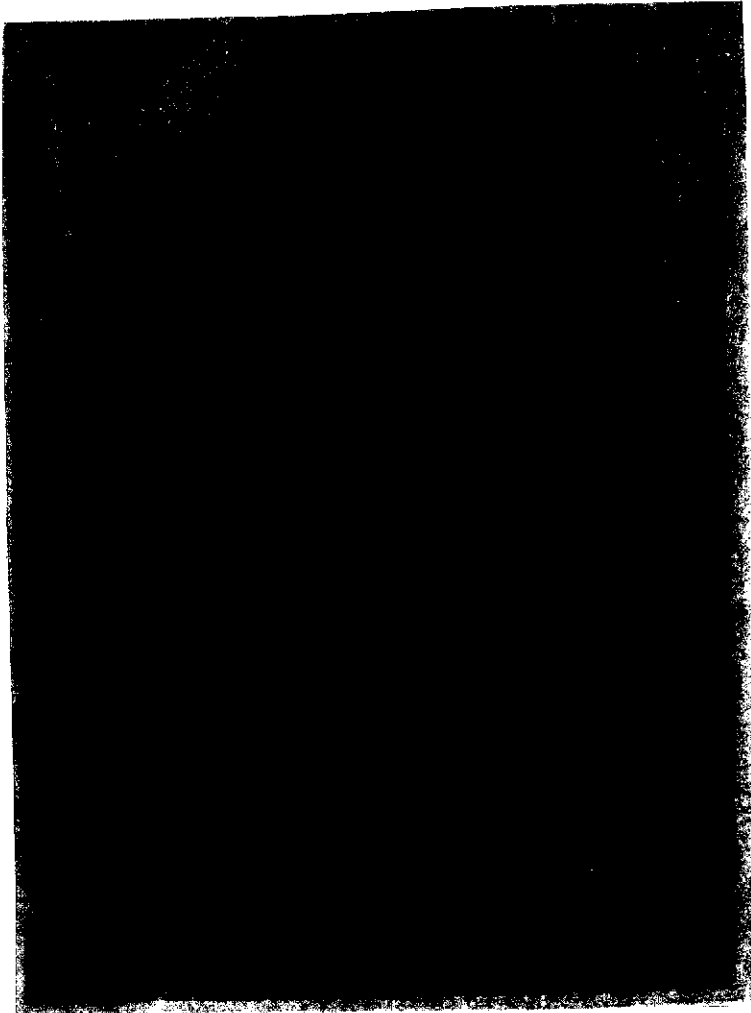


Fig. 91. Interferogram of flow field in a cascade [10]. (Interferometer adjusted to infinite width of fringe.)

rays from both branches of the interferometer pass through the measurement space, i.e. through the same cover glasses. This method is predominately suitable only for supersonic flow when the flow before the shock wave or the front wave of the streamlined body is not disturbed. The compensation chamber is a sealed vessel, whose walls which are perpendicular to the direction of the rays in branch BC, form two parallel glass plates with the same properties as the cover glass of the measurement space. The air inside the chamber is either constantly maintained in the same state, or the chamber is connected by a tube with the opening used for the measurement of the static pressure of the undisturbed flow in the tunnel.

The interference fringes are usually evaluated from photographs. To facilitate this operation, various preparations or apparatus and useful techniques can be used. The basic measurement is the measurement of the distance Δe at the required points. If we want to determine the density ρ at a point M of the layer that is examined, the Δe , which, according to equation (88), must be known, is determined as follows: we find (the shifted) interference fringe which passes in the field of view through the image M' of the point M, and next we find the original position of the same fringe (in this original position the fringe was straight, whereas in the shifted position it is usually not straight), and finally we determine Δe as the perpendicular distance of the point M' on the shifted fringe from the original position of this fringe

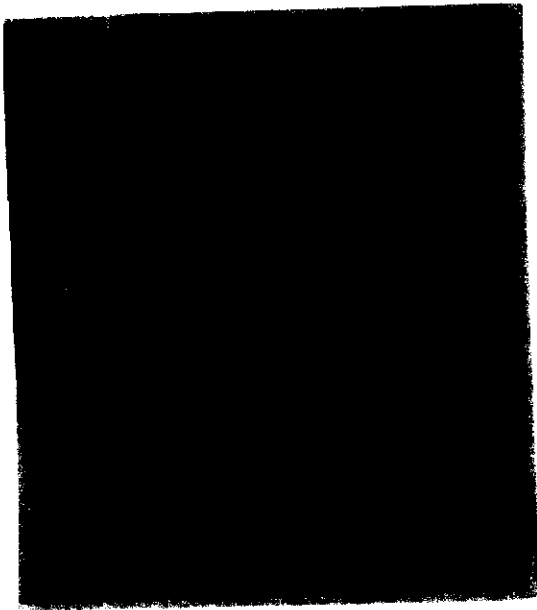


Fig. 92. Interferogram of flow around cylindrical body with conical front part [146]. (Interferometer adjusted to infinite width of fringe.)

the evaluation, or the original positions of the fringes are obtained through extrapolation on the basis of the known behavior of shifted fringes at points (regions) where it can be assumed that the original state did not change, so that the fringes were

(Figs. 94 and 95). The original position of the fringe is the position which it occupied in the case when the examined layer was either not yet inserted in one of the branches of the interferometer, or when it was inserted there but was not yet homogeneous (for example, because the air did not yet circulate in it or circulated in such a way that the flow field was homogeneous) and had the same density ρ_0 everywhere. For example, a comparator with a reading microscope with a capability for mutually perpendicular shifts is used for the measurement of $\Delta\epsilon$.

Since, to determine $\Delta\epsilon$, the original position of the interference fringes must also be known, the original fringes are copied in thin cutouts on the photograph that is evaluated to facilitate



Fig. 93. Interference fringes obtained with the aid of the Mach-Zehnder interferometer adjusted for an infinite width of the fringe. The measurement space is free of inhomogeneities [10].

not shifted at those points. However, this second method may lead to inaccuracies, since the assumption that was made need not be satisfied exactly in the regions under consideration. Although a similar assumption is also used in the mutual pairing of the shifted and original fringes in the first method, the danger of errors is smaller since the original (straight) fringes are copied (in cutouts) on the photograph that is evaluated, so that their direction and positions are known. Another procedure that can be used is that the corresponding grid is prepared in accordance with the original interference image (which was obtained, for example, when the medium in the measurement space was quiescent, the tunnel was blocked), which is copied together with the photograph, or is photographed simultaneously with the flow that is examined (Fig. 96). When photographs of flow fields with large changes in their refractive index are evaluated (for example, at points through which a shock wave passes) the high concentration of the fringes caused by their large shift over a small width causes difficulties. Since, for purposes of accuracy, it is advantageous to adjust the interferometer for very dense interference fringes, in some cases it is not possible to study the interference fringes during the transition through such regions. However, when light which is not perfectly monochromatic is used, usually not all fringes have the same intensity, so that their behavior can be traced more easily in these cases. Mathematical machines, for example, a mechanical analyzer, which calculate and record the pressure distribution from interference images have also been constructed [230].

/138

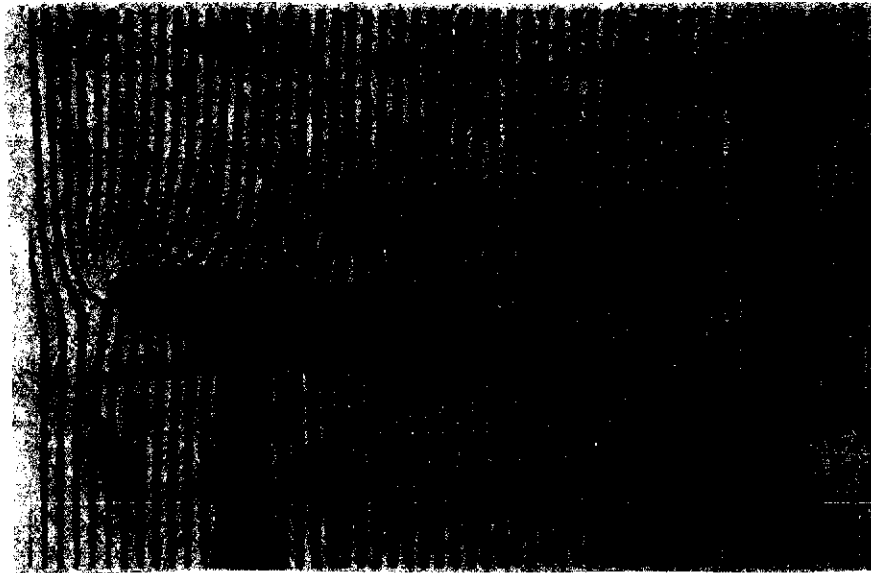


Fig. 94. Interferogram of flow around wing with interferometer adjusted for a finite width of the fringe [5].

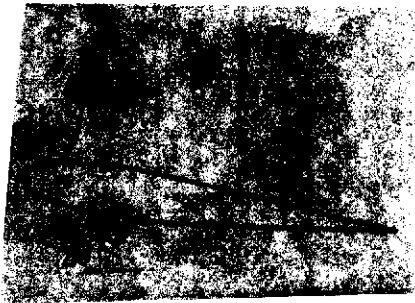


Fig. 95. Diagram for discussion on p. 136.

At first sight, the interferometric method of studying the flow seems to be rather simple. In fact, when the assumed ideal properties of the optical parts are not satisfied and when the disturbing surrounding effects manifest themselves, its use, especially during the adjustment and elimination of disturbing effects by means of various corrections is very laborious and time consuming, which also reduces the accuracy. The inaccuracy of the method itself,

when used as described, is sufficiently small when the density is determined and it depends on the type of the flow field that is studied. In the usual cases, it can be held below 3% up to a Mach number 6 [146, 212]. However, the inaccuracies in the equipment and the deviations from the assumptions that were made in the analysis of the method have a substantial effect on the measurement error. Thus, for example, the glass plates and the cover glasses of the measurement space are not exactly plane parallel, homogeneous, and they do not have the same refractive index; hence, they are not completely identical, for instance, also, due to the effect of the temporary birefringence of the glass caused by mechanical stress. Mirrors are never exactly planar. The uneven temperature in the surrounding air through which the

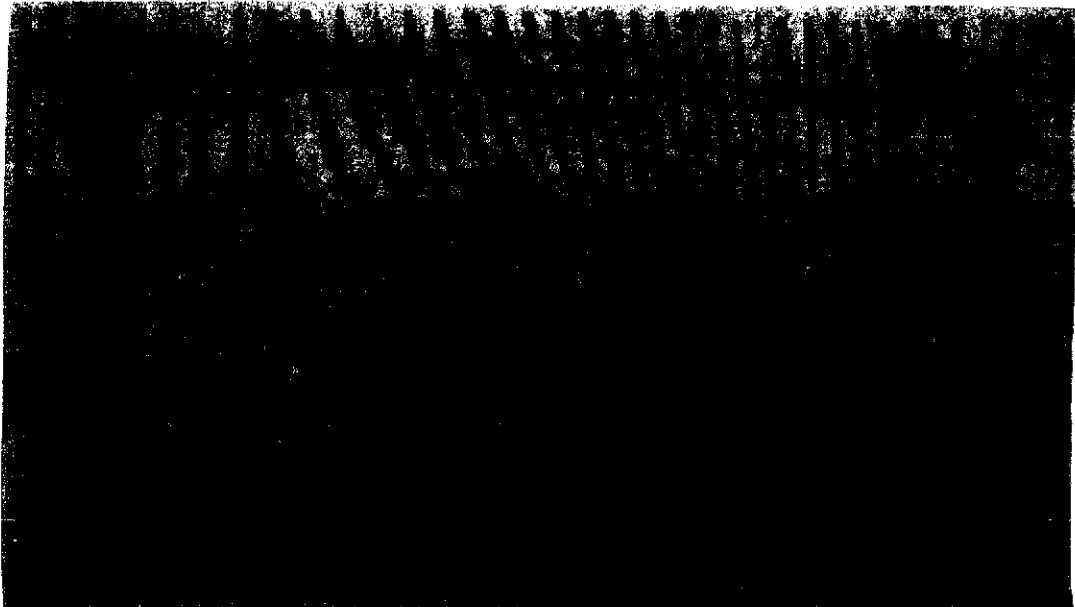


Fig. 96. Interferogram of flow around a wing and grid with original distribution of interference fringes [212].

rays pass, the nonuniform temperature distribution in the glass plates, the vibrations in the entire equipment, and the acoustical waves in the tunnel, the effect of the cover glasses of the measurement space on which the existing boundary layer changes the two-dimensional character of the flow, etc. are the disturbing effects which occur most frequently.

Other problems are introduced by the light source which is not exactly monochromatic. The finite width of its spectrum limits the maximum number of fringes that can be obtained, since it limits the smallest possible width of the fringe for which the entire field of view is covered by fringes. For one end of the spectrum of the light that is used (which is roughly, but not exactly, monochromatic) a dark fringe is formed at a certain point, but, for example, a light fringe from the light at the wavelength belonging to the other end of the spectrum of the source is formed at the same point which distorts the interference image. Another limitation on the number of fringes that can be obtained follows from the fact that the light source is not exactly a point source. Therefore, not all rays pass through the glass plates at the same angle, their paths in the plates are not the same, and undesirable phase shifts in the rays are formed.

/140

Light refraction causes difficulties during the observation of strong inhomogeneities in the layer that is examined [215, 219, 239]. The path of the ray is curved during the passage through such a region (see p. 84), which changes the interference image, the fringes cross one another, spread, and sometimes the photographs at such points become unreadable and the data that are obtained (provided that in this case they can be obtained from the photographs) are inaccurate. Hence, on the whole, it is desirable to now discuss the requirements which must be imposed on the properties that will ensure the best functioning of the individual parts of the equipment and of the equipment as a whole.

The typical method used to assemble the equipment is illustrated in the drawing in Fig. 97, and the photograph is given in Fig. 98. The light beam emanating from the source must be converted by the lens C_1 , the objective of the collimator, into a parallel pencil of rays which passes through the interferometer and then through the lenses C_2 and C_3 which focus the selected plane U in the measurement space (the examined layer) simultaneously with the interference fringes on the photographic plate or screen (focusing screen). Hence, the mirrors and plates must be adjusted so that the pencils of rays passing through the two branches leave the interferometer at such angles that the unreal image of the interference fringes is formed in the desired plane U of the layer that is studied.

/141

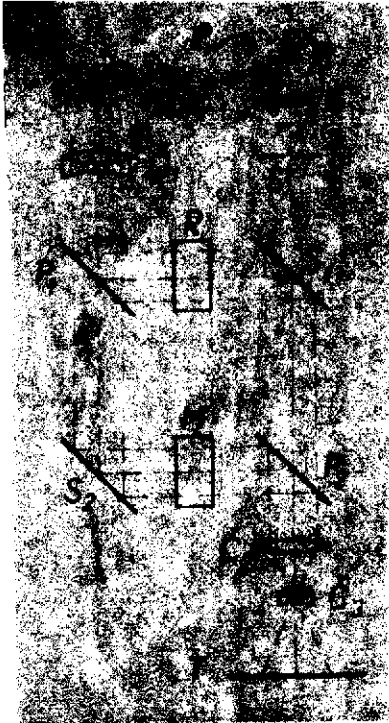


Fig. 97. Schematic diagram of Mach-Zehnder interferometer. (S - light source; C₁ - objective of collimator; P₁ and P₂ - semipermeable glass plates; S₁ and S₂ - mirrors; M - measurement space; R - compensation chamber; C₃ and C₂ - lenses forming the image of the plane selected in the measurement space and simultaneously the interference fringes on the screen, a focusing screen or photographic plate; T - screen). Other versions exist in which instead of the lenses C₁ and C₃, mirrors are used; see, for example, Fig. 106. The right part of the diagram gives the drawing of a detail in the schematic diagram of the light source (V - discharge tube; K - condenser which projects the glowing discharge into the slit S of the collimator; the luminous surface S' of the slit represents the light source S of the interferometer).

If the measurement space is covered by glass plates, identical plates must also be inserted in the second branch of the interferometer, of course, as long as the beams in both branches do not pass through the measurement space [213]. This is done in order that the optical paths of the rays in both branches do not differ much. Sometimes, instead of the other plates, a compensation chamber is also used (see p. 136). The arrangement of the plates and mirrors must not always be such that their planes subtend a 45° angle with the direction of the rays.

A requirement on the interferometric equipment which is not easily satisfied is that parallel interference fringes of the same width be obtained during the observation of a homogeneous layer. Some equipment achieves this with a dispersion which is 1/10 of the width of the fringe. It is obvious that it is much more difficult to retain this dispersion value in plates and mirrors whose dimensions are relatively large. It is difficult to manufacture homogeneous glass plates of large dimensions. In addition to this the flexural deformation of the plate has an unfavorable effect in those cases when the plates are not vertical. Similarly as the plates, the cover glasses of the tunnel and the compensation chambers must have excellent optical properties. In order

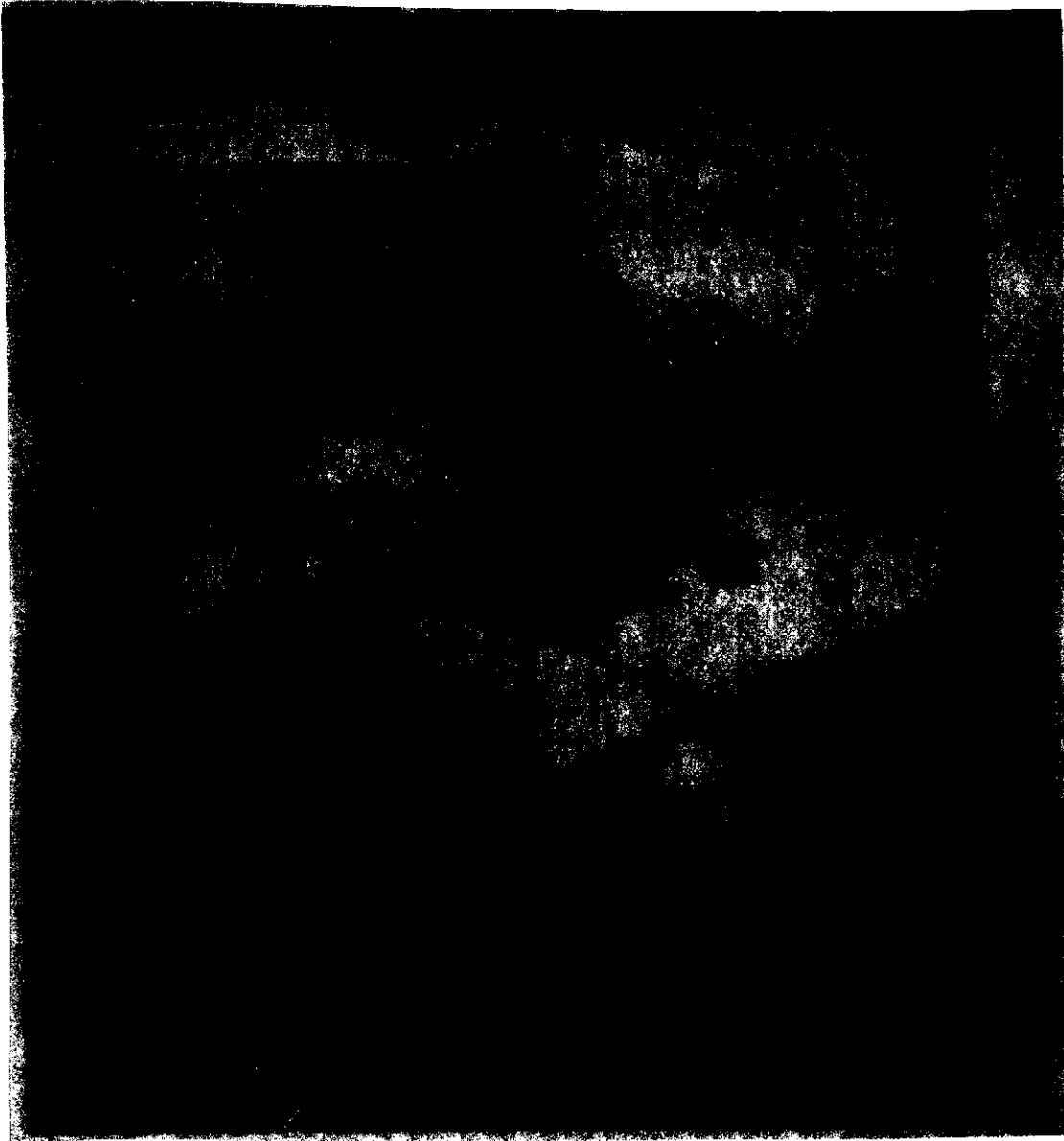


Fig. 98. Mach-Zehner interferometer manufactured in Czechoslovakia, based on a proposal of workers at the VZLU [217]. (The photograph was included with the kind permission of the VZLU management and the author [217].

that the effect of these parts do not cause a distortion in the interference images which is larger than $1/10$ of the width of the fringe for green light at wavelength 5000 \AA , their refractive index must be constant with a tolerance which is equal to $2 \cdot 10^{-6}$ for 2.5 cm thick plates. The thickness of the plates whose dimensions are larger must of course be greater, the ratio of the thickness to the width (in the case of a circular plate to the diameter) which is required for reasons of strength in operation and manufacturing lies between $1:7$ to $1:10$. The largest plates used until now had diameters of approximately 30 cm [231].

The thickness of the semipermeable glass plates must not differ by more than $1/12$ and the thickness of the cover glasses of the measurement space and the compensation chamber by more than $1/3$ of the wavelength of the light that is used. All surfaces reflecting the remaining light must be worked with the same precision. The effect of small local deviations from homogeneity or from a constant thickness of the plates (provided they are not too irregular; hence, for example, in the case of wedges) can be moderated by the mutual turning of the plates about the axes which are perpendicular to their surface, or also be changing very slightly the angle at which the rays are incident to the glass of the compensation chamber, which, in the basic adjustment, is 90° . It also helps when the positives are obtained from the plate or film to incline the plane of the photographic paper so that a positive with parallel fringes corresponding to the still air in the tunnel is obtained. The same inclination must then also be presented when the positives are obtained in the case of an airflow.

The front surface of the glass plates P_1 and P_2 (Figs. 89 and 97) must have an appropriate coating which lets through approximately 50% and also reflects approximately 50% of the intensity of the incident light (among other things, the absorption in such a layer must be very small), and the rear surfaces must have a layer which prevents the formation of undesirable systems of interference fringes from the rays reflected from the rear walls of the plates. The rear walls of the cover glasses and of the lenses must also have such antireflexive layer. Mirrors must reflect more than 90% of the intensity of the incident light [16, 217]. Generally, the absorption in all optical parts must be as small as possible.

All optical parts, especially mirrors and plates must be impeccably clean. Dust, fingerprints or grease spots diffract the rays, whose interference may subsequently form disturbing interference fringes. This danger is great mainly in laser interferometers (see p. 147).

The adjustment of the interferometer requires that it be possible to turn each of the plates P_1 and P_2 about the horizontal and vertical axes, both of which must lie in the plane of the reflecting surface. In addition to this, one of the plates (usually P_2) must be adjusted so that it can move in the direction of the rays, thus changing the relation of the optical paths of the rays in both branches of the interferometer. Therefore, the plates are inserted in frames (in a way which will prevent deformation of the plates even when the inhomogeneities can be corrected by controlling the deformation [213]) and suspended in gimbal suspensions, and the plate P_2 is also mounted on slides. The plates are turned via remote control, since the presence of

a person servicing the equipment would raise the local temperature in the equipment and in the air, which are highly unfavorable disturbing effects. Bowden cables, clock electromotors, selsyns, etc., which are connected with multiple gears and can be adjusted so that the position is determined with an accuracy of 1" are used (see Fig. 99) [217, 212, 213, 232]. For a more perfect adjustment (during the setting of a larger initial path difference; see below p. 145), one of the cover plates of the compensation chamber was also turned [215].

Suitable light sources are high-performance, high-pressure mercury discharge tubes with input powers raised for a short period up to 10 kW, and spark discharges (see p. 108), Fig. 72). The basic requirements are that the dimensions of the source be small, a high intensity of the light, and the exposure times must be very short, on the order of several microseconds, because of the instability of the flow (especially at high velocities). A certain part of the intensity of the source is lost to the monochromatic filter which is indispensable during the normal use of the method. Recently, experiments were made using a laser as a light source for interferometers. Through the use of lasers, certain difficulties which follow from the fact that classical light sources are not perfect point and monochromatic sources and the coherence of their rays is only limited to small path differences, roughly to ten wavelengths of the light used, can be eliminated almost completely. All this facilitates considerably the adjustment of the interferometer [237].

/144

The entire optical equipment from the source to the camera must be firmly secured on a sufficiently rigid frame to prevent vibrations of the parts and of the entire equipment. For these reasons, the grips on the frame in the supporting structure are supplemented by vibration dampers (in smaller equipment, by rubber blocks) or possibly suspensions on rubber ropes [215].

These requirements are especially high on the seating of the mirrors and plates in the interferometer itself. The light source, the condenser, the collimator, the objective, and the camera are often located on an independent optical bench which is separated from the frame of the interferometer. This protects the interferometer from possible shocks that arise during the manipulation of the components in the illumination, image-forming or recording unit.

A pentaprism is used most often for the initial adjustment of the interferometer when the plates and mirrors subtend with the incident rays a 45° angle [225], although other methods can also be used [146, 215, 217]. Then the plates (or only one plate) are turned through a small angle until

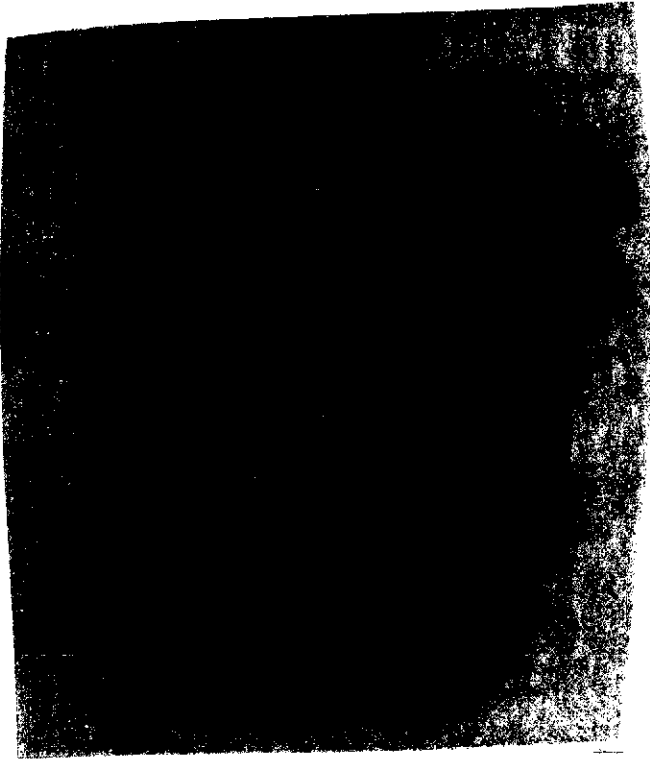


Fig. 99. Plate in gimbal suspension. It is a part in the interferometer in Fig. 98 (the photograph was included with the kind permission of the VZLU and the author [217]).

satisfactory interference fringes are formed. Depending on the axis about which the plates were turned, the fringes that are obtained are either parallel to the plane in which the centers of the plate lie, or the fringes are perpendicular to this plane. Then the equipment must be focused with the aid of the lenses C_2 and C_3 (Fig. 97) on the selected plane in the measurement space and the sharpness and contrast of the fringes must be preserved by turning the plates. The focusing is facilitated by inserting a wire mesh in the selected plane. After the various errors in the equipment, mainly the errors due to the refraction of the rays in the inhomogeneities in the measurement space have been moderated, it is advantageous to focus on the plane in the middle of the measurement space [146, 215]. A monochromatic

source with a lower intensity than that used during the measurement is used. Usually, it is a sodium or cadmium lamp. The additional measures that already have been described prove the quality of the initial interference image, i.e. the parallelism of the fringes.

The adjustment of the interferometer to an infinite width of the interference fringes (see p. 133) is even more laborious. The white light (from the bulb) passes through the interferometer with the plates and mirrors adjusted at a 45° angle, and the zero-th order interference fringe (which has the highest intensity) must be spread over the entire field of view until the illumination in the field of view is uniform. This is achieved by shifting the plate P_2 in the direction of one of the light beams without turning the mirrors or planes. Using this method, the result which must be achieved is that the beams in the two branches of the interferometer have the same optical path. After this basic adjustment of the interferometer to an infinite width of the fringe, it is convenient to set a

certain selected initial trajectory difference before the measurement. This difference (which is constant over the entire field) must be such that it is roughly compensated by the trajectory difference formed in the flow region which is of greatest interest to us during the measurement. We then obtain in this region much clearer interference fringes than we would have without setting the initial trajectory difference, which is especially evident when a source of light that is not sufficiently monochromatic is used [213, 224, 230, 233, 217, 215, 157].

/145

Hence, three different types of interferometric images of the same flow field can be obtained by different basic adjustments of the interferometer. This is evident from the drawing in Fig. 100. The adjustment method yielding an image of type B' is usually preferred over B'', since more data about the shift of the fringes in the vicinity of the leading edge of the profile can be obtained from B', because in the case B' the fringes at this point are denser than in the case B''.

Interference images (Fig. 101 c) which are similar to type B in Fig. 100 can also be obtained photographically, by copying on one paper the positive of the image 101 a and the negative of the image 101 b. A photograph of the same flow field obtained with the aid of an interferometer adjusted to an infinite width of the fringe is given in Fig. 101 d for a comparison.

The functioning of the entire equipment depends on the proper choice of the type of tunnel and its dimensions to be used together with the interferometer. For two-dimensional studies, the measurement space should have a rectangular cross section and for the study of flow around axisymmetric bodies, the measurement space should be cylindrical. The tunnel and the measurement space must be adjusted so that the flow in the measurement space is not disturbed. The selection of an open or closed circuit in the tunnel must be considered from several points of view. In a closed circuit it is mainly the disturbing effect of the air which is heated during the flow, and in the measurement space, the disturbing sound waves which propagate from the blower in the direction of the flow or possibly against it. The first unfavorable property of closed circuits can be moderated sufficiently well by cooling; however, the second cannot be moderated easily; the design of the tunnel must be changed. In an open tunnel, these effects are eliminated; however, the condensed vapors in the air have a very unfavorable effect.

/147

The suspension of the model in the tunnel must not disturb the flow. Recently, the ONRA [expansion unknown] magnetic suspension has been used advantageously [202]. When the model is mounted on the pins in the openings of the cover plate of the

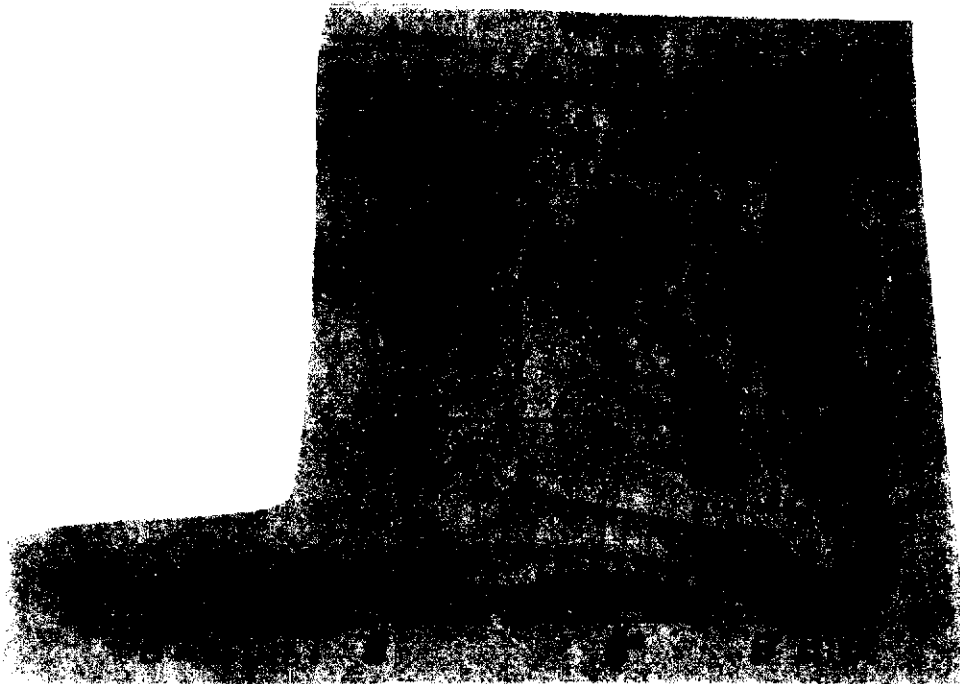


Fig. 100. Principle for various methods used to adjust the Mach-Zehnder interferometer:
B - adjustment to infinite width of fringe;
B', B'' - adjustment to finite widths of fringe;
A - investigated layer; C - screen.

measurement space or glued to them, the plates must not be bent as a result of stress. The depth of the measurement space must be selected taking into consideration the processes that will be studied, so that the refracted light does not distort the interference fringes at a great depth. Since the number of fringes also depends on the density in the measurement space, it is convenient to vary the density (tunnels with a variable density of air).

Interferometric methods can be used for the study of a large number of different cases of flows in a wide range of Mach numbers from $M = 0.2$ up to highly supersonic cases. They can also be used at very low pressures [236], for example, a shock wave was determined in nitrogen already at a density of $1.5 \cdot 10^{-3} \text{ kg/m}^3$. Some illustrations which indicate their use have already been presented earlier, and several other illustrations are given in Figs. 102 through 104. Although the boundary layer is very clear in Fig. 104 c, the quantitative evaluation caused problems, since the effect of temperature changes caused by friction also contributes to the shift in the interference fringes. The method is also very suitable for the study of

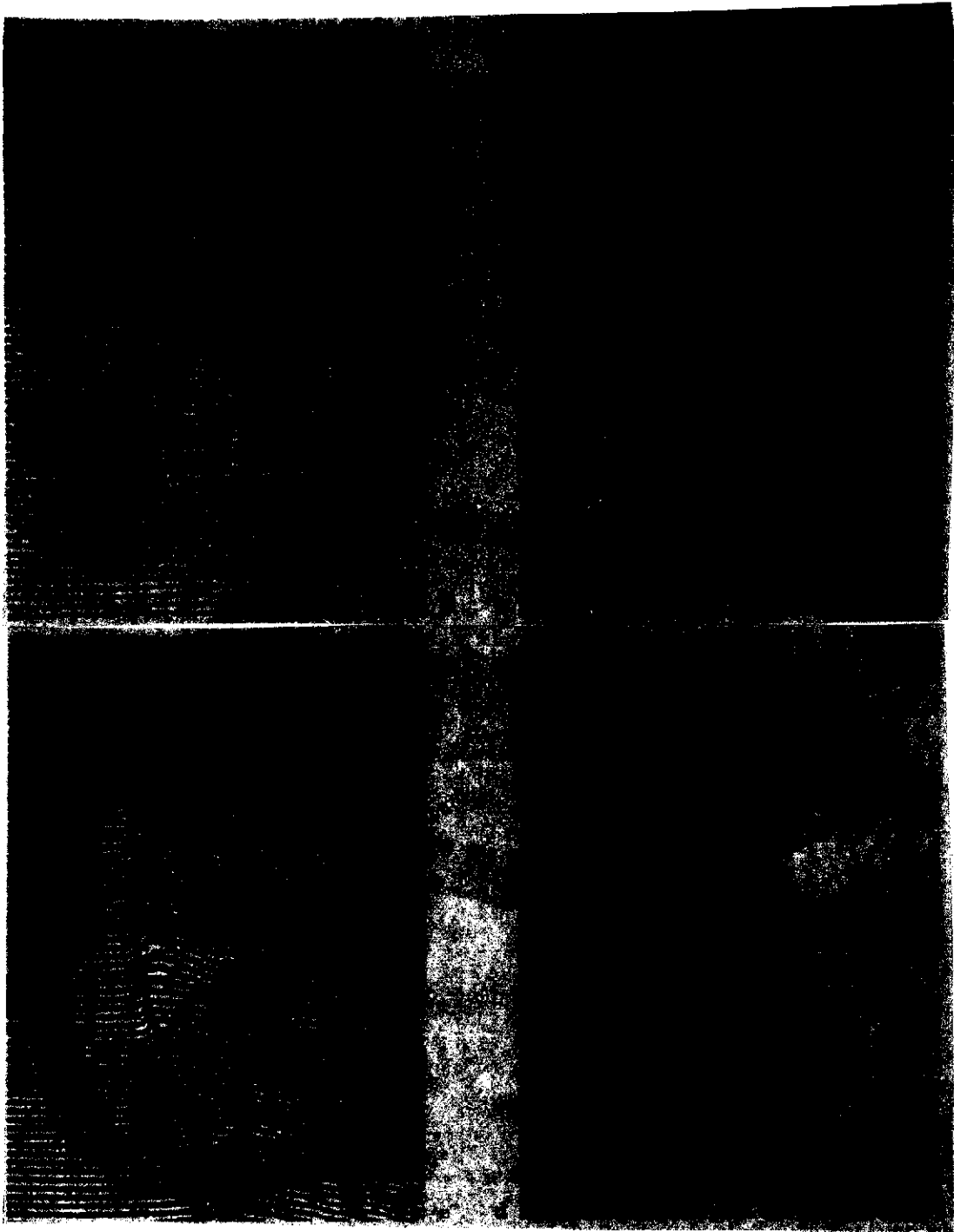


Fig. 101. a) Interferogram of quiescent field (flow field without inhomogeneities). Interferometer adjusted to finite width of fringe. b) Interferogram of flow field with inhomogeneities (adjusted to finite width of fringe). c) Moaré image resulting from superposition of interferograms of type 101 a and 101 b. d) Interferogram of the same flow field obtained with the aid of an interferometer adjusted to an infinite width of the fringe [146].

unstable processes. Photographs obtained by the shadow method can also be obtained with interferometric equipment (see p. 154) by stopping down the branch of the interferometer which contains the compensation chamber. Equipment which makes it possible to obtain from the same measurement space simultaneously photographs using the interference method and the diaphragm schlieren method has also been designed (see p. 153). Drawings of these modifications are given in Figs. 105, 106 [146, 159, 218, 219, 220, 221, 238, 242 and others].

The method taking advantage of the interferometric method that was described is used most frequently and yields the best results. In spite of this several attempts were made to use other types of interferometers [227, 228, 230].

In the last few years a laser has been used as the light source for interferometers. Due to the the differences between the properties of a laser light source and the properties of classical sources, the bases for new designs of interferometers for use in the mechanics of fluids have been obtained. For example, a ruby laser can be used for these purposes, which gives single light pulses whose duration is 0.1 microsecond. The coherence of its rays is adequate for use in interferometers; however, the energy of the pulse must be limited so that the optical parts of the interferometer are not damaged during strong pulses, and there is also the danger of injury to the eyes.

The advantages of using a laser are primarily that the time coherence is preserved sufficiently well even when the differences in the trajectory of the particles are large, on the order of several to several tens of centimeters. This eliminates the requirement that the mirrors and plates in the individual branches of the interferometer have the same thicknesses. This fact together with the good spatial coherence of the rays manifests itself in a substantial reduction of the laboriousness with which the Mach-Zehnder interferometer is adjusted. In addition, it also facilitates the assembly of new types of interferometers. In addition to using a laser as the light source in a Mach-Zehnder interferometer when the necessary light beam is formed from the narrow pencil of parallel light rays emanating from the laser with the aid of the lens, simpler interferometric devices can be assembled with the aid of a laser. Advantage is taken of the fact that the ray passing through the second branch of the interferometer can remain very narrow, so that it can pass through the measurement space at a suitably chosen point, or possibly through a certain point in a separate part of the measurement space which represents the compensation chamber. From the narrow beam emanating from the laser, using, for example, a double prism and a diverging lens (Fig. 107), a thin reference ray and a

/150

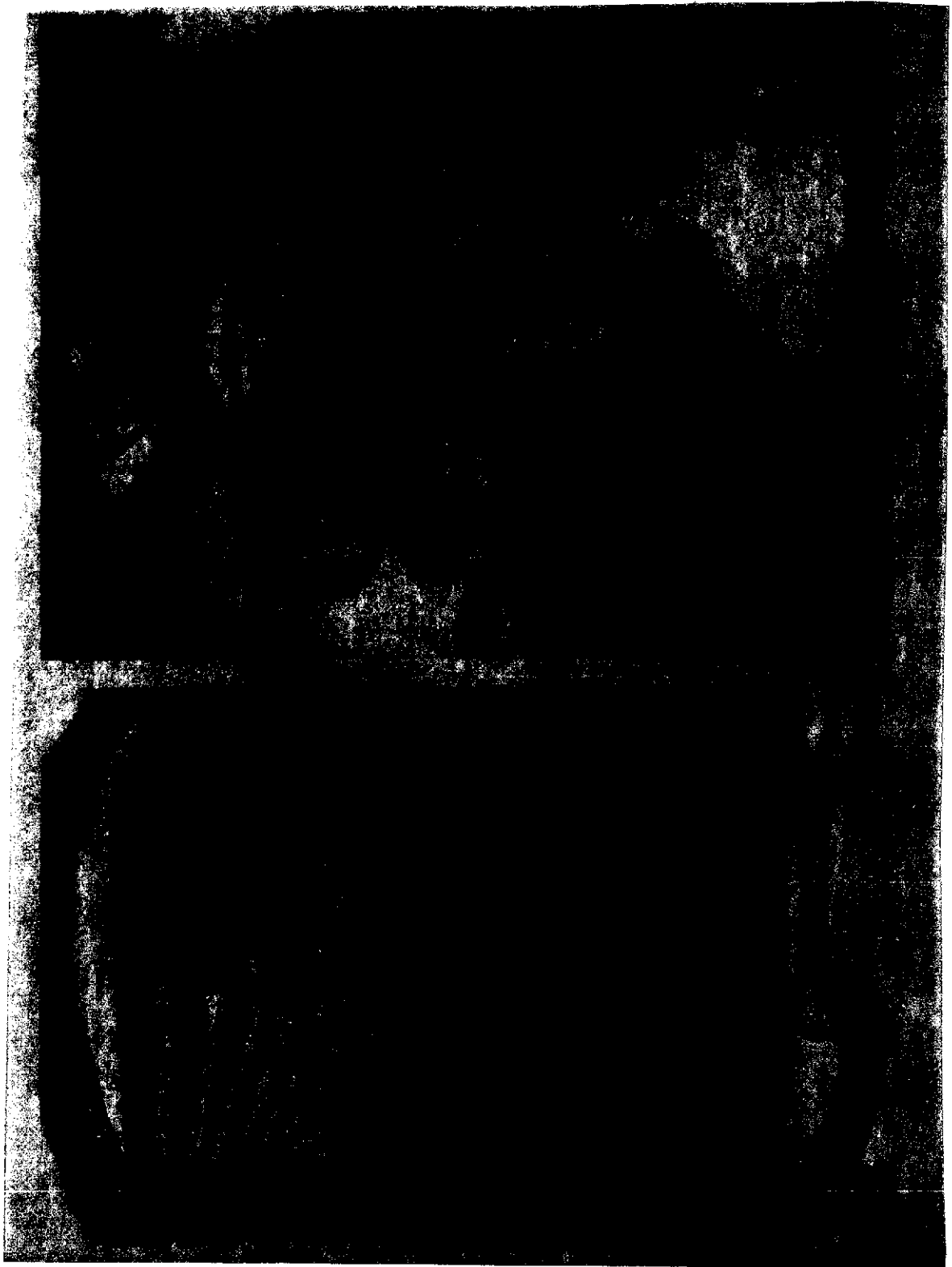
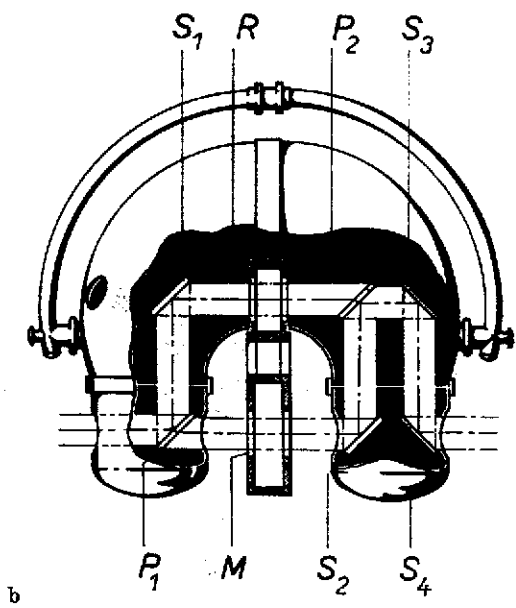


Fig. 102 a, b. Interferograms obtained with interferometer manufactured by the firm Novotechnika, FRG; a) flow through cascade; b) flow through nozzle.



a



b

Fig. 103. Interferometer manufactured by the firm Novotechnik, FRG. a) Interferometer in position for basic adjustment. b) Schematic diagram of interferometer. The meaning of the symbols is the same as in Fig. 97. S_3 and S_4 are accessory mirrors forming a periscope whose use is of no essential importance. It is used to achieve the result that the axis of the emanating beam is identical with the axis of the entering beam so that the illuminating and image-forming parts have colinear optical axes.



Fig. 103. Interferometer manufactured by the firm Novotechnik, FRG. c) Relatively large type of interferometer manufactured by the firm Novotechnik in operating position near wind tunnel at the Institute of Thermodynamics of the Czechoslovak Academy of Sciences.

diverging beam are formed from which a beam which fills the entire cross section of the measurement space is obtained 153 by a converging lens. The reference ray must pass through the image focal plane of the second lens, outside the area occupied by the principal beam in this plane. The reference beam is spread on the screen (the focusing screen of the camera) with the aid of a small diverging or converging lens placed in this plane so that the areas illuminated by the two beams on the screen cover one another (Fig. 108).

If the reference ray cannot pass through the measurement space, it can be guided outside the measurement space with the aid of a periscope consisting of four small mirrors or prisms, taking advantage of fiber optics. If, as a result of this measure, the trajectory difference is large so that, after the two rays are combined, coherence is not preserved, the optical path of the measurement beam must be lengthened and the equipment must be adjusted similarly as the Mach-Zehnder

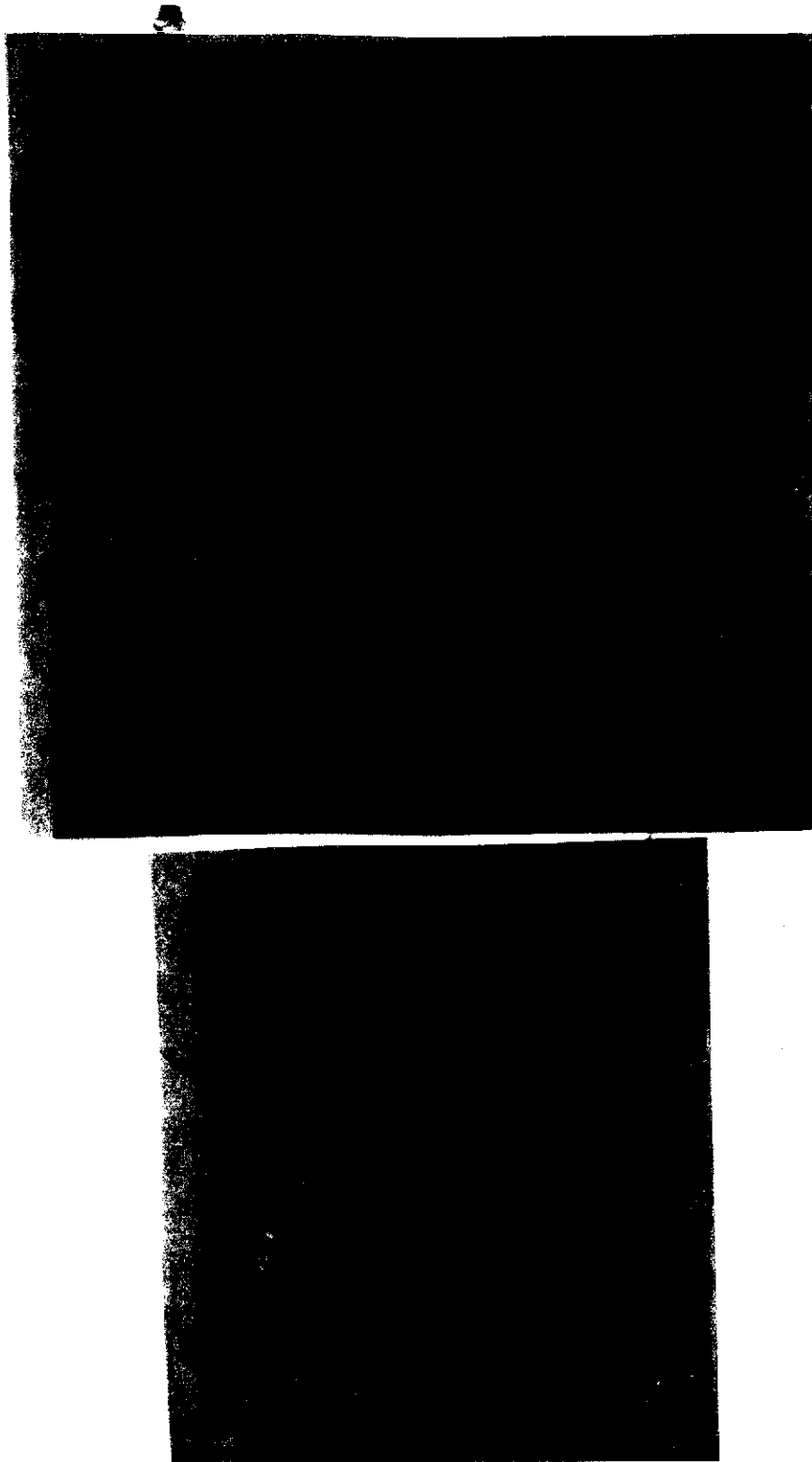


Fig. 104. Interferograms obtained with interferometer adjusted to a finite width of the fringe: a) flow around a projectile [146]; b) flow through cascade.

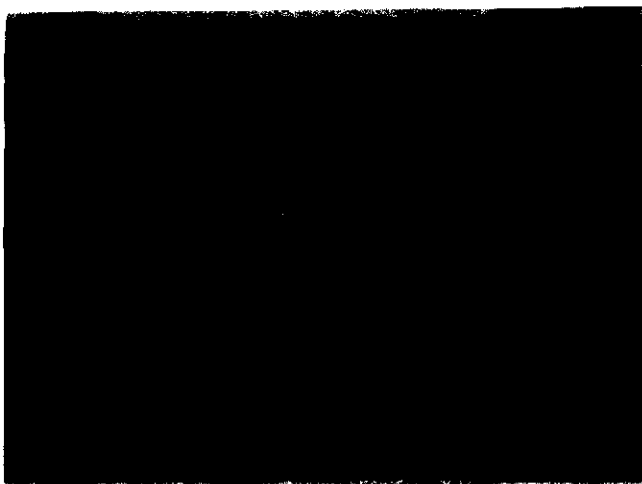


Fig. 104. Interferograms obtained with interferometer adjusted to a finite width of fringe: c) flow around plate with a sharp edge [146].

interferometer. Very small mirrors can be used in the branch of the reference ray in the process.

Hence, interferometers with a laser light source have many advantages. In addition to those that were already mentioned, the additional advantages are the simplicity of the optical equipment requiring a substantially smaller number of high precision optical parts than the Mach-Zehnder interferometer and also the smaller sensitivity to vibrations. On the other hand, however, complications arise during

the operation and when the laser is adjusted. The possibility that disturbing interference fringes caused by the interference of the rays reflected from the optical parts or possibly diffracted on the impurities (dust, grease and fingerprints on the optical parts) are also a disadvantage. The possibility that this may happen is considerable due to the high spatial and time coherence of the light from the laser [237].

/154

Attempts were also made to apply a procedure used in holography. The principle of this procedure during the analysis of the density field in the measurement space is as follows: a coherent beam of light with the required cross section is obtained from the laser, for example, with the aid of a lens. It is split by diaphragms into two beams, one of which, the measurement beam passes through the measurement space, and the second, the reference beam passes outside the measurement space. Using a wedge or mirror, etc., the result is achieved that the two beams are mutually incident at some small angle at the photographic plate in whose plane they subsequently interfere. This arrangement represents a simple laser interferometer (Fig. 109).

In the case when both beams consist of parallel rays and there is no inhomogeneity in the measurement space, equidistant interference fringes are formed on the photographic plate after it is developed similarly as in the Mach-Zehnder interferometer adjusted to a finite width of the fringe. If there is an inhomogeneity in the measurement space, we obtain, as a result of interference, an image which records the changes that

/155

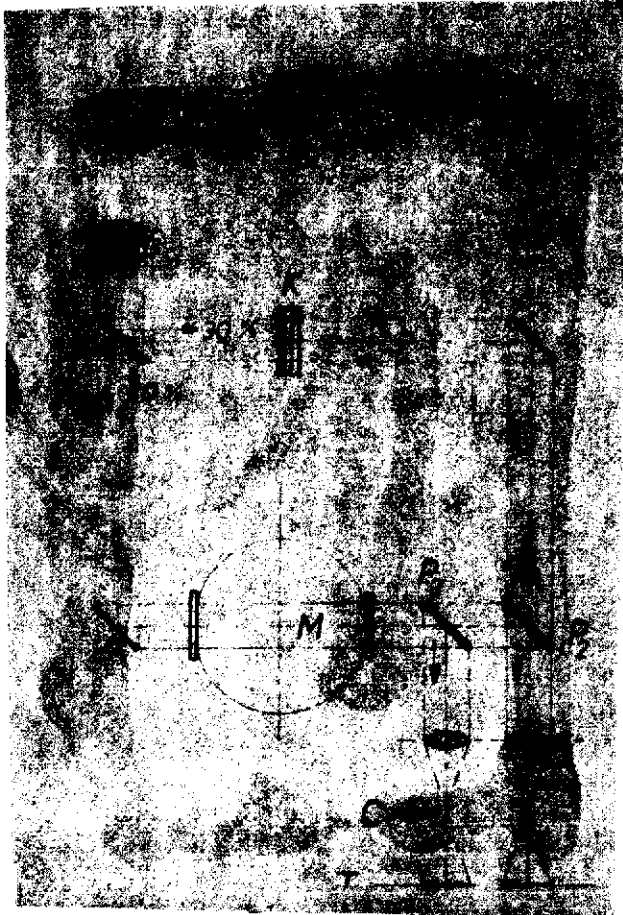


Fig. 105. Schematic diagram of equipment layout for obtaining simultaneously photographs by diaphragm and interference methods (Z - light source; K - compensation plate; M - measurement space; C - knife diaphragm; T - plane of image; the permeability P_1 of the plate is 70%).

occurred in the measurement space. The photographs that are obtained are called holograms, which are analogous to the interference photographs from the Mach-Zehnder interferometer with the exception that no plane in the measurement space is focused on the photographic plate, and also that the maximum density of the interference fringes (the number of intersection points per unit length of the orthogonal) is much higher, up to 100 fringes per 1 mm.

Such a hologram is now inserted in the path of the light beam (the so-called reconstruction beam), which must have the same properties as the reference beam, the same wavelength, the same shape, the same incidence direction as during the hologram exposure (this means that when the hologram was obtained and the reference beam consisted of parallel rays, the rays of the reconstruction beam must be parallel, whereas when the reference beam was divergent, the reconstruction beam must have the same divergence). The hologram represents an optical grid on which the rays of the reconstruction beam

diffract and form diffraction maxima. Only first-order maxima can be observed clearly which are given by two images, one real and the second unreal. The wave fronts of both maxima are the same as the wave fronts of the measurement beam during the hologram exposure, so that the original wave front of the measurement beam is reconstructed.

Two exposures are made on the same photographic plate (film) produced by two identical light pulses from the laser when the interferograms are obtained from the holograms of the flow fields, the first without the flow field, produced by the

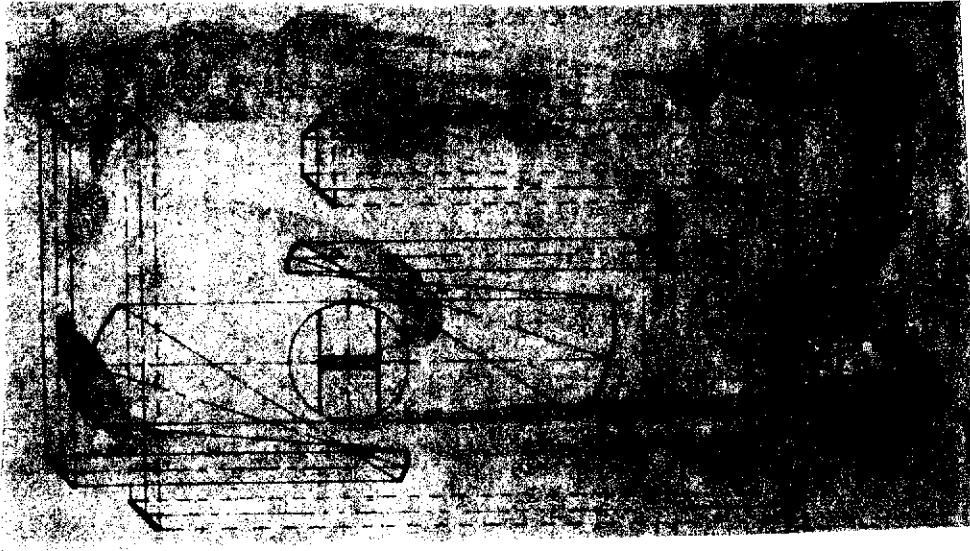


Fig. 106. Schematic diagram of layout for simultaneous analysis by diaphragm and interference methods (1. position of image obtained by interferometer; 2. position of image obtained by diaphragm method).



Fig. 107. Schematic diagram for forming the thin reference beam 1 and the diverging beam 2 from beams from the laser 3.

measurement and reference beam, which gives a system of equidistant parallel interference fringes, and the second with the flow field in the measurement space also produced by the reference and measurement beam. After development of the photographic plates that were exposed twice, we obtained the hologram.

Next, by inserting the hologram in the reconstruction beam of light, we reconstruct the wave front which would impinge on the photographic plate during the simultaneous action of the measurement beams from both exposures. After

circling out the zero order maximum, we obtain on the next photographic plate (possibly with the aid of a camera) placed behind the hologram the interferogram whose fringes denote the points with the same difference in the optical paths of the rays during both exposures, i.e. an interferogram which is analogous to that which we would obtain from a Mach-Zehnder interferometer when it is adjusted to an infinite width of the fringe.

If the first and second hologram exposures have fringes corresponding to the same inhomogeneity, this inhomogeneity will



Fig. 108. Schematic diagram of laser interferometer [237] (1. beam from laser; 2. reference beam; 3. measurement beam; 4. measurement space; 5. plane of image).



Fig. 109. Schematic diagram of two simple laser interferometers for holography [244] (1 and 2. two coherent beams obtained through separation by diaphragms 3 and 4; 1. reference beam; 2. measurement beam; 5. measurement space).

not appear on the interferogram obtained by reconstruction from the hologram, since here only the differences in the optical paths which occurred between the two exposures will appear. This is the great advantage of this method, since the errors in the optical paths which do not

change do not appear on the final interferogram. It is obvious that the configuration of the optical equipment must not change between the two exposures.

/156

Another advantage follows directly from the basic principle of holography. This procedure makes it possible to obtain from the same hologram images of the flow field from different observation directions (in accordance with the position of the photographic plate or camera). The data for an analysis of three-dimensional flow fields can be obtained in this manner [243, 244].

3.2.5. The Method of Phase Contrast

In addition to such classical methods as the diaphragm schlieren method and interferometric methods which have been commonly used for a relatively long period in large aerodynamic laboratories, another new method should also be mentioned, which from the

standpoint of adjusting the apparatus, its substance and effectiveness, lies between the two classical methods that were

mentioned. This method uses the phase contrast and other modifications of this principle [245, 246, 247, 16].

In this method, which requires the same basic equipment as the diaphragm schlieren method, the differences in the phases of the rays, i.e. the phase difference in the rays passing through undisturbed points in the layer that is examined, and the phases of the rays passing through invisible inhomogeneous layers, i.e. points with a different refractive index than that in their vicinity, are converted into amplitude differences, i.e. for example, into changes in the illumination on the screen. The conversion of the phase differences into differences in the illumination (i.e. contrast) is achieved by the interference of the rays that were deflected by the inhomogeneities in the layer that is examined with the rays that were not deflected in the image plane of this layer. The phase differences are converted into amplitude differences that can be well observed by a phase plate or possibly another absorption plate inserted at the point where the image of the source is formed.

The phase plate has two fields whose optical thickness differs, for example, by a quarter of a wavelength. The adjustment of the plate and the form of the field are such that one field exactly covers the basic image of the light source formed by the beam that was not deflected, and the second field covers the remaining images of the source, the images formed by the beams diffracted by the inhomogeneity. This means that the phase of the rays forming the basic image of the source is shifted by $\pi/2$ which corresponds to a displacement along the trajectory equal to one-fourth of the wavelength of the light used. The absorption plate is similar to the phase plate, and it also has two fields. One of these, however, does not cause a phase shift, but absorbs strongly the light of the beam that was not deflected [16].

The interference images that are obtained provide data about the density field of the object, since they contain lines where the density is constant. (In this case, we have the analogy of the Mach-Zehnder interferometer adjusted to an infinite width of the fringe.) However, systems of fringes can also be obtained along which a particular component of the density gradient is constant, which is the analogy of the diaphragm schlieren method with a grid diaphragm. Next, by using clear diffraction fringes that are formed in the plane of the image of the source when a very narrow source with a slit is used, a system of parallel fringes can be obtained on the screen provided the examined layer is homogeneous (similarly as in the Mach-Zehnder interferometer adjusted to a finite length of the fringes). The density field of the layer is determined from the deformations of these fringes caused by the inhomogeneities.

/157

The necessary equipment for the method of phase contrast and the requirements on it are basically the same as in the diaphragm schlieren method. However, monochromatic light is used. Hence, the equipment is less expensive and less sensitive and it can be adjusted and serviced more easily than the Mach-Zehnder interferometer. The advantage is that the method of phase contrast also records weaker inhomogeneities than those obtained with the aid of the Mach-Zehnder interferometer, provided these are relatively small local inhomogeneities in the center of the undisturbed field. Another advantage compared to the normal diaphragm schlieren method is that the evaluation is based on length measurements in the interference image, and not on sensitive photometric measurements. Finally, the fact that the rays which ultimately interfere with one another are separated directly (immediately) before the image is formed is responsible for the fact that the accuracy of this method is affected much less by the inhomogeneities in the surrounding medium than in other sensitive methods used to determine the inhomogeneities in a transparent medium. Therefore, the acoustical or mechanical vibrations to which the Mach-Zehnder interferometer is very sensitive, do not affect considerably the proper functioning of the equipment. However, compared to the Mach-Zehnder interferometer, the disadvantage of the apparatus that was described is the lower average illumination of the observed field which is due to the use of an absorption plate (Fig. 110).

This method is not widely used insofar as we can base our judgment on the single available published study on this subject, although it can be applied very successfully because of the advantages that were already mentioned [245]. The results that were obtained in this study merit a deeper analysis and a comparison with measurements on a Mach-Zehnder interferometer.



Fig. 110. Visualization of flow in a nozzle using the method of phase contrast [245].

3.2.6. Methods Taking Advantage of the Attenuation of the Electromagnetic or Corpuscular Radiation during Passage Through the Gas Flow

/158

The shadow method, the diaphragm schlieren method, and interferometric methods have by now been developed to a high degree of perfection so that very small differences in the density of the gas in the measurement space of the usual type can be determined by them. However, none of these methods can be used at low density values of the gas that is studied. This limitation becomes clearly evident at pressures below 10 torr, when the optical thickness of the gas layer that is studied in a tunnel with the usual dimensions is no longer adequate for obtaining conclusive results. However, tunnels exist in which the static pressure of the free flow is on the order of 10^{-1} torr. New methods were developed for measurements under these conditions. In addition to the methods that take advantage of luminescence (see p. 56) these methods are mainly based on the attenuation of the radiation passing through the gas flow that is examined caused by the effect of absorption or possibly dispersion. The following are used:

- absorption of ultraviolet radiation by oxygen (for wavelengths in the range 1400-1500 Å,
- absorption of ultraviolet radiation by ozone (at wavelength 2537 Å),
- attenuation of soft X-rays,
- attenuation of corpuscular rays (electrons, protons, α particles, potassium atoms).

The attenuation of the radiation during the passage through the measurement space can be described by the well-known relation

$$J(x) = J_0 \exp \left[- \int \mu \rho(x) dx \right], \quad (90)$$

where $J(x)$ is the intensity of the rays after they have covered the path x in the layer that is examined, J_0 is the original intensity of the rays when they enter the layer that is examined (at the point $x = 0$), $\rho(x)$ is the density of the gas examined which is a function of x , since generally it varies along the ray, and μ is the attenuation factor which depends on the type of gas, but is independent of the density of the gas and does not change along the ray, i.e. is independent of x .

Using the methods that were presented, the flow field can be analyzed, i.e. the changes in the density ρ caused by the flow. The basic data about these methods are presented in the following table [248].

Type of radiation used	Ultraviolet radiation	Ultraviolet radiation	X-ray radiation	Electron beams
Properties of the radiation (λ = wavelength)	$\lambda = 1470 \text{ \AA}$ resonance line Xe	$\lambda = 2437 \text{ \AA}$ resonance line Hg	$\lambda \approx 10 \text{ \AA}$	Energy from 4 keV to 60 keV
Type of gas examined	Only O_2	Only O_3	Any	Any
μ Attenuation factor in m^2/kg	$2.5 \cdot 10^4$	$1.7 \cdot 10^4$	79	$10^4 - 10^5$
Density of undisturbed flow in kg/m^3	$7.7 \cdot 10^{-4}$	$1.2 \cdot 10^{-3}$	$2.5 \cdot 10^{-1}$	$2 \cdot 10^{-3} - 2 \cdot 10^{-4}$
p_0 Static pressure in measurement space in torr	0.46	0.7	150	1.2-0.12

Fig. 11 gives the schematic diagram of the equipment for the method taking advantage of the absorption of ultraviolet radiation by oxygen. For example, the image of a shock wave in oxygen in front of the apex of a cone with a 90° apex angle at a Mach number approximately 3.9 was obtained with the aid of this equipment. The diameter of the field that is studied in the measurement space was 3 cm. The source of ultraviolet radiation that was used was an oil-cooled xenon discharge tube with a calcium difluoride window. A pressure below 10^{-4} torr must be maintained in the entire optical equipment. Although the shock wave can be seen on the photograph obtained with the aid of this equipment, it is not possible to obtain conclusive quantitative results by a photographic analysis because of the nonuniformity of the photographic material. These results can be obtained during the study of the measurement space by a narrow pencil of rays from point to point with the aid of a photocoell as long as it is possible to maintain a stationary flow during the measurement period [250].

The attenuation of X-rays during the passage through the measurement space was first used to measure the flow field point by point with the aid of a narrow pencil of X-rays with a 0.05 mm diameter. An attempt has also been made to obtain a photograph of the entire flow; however, here basic difficulties arise and for the time being the results are meaningless. This is due to the fact that the photographic film in comparison with

chambers and counters is relatively insensitive to X-rays. Since the attainable intensity of the soft rays which are suitable for this method is small, the required photographic time is large, on the order of 1 min.

The basic scheme for the method which takes advantage of the attenuation of soft X-rays is simple. The X-ray tube and the intensity reader (detector) of the X-rays, hence, for example, an ionization chamber or a Geiger-Muller counter are placed opposite to one another at opposite sides of the measurement space of the wind tunnel. They are positioned so that they can be jointly moved across and around the measurement part of the tunnel. However, they can also be placed in a fixed position and the model can be moved in the tunnel. The emission from the X-ray tube must be high and the anode must have a small surface [248, 252]. /160

The attenuation of electron beams during the passage through the measurement space was used to measure the measurement space first so that the measurements were made from point to point. The density changes in the flow field were determined on the basis of the intensity of the beam current of the electron beams that passed through that were measured, for example, with the aid of an electrometer or photomultiplier.

A numerical comparison of the discrimination boundaries of the interferometric method and the method using the attenuation of electron beams will demonstrate best the advantage of the second method during the study of gas flows at low pressures. We will start out with equation (90) and assume a constant density $\rho = \text{const}$ along the ray. Since μ also does not vary, as already mentioned, along the ray, we obtain from equation (90), the relation

$$J = J_0 \exp(-\mu \rho l), \quad (91)$$

where l is the thickness of the layer that is examined. If we carry out, for the same initial energy of the electrons and the same initial intensity J_0 of the electron beam, two measurements during which we measured the intensity J_1 of the electron beam after passage through the point with density ρ_1 , and the intensity J_2 of the same beam after passage through the point with density ρ_2 , we obtain, for the difference $\Delta\rho = \rho_1 - \rho_2$ of these two densities from the previous equation, the relation

$$-\Delta\rho = \frac{1}{\mu l} \ln \frac{J_2}{J_1}, \quad (92)$$

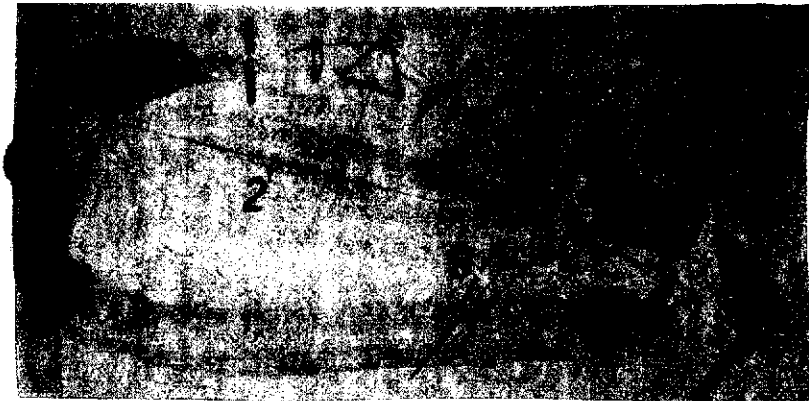


Fig. 111. Schematic diagram of equipment for the visualization method taking advantage of the absorption of ultraviolet radiation by oxygen [250] (1. source of ultraviolet radiation; 2. monochromator; 3. nozzle; 4. measurement space; 5. plane of image).

from which we can clearly write from small changes ΔJ

$$-\Delta e = \frac{1}{\mu l} \frac{\Delta J}{J} \quad (93)$$

Finally, after introducing in this relation the so-called linear attenuation coefficient α defined by the relation $\alpha = \mu\rho$, we obtain:

$$-\frac{\Delta e}{e} = \frac{1}{\alpha l} \frac{\Delta J}{J} \quad (94)$$

We will assume for the numerical comparison that the thickness of the layer that is examined is $l = 6$ cm, its density is $\rho = 4.7 \cdot 10^{-3}$ kg/m³, which corresponds, in the case of air, to a pressure of 3 torr at a temperature of 25°C, an initial energy of the electrons of 5 keV and an attenuation factor $\alpha = 0.9$ cm⁻¹. Given the high sensitivity of modern instruments for the measurement of electrical current, current intensities on the order of 10^{-9} A can be measured well with a 1% accuracy. Hence, we will determine $\Delta J/J$ with such accuracy. From equation (94) it follows that 0.2% changes in the density can be measured well, so that in our case $\Delta\rho = 9.4 \cdot 10^{-6}$ kg/m³, which corresponds to a difference in the pressures of 0.006 torr.

When we use the interferometer, we will distinguish the shift of interference fringes which is 1/10 of the width of the fringe. This shift is caused by a change in the optical path of one of the interfering beams by 1/10 of the wavelength λ of the light that is used, to which corresponds the difference $\Delta n = 0.1\lambda/l$ in the refractive indices. Now, using equation (47) and letting the constant in it be $K_0 = 2.26 \cdot 10^{-4}$ kg⁻¹m³ which we calculated for air in the lines following equation (47), we find that the difference $\Delta\rho$ in the density which is equal to

$$\Delta e = \frac{0.1\lambda}{lK_0}$$

corresponds to the difference Δn in the refractive indices that was given. If we also take into consideration that green light at wavelength $\lambda = 5 \cdot 10^{-5}$ cm was used and let, as in the preceding paragraph, $l = 6$ cm, we find that densities greater than $\Delta \rho = 3.6 \cdot 10^{-3}$ kg/m³ can be measured interferometrically. Hence, the method which takes advantage of the attenuation of electron beams is more sensitive by two orders of magnitude than the interferometric method in the case under consideration.

A further substantial increase in the sensitivity of the method taking advantage of the attenuation of electron beams cannot be achieved sufficiently well by increasing the factor αl in equation (94), since the intensity of the measured electron beam would drop sharply and could not be measured so accurately. This difficulty cannot be eliminated by increasing the input intensity of the beam current, since at higher values of the input intensity of the beam current, the gas is heated, Article [253] states that for an electron probe the heating is negligible at an input intensity of the beam current less than 10^{-7} A.

/162

The equipment for the method which takes advantage of the attenuation of electron beams consists of the source of the narrow electron beam and the detector. Diaphragms are placed in front of the detector which prevent the impinging of electrons that were deflected from their original direction. The entire equipment can be placed inside the measurement space [247] where it must be shifted and turned, or the walls of the measurement space must have appropriate windows. Another method was used to record the behavior of the density across a shock wave in the gas flow in a shock tube at a low pressure (0.5 torr) when neither the interferometric method nor the X-ray method could be used [254]. The windows in the shock tube had openings with a 10-15 μ m diameter in a platinum foil which was 25 μ m thick. The source of the electrons was mounted on a spherical suspension whose center of rotation was in the inlet window, which made it possible to adjust correctly the direction of the electron beam. Other types of corpuscular radiation can be handled similarly.

The disadvantage of the method that was described which takes advantage of the attenuation of the electron beam is that it does not furnish simultaneously the entire image of the flow field. However, since, in comparison with the method taking advantage of the absorption of X-rays the reaction time of the detector is much shorter (on the order of several microseconds) the image of the entire flow field can conceivably be obtained with the aid of a special cathode ray tube.

However, in an attempt to obtain on the fluorescent screen simultaneously the electron shadow image of the entire flow field, experiments were also made with a bundle of diverging

electron beams with a larger cross-sectional area of the bundle [254]. When a bundle of parallel electron beams enters a gas, the electrons are deflected from the original direction of motion as a result of diffusion and the bundle widens, acquiring the shape of a spindle, until it occupies roughly a spherical space whose diameter is approximately equal to the range of the electron. The air in the region which the electrons enter has a bluish-violet glow.

The schematic diagram of the equipment that was used in [254] to obtain the electron shadow image of the flow is given in Fig. 112. It consists of an air-tight chamber sealed at one end with a glass window through which the screen is observed or photographed from the outside. The gas flow which is studied enters into the chamber from the sides through a nozzle. The required vacuum is maintained in the chamber with the aid of a vacuum pump which is connected to the neck at the side of the chamber. The source of the electron beams, the electron gun, is inside the chamber. The transparent fluorescent screen on which the bundle of impinging electrons forms a circular luminous trace is placed at the distance s_0 from the gun perpendicularly to the axis of the electron beam. When the input energy of the electrons is in the range 3-25 keV, and the pressure in the chamber in the range 1-20 torr, at a distance $s_0 = 65$ mm the part of the luminous circular trace at any point of which the luminance can be considered to be the same, has roughly a 20 mm diameter. However, beyond this diameter, the luminance of the trace is reduced considerably. Nevertheless, shadow images can be observed under the conditions that were described even when the diameter of the trace is 40 mm. During visual observation, this attenuation of the luminance of the periphery of the field of view does not cause great difficulties. However, it makes the photography more difficult, since the ratio of the luminance on the periphery of the trace to the luminance at the center of the trace is about 1:10. This shortcoming can be eliminated by using an absorption equalizing filter. It can be obtained by photographing the luminous trace on the screen on a photographic plate on a 1:1 scale when the gas whose flow is to be studied does not enter the chamber. The energy of the electrons and the pressure inside the chamber are adjusted to values at which the gas flow will be studied later. The negative is then used as the base to which a fluorescent layer is applied. A transparent fluorescent screen is obtained in this way which must be inserted in the chamber instead of the screen without the filter.

/163

A field of view with larger dimensions can be obtained by using a magnetic lens which expands the originally narrow beam. From the published photographs of the shadow electron image of an airflow from a cylindrical nozzle with a 1 mm diameter into a chamber in which the pressure was 3.2 torr



Fig. 112. Schematic diagram of equipment used to obtain the electron shadow image of the flow [245] (1. source of electrons; 2. nozzle; 3. connection for pump; 4. fluorescent screen; 5. glass window).

(the pressure drop on the nozzle was 600 torr) produced by an electron beam with an initial energy of 7.5 keV [254], it can be seen that sufficiently clear images cannot be obtained by this method. Due to this and also due to the entire character of the method, the assertion of the author of the method that quantitative data about the flow field can be obtained with its aid should be accepted with certain reservations. The acquisition of quantitative data would naturally require calibration equipment, i.e. it would require that the relations between the luminance of the trace on the screen, the pressure and the density of the gas layer in the chamber, the thickness of this layer and the deflection of the electron beams from the original direction be determined.

Conclusion

From the survey of the methods that was presented, it follows /164 that the visualization possibilities are far-ranging and that they can be used on a very wide scale. The significance of visualization was already discussed in the introduction. The great number of methods used until now makes it possible to visualize almost any case of flow. Thus, for example, airflow can be visualized from the lowest velocities up to the highest supersonic velocities, by using smoke up to velocities of 30 m/sec, aluminum powder up to velocities of 90 m/sec, and with the aid of interferometric methods, or possibly diaphragm schlieren methods starting with velocities of 60 m/sec, and, finally, for high subsonic and supersonic flows, with the aid of the shadow method. Images of the flow at very low pressures (fractions of a torr) can be obtained, for example, by taking advantage of luminescence exactly like images of the flow of highly viscous fluids by taking advantage of temporary birefringence.

With regard to the cost of the individual methods, the conclusion can be made, on the basis of the survey, that the requirement to obtain quantitative values entails greater expenditures on the equipment. Certain methods in group 3 (the interferometric method and the diaphragm schlieren method) require the most expensive equipment. Further development of methods in this group should be expected in conjunction with the use of laser light sources.

The majority of the methods that were described have already been used many times and in many cases the equipment required for their use has been thoroughly elaborated. On the other hand, very little is known about other newer methods. These are mainly luminescence methods (see p. 56), the temporary birefringence (see p. 75), and the phase contrast methods (see p. 158). For the time being, these methods have not been analyzed and worked out thoroughly, and thus cannot be used on a wider scale.

REFERENCES

General Bibliography

1. Zaks, N. A., Visual'nyye metody izucheniya obtekaniya tel potokom, [Visualization Methods for the Study of Flow around Streamlined Bodies], VVIA im. Zhukovskogo, 1949.
2. Zaks, N. A., Osnovy ekperimental'noy aerodynamiki, [Foundations of Experimental Aerodynamics], Oborongiz, 1953.
3. Balint, E., Techniques of Flow Visualization, Aircraft Engng, June 1953.
4. Popov, S. T., Nekotoryye zadachi i metody eksperimental'noy aeromekhaniki, [Some Problems and Methods in Experimental Flight Mechanics], "Gos. isdat. teknikoteoretich. lit." Press, Moscow, 1952.
5. Pankhurst, R. C., and Holder, D. W., Wind-Tunnel Technique, I. Pitman, London, 1952.
- 5a. Pankhurst, R., and Holder, D., Tekhnika eksperimenta v aerodinamicheskikh trubakh, [Experimental Techniques in Wind Tunnels] (translation), "Izdat. inostr. lit." Press, Moscow, 1955.
6. Řezníček, R., Výzkum optických vlastností proudících tekutin. Research on [Optical Properties of Fluid Flows], Final report on project M-21, Mechanization Department, School of Agriculture, Prague, 1958.
7. Outurquin, R., La visualition au service de l'aeronautique, [Visualization in the Service of Aeronautics], "Technique et Science Aeronautique" Press, 1955.
8. Kurganov, M. M., Vizual'nyye metody issledovaniya potokov [Visualization Methods for the Study of Flows], CAGI [Central Institute of Aerohydrodynamics im. N. Ye. Zhukovskiy], Technical Notes, 1939.
9. Hošek, J., Aerodynamika vysokých rychlostí, [High-Speed Aerodynamics], "Nase vojsko" Press, Prague, 1949.
- 9a. Hošek, J., Aerodynamika bol'shikh skorostey, [High-Speed Aerodynamics] (translation), "Izdat. inostr. lit." Press, Moscow, 1954.

10. Řezníček, R., Müller, U., and Badin, J., Soubor experimentálních prací v oboru visualisace proudění, prováděných v rámci výzkumné činnosti katedry fyziky VSZ v Praze [Collection of Experimental Studies in the Field of Flow Visualization Carried Out as Part of the Research at the Physics Department of the School of Agriculture in Prague] (unpublished).
11. Eck, B., Technische Strömungslehre, [Flow Theory in Engineering], "Springer" Press, Berlin, 1954.
12. Brodovicz, K., "Visualization methods applied to the study of media with a nonuniform density distribution," Technika Lotnicza 44 (March-June 1957).
13. Matula, D., "An analysis of methods for the visualization of airflows at low velocities," VZLU, Letnany, Report, Collection E-70/25-V, 1954.
14. Preston, J. M., "Visualization of boundary-layer flow," Reports and Memoranda 2267 (1946).
15. Horák, Z., and Krupka, F., Fyzika, [Physics], "SNTL/SVTL" Press, 1966.
16. Fuka, J., and Havelka, J., Optika, [Optics], "SPN" Press, Prague, 1961.
17. Brdička, M., Mechanika kontinua, [Continuum Mechanics], "NČSAV" Press, Prague, 1959.
18. Lojčjanskij, L. G., Mechanika kapalin a plynů, [Mechanics of Fluids and Gases], Part I, "SNTL" Press, Prague, 1954.
19. Symposium of Flow Visualization, Collection ASME, 1960.
20. Rektorys, K. et al., Préhled užité matematiky [Survey of Applied Mathematics], "SNTL" Press, Prague 1963.
21. Lau, E., and Krug, W., Die Äquidensitometrie, [Equidensitometry], "Akademie" Press, Berlin, 1957.
22. Lambourne, N. C., and Pusey, P. S. "Some visual observations of the effects of sweep on the low-speed flow over a sharp-edged plate at incidence," Report and Memoranda 3106 (1958). /166
23. Gukosova, Ya. A. et al., Aerodinamicheskoye sovershchenstvovniye lopatochnykh apparatov parovykh i gazovykh turbin, [Aerodynamic Improvement of Bladed Apparatus in Steam and Gas Turbines], "GEI" Press, Moscow-Leningrad, 1960.

Section 1.1.1.

24. Reynolds, O., Papers on Mechanical and Physical Subjects, Cambridge, 1890.
25. Hele-Shaw, H. S., "Experimental Investigation of the motion of a thin film of viscous fluid," Rep. Brit. Assoc. (1898).
26. Hele-Shaw, H. S., "Nature of surface resistance of water and streamline motion under certain experimental conditions," The Engineer (1898).
27. Wortman, F. X., "A method for the observation and measurement of water flows with the aid of tellurium," Zeitschrift für Angewandte Physik 5 (June 1953).
28. Werlé, H., "Nonstationary motion in constant circulation. Results obtained on the basis of hydrodynamic visualization," La Recherche Aeronautique 26 (1952).
29. Werlé, H., "Some experimental results on backswept wings at low velocities obtained in a hydrodynamic tunnel," La Recherche Aeronautique (September-October 1954).
30. "Visualization in a hydrodynamic tunnel," La Recherche Aeronautique (May-June 1953).
31. Jordan, P., "Bouyancy calculations and flow processes when maximum bouyancy is not attained," Luftfahrtforschung 16 (1939).
32. Richardson, "Velocity-gradient methods in rheology," Physics 6 (1935).
33. Van Meel, D. A., and Vermij, H., "A method for flow visualization and measurement of velocity vectors in three-dimensional flow patterns in water models by using color photography," Appl. Sci. Res., Section A 10(2) (1961).
34. Winter, E. F., "Flow visualization techniques applied to combustion problems," J. Roy. Ae. Soc. 62(568) (1958).
35. Myl, J., and Solc, Z., "A method for determining the velocity and direction of streamlines," Chemický průmysl 13(4) (1963).
36. Werlé, H., "Simulation of the effect of the soil in a hydrodynamic tunnel," La Recherche Aeronautique, No. 95 (1963).

37. Howland, B., and Springer, G. S., "Use of electrochemoluminescence in visualizing separated flows," J. Fluid Mech. 24, 697 (1966).
38. Springer, G. S., "Use of electrochemoluminescence in the measurement of mass transfer rates," Rev. Sci. Instr. 35, 1277 (1964).
39. Goldish, L. H., "Tracer introduction by flash photolysis," Chem. E. Sci. 20, 1011 (1965).
40. McMaster, "Flash photolysis tracer studies," Sen. Project, Rep. University of Delaware, 1964.
41. Allen, M., "Visualization of 3-dimensional flow," Instr. Control system, No. 3, 1966-93.
42. Allen, M., "Better way to trace liquid flow patterns," Ch. Engng 66 (may 1959).
43. Allen, M., "Fluorescent particles for tracing liquids," Chem. Engng. 67 (June 1960).
44. Baker, D. J., "A technique for the precise measurement of small fluid velocities," J. Fluid Mech. 26 (November 1966).
45. Adams, F. G., "A study of the technique of electrochemoluminescence in determining points of separation and transitions," S. M. Thesis, Mass. I. T., 1965.
46. Schiller, T. R., "An apparatus for applying the technique of electrochemoluminescence to boundary layer studies," S.M. Thesis, Mass. I. T., 1964.

Section 1.1.2.

/167

47. Relf, E. F., "Photographic investigation of the flow around a model aerofoil," Rep. and Mem. 76 (March 1913).
48. Relf, E. F., Rep. and Mem. 50 (1911-12).
49. Walker, P. B., Rep. and Mem. 1402 (1931-32).
50. Jones, B. M., Farren, W. S., and Lockyer, Rep. and Mem. 1065 (1926-27).
51. Prandtl, L., and Teitjens, O., Applied Hydro- and Aeromechanics, McGraw-Hill, 1934.
52. Prandtl, L., Hydro- und Aeromechanik, [Hydro and Aeromechanics], Vol. II, "Julius Springer" Press, Berlin, 1929.

53. Jerie, J., "Flow through a labyrinth seal," in the collection Výzkum v oboru proudění, [Research in the Field of Flow], Vol. I., "NCSAV" Press, Prague, 1955.
54. Schiegler, L. "The flow process in grate-firing combustion chambers," Z. Ver. Deut. Ing. 82(29).
55. Ahlborn, F., "The hydrodynamic resistance mechanism," Abhandl. geb. d. Naturwiss., Hamburg 17 (1902).
56. Rubach., H., "The origin and motion of a pair of vortices in cylindrical bodies," Forschungshefte des VDI 185 (1916).
57. Timme, A., "The velocity distribution in vortices," Ingenieur-Archiv, No. 1,3 (1957).
58. Pešek, R., "Some results obtained from the visualization of flow," paper read at the scientific conference at the Department of Mechanical Engineering at the Czechoslovak Research Institute for Technology on February 22, 1957.
59. Birkhoff, G., and Caywood, T. E., "Use of air bubbles," J. Appl. Phys. 20, 646 (1949).
60. Caffyn, and Underwood, "An improved method for the measurement of velocity profiles in liquids," Nature (February 9, 1952).
61. Barth, "Application of model experiments to solution of flow problems," Z. Ver. Deut. Ing. 92, 105 (1950).
62. Wuest, W., "Visualization of flows," ATM, No. 329 (1963).
63. Danckwerts, P. V., "Flow visualization by means of a time reaction," J. Fluid Mech., No. 3 (1963).
64. Smith, A.M.O., and Clutter, D. W., "The electrochemical technique of flow visualization," in the collection Symposium on Flow Visualization, ASME, 1960.
65. Schraub, "Use of hydrogen bubbles for quantitative determination of time-dependent velocity fields in low-speed water flows," ASME Paper 64, WA/FE-20.

Section 1.2.1.

66. Preston, J. H., and Sweeting, N. E., "Wood smoke as a means of visualizing boundary-layer flow at high Reynolds number," Rep. and Mem. 2023 (1943).

67. Lippisch, A., "Results from the Deutsche Forschungsanstalt für Segelflug smoke tunnel," J. Roy. Ae. Soc. 43, 93 (1939).
68. Drees, I. J. M., and Hendaal, I. W. P., "Airflow patterns in the neighborhood of helicopter rotors," Aircraft Engng 23(266) (April 1951).
69. Salter, C., "Multiple-jet white-smoke generators," Rep. and Mem 2657 (March 1950).
70. "Smoke traces aerodynamic patterns," Aviation Week 64, 12 (1956).
71. Brat, J. S., "Flow patterns in the wake of an oscillating aerofoil," Rep. and Mem. 2773 (March 1950).
72. Brown, F. N., "An American method of photographing flow patterns," Aircraft Engng 24, 280 (1952).
73. Herzig, H. Z., and Hansen, A. G., "Visualization studies of secondary flows with applications to turbomachines," Trans. ASME 77, 3 (1955).
74. Herzig, H. Z., and Hansen, A. G., "Airflow studies in miniature smoke jet wind tunnels," Aero Digest 72, 6 (1956).
75. Brown, F. N., "Fundamental flow patterns," Aircraft Engng. 28, 331 (1956). /168
76. Preston, J. H., and Sweeting, N. E., "An improved smoke generator for use in the visualization of airflow particularly boundary-layer flow at high Reynolds number," Rep. and Mem. 2023 (1943).
77. Farren, W. S. "Airflow with demonstration on the screen by means of smoke," J. Roy. Ae. Soc. 36, 454 (1932).
78. Clark, K. W., "Methods of visualizing airflow with observations on several aerofoils in the wind tunnel," Rep. and Mem. 1552 (1933).
79. Tanner, T., "Movement of smoke in the boundary layer of an aerofoil without and with slot," Rep. and Mem. 1352 (1933).
80. Simons, F. G., and Dewoy, N. S., "Wind tunnel experiments with circular discs," Rep. and Mem. 1334 (1930).
81. Simons, F. G., and Dewoy, N. S., "Photographic records of flow in the boundary layer," Rep. and Mem. 1335 (1931).

82. Simons, F. G., and Dewoy, N. S., "Results from the aerodynamic testing station in Göttingen," Lieferung 2 (1923).
83. Hazen, D. C., "On visual aerodynamics," The Aeroplane (July 15, 1955).
84. Jacobs, E. N., and Sherman, A., "Airfoil characteristics as affected by variations of the Reynolds number," NACA T.R. 586, 1937.
85. Townend, H.C.H., "On rendering airflow visible by means of hot wires," Rep. and Mem. 1349 (1931).
86. Townend, H.C.H., "Hot wire and spark shadowgraphs of the airflow through an airscrew," Rep. and Mem. 1434 (1932).
87. Hampl, J., and Holý, S., "Visualization of flow by means of the shadow method at low velocities," report from SVK [expansion unknown] to the Czechoslovak Technical Research Institute under the leadership of Professor Pesek.
88. Schrüfer, E., "The form of the ray during airflow in a vacuum," Zeit. f. Angewandte Physik 9, 2 (1957).
89. Kunkel, W. B., and Hurlbut, F. C., "Luminescent gas visualization for low-density wind tunnels," J. Appl. Phys. 28, 8 (1957).
90. Fowler, H. S., "A smoke generator for use in wind tunnels," NRC 8225 (research report MET-452), 1964.
91. Hansen, A. G., "Smoke studies of secondary flows in bends, tandem cascades and high turning configurations," NACA Res. Mem.
92. Hansen, A. G., Aero Digest 72(6) (1956).
93. Lippisch, A. M., "Flow visualization," Aero. Eng. Rev. 30(2) (1958).
94. Früangel, F., Impulsetechnik, [Pulse Technique], Leipzig, 1960, p. 378.
95. Bomelburg, H. J., et al., "The electric spark method for quantitative measurements in flowing gases," ZFW 7(11) (1959).
96. Gregore, I. Mc., "The vapor-screen method of flow visualization," J. Fluid Mech. 11(4) (1961).

97. Hall, I. M. et al., "Experiments with inclined blunt-nosed bodies at $M_0 = 2.45$," Rep. and Mem. 3128 (1957).

Section 1.2.2

98. Bourot, J. M., Chronofotographie des Champs Aérodynamiques, [Chronophotography of aerodynamic fields], "SDITA" Press, Paris, 1949.
99. Bourot, J. M., "Balsa dust shows rotor flow geometry," Aviation Week 53, 1 (1950).
100. Taylor, M. K., "A balsa dust technique for air-flow visualization and its application to flow through model helicopter rotors in static thrust," NACA T.N. 2220, November 1950.
101. Lebouf, R., and Voret, C., "Microphotography of carbide particles pulverized in a combustion chamber," Rech. Aeronautique 45 (1955).
102. Girard, A., and Robert, E., "Stereoscopic chronophotography of particles in a suspension in an aerodynamic flow," Rech. Aeronautique 49 (January, February 1956). /169
103. Townend, H. C., "A method of air cinematography capable of quantitative analysis," J. Ae. Sci. 3 (1936).
104. Townend, H. C., "Visual and photographic methods of studying boundary-layer flow," Rep. and Mem. 1803 (1937).
105. Townend, H. C., "Abstract of a film illustrating the theory of flight," Rep. and Mem. 1767 (1937).
106. Laniece, F., and Tisseau, R., "A study of the aerodynamic field by means of a perturbation method," Rech. Aeronautique 34 (July, August 1953).
107. Tisseau, M., "Measurement of aerodynamic velocities by means of a perturbation method," Rech. Aeronautique 5 (1948).
108. Bird, J. D., "Visualization of flow fields by use of tuft grid technique," J. Ae. Sci. 19, 7 (1952).
109. Kubeš, J., "Flow in a drum blower with blades bent forward, in the collection Výzkum v oboru proudění, [Research in the Field of Flow], Part I, "NCSAV" Press, Prague, 1955.
110. Schlichting, H., "Aerodynamics of the mutual interference of aircraft parts," British R.A.N. Library Transl. 275 (1948).

111. Purser, P. E., Spearman, M. L., and Bates, W. R., "Investigation of low speed of downwash characteristics of small-scale swept-back wings," NACA T.N. NO. 1378, 1947.
112. Kedi, U. M., "Velocity measurement with the aid of illuminated or luminescent particles," article in [146a], p. 147.
113. "Method for the visualization of flows in gaseous media," Die Technik 15(6) (1960).
114. Benetka, J., Cejchování směrových sond, [Calibration of directional Probes], "VZLÚ" Press, Letnany, 1964.
115. Maltby, R. L., "Flow visualization in wind tunnels using indicators," AGARDograf 70, 1962.

Section 2.1

116. Main-Smith, J. D., "Chemical solids as diffusible coating film for visual indications of boundary-layer transition in air and water," Rep. and Mem. 2755 (February 1950).
117. Walker, W. P., "Detection of laminar flow on ship models," Trans. Inst. Nav. Arch. (April 1949).

Section 2.2

118. Jaňour, Z., "Experimental analysis of the development of the boundary layer on a profile," Report of the Aeronautical Research Institute, Letňany, No. 6, 1949.
119. Preston, J. H., and Sweeting, N. E., "experiments on the measurement of transition position by chemical methods," Rep. and Mem. 2014 (1945).
120. Owen, P. R., and Ormerod, A. O., "Evaporation from the surface of a body in an airstream," Rep. and Mem. 2875 (September 1951).
121. Richards, E. J., and Burstall, F. H., "The china-clay method of indication transition," Rep. and Mem. 2126 (1945).
122. Holder, D. W., "Transition indication in the National Physical Laboratory 20 in x 8 in high-speed tunnel," Rep. and Mem. 2079 (1945).

123. Gray, W. E., "A simple visual method of recording boundary layer (liquid film)," Tech. Note Aero., RAE 1816 (1946).
124. Jones, B. M., "Airflow about stalled and spinning aeroplanes shown by cinematograph records of the movements of wool tufts," Rep. and Mem. 1494 (1932).
125. Abbot, I. H., and Sherman, A., "Flow observation with tufts and lampblack of the stalling of four typical airfoil sections in the NACA variable density tunnel, " NACA T.N. 672, 1938. /170
126. Smith, A.M.O., "A dust method for locating the separation point," J. Ae. Sci. 22, 4 (1955).
127. Khabinskaya, S. P., Opyty po opredeleniyu oblasti sryva na trokh krylyakh so shchitkami i eleronamy, [Experiments in Determining the Stall Region on Three Wings with Flaps and Ailerons], CAGI [Central Institute of Aerohydrodynamics im. N. Ye. Zhukovskiy], Technical Notes, 1939,
128. Murphy, J. S., "Measurement of wall shearing stress in the boundary layer by means of an evaporating liquid film," J. Appl. Phys. 27(9) (1956).
129. Hignett, E. T., The Use of Dust Deposition as a Means of Flow Visualization, Her Majesty's Office, London, 1963.
130. Hignett, E. T., "Surface flow pattern as visualized by dust deposits on the blades of a fan," J. Roy. Ae. Soc. 67, 633 (1963).
131. Persoz, B., and Gernier G., "Visualization by means of tufts with a fatty base," Rech. Aéron., No. 60 (1957).
132. Garner, H. C., and Bryer, D. W., "Experimental study of surface flow and part-span vortex layer on a cropped arrowhead wing," Rep. and Mem. 3017 (1957).
133. Tighe, J. G. Mc. et al., "Two techniques for detecting boundary layer transition in flight at supersonic speeds and at altitudes above 20,000 feet," NASA T.N. D-18, 1959.
134. Haines, A. B., Some Notes on the Flow Patterns Observed over Various Sweptback Wings at Low Mach Numbers, H. M. Stationary Office, London, 1960.
135. Hopkins, E. J. Et al., "Photographic evidence of stream-wise arrays of vortices in boundary-layer flow," NASA, T.N., D-328, 1960.

136. Loving, D. L., and Katzoff, S., "The fluorescent-oil film method and other techniques for boundary-layer flow visualization," NASA Memo 3-17-59 L, 1959.
137. Stalder, J. R., et al., "The use of a luminescent lacquer for the visual indication of boundary-layer transition," NACA T. N. 2263, 1951.

Section 3.1

138. Boeder, P., "Birefringence in flow," Zeitschr. für Physik 75 (1932).
139. Cvětkov, V. N., "Some optical methods for the study of micromolecular structures in solutions," Chemické listy 49, 10 (1955).
140. Wellwer, R., Middlehurst, D. J., and Steiner, R., "The photo viscous properties of fluids," NACA T.N. 841, 1942.
141. Weller, R., "The optical investigation of fluid flow," J. Appl. Mech. 14 (1947).
142. Lindgren, E. R., "Note on the flow of liquids in tubes," Appl. Sci. Research 44 (1954).
143. Leaf, W., "Fluid flow study of locomotive firebox design," Mech. Engng. 67 (1945).
144. Řezníček, R., "The use of temporary birefringence of fluid flows in the visualization of flows," paper read at the scientific conference at the Mechanical Engineering Department at the Czechoslovak Research Institute for Technology on February 22, 1957.
145. Maxwell, I. C., Proc. Roy. Soc. 22 (1873-74).

Section 3.2

146. Landenburg, R. W., Lewis, B., Pease, R. N., and Taylor, H. S., Physical Measurements in Gas Dynamics and Combustion, Princeton Univ. Press, Princeton, 1954.
- 146a. Landenburg, R. W., Lewis, B., Pease, R. N., Fizicheskiye izmereniya v gazovoy dinamike i pri gorenii, [Physical Measurements in Gas Dynamics and Combustion] (translation), "Izd. inostr. lit." Press, Moscow, 1957.

147. Kašpar, J., "Application of shadow and mist method to the visualization of density changes in the flow and temperature field," Research report No. V 857/66, VZLU, 1966.
148. Shitov, V. A., and Sokolova, V. A., "Methods for the photography of aerodynamic spectra at supersonic velocities," Trudy VVLA 62 (1940).
149. Horwath, L., Squire, H. B., and Lock, C. N. H., Modern Developments in Fluid Dynamics in High-Speed Flow, Vol. II, Oxford, 1953. /171
150. Lemens, P. et al., "Development of apparatus for a hypersonic ballistic installation..." in the collection Sovremennaya tekhnika aerodinamicheskikh issledovaniy, [Modern Techniques for Aerodynamic Studies], Moscow, 1965, p. 186.
151. Hotz, R., "NACA shows Ames Laboratory progress," Aviation Week 49(4) (1948).
152. Ferri, A., Aerodinamika sverkhzvukovykh techeniy, [Aerodynamics of Supersonic Flows], "Gos. izd. tekhn. teoret. literatury" Press, Moscow, 1953.
153. Chilton, U. F., Aerodinamika bol'shikh skorostey, [High-Speed Aerodynamics], "Izd. inostr. literatury" Press, Moscow, 1955.
154. Wilson, M. R., and Hiemenz, R. J., "High-speed multiple-spark light sources," Rev. Sci. Instr. 29(11) (1958).
155. Kumar, S. S., "A high-intensity spark light source for schlieren and direct shadow photography," NAL Tech. Note, 1964.
156. Ferri, A., "Method for evaluating from shadow or schlieren photographs," NACA Tech. Note 1808, 1949.
157. Price, E. W., et al., "Contrast and color in interference fringes," Rev. Sci. Instr. 24 (1953).
158. Holder, D. W. et al., "A high-speed camera for the photography of shock-wave oscillation in a wind tunnel," Rep. and Mem. 2901 (1949).
159. Seiff, A., and Short, B. J., "An investigation of supersonic turbulent boundary layers on slender bodies of revolution in free flight by use of Mach-Zehnder interferometer and shadowgraphs," NACA Tech. Note, 1958.

160. Sammonds, R. I., "The shock-wave patterns on a cranked-wing configuration," NACA Tech. Note D-346, 1960.

Section 3.2.1

161. Dvorak, V., "A new simple method for schlieren observations," Ann. d. Phys. u. Chem. 9, 502 (1880).
162. Schardin, H., "The schlieren method and its applications," Ergebnisse d. exakten Naturwissenschaften 20 (1942).
163. Hankins, G. A., and Cope, W. F., "The flow of gases at sonic and supersonic speeds," Proceedings of the Institution of Mechanical Engineers, 1946, p. 155.
164. Bukovský, J. J., "Research on cascades in turboengines at high velocities," in the collection Proudění v lopatkových strojích, [Flow in Cascade Machines], "NCSAV" Press, Prague, 1958.
165. Ormerod, A. O., "Note on the use of the three-dimensional shock-wave recorder for studying interference in supersonic wind tunnel," Reports and Memoranda 2798 (December 1950).
166. Kovasznay, L. S. G., Technique for the Optical Measurement of Turbulence in High-Speed Flow, Publications of the Am. Soc. Mech. Engrs., 1949.
167. Petrov, G. I., Primeneniya tenevogo metoda dlya issledovaniya spektrov vozdušnogo potoka, [Application of Shadow Method to the Study of Airflow Spectra], "CAGI [Central Institute of Aerohydrodynamics im. N. Ye. Zhukovskiy], Technical Notes, No. 107, 1936.
168. Lamplough, F. E., "Shock-wave shadow photography in tunnel and in flight," Aircraft Engng (April 1951).
169. Véret, C., "Shadowgraph apparatus for the S2 Modane wind tunnel," La Rech. Aéron. 90 (1962).
170. Love, E. S., "A new shadowgraph technique for the observation of conical flow phenomena in supersonic flow and preliminary results obtained for a triangular wing," NACA Tech. Note 2950, 1953.

Section 3.2.2

171. Schardin, H., "The Töpler schlieren method," VDI Forschungsheft 5, 367 (1934).
172. Schardin, H., Vozmozhnosti eksperimental'nogo issledovaniya snaryadov v polete, [The Possibility of an Experimental Study of Projectiles in Flight], technical translation No. 106, NII-I, 1949.
173. Töpler, A., "Observations based on a new method," Poggendorfs Ann. d. Phys. u. Chem. 127, 128, 131, and 134 (1866-1868) /172
174. Holder, D. W., "The toepler schlieren apparatus," Rep. and Mem. 2780 (April 1950).
175. Speak, G. S., and Walter, D. J., "Optical considerations and limitations of the schlieren method," Rep. and Mem. 2859 (January 1950).
176. Mair, W. A., "The sensitivity and range required in a Toepler schlieren apparatus for photography of high-speed airflow," The Aeronautical Quarterly 4 (August 1952).
177. Kantrowitz, A., and Trimpf, R. L., "A sharp-focusing schlieren system," J. Ae. Sci. 17 (1950).
178. Jeffree, H., "A wide-range schlieren system," J. Sci. Instr. (January 1956).
179. Barry, F. W., and Edelman, G. M., "An improved schlieren apparatus," J. Ae. Sci. 15 (June 1948).
180. Sukhorukikh V. S., "The functioning of the Töpler apparatus from the standpoint of geometric and wave optics," report No. 231, State Red Banner Scientific Testing Institute of the Air Force, 1944.
181. Tatarenchik, V. S., "Application of the Töpler optical method to a study of flow around airfoils at high subsonic velocities," Report of the State Red Banner Scientific Research Institute of the Air Force, 1944.
182. Sukhorukikh, V. S., "Testing of the Töpler instrument in a high-velocity wind tunnel," Report of the State Red Banner Scientific Research Institute of the Air Force, p. 231.
183. Veret, C., "Stereoscopic schlieren photography," La Recherche Aéronautique (September-October 1952).

184. Picard, C., "Schlieren photographic analysis of three-dimensional supersonic flows," La Recherche Aéronautique (March-April 1953).
185. Barnes, N. F. and Belinger, S. L., "Schlieren and shadow-graph equipment for airflow analysis," J. Opt. Soc. Am. 35, 497 (1945).
186. Ronchi, V., "Optical systems test," Rev. Opt. (Bologna) 5 (1926).
187. Ronchi, V., "Camera catches shock waves in flight," Aviation Week 49 (September 13, 1948).
188. Valensi, J., and Pruden, F. Q., "Some observations on sharp-nosed profiles at supersonic speed," Rep. and Mem. 2482 (May 12, 1947).
189. Hilton, W. F., and Fowler, R. G., "Photographs of shock wave movements," Rep. and Mem. 2692 (Dember 1947).
190. Dunsby, J. A., "Schlieren tests on some conventional turbine cascades," Rep. and Mem. 2728 (September 1949).
191. Kaspar, J., "Visualization of flow in the study of turbine cascades," Die Schwerindustrie der Tschechoslowakei 8 (1966).
192. Kaspar, J., Schlierengeräte, [Schlieren Apparatus], Mess 32-280-1 Jena.
193. Brandfield, W. S., and Fish, W. Y., "A high-speed schlieren technique for investigation of aerodynamic transients," J. Ae. Sci. (June 1952).
194. Véret, C., "Schlieren photograph apparatus for the S3 Modane wind tunnel," Rech. Aéron. 78 (1960).
195. Bradfield, W. S., and Sheppard, J. J., "Microschlieren," Aerospace Eng. 18(5) (1959).
196. Thomas, G. M., "Measurement technique for nonequilibrium flow and studies of blast wave propagation," ARS 32(8) (1962).
197. Leonard, D. A., and Keck, J. C., "Schlieren photography of projectile wakes using resonance radiation," ARS 32(7) (1962).
198. Nebbeling, C., "A simple method for simultaneous projection of a schlieren image on a viewing screen and into a camera," J. Roy. Ae. Soc. 67, 631 (1963).

199. Creedon, J. E., and Sterling, J., "Multiple simultaneous imaging schlieren system," J. Roy. Aer. Soc. 68(2) (1964).
200. Creedon, J. E., and Sterling, J., "Photographs obtained with the schlieren No. 80 photographic equipment on microfilm," Jenaer Rundschau 9(2) (1964).
201. Lawrence, L. F. et al., "A self-synchronizing stroboscopic schlieren system for the study of unsteady air flows," NACA Techn. Note 2509, 1951.
202. Dubois, G., "A method for visualizing supersonic flows," Rech. Aéron., No. 53 (1956). /173
203. Vas, I. E., "An experimental investigation of the flow over simple two-dimensional and axial symmetric bodies at hypersonic speeds," Jet Propulsion 28(2) (1958).
204. Nebe, V., "Schlieren photographic equipment NO. 80, universal equipment for optical studies," Jenaer Rundschau 3, 4(1958).
205. Grubman, D. H., "Method of determining boundary layer thickness from schlieren photographs," ARS 32(8) (1962).
206. "Basic optical studies of the change in the boundary layer of a supersonic airflow," Feingerätetechnik 11(12) (1962).
207. "Optical schlieren observations in heat flows," Jenaer Rundschau 8(3)(1963).
208. Earnshaw, K. B., and Benedict, Ch. M., "An ultra-high speed image dissecting camera for photographing strong shock waves," Eng. and Instr. 66C(4) (1962).
209. Lebduška, J., "Experimental methods for a high-speed tunnel," in the collection Výskum v oboru proudění [Research in the Field of Flow], Part I, "NCSAV" Press, Prague, 1955.
210. Surget, J., "Quantitative schlieren photography with a color grid with multiple input slits," Rech. Aérospat., No. 97 (1963).

Section 3.2.3

211. Holder, D. W., and North, R. J., "Color in the wind tunnel," The Aeroplane (January 4, 1952).

Section 3.2.4.

212. Hutton, S. P., "The use of interferometers in aerodynamics at the L.F.A Brunswick, Germany," Rep. and Mem. 2366 (July 1946).
213. Ashkenas, H. I., and Bryson, A. E., "Design and performance of a simple interferometer for wind-tunnel measurements," J. Ae. Sci. 18 (February 1951).
214. Zobel, Th., Hochgeschwindigkeitskanal der Luftfahrtforschungsanstalt Braunschweig und seine Messeinrichtungen, [The High-Speed Wind Tunnel of the Braunschweig Aeronautical Research Facility and Its Measurement Apparatus], German Academy for Aeronautical Research, Berlin, 1944.
215. Mokřý, M., "Aerodynamical measurements using the Mach-Zehnder interferometer," report No. Z-239/67 of the Thermomechanics Institute at the Czechoslovak Academy of Sciences, 1967.
216. Zeiss, C., "Mach-Zehnder interferometer," Report G-41-270-1, Jena.
217. Kašpar, J., "Mach-Zehnder interferometer," VZLU Report No. V 784/65, 1965; also published in Zpravodaj VZLU 3, 51 (1965) and in Trojnický časopis SAV 17(1) (1965).
218. Faulders, C. R., "An interferometric study of the boundary layer on a turbine nozzle blade," Transactions of the ASME 76 (January 1954).
219. Bershader, D., "An interferometric study of supersonic channel flow," Rev. Sc. Instr. 20 (1949).
220. Bryson, A. E., "An experimental investigation of transonic flow past two-dimensional wedge and circular section using a Mach-Zehnder interferometer," NACA report 1094, June 1, 1951.
221. "Interferometric analysis of airflow about projectiles in free flight," J. Appl. Phys. 23 (April 1952).
222. Eckert, E., Strömungsuntersuchungen in Turbomaschinen, [Studies of Flow in Turboengines], German Academy for Aeronautical Research, Berlin, 1944.
223. Mach, L., "An interference refractometer," session on report to the Academy of Sciences, Math., Natural Science Department, Section 2A, 102, 1035-1056 (1893) 101, 5-10 (1892).

224. Bouniol, F. and Chevalierias, R., "Interferometer with large field for a supersonic blower," La Recherche Aéronautique, No. 30 (1952).
225. Lamla, E., "Adjustment of the Mach-Zehnder interferometer," Z. Instrumentech. 62 (1942). /174
226. Kinder, W., "Theory of the Mach-Zehnder interferometer and a description of apparatus with a single mirror adjustment," Optik 1 (1946).
227. Kraushaar, R., "A diffraction grating interferometer," Opt. Soc. Amer. 40 (1950).
228. Sterret, J. R., "Investigation of a diffraction grating interferometer for use in aerodynamic research," NACA Tech. Note 2827, 1952.
229. Schardin, H., "Theory and application of the Mach-Zehnder interference-refractometer," Z. f. Instrumentenk. 53 (1933).
230. Tanner, L. H., The Design and Use of Interferometers in Aerodynamics, H.M. Stationary Office, London, 1959.
231. Richter, W., Interferenzgeräte grosser Spiegelabmessungen für optische Strömungsuntersuchungen, [Interference Devices for Large Mirror Measurements for Optical Flow Studies], Jahrbuch WGL, 1958.
232. Constans, M., "Causes of errors in interferential interferometry and schlieren photography," Rech. Aéron., No. 86 (1965).
233. Johnstone, R. K. M. et al., "A design for a 6 in. field Mach-Zehnder interferometer," J. Sci. Instr. 42(4) (1965).
234. Motyčka, J., Interferometry a fotoelectrické přístroje, [Interferometers and Electric Photographic Instruments], "CVUT" Press, Prague, 1965.
235. Dubois, G., and Rugué, C., "A method for measuring base pressure," Rech. Aéron., No. 79 (1960).
236. Philbert, M., and Dubois, G., "The visualization of aerodynamic flows at low densities," Rech. Aéron., No. 81 (1961).
237. Tanner, L. H., "The design of laser interferometers for use in fluid mechanics," J. Sci. Instrum., 43(12) (1966).

238. Wood, G. P. et al., "Investigation with an interferometer of the flow around a circular-arc airfoil at Mach numbers between 0.6 and 0.9," NACA Tech. Note 2693, 1952.
239. Howes, W. L. et al., "A theory and method for applying interferometry to the measurement of certain two-dimensional gaseous density fields," NACA Tech. Note 1693, 1952.
240. Zobel, Th., "Flow measurement by means of light interference," NACA Tech. Note 1253, 1949.
241. Werner, F. D., and Leadon, B. N., "Very accurate measurements of fringes shifts in an optical interferometer study at gas flow," Rev. Sci. Instr. 24 (1953).
242. Guinne, P., and Bouniol, F., "Determination of the velocity field in front of a shock wave on the basis of an interferogram," Rech. Aéron., No. 53 (1956).
243. Tanner, L. G., "Some applications of holography in fluid mechanics," J. Sci. Instrum. 43(2) (1966).
244. Helfinger, L. O., et al., "Holographic interferometry," J. Appl. Phys. 37(2) (1966).

Section 3.2.5

245. Erdmann, S. F., "A new very simple interferometer for obtaining flow images that can be evaluated quantitatively," Appl. Sci. Research B2 (1951).
246. van der Vorren, A. I., "Theory of the Erdmann interferometer for investigation of compressible flows," Appl. Sci. Research B3 (1952).
247. Saunder, M. J., and Smith, A. G., "Phase contrast observations," J. Appl. Phys. 27 (1956).

Section 3.2.6

248. Hurlbut, F. C., Techniques of Flow Visualization Applicable on Low Density Fields (see [19]).
249. Dimeff, J., et al., "X-ray instrumentation for density measurements in supersonic flow field," NACA Tech. Note 2845, 1952. /175
250. Sherman, P. M., "Visualization at low-density flows by means of oxygen absorption of ultraviolet radiation," J. Ae. Sci. 24(2) (1957).

251. Evans, R. A., "A new visualization method in wind tunnels at low densities," Voprosy raketnoy tekhniki 8(4) (1958).
252. Winkler, E. M., "X-Ray Technique (see [146 and 146a]).
253. Grün, A. E. et al., "Electron shadowgraphs and afterglow pictures of gas jets at low densities," J. Appl. Phys. 24 (1953).
254. Schumacher, B., "Images of gas flows obtained by electron beams," Ann. Physik, Ser. 6 (1953).
255. Venable, D., and Kaplan, D., "Electron beam method of determining density profiles across shock waves in gases at low densities," J. Appl. Phys. 26 (1955).

The literature that was presented in this bibliography can also be obtained, with certain exceptions, in our libraries, namely in

1. the State Technical Library in Prague,
2. the VZLU Library in Letnany
3. the Mathematics-Physics Department Library at Charles University in Prague.